Methods in Molecular Biology 1242

Springer Protocols

José M. Estevez *Editor*

Plant Cell Expansion

Methods and Protocols

Humana Press

METHODS IN MOLECULAR BIOLOGY

Series Editor
John M. Walker
School of Life Sciences
University of Hertfordshire
Hatfield, Hertfordshire, AL10 9AB, UK

For further volumes:
http://www.springer.com/series/7651

Plant Cell Expansion

Methods and Protocols

Edited by

José M. Estevez

Instituto de Fisiología, Biología Molecular y Neurociencias (IFIBYNE-CONICET), Facultad de Ciencias Exactas y Naturales, Universidad de Buenos Aires, Argentina

Humana Press

Editor
José M. Estevez
Departamento de Fisiología
Biologia Molecular y Celular (DFBMC)
University of Buenos Aires IFIByNE-CONICET
Buenos Aires, Argentina

ISSN 1064-3745 ISSN 1940-6029 (electronic)
ISBN 978-1-4939-1901-7 ISBN 978-1-4939-1902-4 (eBook)
DOI 10.1007/978-1-4939-1902-4
Springer New York Heidelberg Dordrecht London

Library of Congress Control Number: 2014954228

Printed on acid-free paper

Humana Press is a brand of Springer
Springer is part of Springer Science+Business Media (www.springer.com)

Preface

Plant cells differ enormously in size and shape and cell volumes can vary 10,000-fold within a species, increasing in size from meristems to differentiated cells. Plant cells can be cylindrical, tubular, spherical, stellate, etc., and this complex cell shapes are produced by tight regulation of growth and need to be maintained by structural reinforcement after the cessation of growth. Plant cell expansion occurs through the controlled growth of the cell wall, which results from the interplay between turgor pressure and cell wall elasticity and extensibility. The understanding of growth at the cellular level is vital because final plant shape is dictated by two factors: cell number and cell size. The improvement of existing methods and the development of new ones to follow and study how single plant cells change over the time is one exciting area of research within plant biology.

By presenting this new volume of *Plant Cell Expansion*, I wanted to cover selected aspects of plant cell growth in different single-cell types such as root hairs and pollen tubes as well as at tissues-organ level like hypocotyls and whole roots. This volume is focused on methods to study in detail several complex aspects of cell expansion such as secretion and endocytosis, reactive oxygen species (ROS) production, and Ca^{2+} imaging as well as quantification of growth in real time. In addition, two chapters described methods for the structural and mechanical as well as the biochemical characterization of growing plant cell walls. On top, there are chapters only dedicated to the green algae *Penium margaritaceum* as a new model for single-cell growth and cell wall formation. Finally, several methods currently used in plant molecular and cell biology are described for identification of new genes related to cell growth and expansion.

As in previous books of the series, all the authors in each single chapter of this book have tried to present a collection of step-by-step protocols, described at a level of detail enough to be followed by experienced researchers and beginners. I wish this book would become an important reference book for plant scientists working on any aspect of molecular and cell biology that relates to cell growth and expansion. Finally, I would like to thank all the contributing colleagues whose knowledge, expertise, and effort have been vital for attaining the highest scientific level of this book.

Buenos Aires, Argentina — *José M. Estevez*

Contents

Contributors

Charles T. Anderson • *Department of Biology and Center for Lignocellulose Structure and Formation, The Pennsylvania State University, University Park, PA, USA*

Amanda Andreas • *Department of Biology and Skidmore Microscopy Imaging Center, Skidmore College, Saratoga Springs, NY, USA*

Logan Bashline • *Department of Biochemistry & Molecular Biology, Pennsylvania State University, University Park, PA, USA*

María Laura Barberini • *Instituto de Investigaciones en Ingeniería Genética y Biología Molecular, Dr. Héctor Torres (INGEBI-CONICET), Buenos Aires, Argentina*

Cecilia Borassi • *Instituto de Fisiología, Biología Molecular y Neurociencias (IFIBYNE-CONICET), Facultad de Ciencias Exactas y Naturales, Universidad de Buenos Aires, Buenos Aires, Argentina*

Federica Brandizzi • *MSU-DOE Plant Research Lab, Michigan State University, East Lansing, MI, USA*

Ingo Burgert • *Applied Wood Research Laboratory, Empa-Swiss Federal Laboratories for Material Testing and Research, Institute for Building Materials, Duebendorf, Switzerland*

Jose R. Dinneny • *Department of Plant Biology, Carnegie Institution for Science, Stanford, CA, USA*

Lina Duan • *Department of Plant Biology, Carnegie Institution for Science, Stanford, CA, USA*

David S. Domozych • *Department of Biology and Skidmore Microscopy Imaging Center, Skidmore College, Saratoga Springs, NY, USA*

Siamsa M. Doyle • *Department of Forest Genetics and Plant Physiology, Umeå Plant Science Centre, Swedish University of Agricultural Sciences (SLU), Umeå, Sweden*

G. Drakakaki • *Department of Plant Sciences, University of California Davis, Davis, CA, USA*

Michaela Eder • *Department of Biomaterials, Max-Planck-Institute of Colloids and Interfaces, Potsdam, Germany*

V. Esteva Esteve • *Department of Plant Sciences, University of California Davis, Davis, CA, USA*

José M. Estevez • *Departamento de Fisiología, Biologia Molecular y Celular (DFBMC), University of Buenos Aires IFIByNE-CONICET, Buenos Aires, Argentina*

Jose Sebastian • *Department of Plant Biology, Carnegie Institution for Science, Stanford, CA, USA*

Jonatan U. Fangel • *Department of Plant and Environmental Sciences, Faculty of Life Sciences, University of Copenhagen, Copenhagen, Denmark*

Andrew P. French • *Centre for Plant Integrative Biology, School of Biosciences, University of Nottingham, Sutton Bonington, UK*

Yoichiro Fukao • *Graduate School of Biological Sciences, Nara Institute of Science and Technology, Ikoma, Japan; Plant Global Educational ProjectNara Institute of Science and Technology, Ikoma, Japan*
Ying Gu • *Department of Biochemistry & Molecular Biology, Pennsylvania State University, University Park, PA, USA*
Jesper Harholt • *Department of Plant and Environmental Sciences, Faculty of Life Sciences, University of Copenhagen, Copenhagen, Denmark*
I. Elisabeth Johansen • *Department of Plant and Environmental Sciences, Faculty of Life Sciences, University of Copenhagen, Copenhagen, Denmark*
Bodil Jørgensen • *Department of Plant and Environmental Sciences, Faculty of Life Sciences, University of Copenhagen, Copenhagen, Denmark*
Paola Silvina Denita Juarez • *Laboratorio de Fisiología y Biología Molecular, IFIByNE (CONICET), FCEyN, Universidad de Buenos Aires, Buenos Aires, Argentina*
Joanna Kacprzyk • *School of Biology and Environmental Science, University College Dublin, Dublin, Ireland*
Jürgen Kleine-Vehn • *Department of Applied Genetics and Cell Biology, University of Natural Resources and Life Sciences, Vienna (BOKU), Austria*
Rie Kurata • *Graduate School of Biological Sciences, Nara Institute of Science and Technology, Ikoma, Japan*
Christian Löfke • *Department of Applied Genetics and Cell Biology, University of Natural Resources and Life Sciences, Vienna (BOKU), Austria*
Silvina Mangano • *Laboratorio de Fisiología y Biología Molecular, IFIByNE (CONICET), FCEyN, Universidad de Buenos Aires, Buenos Aires, Argentina*
Paul F. McCabe • *School of Biology and Environmental Science, University College Dublin, Dublin, Ireland*
Maria Dalgaard Mikkelsen • *Department of Plant and Environmental Sciences, Faculty of Life Sciences, University of Copenhagen, Copenhagen, Denmark*
Jorge Muschietti • *Instituto de Investigaciones en Ingeniería Genética y Biología Molecular, Dr. Héctor Torres (INGEBI-CONICET), Buenos Aires, Argentina; Departamento de Biodiversidad y Biología Experimental, Facultad de Ciencias Exactas y NaturalesUniversidad de Buenos Aires, Buenos Aires, Argentina*
Juliana Pérez Di Giorgio • *Instituto de Investigaciones en Ingeniería Genética y Biología Molecular, Dr. Héctor Torres (INGEBI-CONICET), Buenos Aires, Argentina*
Michael Pound • *Centre for Plant Integrative Biology, School of Biosciences, University of Nottingham, Sutton Bonington, UK*
Randeep Rakwal • *Organization for Educational Initiatives, University of Tsukuba, Tsukuba, Japan*
Luciana Renna • *MSU-DOE Plant Research Lab, Michigan State University, East Lansing, MI, USA*
Adeline Rigal • *Department of Forest Genetics and Plant Physiology, Umeå Plant Science Centre, Swedish University of Agricultural Sciences (SLU), Umeå, Sweden*
Stéphanie Robert • *Department of Forest Genetics and Plant Physiology, Umeå Plant Science Centre, Swedish University of Agricultural Sciences (SLU), Umeå, Sweden*
Maja G. Rydahl • *Department of Plant and Environmental Sciences, Faculty of Life Sciences, University of Copenhagen, Copenhagen, Denmark*
Arun Sampathkumar • *Division of Biology and Biological Engineering, California Institute of Technology, Pasadena, CA, USA*

Friederike Saxe • *Department of Biomaterials, Max-Planck-Institute of Colloids and Interfaces, Potsdam, Germany*
María R. Scarpin • *Instituto de Investigaciones en Ingeniería Genética y Biología Molecular, Dr. Héctor Torres (INGEBI-CONICET), Buenos Aires, Argentina*
David Scheuring • *Department of Applied Genetics and Cell Biology, University of Natural Resources and Life Sciences, Vienna (BOKU), Austria*
Maria Schöller • *Department of Applied Genetics and Cell Biology, University of Natural Resources and Life Sciences, Vienna (BOKU), Austria*
Giovanni Stefano • *MSU-DOE Plant Research Lab, Michigan State University, East Lansing, MI, USA*
Richard Strasser • *Department of Applied Genetics and Cell Biology, University of Natural Resources and Life Sciences, Vienna, Austria*
Peter Ulvskov • *Department of Plant and Environmental Sciences, Faculty of Life Sciences, University of Copenhagen, Copenhagen, Denmark*
Ulrike Vavra • *Department of Applied Genetics and Cell Biology, University of Natural Resources and Life Sciences, Vienna, Austria*
Christiane Veit • *Department of Applied Genetics and Cell Biology, University of Natural Resources and Life Sciences, Vienna, Austria*
Silvia M. Velasquez • *Instituto de Fisiología, Biología Molecular y Neurociencias (IFIBYNE-CONICET), Facultad de Ciencias Exactas y Naturales, Universidad de Buenos Aires, Buenos Aires, Argentina*
Darren M. Wells • *Centre for Plant Integrative Biology, School of Biosciences, University of Nottingham, Sutton Bonington, UK*
Raymond Wightman • *Sainsbury Laboratory, University of Cambridge, Cambridge, UK*
William G.T. Willats • *Department of Plant and Environmental Sciences, Faculty of Life Sciences, University of Copenhagen, Copenhagen, Denmark*
N. Worden • *Department of Plant Sciences, University of California Davis, Davis, CA, USA*
Chaowen Xiao • *Department of Biology and Center for Lignocellulose Structure and Formation, The Pennsylvania State University, University Park, PA, USA*
Sajad Majeed Zargar • *Graduate School of Biological Sciences, Nara Institute of Science and Technology, Ikoma, Japan; School of Biotechnology, SK University of Agricultural Sciences and Technology, Chatha, Jammu, Jammu and Kashmir, India*

Chapter 1

Penium margaritaceum as a Model Organism for Cell Wall Analysis of Expanding Plant Cells

Maja G. Rydahl, Jonatan U. Fangel, Maria Dalgaard Mikkelsen, I. Elisabeth Johansen, Amanda Andreas, Jesper Harholt, Peter Ulvskov, Bodil Jørgensen, David S. Domozych, and William G.T. Willats

Abstract

The growth of a plant cell encompasses a complex set of subcellular components interacting in a highly coordinated fashion. Ultimately, these activities create specific cell wall structural domains that regulate the prime force of expansion, internally generated turgor pressure. The precise organization of the polymeric networks of the cell wall around the protoplast also contributes to the direction of growth, the shape of the cell, and the proper positioning of the cell in a tissue. In essence, plant cell expansion represents the foundation of development. Most studies of plant cell expansion have focused primarily upon late divergent multicellular land plants and specialized cell types (e.g., pollen tubes, root hairs). Here, we describe a unicellular green alga, *Penium margaritaceum* (Penium), which can serve as a valuable model organism for understanding cell expansion and the underlying mechanics of the cell wall in a single plant cell.

Key words *Penium margaritaceum*, Live cell labeling, Cell expansion, Confocal laser scanning microscopy, Variable pressure scanning electron microscopy, Manipulation of cell wall, Isolation of pure cell wall

Abbreviations

AGP	Arabinogalactan protein
CBM	Carbohydrate-binding module
CGA	Charophycean Green Algae
CLSM	Confocal laser scanning microscope
HG	Homogalacturonan
LM	Light microscope
LRW	London Resin White
PBS	Phosphate-buffered saline
PBST	PBS with 1 % Triton-X
Penium	*Penium margaritaceum*
PME	Pectin methyl esterase
RT	Room temperature

José M. Estevez (ed.), *Plant Cell Expansion: Methods and Protocols*, Methods in Molecular Biology, vol. 1242,
DOI 10.1007/978-1-4939-1902-4_1,

TEM	Transmission electron microscopy
VPSEM	Variable pressure scanning electron microscopy
WFLM	Wide-field fluorescence microscope
WHS	Sterile Woods Hole medium supplemented with sterile soil extract (Woods Hole Soil)

1 Introduction: *Penium* and Its Taxonomic Position in the Plant Kingdom

The evolution of land plants from an ancestral stock of Charophycean Green Algae (CGA; also called the Streptophyta), 470–450 million years ago, profoundly changed our planet [1–3]. The consequences of this event allowed for further expansion onto *terra firma* by green plants as well as the introduction of other life forms to these ecosystems [4–6]. The cell wall was central to the invasion of land by green plants and is profoundly essential to the life processes of virtually all plants. The cell wall is a fibrous composite primarily comprising a diverse set of polysaccharides along with a subset of proteoglycans and in some cases, phenylpropanoids. These macromolecules assemble into an intricate microarchitecture that is essential to rigidity, defense, adhesion, and transport of water and ions [7–10]. However, the most important function of the cell wall in the life of a plant cell is most likely in the regulation of cell expansion and morphogenesis. While our understanding of the cell wall and its role in expansion has dramatically increased over the past decades, we are only just beginning to understand the evolutionary processes associated with cell wall biochemistry, biology, complexity, structure, and dynamics [6, 11].

For CGA to have first colonized land, significant molecular adaptations would have been necessary in order to adapt to the inhospitable environmental pressures such as UV radiation and desiccation [3, 12, 13]. Cell wall evolution and diversification were inevitably required to respond to these pressures as well as to provide a rigid "skeleton" in order for a plant to stand upright. However, recent studies have shown that many land plants do not have a significantly more advanced cell wall than those found in the CGA [12, 14–18]. This suggests that the terrestrial invasion and evolution of morphological complexity displayed in land plants required a restructuring of the wall molecular architecture already found in CGA rather than the creation of significantly new wall components. However, it is not fully understood to what degree land plant cell wall polymers, like pectin, hemicellulose, lignin, and glycoprotein, predates back to their algal ancestors [19].

The precise identity of CGA taxa that yielded land plants is still not resolved [3, 4, 20–22]. One major factor is that the 450+ million years that passed after the invasion of land by green plants has also naturally yielded significant changes in extant CGA. However, over the past few decades data derived from multiple

modern technologies has shown that the later diverging clades of the CGA, i.e., Charales, Coleochaetales, and Zygnematales, are the closest related to modern land plants within the CGA taxa [4, 15, 18, 23–27]. Transcriptomic data has recently suggested that the unicellular desmid, Penium, of the Zygnematales clade, has perhaps the most advanced extant CGA taxon, thereby placing it closest to land plants [23, 24, 26–28]. Concurrent studies furthermore suggest that Penium may be the best candidate as an experimental model system for studying the CGA, their cell walls, cell and wall expansion and for identifying the evolutionary adaptations important for colonization of land [12, 29, 30].

Model organisms are carefully chosen species that possess attributes highly desirable for studying basic biological phenomena. In some ways, model organisms represent a major foundation upon which modern biology has been built. In plants, *Arabidopsis thaliana* (Brassicaceae; Angiospermae), is the most well-studied model system, especially for molecular analyses. This is due to its small and fully sequenced genome and a short generation time [31, 32]. Other plants such as rice, corn, tobacco, *Brachypodium*, and the moss, *Physcomitrella patens*, have also become valuable model organisms for the study of various biological phenomena and applications. However, most of these multicellular taxa have some major inherent disadvantages. These include deciphering basic cellular processes, especially those used in expansion and differentiation. It is extremely difficult to study and interpret data concerning subcellular phenomena that occurs in a *single* cell embedded in a *multicellular* tissue and organ. Likewise, many model multicellular plants express heterogeneous developmental patterning in the different tissues and must be studied over relatively long generation times. Attempts to create and utilize unicellular plant systems have provided some help in understanding biological processes at the cellular level. For example, suspension culture cell lines like the tobacco BY-2 line have successfully been employed in many studies [33, 34]. However, these tissue culture-derived cells represent highly artificial systems whose physiology has been significantly altered. The identification and use of a "natural" unicellular plant system would represent a simple, convenient, and valuable tool for analyzing expansion phenomena in a cell with the same physiological and developmental status. Penium represents one such unicellular model system for plant biology research. This alga may be grown rapidly in large, developmentally synchronized cultures and possesses multiple features that are highly useful for experimental work. This includes application in high-throughput technologies that allow for quick and diverse analyses.

Penium is a unicellular placoderm desmid (Desmidiacae, Zygnematales) that has a simple cylindrical phenotype. Like all desmids, the cell is made up of two identical semicells, each containing a large chloroplast and surrounding a central nucleus located in an

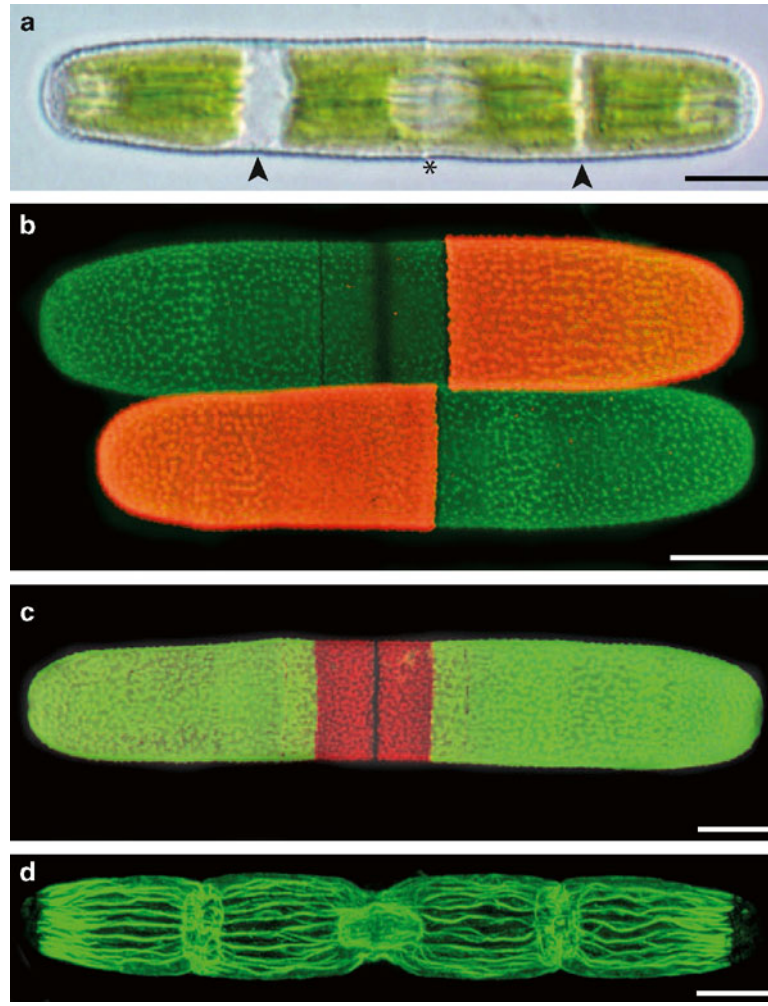

Fig. 1 *Penium margaritaceum*. (**a**) Light microscopy differential interference contrast (DIC) image of a whole cell. Central isthmus zone (*asterisk*), and the plastids found in each of the semicell (*arrow*). (**b**) Overlay of dual live cell labeling with JIM5 (HG w. low %DE) on day zero (TRITC) and day one (FITC). Orange channel; older JIM5-TRITC wall, green channel; new JIM5-FITC, indicating that new wall production is not always perfectly symmetric (*see* method 3.1 and 3.2). (**c**) Same type of labeling as (**b**), green channel; older JIM5-TRITC wall, red channel; new JIM5-FITC. (**d**) F-actin network labeled with Rhodamine phalloidin (*see* method 3.8). Scale bar 10 μm. Taken with blue and green lasers on an Olympus Fluoview 1200 confocal laser microscope

isthmus zone (*see* overview in Fig. 1). Penium produces only a primary cell wall that consists of a distinct calcium (Ca^{2+})-complexed homogalacturonan (HG)-rich outer layer and an inner layer of cellulose [29, 35–38]. Biochemical analysis and immunocytochemistry have furthermore identified components and epitopes of the pectin

rhamnoglacturonan I, proteoglycans, extensins, arabinogalactan protein (AGP), and hemicelluloses, including mannan and xylan [30]. Immunocytochemical labeling has shown that during predivision expansion, highly esterified HG is secreted in a narrow band at the isthmus. The HG is most likely de-esterified by pectin methyl esterase (PME) and then complexed with Ca^{2+} to form a distinct lattice constituting the outer wall layer [29, 38]. This process is distinctly bidirectional or "bipolar," as older pectin is pushed outward toward both poles by newly secreted pectin. Once cytokinesis has occurred, residual HG secretion occurs for a short period of time at the expanding pole of the daughter semicell [29, 39]. Pectin secretion also entails the activity of an elaborate endomembrane system consisting of over 100 Golgi bodies and a mobile pool of vesicles circulating in a peripheral cytoplasmic streaming network [40]. The expansion mechanism of Penium may also be manipulated in high-throughput studies including single cell experiments [29]. It is also important to reconsider the type of model system that the Penium wall expansion represents. We propose that it models a *primordial* cell expansion mechanism that has been elaborated upon in vascular plants. Vascular plants will expand at constant wall thickness, i.e., tightly coupled to wall biosynthesis, if carbon is available, but also have programs that uncouple wall biosynthesis and cell expansion [41, 42] when carbon availability is limiting. A term, "extensial," has been proposed long ago for the incorporation of wall material that leads to wall loosening and thus drives expansion as opposed to "intensial" for the apposition of material that stiffens the wall [43]. The underlying mechanisms of wall incorporation are unknown and the apparent existence of biosynthesis driven expansion in its pure form in Penium makes it an ideal organism for elucidating basic expansion mechanisms in plants including pectin dynamics, membrane trafficking, and adaptation to experimental/environmental stress.

As important, efforts to reveal the molecular biology of Penium have recently begun and soon will provide powerful tools for analyzing cell expansion dynamics. We and other research groups have developed biolistic and *Agrobacterium* based transformation protocols for application to the CGA including Penium (e.g., *Closterium peracerosum* [44]; *Penium margaritaceum* [45]). Considerable transcriptomic data is currently available for Penium and other CGA taxa [23] and we and other research groups (personal communication, Jocelyn K.C. Rose, Cornell University) are now working on defining and annotating the Penium genome. In the near future, molecular analyses will significantly complement cell biology and biochemistry-based approaches to the study of among other expansion in Penium. The procedures described below provide the reader with basic techniques dealing with Penium. These protocols provide a foundation for future research with this unicellular model organism.

2 Materials

2.1 Growth, Synchronization, and Cell Collection

Penium margaritaceum culture (e.g., from Skidmore College Algal Culture Collection; clone number Skd#8).

Growth Medium

Sterile Woods Hole medium supplemented with Sterile soil extract (Woods Hole Soil; WHS) [46].

1,000× Stock solutions (always use dH_2O, i.e., deionized or double distilled water; 18 MΩ resistance preferred; stock solutions may be stored for up to 6 months at 4 °C):

1. $CaCl_2 \cdot 2H_2O$—36.80 g in 1 L of dH_2O.
2. $MgSO_4 \cdot 7H_2O$—37.00 g in 1 L of dH_2O.
3. $NaHCO_3$—12.60 g in 1 L of dH_2O.
4. $K2HPO_4 \cdot 3H_2O$—11.40 g in 1 L of dH_2O.
5. $NaNO_3$—85.00 g in 1 L of dH_2O.
6. Combined trace elements: $EDTANa_2$—4.36 g, $FeCl_3 \cdot 6H_2O$—3.15 g, $CuSO_4 \cdot 5H_2O$—0.01 g, $ZnSO_4 \cdot 7H_2O$—0.022 g, $CoCl_2 \cdot 6H_2O$—0.01 g, $MnCl_2 \cdot 4H_2O$—0.18 g, $Na_2MoO_4 \cdot 2H_2O$—0.006 g, H_3BO_3—1.00 g in 1 L of dH_2O.
7. Vitamin mix: Sigma-Aldrich Gamborg's Vitamin Solution (already in solution).
8. 1.5 mM Tris–HCl: 121 g of Tris–HCl in 1 L of dH_2O—adjust pH to 7.2.

Medium per liter: Add 1 mL of stock solutions #1-7, 2 mL of stock #8, 100 mL of soil supernatant (e.g., Soil–Water Supernatant from http://www.carolina.com/) to 1 L of dH_2O, and check pH (should be 7.2). Autoclave at 15 psi for 15 min.

Equipment

1. Growth chamber: 35 W/m^2 of cool white fluorescent light.
2. Sterile 250 mL Erlenmeyer flasks with cotton or foam plugs.
3. Sterile 10 or 25 mL pipettes.
4. Sterile 15 mL falcon tubes.
5. Autoclave.
6. Table top centrifuge that holds 15 mL centrifuge tubes.

2.2 Live Cell Labeling

1. Table top centrifuge (as above).
2. Microcentrifuge.
3. Sterile 15 mL falcon tubes.
4. Sterile 10 or 25 mL pipettes.
5. 1.5 mL Eppendorf tubes.

6. Microtube rotator.
7. Micropipettes and tips.
8. Platform shaker.
9. WHS.
10. Instant nonfat milk powder.
11. Molecular probes (carbohydrate binding modules, monoclonal antibodies, etc., *see* **Note 1**).
12. Secondary antibodies specific for primary molecular probe (e.g., Anti-Rat IgG-FITC conjugate).
13. Calcofluor White stock solution: 1 mg/mL in dH_2O stored in the freezer.
14. Light microscope (LM) or wide field fluorescence microscope (WFLM) or confocal laser scanning microscope (CLSM) for viewing cells.

2.3 Monitoring Cell and Wall Expansion Over Time

1. Molecular probes (e.g., JIM5 or LM18).
2. WHS.
3. Petri dishes or multiwelled tissue culture plates.
4. Microscopes (WFLM or CLSM).

2.4 Transmission Electron Microscopy (TEM)

1. Artist's airbrush (*see* **Note 2**).
2. Freezer (–80 or –90 °C).
3. Air compressor or house compressed air.
4. Propane (*see* **Note 3**).
5. Liquid nitrogen.
6. 200–500 mL dewar for holding porcelain dishes.
7. 99 or 100 % ethanol.
8. Molecular sieves (Sigma Chemical).
9. 1 % uranyl acetate (Sigma Chemical).
10. 0.1 % lead citrate (Sigma Chemical).
11. Porcelain dishes (20 mL) with covers.
12. EM supplies (EM supplies may be purchased from Electron Microscopy Sciences (EMS), Ft. Washington, PA, USA).
    - 20 mL glass scintillation vials with caps.
    - 70 % glutaraldehyde.
    - 1/10 g vials of osmium tetroxide.
    - Acetone.
    - Spurrs Low Viscosity resin.
    - London Resin White (LRW).
    - Aclar plastic.

- Beem capsules.
- Formvar.
- Gold, copper, and nickel grids.

13. PBS and PBS with 1 % Triton-X (PBST) (both pH 7.2); 10× concentrated PBS and PBST may be purchased from BioRad (CA, USA).
14. Ultramicrotome and diamond/glass knife for sectioning.

2.5 Variable Pressure Scanning Electron Microscopy (VPSEM)

1. 0.8 cm circles of nitrocellulose (*see* **Note 4**).
2. Small dewar and liquid nitrogen.
3. Filter paper.
4. Pipette.
5. Forceps.
6. Cryo-stub (JEOL, Peabody, MA, USA) or Peltier cooled stage used on many scanning electron microscopes.

2.6 Isolating Pure CW

1. Sonicator with horn (probe) for processing 5–100 mL samples.
2. 50–100 mL beakers.
3. 15 mL falcon tubes.
4. Clinical centrifuge.
5. 0.1 M Tris–HCl buffer, pH 7.2.
6. Wall isolation buffer: 0.5 % Triton X-100 in 0.1 M Tris–HCl buffer (pH 7.2).
7. Deionized water (dH_2O).
8. Ice.

2.7 High-Throughput Manipulation and Assessment of Cell and Cell Wall Expansion

1. Plastic multiwelled tissue culture plates, 24-, 48-, and 96-welled, uncoated.
2. WHS.
3. Micropipettes and plastic tips.
4. Growth chamber (*see* Subheading 2.1).
5. Experimental chemicals (e.g., cytochalasin B or E for actin studies, oryzalin for microtubule studies; Sigma Chemical).

2.8 Rhodamine Phalloidin Labeling

Stock solutions (Solutions 1-5 may be stored for up to 6 months at 4 °C).

1. 10× PIPES—500 mM PIPES buffer (7.05 g PIPES/50 mL dH_2O—adjust pH to 6.9).
2. 10× $MgCl_2$—50 mM $MgCl_2$ (1.01 g/100 mL dH_2O).
3. 10× KCl—250 mM KCl (1.85 g/100 mL dH_2O).
4. 10× $CaCl_2$—50 mM $CaCl_2$ (0.735 g/100 mL dH_2O).

5. 10× EGTA—50 mM EGTA (Ethylene Glycol Tetraacetic Acid; 1.9 g/100 mL dH_2O; adjust pH to 6.9).
6. 1,000× MBS—100 mM MBS (3-Maleimidobenzoic acid *N*-hydroxy-succinimide ester; 6.3 mg/200 µL DMSO, store in freezer).
7. 37 % formaldehyde (alcohol free).
8. Rhodamine phalloidin (Molecular Probes/Invitrogen)—Rhodamine phalloidin is dissolved in 300 µL of methanol and stored in the dark at −20 °C until further use. At the time of labeling, for each sample, 30 µl rhodamine phalloidin is placed in a 1.5 mL microcentrifuge tube. The tubes are placed in a 37 °C incubator for 2H to evaporate methanol (*see* **Note 5**).
9. Working buffer A: 20 mL of stock solution #1-5 to 50 mL of dH_2O. Adjust pH to 6.9 and bring total volume to 200 mL with dH_2O.
10. Buffer/Triton-X100: 10 µL Triton-X100/100 mL of Working buffer A.
11. Fixative: add 2.7 mL formaldehyde/50 mL of Buffer/Triton-X100 (under hood).

Working rhodamine phalloidin solution: Dissolve dried rhodamine phalloidin in tube (*see* **item 8** above) with 1 mL of Buffer/Triton-X100 (requires shaking; keep in dark when not using).

3 Methods

3.1 Growth, Synchronization, and Cell Collection

1. Cell cultures are maintained in sterile 250 mL sterile Erlenmeyer flasks containing 100 mL of WHS (*see* Subheading 2.1). Flasks are maintained in a growth chamber, set at 18 ± 1 °C with a 14:10 light/darkness regime, 35 W/m^2 of cool white fluorescent light.
2. Subcultures are made every 5 days by taking 5 mL of cell suspension from stock cultures and adding to a new flask (*see* **Note 6**).
3. Washing of cells: Cells are collected in a centrifuge tube and centrifuged at 250–400 × *g* on a table top centrifuge for 1 min. The supernatant is discarded, new WHS is added to disrupt the pellet, and the tubes are vortexed for 30 s. Cells are centrifuged again and this washing procedure is repeated twice (*see* **Note 7**).
4. Synchronizing cultures using dark starvation, aseptically collect a 10 mL cell suspension in 15 mL falcon centrifuge tube and washed as described in **step 3** of Subheading 3.1.
5. Resuspend in sterile WHS and wrap in a double layer of aluminum foil. The tube is kept in the growth chamber for at least 3 weeks and up to 4 months.

6. Remove aluminum foil and washed cells as described in **step 3** of Subheading 3.1.
7. Resuspend the pellet in 5 mL of sterile WHS, and pour it into a sterile culture flask containing 100 mL of sterile WHS. The flask is placed in a growth chamber at the beginning of the 14 h light sequence as described in **step 1** of Subheading 3.1.
8. Cell and wall expansion stages may be monitored by removing a small aliquot of cells from the flask with a sterile pipette at various times and viewing with a LM (*see* **Note 8**).

3.2 Live Cell Labeling

1. Cells are collected in 15 mL sterile plastic centrifuge tubes and washed as described in **step 3** of Subheading 3.1. The final pellet is resuspended in 500 μL WHS and transferred to a 1.5 mL Eppendorf tube.
2. Block the cells by centrifuging at 1,500 × *g* on a microcentrifuge for 1 min, discard the supernatant, and resuspend in 500 μL of WHS containing 0.5 % nonfat instant milk. Place tube in a laboratory rotator or platform shaker and rotate for 30 min (*see* **Note 9**). The cells are centrifuged at 4,000 rpm on a microcentrifuge for 1 min and washed as described in **step 3** of Subheading 3.1.
3. Incubate cells with 200 μL of various molecular probes diluted in WHS (*see* **Note 10**). Incubated tubes in the dark on a rotator or platform shaker at room temperature (RT) for 90 min.
4. Cells are centrifuged and washed, as described in **step 3** of Subheading 3.1.
5. Block pellet once again with WHS containing 1 % nonfat instant milk for 30 min, and washed as described in **step 3** of Subheading 3.1.
6. Incubate cells in 200 μL fluorescently labeled secondary antibody at a 1/50 dilution in WHS. Incubated tubes in the dark on a rotator or platform shaker at RT for 90 min.
7. Cells and washed as described in **step 3** of Subheading 3.1.
8. Cells may then be costained in 1:1,000 dilution of Calcofluor White derived from a 1 mg/mL stock solution in WHS. Cells are labeled for 15 min and then washed, as described in **step 3** of Subheading 3.1. The pellet is suspended in a small volume of fresh WHS (~100 μL). The cells are now ready for microscopic observation.

3.3 Monitoring Cell and Wall Expansion over Time

1. Cultures are synchronized using dark starvation as described in Subheading 3.1.
2. After the cells are removed from the aluminum foil and washed (as described in **step 3** of Subheading 3.1), they may be labeled

with fluorescent molecular probes like the monoclonal antibodies JIM5 and LM18, followed by anti-rat-FITC or -TRITC labeled secondary antibody as described in Subheading 3.2 (*see* **Note 11**).

3. Aliquots of cells are placed in fresh WHS in petri dishes, multiwelled petri dishes or flasks.
4. Aliquots of cells may be aseptically removed from the cultures at various times, concentrated by centrifugation at 1,500×*g* on a microcentrifuge for 1 min and viewed with WFLM or CLSM.
5. Quantitative analysis of wall surface areas may be determined as described in ref. [29]. Further developmental data may be obtained by taking labeled cells and labeling with other molecular probes (*see* **Note 12**).

3.4 Transmission Electron Microscopy (TEM)

An acetone-based substitution solution is used for osmicated preparations while an ethanol-based solution is employed for nonosmicated preparations (*see* **Note 13**). One to two days before cryofixation, prepare freeze substitution vials as follows:

3.4.1 Prefixation

1. Wash approximately 50–100 g of molecular sieves with either 100 % acetone or 100 % ethanol.
2. With a spatula, cover the bottom of the 20 mL substitution vials with a layer of washed molecular sieves. Add 10 mL of 100 % acetone or 99 % ethanol, cap, shake, and let stand for 24–48 H, to "dry" the acetone/ethanol (i.e., remove residual water).
3. 24 H before fixation, place 10 mL of 70 % glutaraldehyde into the bottom of a clean scintillation vial. Add dry molecular sieve and mix until no glutaraldehyde is observed above sieves. Let stand for 24 H in a fume hood. This process removes water from the 70 % glutaraldehyde. A clearly sticky mass of glutaraldehyde will cover the sieves when residual water is removed.
4. 3-4 H before cryofixation, weigh out under a fume hood 0.5 g of the "dried" glutaraldehyde-molecular sieves and place into either a vial containing dried acetone (for osmicated preparations) or ethanol (nonosmicated preparations). This amount will provide a final 1 % glutaraldehyde acetone or ethanol substitution medium.
5. Cap the vial and swirl the vials for 1 min and let stand for 1 h with occasional swirling to dissolve the glutaraldehyde.
6. Place the vials into a –80 °C freezer for at least 2 h. These vials represent the freeze substitution chambers and can be kept in the freezer for up to 2 weeks.

3.4.2 Cryofixation

The following procedures must be performed in a fume hood and no flames should be ignited in the laboratory.

1. Place a 20 mL porcelain dish into a shallow liquid nitrogen-tolerant dewar so that its opening is slightly above that of the dewar (*see* **Note 14**).
2. Position the artist's airbrush approximately 20 cm above the center of the porcelain dish using a bunsen burner stand and clamps. Connect the air inlet port of the airbrush to an air compressor (or a building air source). Adjust the spray setting on the airbrush to a fine spray. Test that liquid will spray into the dish by covering the dish with a paper towel and using water as the test solution. Adjust the positioning of airbrush as needed.
3. Collect Penium suspensions and wash three times as described in **step 3** of Subheading 3.1 with fresh growth medium or test solution. After the last centrifugation, add 500 μL of growth medium or test solution to resuspend the pellet.
4. Cool the porcelain dish with liquid nitrogen.
5. Attach a plastic hose to the outlet of a propane gas source. Attach the large opening of a glass Pasteur pipette to the other end of the hose.
6. Gently turn on the outlet of the propane tank/bottle/outlet and place the tip of the pipette onto the bottom of the cooled porcelain dish. In 30–60 s, a gurgling will be heard as the propane liquefies. Increase the flow of gas release and in a few minutes, the porcelain dish will fill with propane.
7. Once filled, cover the porcelain dish with its porcelain cover or a piece of thick aluminum foil. Be sure to continually add more liquid nitrogen around the dish (not into the dish). In 3–5 min, the temperature of the propane will reach −180 C or lower.
8. Place a 100–200 μl drop of Penium cell suspension into the side port of the airbrush. Quickly remove the cover off the porcelain dish. Spray the cell suspension from the airbrush into the propane. Repeat until all of the cell suspension is used and then recover the porcelain dish.
9. In a fume hood, pour off the top 2/3 of the propane into a waste container. Pour the remaining liquid propane containing the cryofixed cells into either a cooled glutaraldehyde–acetone scintillation vial or glutaraldehyde–ethanol vial (from step 3.4.1.6). Tighten the cap of the vial, gently swirl and then open the cap to release any residual propane. Place the vial in a −80 °C freezer for substitution.

3.4.3 Osmicated

Preparations

1. 24 h after cryofixation, add 1/10 g of osmium tetroxide to each glutaraldehyde–acetone vial in a fume hood. Swirl and place back into the freezer.

2. Every 12 h, swirl the vials and let sit in the −80 °C freezer for 48–96 h. This period of time constitutes the freeze substitution period.
3. Place vials in a −20 °C freezer (commercial freezer) for 4 h, then in a 4 °C refrigerator for 2 h and then at RT for 1 h, to slowly adjust them to RT.
4. Pour the glutaraldehyde–acetone medium containing the cells into a 12 mL glass centrifuge tube and centrifuged (400 × *g* for 1 min) in a fume hood.
5. Pour off supernatant into a waste container leaving the freeze substituted and osmicated cells in the pellet.
6. Wash the pellet three times with 100 % acetone.
7. The cells are infiltrated and embedded with Spurrs Low Viscosity resin (*see* **Note 15**).
8. For infiltration: resuspend the pellet in a solution of 25 % Spurrs resin/75 % acetone and gently shaken for 2 h. Between each infiltration step cells are centrifuged and supernatant discarded.

   Place in a 50 % Spurrs resin/50 % acetone solution for 2 h, a 75 % Spurrs resin/25 % acetone solution for 4 h or overnight and then in 100 % Spurrs resin for 12–24 h.
9. Embedding Cells are placed into the bottom of beem capsules and the capsules filled with fresh Spurrs resin. Alternatively, they may be suspended in a thin layer of Spurrs resin sandwiched between two sheets of Aclar plastic.
10. Capsules or plastic sandwiches are polymerized for 9–12 h at 70 °C (*see* **Note 16**).

3.4.4 Nonosmicated

Preparations

1. The glutaraldehyde–ethanol vials kept at −80 °C for 48 h are warmed to −20 °C by placing them in a commercial freezer.
2. The substitution medium with cells is poured into 12 mL glass centrifuge tubes precooled to −20 °C and centrifuged in a cooled centrifuge.
3. Wash the pellet three times with precooled 100 % ethanol.
4. The pellet is then infiltrated in a solution of 50 % LRW/50 % ethanol cooled to −20 °C for 12 h. Cells are centrifuged and supernatant replaced by 100 % LRW for 24 h with two replacements of the 100 % LRW during that time.
5. The cells are then collected into precooled beem capsules and polymerized with a UV light for 24 h at −20 °C (*see* Fig. 2 for images of this).

3.4.5 Sectioning

For routine ultrastructural observation we use osmicated cells and for immunolabeling, either osmicated or nonosmicated cells.

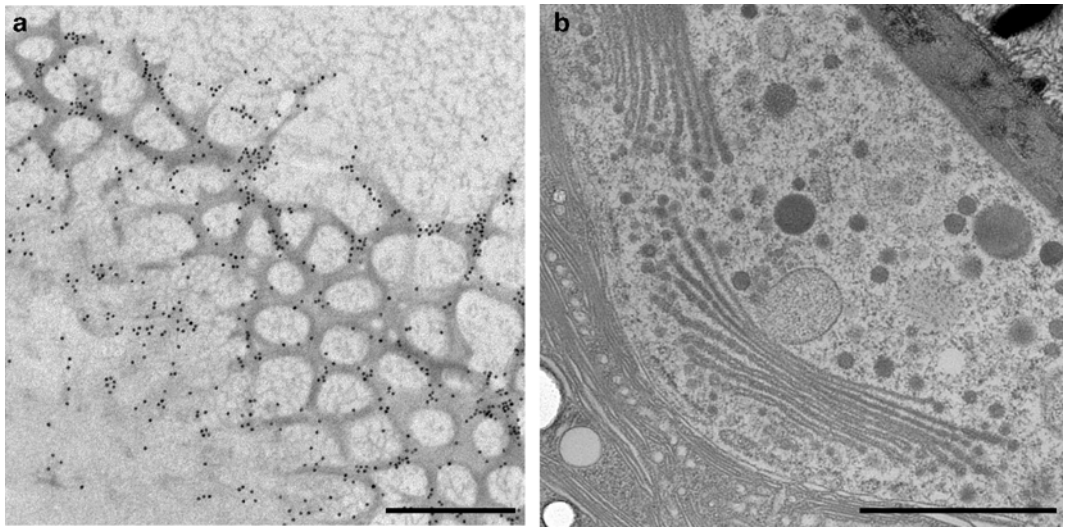

Fig. 2 TEM analysis of the Penium cell wall. (**a**) Cross section through the outer cell wall immunogold labeled with LM18 (Partially esterified HG). (**b**) Ultrastructural analysis of the Golgi apparatus of Penium, indicating ER, golgi bodies, and vesicles. Scale bar 500 nm. Taken with a Zeiss Libra120 TEM

For immunolabeling, 50–70 nm sections are collected on Formvar-coated gold or nickel grids. For routine observations, copper grids are employed.

3.4.6 Staining and Labeling

For Immunolabeling

1. Grids containing sections of osmicated cells are first floated in drops (section-side into the drop) of 5 % H_2O_2 for 3–5 min to remove residual free osmium tetroxide.
2. Wash grids with deionized water.
3. Peroxide-treated grids or grids containing sections of nonosmicated cells are incubated for 10 min in a solution of 0.25 % ammonium chloride and then washed to remove residual glutaraldehyde.
4. Grids are then immunolabeled using the technique of Domozych et al., 2007 [30]. Here, the grids are placed in drops of a blocking solution consisting of PBS with 1 % nonfat Instant Milk for 30 min at RT, washed thoroughly with PBS and then incubated in 1/10 to 1/100 dilutions of wall-specific antibodies (i.e., primary antibodies) in PBST for 90 min at 37 °C or at 4 °C overnight. The grids area then washed thoroughly with PBS, placed in blocking solution for 30 min at RT, and then incubated in secondary antibodies for 37 °C for 90 min. Secondary antibodies include anti-rat or anti-mouse antibodies conjugated with 10 or 15 nm gold particles. The grids are then washed with dH_2O and then conventionally stained with uranyl acetate/lead citrate.

3.5 Variable Pressure Scanning Electron Microscopy (VPSEM)

VPSEM is a rapid and simple technique for imaging changes to cell expansion, cell morphology, and wall surface structure. We use a JEOL (Peabody, MA, USA) 6480 VPSEM. Small amounts of cell suspension may be used and images of cells may be obtained within 1 h without fixation, drying, or sputter coating.

1. Cells untreated or treated with various agents are collected and washed three times as described in **step 3** of Subheading 3.1.
2. The pellet is resuspended in WHS and a 30 μL drop is placed on a 0.8 cm circle of nitrocellulose (*see* **Note 17**). The cells are allowed to settle (10–20 s) and extra medium is gently removed with ripped filter paper. It is important that the cells are still wet but most medium has been removed.
3. The nitrocellulose circle containing the cells is gently collected with forceps and carefully plunged into a small dewar of liquid nitrogen and attached to a liquid nitrogen-cooled cryo-stub (JEOL) using the inclusive clips, making sure not to break the now brittle nitrocellulose.
4. The cooled cryo-stub is inserted into a JEOL VPSEM and the following conditions are set: 10 kV, 30–50 Pa low vacuum pressure mode, spot size = 40–60. These settings may be adjusted to improve imaging.
5. The nitrocellulose circle containing the cells should be located and focused on after the microscope allows for the high voltage to be turned on. Cells will generally not be immediately visible as they are initially coated with ice crystals.
6. Within 15–20 min, ice crystal sublimation starts at the edges of the circle and works inward. It is at this time that images may be taken of the whole intact cells and the cell wall. Typically, 15–30 min is allowed to take high resolution images before sublimation continues and the chamber vacuum pressure deteriorates the cells' surfaces.

3.6 Isolating Pure CWs

1. Cells are collected from cultures that are 2–3 weeks old or younger by centrifugation in a 15 mL falcon tube. The pellet is washed as described in **step 3** of Subheading 3.1.
2. The cell pellet is resuspended in ice cold wall isolation buffer (15 mL is sufficient; *see* **step 6** of Subheading 2.6) and stored on ice until further use.
3. The suspension is then placed in a clean beaker maintained on ice, and sonicated to cavitation for 10 s. The suspension is allowed to cool for 10 s and resonicated. This is done ten times.
4. The suspension is placed in a falcon centrifuge tube and centrifuged on a table top centrifuge at $250 \times g$ for 1 min. The green supernatant is poured off leaving an off-white pellet.

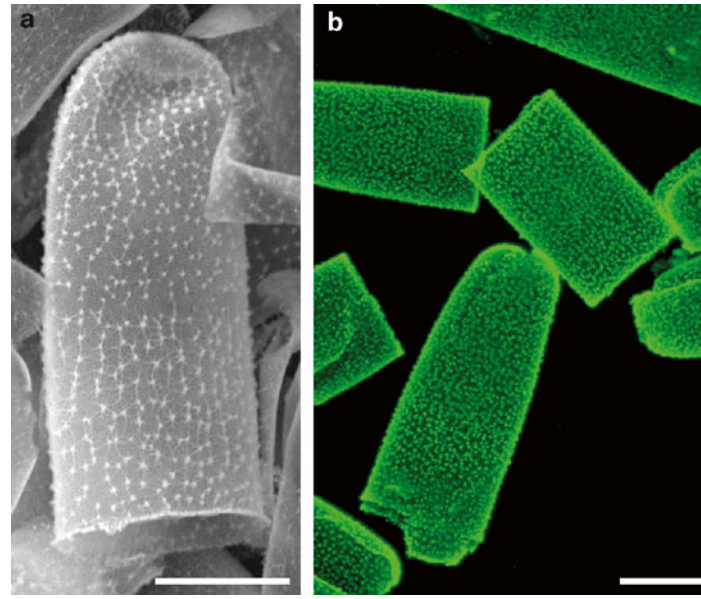

Fig. 3 Isolated pure cell wall of Penium. (**a**) VPSEM of isolated cell wall. (**b**) CLSM of isolated cell wall labeled with JIM5-TRITC (HG w. low %DE). Scale bar 10 μm. Captured with (**a**) JEOL 6480 variable-pressure scanning electron microscope visualized at 10 kV (**b**) Olympus Fluoview 1200 confocal laser microscope

5. **Steps 2–4** are repeated again.
6. The pellet is now resuspended in cold dH_2O, vortexed and centrifuged again. This is repeated three times. The contents of the pellet may be determined by placing a small amount of pellet in a drop of water on a glass microscope slide, mixing with a micropipette tip, covering with a coverslip and viewing with a LM (*see* Fig. 3). Typically after two sonication treatments, only cell walls remain. If there are intact cells in the pellet, **steps 2–4** are repeated.
7. When the pellet is judged to be pure, the pellet is suspended in cold dH_2O, vortexed and centrifuged. The supernatant is discarded. This process is repeated five times. The resulting pellet will be pure white.
8. The cell wall pellet may then be directly used for biochemical and/or enzymatic analyses. Likewise, it may be used for SEM/TEM imaging (*see* Fig. 3). Alternatively, the pellet may be frozen in liquid nitrogen, stored at −80 °C, or freeze-dried for long-term storage in a refrigerator.

3.7 Experimental Manipulation of Cell and Cell Wall Expansion

1. For initial experiments, we typically employ 24- or 48 multi-welled tissue culture plates, with either 2 or 1 mL of WHS added, respectively.

2. 1,000× stock solutions of chemical agents (e.g., oryzalin, cytochalasin E, latrunculin), cation solutions (e.g., $BaCl_2$, $SrCl_2$,), enzymes (e.g., PME, pectate lyase, cellulase), or various exogenous pectins are made. Each agent is diluted to diverse concentrations in a well and mixed.
3. Both cells labeled and unlabelled are washed as described in **step 3** of Subheading 3.1, centrifuged, supernatant discarded, and pellet resuspended in 100 μL of WHS.
4. To each well of the multiwelled tissue culture plates, 10 or 20 μL of dense pellet suspension is added. The cells are mixed by gentle swirling and the plate is sealed with parafilm. The plate is then placed in a growth chamber with setting as **step 1** of Subheading 3.1.
5. After various time intervals, the multiwelled dish is placed on an inverted LM and changes to cell or wall morphology is noted.
6. Aliquots of cells may be removed from a well and live cell labeled (*see* Subheading 3.2) and viewed with a CLSM to monitor fine changes to expansion sites of the cell wall or abnormalities to cell morphology. Cells may also be processed for TEM (*see* Subheading 3.4) or SEM.
7. If changes to cell or wall expansion are noted, aliquots of treated cells are collected and washed as described in **step 3** of Subheading 3.1. They are returned to wells of a multiwelled plate containing fresh WHS. Wall or cell shape or structure is monitored via microscopy 48–72 h later to see if recovery has occurred.

3.8 Rhodamine Phalloidin Labeling

1. Collect cells and wash as described in **step 3** of Subheading 3.1.
2. Resuspend pellet in 1 mL of WHS and add 1 μL of MBS. Shake and place on rotator for 30 min.
3. Wash cells as described in **step 3** of Subheading 3.1 and suspend cells in Fixative (5 mL). Place on rotator for 30 min.
4. Wash cells with Buffer/Triton-X100 three times over a 30-min period.
5. Resuspend cells in rhodamine phalloidin working solution. Shake, cover in aluminum foil, and place on rotator for 90 min.
6. Wash cells with Buffer/Triton-X100 three times (as described in **step 3** of Subheading 3.1, but with Buffer/Triton-X100 instead of WHS) and then Working buffer A two times over 30 min.
7. Observe in WFLM or CLSM using green light/laser and rhodamine filter set. Observe within 4-8 h.

4 Notes

1. May be purchased at Plant Probes, University of Leeds (www.plantprobes.net/index.php), or at the Complex Carbohydrate Research Center, University of Georgia (www.ccrc.uga.edu/~carbosource/CSS_mabs7-07.html).
2. Available at art shops or online at www.amazon.com or www.amazon.co.uk.
3. We have successfully used propane from high purity pressure tanks, a commercial bottle of camping stove propane.
4. Circles may also be hand cut or with a hole punch.
5. The dried rhodamine phalloidin can be stored in a refrigerator for 48 h before use.
6. For most experiments, we use cells from 5- to 10-day-old cultures.
7. This procedure helps remove the gel-like EPS produced by Penium [37, 40], but is also used as a general washing protocol during diverse methods in this chapter.
8. Approximately 60–80 % of the cells will enter predivision expansion and cell division at approximately the same time (±1 h, 2–4 h into the dark cycle).
9. It is important to employ a rotation or shaking speed that allows for good mixing of the contents of the tube.
10. The dilution factors for monoclonal antibodies are as a general rule 1/10, and 1/50 for CBMs, depending on the producer.
11. These monoclonal antibodies are specific for the HG of the outer cell wall layer and the fluorescent regions on the cell surface allow for easier recognition of cell cycle events and quantitative assessment of growth.
12. Nonfluorescent or dark zones between labeled regions of the wall represent newly formed cell wall (also *see* ref. [30]). We have used this protocol to determine the location of high esterified and low esterified HG [30] and cellulose/HG.
13. Osmium tetroxide is a postfixative employed to significantly enhance contrast in TEM preparations. Though not recommended for immunolabeling of proteins, osmium does not, in our experience, affect labeling when using polysaccharide-based antibodies.
14. The height of the vials can be adjusted by placing aluminum foil wads under the vials.
15. Several plastics can be used, but we prefer using Spurrs Low Viscosity resin. This is one of the most commonly used plastics in plant cell studies.

16. For the thin sheets of plastic formed in the sandwich, individual cells may be chosen using a dissecting microscope, cut out with a razor blade, and then super-glued to the tip of a beem capsule.
17. It is important to be sure that the pellet is sufficiently diluted so that cells make contact with the nitrocellulose surface but are not piled on top of each other.

Acknowledgments

The authors thank J. Paul Knox (University of Leeds, UK), Marie-Christine Ralet (Institut National de la Recherche Agronomique, Nantes, France), and Harry J. Gilbert (Newcastle University, UK) for monoclonal antibodies and CBMs. We are grateful to Iben Sørensen and Jocelyn K.C. Rose of Cornell University for rewarding and helpful discussion. This work was funded by The Danish Strategic Research Council, The Danish Council for Independent Research, Technology and Production Sciences, and The Villum Foundation's Young Investigator Programme. Some techniques described here were derived from research funded by the National Science Foundation (USA) grants, NSF-MCB 0919925, NSF-MRI 0922805, and NSF-MRI 0419131.

References

1. Niklas KJ, Kutschera U (2010) The evolution of the land plant life cycle. New Phytol 185: 27–41
2. Sanderson MJ, Thorne JL, Wikström N et al (2004) Molecular evidence on plant divergence times. Am J Bot 91:1656–1665
3. Becker B, Marin B (2009) Streptophyte algae and the origin of embryophytes. Ann Bot 103: 999–1004
4. Bowman JL (2013) Walkabout on the long branches of plant evolution. Curr Opin Plant Biol 16:70–77
5. Kenrick P, Crane PR (1997) The origin and early evolution of plants on land. Nature 389: 33–39
6. Niklas KJ (2004) The cell walls that bind the tree of life. Bioscience 54:831–841
7. Fry SC (2004) Primary cell wall metabolism: tracking the careers of wall polymers in living plant cells. New Phytol 161:641–675
8. Mohnen D (2008) Pectin structure and biosynthesis. Curr Opin Plant Biol 11:266–277
9. Caffall KH, Mohnen D (2009) The structure, function, and biosynthesis of plant cell wall pectic polysaccharides. Carbohydr Res 344: 1879–1900
10. Harholt J, Suttangkakul A, Vibe Scheller H (2010) Biosynthesis of pectin. Plant Physiol 153:384–395
11. Popper ZA, Tuohy MG (2010) Beyond the green: understanding the evolutionary puzzle of plant and algal cell walls. Plant Physiol 153: 373–383
12. Popper ZA, Michel G, Hervé C et al (2011) Evolution and diversity of plant cell walls: from algae to flowering plants. Annu Rev Plant Biol 62:567–90
13. Waters E (2003) Molecular adaptation and the origin of land plants. Mol Phylogenet Evol 29:456–463
14. Domozych DS (2012) The quest for four-dimensional imaging in plant cell biology: it's just a matter of time. Ann Bot 110: 461–474
15. Sørensen I, Pettolino FA, Bacic A et al (2011) The charophycean green algae provide insights into the early origins of plant cell walls. Plant J 68:201–11

16. Popper ZA (2003) Primary cell wall composition of bryophytes and charophytes. Ann Bot 91:1–12
17. Eder M, Lütz-Meindl U (2010) Analyses and localization of pectin-like carbohydrates in cell wall and mucilage of the green alga Netrium digitus. Protoplasma 243:25–38
18. Sørensen I, Rose JKC, Doyle JJ et al (2012) The Charophycean green algae as model systems to study plant cell walls and other evolutionary adaptations that gave rise to land plants. Plant Signal Behav 7:1–3
19. Fangel JU, Ulvskov P, Knox JP et al (2012) Cell wall evolution and diversity. Front Plant Sci 3:152
20. Leliaert F, Verbruggen H, Zechman FW (2011) Into the deep: new discoveries at the base of the green plant phylogeny. Bioessays 33:683–692
21. Lewis LA, McCourt RM (2004) Green algae and the origin of land plants. Am J Bot 91: 1535–56
22. Leliaert F, Smith DR, Moreau H et al (2012) Phylogeny and molecular evolution of the green algae. Crit Rev Plant Sci 31:1–46
23. Timme RE, Bachvaroff TR, Delwiche CF (2012) Broad phylogenomic sampling and the sister lineage of land plants. PloS One. 7, e29696
24. Wodniok S, Brinkmann H, Glöckner G et al (2011) Origin of land plants: do conjugating green algae hold the key? BMC Evol Biol 11:104
25. Finet C, Timme REE, Delwiche CFF et al (2010) Multigene phylogeny of the green lineage reveals the origin and diversification of land plants. Curr Biol 22:1456–1457
26. Laurin-Lemay S, Brinkmann H, Philippe H (2012) Origin of land plants revisited in the light of sequence contamination and missing data. Curr Biol 22:R593–R594
27. Finet C, Timme RE, Delwiche CF et al (2010) Multigene phylogeny of the green lineage reveals the origin and diversification of land plants. Curr Biol 20:2217–2222
28. Timme RE, Delwiche CF, Marle F (2012) Erratum: multigene phylogeny of the green and diversification of land plants. Curr Biol 22(15):1456–1457
29. Domozych DS, Brechka H, Britton A et al (2011) Cell wall growth and modulation dynamics in a model unicellular green alga—Penium margaritaceum: live cell labeling with monoclonal antibodies. J Bot. doi. org/10.1155/2011/632165
30. Domozych DS, Serfis A, Kiemle SN et al (2007) The structure and biochemistry of charophycean cell walls: I. Pectins of Penium margaritaceum. Protoplasma 230:99–115
31. Liberman LM, Sozzani R, Benfey PN (2012) Integrative systems biology: an attempt to describe a simple weed. Curr Opin Plant Biol 15:162–167
32. Wienkoop S, Baginsky S, Weckwerth W (2010) Arabidopsis thaliana as a model organism for plant proteome research. J Proteome 73: 2239–2248
33. Kato K, Matsumoto T, Koiwai A et al (1972) Liquid suspension culture of tobacco cells. In: Terui G (ed) Fermentation technology today: proceedings of the IVth international fermentation symposium. Society of Fermentation Technology, Kyoto, Japan, pp 689–695
34. Nagata T, Yasuyuki N, Seiichiro H (1992) Tobacco BY-2 cell line as the "HeLa" cell in the cell biology of higher plants. Int Rev Cytol 132: 1–30
35. Brook AJ (1981) The biology of desmids. University of California Press, Oakland, CA
36. Gerrath JF (2003) Conjugating green algae and desmids. In: Wehr, J.D. (ed.) Freshwater Algae of North America: Ecology and Classification. Elsevier Science, San Diego, CA, pp 353–381
37. Domozych DS, Kort S, Benton S et al (2005) The extracellular polymeric substance of the green alga Penium margaritaceum and its role in biofilm formation. Biofilms 2:129
38. Domozych DS, Lambiasse L, Kiemle SN et al (2009) Cell-wall development and bipolar growth in the desmid Penium margaritaceum (Zygnematophyceae, Streptophyta). Asymmetry in a symmetric world. J Phycol 45:879–893
39. Domozych D, Fujimoto C, LaRue T (2013) Polar expansion dynamics in the plant kingdom: a diverse and multifunctional journey on the path to pollen tubes. Planta 2:148–173
40. Domozych DS (2007) Exopolymer production by the green alga Penium argaritaceum: Implications for biofilm residency. Int J Plant Sci 168:763–774
41. Bret-harte MS, Talbott LD (1993) Changes in composition of the outer epidermal cell wall of pea stems during auxin-induced growth. Planta 190:369–378
42. Refrégier G, Pelletier S, Jaillard D et al (2004) Interaction between wall deposition and cell elongation in dark-grown hypocotyl cells in Arabidopsis. Plant Physiol 135:959–968
43. Baker DB, Ray PM (1965) Relation between effects of auxin on cell wall synthesis and cell elongation. Plant Physiol 40:360–368

44. Abe J, Hori S, Tsuchikane Y et al (2011) Stable nuclear transformation of the Closterium peracerosum-strigosum-littorale complex. Plant Cell Physiol 52:1676–1685
45. Sørensen I, Fei Z, Andreas A, et al. (2014) Stable transformation and reverse genetic analysis of Penium margaritaceum: a platform for studies of Charophycean Green Algae, the immediate ancestors of land plants. Plant J 77:339–351
46. Nichols HW (1973) Handbook of phycological methods: culture methods and growth measurements. Cambridge University Press, New York, NY

Chapter 2

Using Chemical Genomics to Study Cell Wall Formation and Cell Growth in *Arabidopsis thaliana* and *Penium margaritaceum*

N. Worden, V. Esteva Esteve, D.S. Domozych, and G. Drakakaki

Abstract

The cell wall is directly involved in cell growth, and its ability to loosen and rearrange allows for cell expansion through the existing turgor pressure. Thus, information on cell wall deposition and rearrangement can provide insights into the overall plant growth. This chapter describes two methods that can be used to evaluate cell expansion (1) in the model plant *Arabidopsis thaliana* and (2) the model alga *Penium margaritaceum*. These methods are further used to screen for small molecules that induce cell growth phenotypic changes affecting cell wall. Identification of such small molecules is beneficial due to their posttranslational mechanism of action that can be controlled in a temporal and spatial manner. Chemical genomics has the ability to overcome issues of genetic redundancy and lethality, which can hinder traditional genetic methods. The identification of small molecules in these screens will provide useful information on plant cell wall biology and overall plant growth.

Key words *Penium margaritaceum*, *Arabidopsis thaliana*, Chemical genomics, Cell wall biology

1 Introduction. Cell Wall and Cell Growth

The cell wall is a dynamic network of polysaccharides and proteins that constitute the extracellular matrix of the plant cell. It provides structural support and serves as a protective barrier for the protoplast against biotic and abiotic stresses [1]. The cell wall also plays a vital role during plant cell growth as its tensile strength serves as the structural regulator of turgor-driven expansion. Plant cell expansion typically occurs in one of two ways: *diffuse* expansion, where new cell wall materials are deposited and incorporated into the cell wall uniformly along the expanding cell and *polar* expansion, where growth is focused at a specific point or front of the cell [2]. In both types, changes in cell wall polymer arrangement lead to a weakening of the wall architecture, which permits the existing, constant turgor pressure to expand into the weakened cell wall via a process known as "creep" [1–4]. In pollen tubes, the rates of

José M. Estevez (ed.), *Plant Cell Expansion: Methods and Protocols*, Methods in Molecular Biology, vol. 1242,
DOI 10.1007/978-1-4939-1902-4_2,

growth correlate with rates of cell wall deposition, suggesting a dynamic model of continuous cell wall loosening, rearrangement, and polysaccharide deposition which allows turgor-driven cell expansion and reorientation for cell growth [5, 6]. In fact, the amount of cell wall material deposited can predict with up to 90 % accuracy the degree of pollen cell expansion [5].

The generation of plants with altered cell wall and expansion characteristics has been very valuable in the dissecting mechanisms of plant cell growth. Derived from either genetic mutations or application of pharmacological agents, wall associated structures or events may be specifically "tested" to elucidate their roles in the expansion process.

1.1 Using Chemical Genomic Approaches to Study Cell Wall Modifications During Cell Growth

Chemical genomics is the use of small molecules rather than genetic mutations to perturb, study, and control the cellular and physiological function of proteins [7]. This approach is similar to that employed in the screening of chemicals for pharmacological drug and herbicide applications [8].

As a result of the altered cell wall function in plant cell growth and development, mutations in biosynthetic genes can be lethal [9, 10]. Chemical genomic screens can be performed at specific developmental stages using sublethal concentrations of small molecules that overcome lethality limitations [7, 8]. Additionally, redundancies that are observed in gene products involved in cell wall biosynthesis and metabolism [11, 12] and phenotypes of knockout mutations may be difficult to detect. Small molecules can be highly specific and be used to distinguish a single protein from a large family of proteins, or they can target proteins with conserved active sites, thus addressing redundancy. Despite these advantages, fundamental challenges in plant chemical biology remain, including target identification and off-target effects [8]. The protocols described below illustrate chemical genomic screens for plant and algal cell wall and growth modifications.

1.2 Model Organisms to Study Cell Wall Development and Cell Growth: Arabidopsis thaliana and Penium margaritaceum

The small flowering plant, *Arabidopsis thaliana* (Brassicaceae, Angiospermae), is commonly used as a model organism in cell expansion and cell wall deposition studies [13]. Many *Arabidopsis* mutants with altered cell wall properties have already been characterized [14], providing a useful toolset for future chemical genomic screens.

Penium margaritaceum (Peniaceae, Zygnematales, Streptophyta) is a green alga that has recently attracted attention as another efficacious model organism for cell wall studies. *Penium* is single celled, easy to grow, and produces only a simplified primary cell wall predominately composed of cellulose and pectic polysaccharides [15]. The alga also has a simple cylindrical shape that makes genetic or experimental alterations to cell wall/cell expansion easy to monitor and quantitative growth measurements easy to

Table 1
Examples of chemicals affecting cell wall composition and cell growth

Chemical	Effect	References
Isoxaben	Cellulose biosynthesis, targeting CESA3 and CESA6	Scheible et al. [20] and Desprez et al. [21]
BFA	Disruption of Golgi-mediated trafficking, alters cell wall secretion	Nebenführ et al. [28] and Hörmanseder et al. [29]
Oryzalin	Depolymerizes microtubules, alters cell wall texture	Morejohn et al. [30] and Chan et al. [31]
Morlin	Alters microtubule organization and CESA velocity	DeBolt et al. [22]
Chemical A	Inhibits UDP-glucose transfer activity in Golgi-enriched fractions	Zabotina et al. [27]
DCB	Inhibits cellulose biosynthesis	Montezinos et al. [23]
CGA	Inhibits cellulose biosynthesis	Peng et al. [26]
Cobtorin	Disrupts microtubule/cellulose relationship	Yoneda et al. [24, 25]

calculate. The rapid growth of *Penium* also allows for acquisition of abundant cell wall material that may be subsequently used for specific biochemical analyses [16]. Additionally, live *Penium* may be labeled with monoclonal antibodies (mAbs), placed back in culture, and subsequently monitored for growth dynamics [15, 17]. Finally, a new protocol for transforming *Penium* has recently been developed that allows for the generation of cell lines that are useful for the study of cell wall mechanics including knockouts, overexpressed lines, and ones expressing fluorescent protein fusions [18].

Here, we describe the protocol for using chemical genetics with these two model organisms to identify potentially important pharmacological inhibitors that may be used to dissect the processes of plant cell wall expansion. The notable similarities in cell wall biochemistry found throughout the plant kingdom [16] allow for reasonable and valuable translation of chemical hits from these model systems to plants of agricultural importance.

1.3 Examples of Small Molecules Affecting Cell Wall Deposition

Chemical genomics has been a powerful tool in enhancing our understanding of cell wall biology. An arsenal of bioactive molecules have been identified and have had significant impacts in cell wall studies [19]. These include (Table 1): *isoxaben* (N-[3-(1-ethyl-1-methylpropyl)-5-isoxazolyl]-2,6-dimethoxybenzamide), which inhibits incorporation of UDP-Glucose into cellulosic regions of the cell wall and has played an instrumental role in identifying members of cellulose synthase complexes (CESA), CESA3 and CESA6 [20, 21]. The inhibition specificity of isoxaben for only two members of the cellulose synthase superfamily also illustrates the power of small molecules in overcoming functional

redundancy. *Morlin* (7-ethoxy-4-methyl chromen-2-one) was identified in a screen for swollen organ morphology, such as roots. It affects microtubule organization in the cell cortex and the velocity of CESA movement in the plasma membrane, possibly targeting the interaction between the CESA complex and the microtubules [22]. The herbicide, *DCB* (2,6,-dichlorobenzonitrile), is a cellulose biosynthesis inhibitor that arrests movement of CESA complexes at the plasma membrane [23]. *Cobtorin* (4-[(2-chlorophenyl)-methoxy]-1-nitrobenzene) also alters the relationship between cortical microtubules and the production of cellulose microfibrils [24, 25]. Yoneda et al. [25] used cobtorin in showing that pectin plays a critical role in the deposition and maintenance of cellulose microfibril orientation. *CGA* (1-cyclohexl-5-(2,3,4,5,6-pentafluorophenoxy)-1λ4,2,4,6-thiatriazin-3-amine) also inhibits cellulose biosynthesis [26]. *Chemical A* (methyl 3-(2,5-dioxo-2,5-dihydro-1H-pyrrol-1-yl) benzoate) inhibits the transfer of UDP-glucose in Golgi membranes [27] and consequently affects downstream deposition of cell wall components. In addition, *Brefeldin A* (BFA; 4-Dihydroxy-2-(6-hydroxy-1-heptenyl)-4-cyclopentanecrotonic acid) blocks Golgi-dependent trafficking and has been shown to inhibit secretion of cell wall components [28, 29]. *Oryzalin* (4-(dipropylamino)-3,5-dinitrobenzenesulfonamide) targets tubulin and alters cellulose crystallinity [30–32].

1.4 High-Throughput Chemical Screening for Growth Defects in Arabidopsis thaliana and Penium margaritaceum

An effective strategy for the identification of novel inhibitors of cell wall deposition is the assessment of the effects of large arrays of small molecules on the phenotype of specific cell wall/growth mutants. Forward chemical genomic screens can be performed by employing a chemical library (*see* **Note 1**) of small molecules that yield a specific phenotype such as root swelling [22] in specific mutant or wild type plants. In addition, chemical screens can be based directly on biochemically determined cell wall modifications [27, 33]. In this chapter, we describe a screen for *Arabidopsis thaliana* mutants based on hypocotyl length using the herbicide, *isoxaben*.

In the *Arabidopsis*-based procedure, changes in growth are assessed by measuring hypocotyl lengths, a suitable indicator of cell wall perturbation. This approach benefits from the ease of measurement compared to biochemical methods. Resistance to the herbicide isoxaben is observed in the *ixr1* and *ixr2* mutants which carry mutations in cellulose synthase 3 (CESA3) and cellulose synthase 6 (CES6) [20, 21].

This chapter also introduces the methodology to assess the effects of small molecule inhibitors on *Penium margaritaceum* during cell wall expansion and to detect cell wall structural and biochemical changes. To demonstrate this, BFA was chosen to induce changes in *Penium* cell growth. The protocols below provide examples of chemical screens that can be adjusted to the specific needs of individual research projects.

2 Materials

2.1 Arabidopsis thaliana

Screening for changes in hypocotyl length in Arabidopsis thaliana after chemical application

To prevent contamination, aseptic laboratory materials and double-distilled or deionized water should be used during germination.

2.1.1 Growth Materials for Arabidopsis thaliana

1. Sterilization solution: 30 % (v/v) sodium chlorate (bleach) in ethanol (absolute) with 30 μL Triton X-100 (Sigma) per 50 mL of solution.
2. 1.5 mL Eppendorf tubes (Fisher, #05-402).
3. 0.5× *Arabidopsis* growth medium (AGM): 2.3 g/L Murashige minimal organics medium (Sigma, #M6899), 10 g/L sucrose (Fisher), and 8 g/L Phytagel (Sigma, #P8169) (*see* **Note 2**). Autoclave for 30 min at 120 °C and store at room temperature (RT).
4. Plant growth incubator set at 24 °C with a 16 h light cycle.
5. Aluminum foil.
6. Seed stock for screening phenotype of interest, this includes both wild type and mutant seeds. In this example we are using *Arabidopsis thaliana* Columbia (Col-0) wild type seeds and *ixr1-1* mutant seeds.
7. Parafilm.
8. 1 μL inoculation loop (Globe scientific, #2801).
9. 6 well plate (Fisher 08-772-1B).
10. Chemical library of interest to be screened in 5 mg/mL stock solution in dimethylsulfoxide (DMSO) (Sigma, #D8418).
11. Flatbed scanner.
12. 4 % v/v formaldehyde solution in water.
13. Gelrite (Research Products International Corp, G35020).
14. A clear plate or lid for holding Gelrite.
15. Vortex Genie 2 (Fisher, #NC9864336).

2.2 Penium margaritaceum

Using small cell molecules to perturb the wall in Penium margaritaceum

Sterile medium and aseptic techniques should be employed during all procedures.

2.2.1 Growing Penium

1. *Penium margaritaceum*, a Skidmore college isolate (Skd-8).
2. Sterile polystyrene 25 cm^2 cell culture flask (Corning Incorporated, #430372).
3. 1.5 mL Eppendorf tubes (Fisher, #05-402).
4. Microcentrifuge tubes (Eppendorf, #5417C).

5. 2 µL pipette and 200 µL pipette (Gilson).
6. MWC (Modified Woods Hole Medium) [34]. To make MWC combine stock solutions 1–17 (1 mL each), 0.115 g/L (final volume) TES dry buffer (Sigma, #T5691-100G), 1.5 % Soil–Water Supernatant (Carolina Biological Supply Company, Burlington, #15-3790) and make up to 1 L with deionized water. Autoclave at 120 °C for 20 min.

(*a*) *Macronutrients* (*stock solutions*):

1. $CaCl_2 \cdot 2H_2O$—36.80 g/L.
2. $MgSO_4 \cdot 7H_2O$—37.00 g/L.
3. $NaHCO_3$—12.60 g/L.
4. $K_2HPO_4 \cdot 3H_2O$—11.40 g/L.
5. $NaNO_3$—85.00 g/L.
6. $Na_2O_3Si \cdot 9H_2O$—28.40 g/L.

(*b*) *Vitamin stocks*:

7. Thiamine HCl—0.1 g/L.
8. Biotin—0.0005 g/L.
9. Cyanocobalamin—0.0005 g/L.

(*c*) *Combined trace elements*:

10. $EDTANa_2$—4.36 g/L.
11. $FeCl_3 \cdot 6H_2O$—3.15 g/L.
12. $CuSO_4 \cdot 5H_2O$—0.01 g/L.
13. $ZnSO_4 \cdot 7H_2O$—0.022 g/L.
14. $CoCl_2 \cdot 6H_2O$—0.01 g/L.
15. $MnCl_2 \cdot 4H_2O$—0.18 g/L.
16. $Na_2MoO_4 \cdot 2H_2O$—0.006 g/L.
17. H_3BO_3—1.00 g/L.

2.2.2 Chemical Treatment and Microscopy

1. 7- to 14-day-old *Penium margaritaceum* culture.
2. Chemicals to be screened.
3. MWC solution.
4. DMSO as control (*see* **Note 3**).
5. Carnation Instant nonfat milk.
6. JIM5 or LM18 monoclonal primary antibodies (Plant Probes, Leeds, UK) (*see* **Note 4**).
7. Fluorescein isothiocyanate (FITC)-Goat Anti-Rat secondary antibody (Invitrogen, #62-9511).
8. LSM 700 confocal laser scanning microscope (Carl Zeiss, Germany), Olympus Fluoview 1200 (Olympus, Center Valley, PA, USA), or other high resolution confocal microscope.

9. Disposable transfer pipettes (Fisher Scientific, #S30467-1).
10. Microscope cover glasses 22×40 mm (VWR international, #16004-306).
11. Microscope slides, Superfrost Plus (VWR).

3 Methods

3.1 *Arabidopsis thaliana*

Perform work with sterile seeds and plates in a laminar flow hood. All procedures may be carried out at room temperature, unless otherwise specified.

3.1.1 Seed Sterilization

1. Add 500 μL of sterilization solution to 50 mg of *Arabidopsis* seeds in a 1.5-mL microcentrifuge tube.
2. Shake on speed 3 or lower for 10 min in a Vortex Genie.
3. In a laminar flow hood, remove sterilization solution and rinse three times with 100 % ethanol, allow to air dry.
4. Store sterilized seeds at 4 °C.

3.1.2 Growth and Chemical Treatment of Arabidopsis thaliana Seedlings

1. Prepare 5 mL of 0.5 AGM/phytagel and add a starting volume of 25 μL of the 5 mg/mL chemical stock. Dispense 5 mL of the AGM supplemented with chemicals into the wells of a 6 well plate, and use DMSO as a control. Here 10 nM of isoxaben is used as treatment. Pipette repeatedly to mix the chemical thoroughly within the media. Allow media to solidify (*see* **Note 5**).
2. Dispense the required number of seeds onto the sterile side of a parafilm slice.
3. Use the needle tip of a sterile 1 μL inoculation loop to transfer the seeds onto the media in the 6 well plate. Between 15 and 20 seeds are recommended per well, positioned in a straight line 2 cm from the top of the well (*see* **Note 6**). In the presented example we will be using both Col-0 and *ixr1-1* seeds, each being allocated a well per chemical treatment and control.
4. Cover completed screening plates with aluminum foil and leave in a 4 °C refrigerator for 48 h to cold vernalize and ensure uniform germination (*see* **Note 7**).
5. After cold vernalization, place plates in a 24 °C growth chamber. Expose to light for 3 h to induce germination and cover with foil to etiolate and allow for hypocotyl expansion while growing vertically (*see* **Note 8**).
6. Image seedlings at 5, 7, and 10 days, this can be easily done using a flatbed scanner. Use a resolution of at least 300 dpi when scanning to allow for accurate measurements (*see* **Note 9**).
7. On the tenth day fix the seedlings using 400 μL of 4 % v/v formaldehyde per well, and allow to rest for at least 2 h.

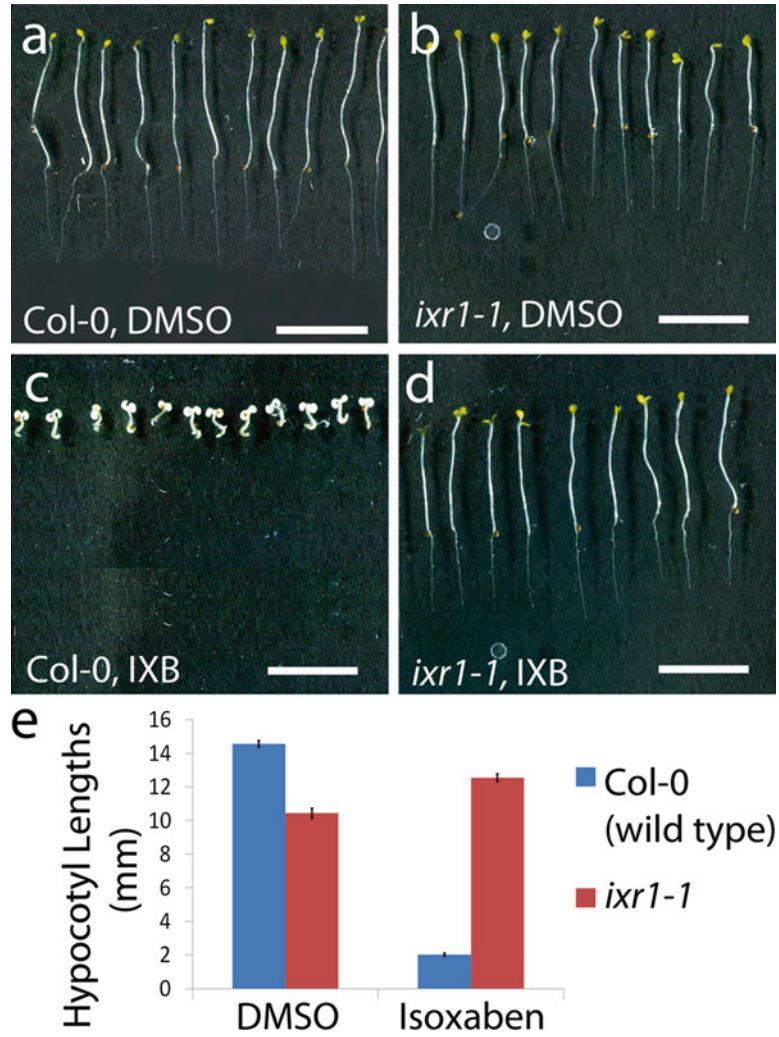

Fig. 1 Hypocotyl growth in the presence of *isoxaben*. Results of *isoxaben* screen against *Arabidopsis thaliana* wild type Columbia (Col-0) (**a**, **c**) and the Cellulose Synthase (CESA3) mutant *ixr1-1* (**b**, **d**). The mutant *ixr1-1* shows resistance to 10 nM isoxaben compared to Col-0 (**d**). Quantification of hypocotyl length (**e**) reveals no growth difference for the mutant, whereas Col-0 exhibits a sevenfold reduction. Two way ANOVA of the growth effects between the two genotypes. $p = <10^{-15}$. Scale = 10 mm

8. Make a solution of 1 % Gelrite in ddH2O, microwave and pour into a clear plate, and let solidify.
9. Transfer fixed seedlings on the top of a 1 % Gelrite agar bed in a clear plate, and align them in parallel for subsequent imaging and accurate measurements. Figure 1 demonstrates the results of the example using the mutant *ixr1-1* and the cellulose inhibitor isoxaben.

3.1.3 Analysis of Hypocotyl Lengths Using ImageJ

1. Measure the seedlings lengths from your scanned photographs using ImageJ [35]. Set scale (Analyze > Set Scale) by using a ruler scanned at the same resolution as the scanned seedlings.
2. Use the segmented line tool to track the plant hypocotyl.
3. Press "Ctrl M" to measure.
4. Transfer measurements to an Excel worksheet, and perform a two-way ANOVA using the statistical package R [36], or other software package of your choice. Compare each genetic background's response to the treatment.

3.2 Penium margaritaceum

3.2.1 Penium Propagation

Perform *Penium* culture transfers (i.e., establishing subcultures) in a laminar flow hood. All the procedures may be carried out at RT unless otherwise specified. Subcultures are performed weekly or as needed. Seven- to fourteen-day-old cultures should be used for screening.

1. Add 30 mL of sterile MWC to a 25 cm^2 cell culture flask.
2. Add 3 mL of 7- to 14-day-old *Penium* cell culture to the flask; disperse the cells by gentle shaking of the flask.
3. Incubate the freshly subcultured *Penium* in a growth chamber at 18–24 °C with a 16:8 h light:dark (L:D) cycle under cool white fluorescent light (74 μmol/m^2 s Photosynthetic Photon Flux).

3.2.2 Harvest of Penium Cells

1. Add 1 mL of 7- to 14-day-old *Penium* cell culture to autoclaved Eppendorf tubes (shake the cell culture flask by hand until all the *Penium* is uniformly suspended in MWC) (*see* **Note 10**).
2. Centrifuge at 1,500 × *g* for 1 min to pellet the cells.
3. Remove supernatant by pipetting the supernatant out, then add 1 mL of *Penium* cell culture and vortex for 10 s to mix the cells.
4. Repeat **steps 1–3** three times (*see* **Note 11**).
5. Remove supernatant from harvested cells by pipetting, then add 1 mL of MWC.
6. Centrifuge at 1,500 × *g* for 1 min to pellet the cells. Repeat **steps 5** and **6** twice to remove any of the extracellular polymeric substance (EPS) that may be secreted while in culture.
7. Resuspend the cell pellet in 300 μL of MWC supplemented with desired small molecules
8. Calculate cell density with a hemacytometer [37].

3.2.3 Chemical Treatment

1. Make chemical treatment solutions in sterile Eppendorf tubes, using selected chemical stock solutions diluted in MWC growth medium. Here, we use 25 μM BFA as the working solution.

2. After harvesting cells from the procedure employed above (**steps 1-8**, Subheading 3.2.2), adjust the final volume to 300 μL with the chemical treatment solution, and incubate for 24 h or other preferred times under the same growth conditions described earlier.

3.2.4 Penium Cell Wall Immunolabeling

After chemical incubation, live cell labeling can be initiated.

1. Centrifuge the treated cells at 1,500 × *g* for 1 min, and discard supernatant.
2. Add 300 μL of blocking solution which consists of 1 % Carnation Instant Nonfat Milk in MWC. Mix by vortexing and let sit for 20 min. This constitutes the primary blocking step of the labeling process.
3. Centrifuge the treated cells at 1,500 × *g* for 1 min, and discard supernatant. Add 300 μL of MWC, vortex cells, recentrifuge, and remove supernatant. Repeat this step twice more. This constitutes the wash.
4. Centrifuge the treated cells at 1,500 × *g* for 1 min, and discard supernatant. Resuspend the pellet in primary antibody solution (1:10 dilution of JIM5 or LM18 in MWC).
5. Mix by vortexing or inverting (*see* **Note 12**).
6. Incubate for 90 min at RT (*see* **Note 13**).
7. Wash three times with fresh MWC—*see* **step 3**.
8. Add 300 μL of blocking solution (prepared as described in **step 2**).
9. Centrifuge the treated cells at 1,500 × *g* for 1 min, and discard supernatant. Resuspend pellet in the secondary antibody solution consisting anti-rat FITC or tetramethylrhodamine (TRITC) (1:50 dilution in MWC) for 90 min at RT. Gentle shaking during this period is recommended.
10. Wash the cells three times with fresh MWC and proceed with microscope imaging or with a secondary chemical treatment.
11. For a postlabeling chemical treatment, return the cells into the same chemical treatment solution, and incubate for additional time periods as described earlier. Aliquots of cells may be taken from the treatment solution and viewed at various periods. Unlabeled zones represent new areas of cell wall.
12. For recovery experiments, treated cells are washed three times with MWC. The pellet is resuspended in fresh MWC and cultured as described earlier. Aliquots of cells may be examined at different time periods thereafter to examine cell recovery.

3.2.5 Microscopy Visualization

1. Transfer 15 μL of cell suspension onto a microscope slide using a disposable transfer pipette and add cover glass of appropriate thickness for the microscope (*see* **Note 14**).

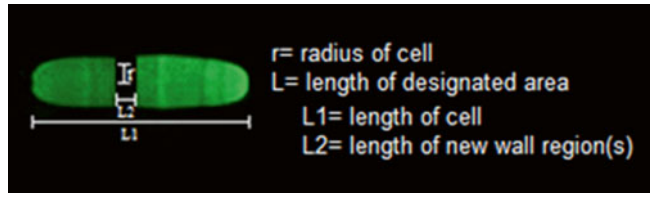

Fig. 2 Quantitative parameters for *Penium margaritaceum* growth. To quantify the effect of chemical treatments on Penium growth the length of the cells (L1) and length of new wall regions (L2) are measured and compared between treated cells and nontreated cells (control)

2. For chlorophyll autofluorescence imaging, one can use the FITC 488 excitation with a filter that allows for emission signals over 580 nm. Alternatively, a Texas Red filter set may be used for chlorophyll autofluorescence.

3.2.6 Calculating Cell Growth Measurements During Treatment

For each of the chemical treatments, perform the following quantitative measurements using Image J and the confocal images acquired as described earlier:

1. Measure the corresponding length of a designated area (L) as shown in Fig. 2. L1 corresponds to the overall length of the cell. L2 corresponds to the length of newly deposited cell wall as shown by nonfluorescent zones produced postinitial JIM5 labeling.
2. Calculate the Surface area (SA) of a cell and the specific area of new cell wall after polysaccharide labeling using the formula: $SA = 2(\pi \times r^2) + (2\pi \times r) \times L$, where r = radius of cell (8.5 μm) (Fig. 5).

3.2.7 Expected Results. Phenotypic Changes in Penium Growth After BFA Treatment

The chemical treatment (25 μM BFA) used in this experiment causes representative phenotypic changes shown in Fig. 3.

3.3 Penium Growth Changes After BFA Treatment

The length (L1) of treated cells decreased significantly under 25 μM BFA ($p = 0.0067$). In addition, new cell wall regions were affected under BFA, suggesting an effect on cell division and growth of new cells. New cell wall regions (L2) were shorter and almost nonexistent in 25 μM BFA ($p = 0.00018$) (Fig. 4).

Quantitative analysis of the surface area (SA) showed a significant reduction in the newly formed cell wall area of BFA treated cells compared to the control ($p = 0.00043$) (Fig. 5). This establishes the effect of BFA on cell division, likely due to perturbation of Golgi-dependent pathways involved in secretion of cell wall components.

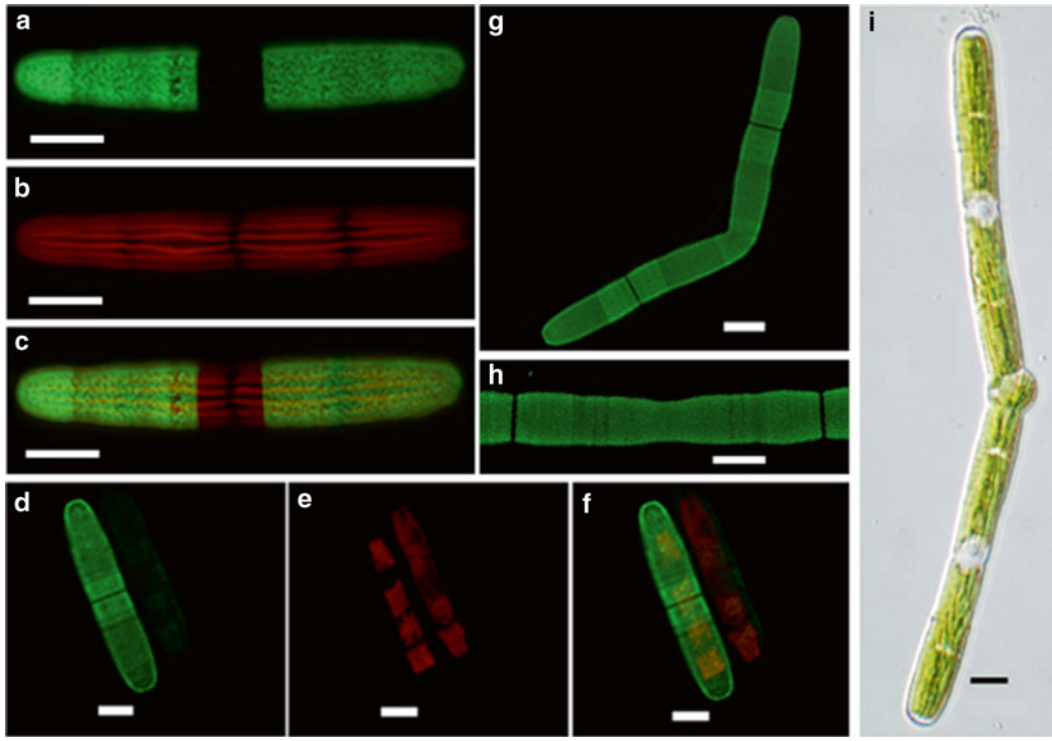

Fig. 3 Effects of BFA treatment on *Penium* growth. Panels **a**–**c** show typical cell morphology of control treated cells after 24 h labeling. JIM 5 labeling shows immunostaining of homogalacturonan (**a**). Panel **b** shows chlorophyll autofluoresence. **c** is an overlay of **a** and **b**. Scale bar = 20 μm. Typically BFA treatment caused reduction of cell growth as shown in panels **d**–**f**. In addition, other cellular effects are observed: inhibition of cell division and cytokinesis effect (**g**, **h**). Highly irregular swollen isthmus (**i**). The panels **g**, **d**, **h** represent JIM5 labeling. Panel **e** represents chlorophyll autofluorescence. **i** represents brightfield image. Scale bar = 20 μm

4 Notes

1. Chemical libraries are commercially available from chemical companies such as ChemBridge or Maybridge. Targeted libraries can be assembled searching for structural similarity to known active compounds or diverse chemicals selected for the same biological activity [38, 39].
2. Phytagel generally shows more consistent, reproducible results in chemical screens because of its increased purity over phytoagar, however best results are obtained in media containing sucrose.
3. DMSO was used as a control at the same dilution as the corresponding chemical. All the other procedures (antibody labeling, washing, and visualization) remain the same.
4. JIM5 binds to a relatively low methyl esterified homogalacturonan found in the walls of diverse plant species. LM19 recognizes the homogalacturonan domain of pectic polysaccharides [40, 41].

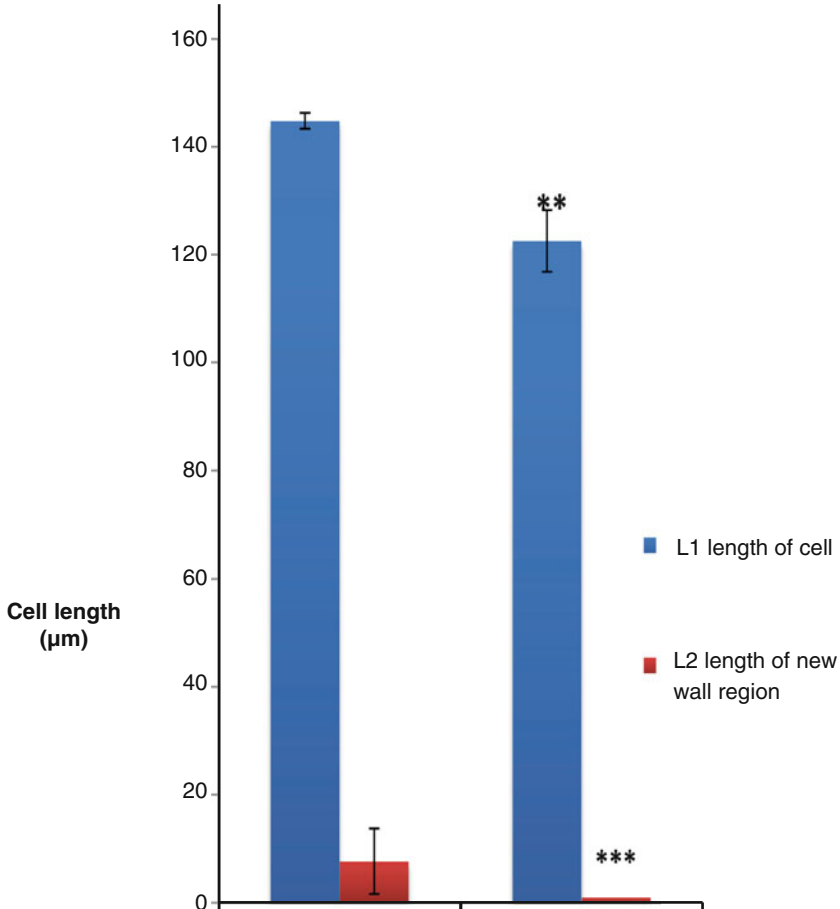

Fig. 4 Cell length analysis of BFA treated *Penium* cells. Calculated length of designated areas (L1 and L2) of *Penium margaritaceum* in control and 25 µM BFA. L1 length of whole cell, L2 length of new wall regions. $^{**}p < 0.01$, and $^{***}p < 0.001$

5. Start with a dilution 1:200 of the original stock (5 mg/mL) and decrease the concentration if plants are not germinating or are too heavily affected. Alternatively, increase concentration if no effect is seen.
6. Perform secondary and tertiary screens to increase the sample number and observe several dilutions in order to confirm the original results.
7. Increase the vernalization time to more than 48 h if seeds are not germinating uniformly.

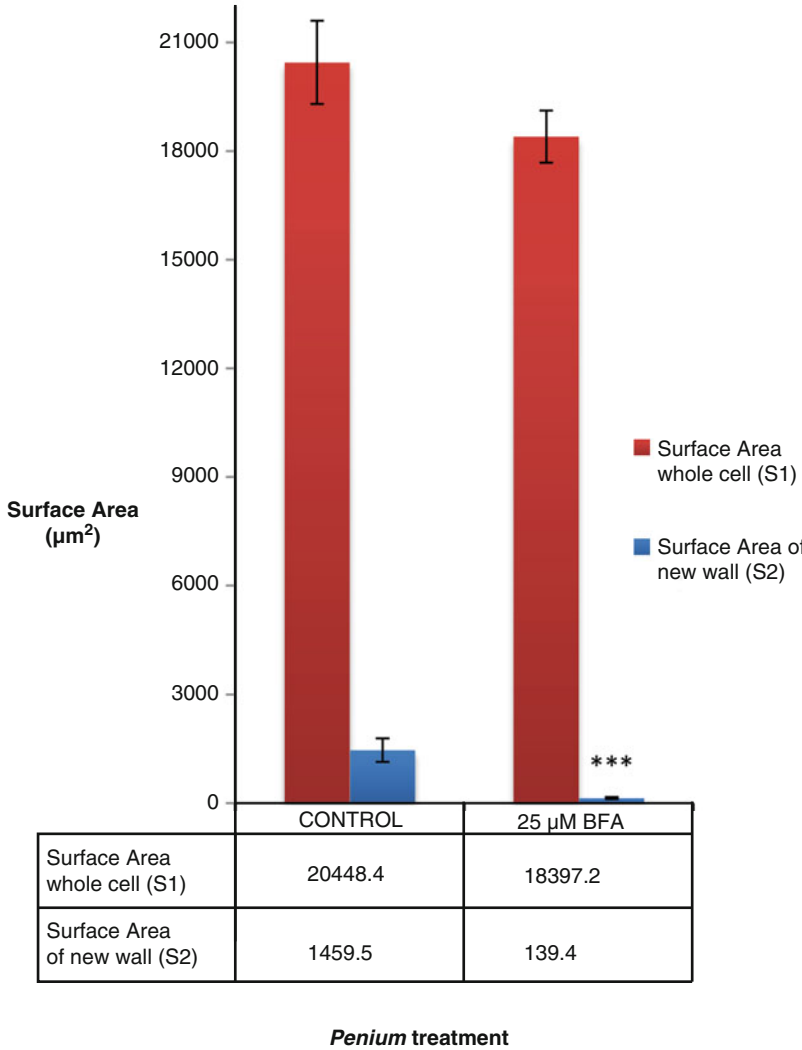

Fig. 5 Calculation of surface areas (SA) for the whole cell, and the new cell wall in *Penium margaritaceum* under 25 μM BFA treatment. ***$p < 0.001$

8. In this protocol we are exploring the effects of isoxaben on hypocotyl expansion; however, the same procedure can be followed for observing changes in root growth by growing the plants under light illumination.
9. Other methods can be used for imaging; scanning is a straightforward approach with high reproducibility.
10. This method can be adapted to 96-well plate high-throughput screens. *Penium* is convenient for microplate assays of pharmacological agents.
11. Harvest 3 mL of *Penium* culture by sequential centrifugation in a 1.5 mL Eppendorf tube.
12. The resuspension of the cell pellet should be slow and uniform.

13. It is recommended that the tubes be gently shaken during this period and/or occasionally vortexed every 30 min.
14. Add the cover glass gently to avoid cell damage.

5 Concluding Remarks

The protocols described here outline simple and straightforward chemical genomics-based methods for the study of plant cell growth via cell wall perturbation. In the *Arabidopsis thaliana* experiment we demonstrated the *ixr1-1* mutant's resistance to the chemical isoxaben, measuring hypocotyl length as a phenotype. We further demonstrated that the same concept can be used for *Penium margaritaceum*, a unicellular alga that serves as an analogous model for higher plant cell wall deposition and cell growth. By applying BFA, a disrupter of Golgi mediated trafficking and cell wall component secretion, cell wall deposition, and cell length were decreased. These detailed protocols may be adjusted for specific research projects to identify new chemical probes and their targets. Valuable insights can be obtained for the relationship of cell wall and cell growth. This in turn can be applied for crop improvement of agronomically important plants.

Acknowledgments

This project was supported by the NSF-IOS-1258135 and a Hellman award to G. Drakakaki. N. Worden was partially funded by the NSF CREATE-IGERT (DGE-0653984), the UCD Plant Sciences GSR, and the Henry A. Jastro Research Scholarship; D. Domozych was supported by the NSF-MCB 0919925 and NSF-DBI 0922805.

References

1. Cosgrove DJ (2005) Growth of the plant cell wall. Nat Rev Mol Cell Biol 6:850–861
2. Carpita NC, Gibeaut DM (1993) Structural models of primary cell walls in flowering plants: consistency of molecular structure with the physical properties of the walls during growth. Plant J 3:1–30
3. Thompson DS (2005) How do cell walls regulate plant growth? J Exp Bot 56:2275–2285
4. Cosgrove D (1993) Wall extensibility: its nature, measurement and relationship to plant cell growth. New Phytol 124:1–23
5. Winship LJ, Obermeyer G, Geitmann A, Hepler PK (2010) Under pressure, cell walls set the pace. Trends Plant Sci 15:363–369
6. McKenna ST, Kunkel JG, Bosch M et al (2009) Exocytosis precedes and predicts the increase in growth in oscillating pollen tubes. Plant Cell 21:3026–3040
7. Drakakaki G, Robert S, Raikhel N, Hicks GR (2009) Chemical dissection of endosomal pathways. Plant Signal Behav 4:57–62
8. Hicks GR, Raikhel NV (2012) Small molecules present large opportunities in plant biology. Annu Rev Plant Biol 63:261–282
9. Persson S, Paredez A, Carroll A et al (2007) Genetic evidence for three unique components in primary cell-wall cellulose synthase complexes in Arabidopsis. Proc Natl Acad Sci U S A 104:15566–15571

10. Harholt J, Suttangkakul A, Vibe Scheller H (2010) Biosynthesis of pectin. Plant Physiol 153:384–395
11. Somerville C (2006) Cellulose synthesis in higher plants. Annu Rev Cell Dev Biol 22: 53–78
12. Cavalier DM, Lerouxel O, Neumetzler L et al (2008) Disrupting two Arabidopsis thaliana xylosyltransferase genes results in plants deficient in xyloglucan, a major primary cell wall component. Plant Cell 20:1519–1537
13. Liepman AH, Wightman R, Geshi N et al (2010) Arabidopsis—a powerful model system for plant cell wall research. Plant J 61:1107–1121
14. Mouille G, Robin S, Lecomte M et al (2003) Classification and identification of Arabidopsis cell wall mutants using Fourier-Transform InfraRed (FT-IR) microspectroscopy. Plant J 35:393–404
15. Domozych DS, Serfis A, Kiemle SN, Gretz MR (2007) The structure and biochemistry of charophycean cell walls: I. Pectins of Penium margaritaceum. Protoplasma 230:99–115
16. Sørensen I, Pettolino FA, Bacic A et al (2011) The charophycean green algae provide insights into the early origins of plant cell walls. Plant J 68:201–211
17. Domozych DS, Brechka H, Britton A, Toso M (2011) Cell wall growth and modulation dynamics in a model unicellular green alga—Penium margaritaceum: live cell labeling with monoclonal antibodies. J Bot 2011:1–8
18. Sørensen I, Fei Z, Andreas A et al (2014) Stable transformation and reverse genetic analysis of Penium margaritaceum: a platform for studies of charophyte green algae, the immediate ancestors of land plants. Plant J 77:339–351
19. Brabham C, Debolt S (2012) Chemical genetics to examine cellulose biosynthesis. Front Plant Sci 3:309.
20. Scheible WR, Eshed R, Richmond T et al (2001) Modifications of cellulose synthase confer resistance to isoxaben and thiazolidinone herbicides in Arabidopsis Ixr1 mutants. Proc Natl Acad Sci U S A 98:10079–10084
21. Desprez T, Vernhettes S, Fagard M et al (2002) Resistance against herbicide isoxaben and cellulose deficiency caused by distinct mutations in same cellulose synthase isoform CESA6 1. Plant Physiol 128:482–490
22. DeBolt S, Gutierrez R, Ehrhardt DW et al (2007) Morlin, an inhibitor of cortical microtubule dynamics and cellulose synthase movement. Proc Natl Acad Sci U S A 104:5854–5859
23. Montezinos D, Delmer D (1980) Characterization of inhibitors of cellulose synthesis in cotton fibers. Planta 148:305–311
24. Yoneda A, Higaki T, Kutsuna N et al (2007) Chemical genetic screening identifies a novel inhibitor of parallel alignment of cortical microtubules and cellulose microfibrils. Plant Cell Physiol 48:1393–1403
25. Yoneda A, Ito T, Higaki T et al (2010) Cobtorin target analysis reveals that pectin functions in the deposition of cellulose microfibrils in parallel with cortical microtubules. Plant J 64:657–667
26. Peng L, Xiang F, Roberts E et al (2001) The experimental herbicide CGA 325'615 inhibits synthesis of crystalline cellulose and causes accumulation of non-crystalline beta-1,4-glucan associated with CesA protein. Plant Physiol 126:981–992
27. Zabotina O, Malm E, Drakakaki G et al (2008) Identification and preliminary characterization of a new chemical affecting glucosyltransferase activities involved in plant cell wall biosynthesis. Mol Plant 1:977–989
28. Nebenführ A, Ritzenthaler C, Robinson D (2002) Brefeldin A: deciphering an enigmatic inhibitor of secretion. Plant Physiol 130: 1102–1108
29. Hörmanseder K, Obermeyer G, Foissner I (2005) Disturbance of endomembrane trafficking by brefeldin A and calyculin A reorganizes the actin cytoskeleton of Lilium longiflorum pollen tubes. Protoplasma 227:25–36
30. Morejohn LC, Bureau TE, Molé-Bajer J et al (1987) Oryzalin, a dinitrile herbicide, binds to plant tubulin and inhibits microtubule polymerization in vitro. Planta 172:252–264
31. Chan J, Crowell E, Eder M et al (2010) The rotation of cellulose synthase trajectories is microtubule dependent and influences the texture of epidermal cell walls in Arabidopsis hypocotyls. J Cell Sci 123:3490–3495
32. Domozych DS, Sørensen I, Sacks C et al (2014) Disruption of the microtubule network alters cellulose deposition and causes major changes in pectin distribution in the cell wall of the green alga, Penium margaritaceum. J Exp Bot 65:465–479
33. Gille S, Hänsel U, Ziemann M, Pauly M (2009) Identification of plant cell wall mutants by means of a forward chemical genetic approach using hydrolases. Proc Natl Acad Sci U S A 106:14699–14704
34. Guillard RR, Lorenzen CJ (1972) Yellow green algae with chlorophyllide c. J Phycol 8:10–14
35. Rasband WS. ImageJ. U. S. National Institutes of Health, Bethesda, Maryland, USA. http://imagej.nih.gov/ij/, 1997–2014
36. Team R core (2013) R: a language and environment for statistical computing

37. Phelan MC (1996) Determining cell number and viability with a hemacytometer and trypan blue staining. In: Kingston R, Moore D, Seidman JG et al (eds) Curr Protoc Mol Biol, vol 3. Wiley, New York, pp A.3F.8–10
38. Drakakaki G, Robert S, Szatmari A et al (2011) Clusters of bioactive compounds target dynamic endomembrane networks in vivo. Proc Natl Acad Sci U S A 108:17850–17855
39. Worden N, Girke T, Drakakaki G (2014) Endomembrane dissection using chemical induced bioactive clusters. Methods Mol Biol 1056:159–168
40. Verhertbruggen Y, Marcus SE, Haeger A et al (2009) An extended set of monoclonal antibodies to pectic homogalacturonan. Carbohydr Res 344:1858–1862
41. Knox JP, Linstead PJ, King J, Cooper KR (1990) Pectin esterification is spatially regulated both within cell walls and between developing tissues of root apices. Planta 181: 512–521

Chapter 3

Optimized Method for Growing In Vitro *Arabidopsis thaliana* Pollen Tubes

Cecilia Borassi, Juliana Pérez Di Giorgio, María R. Scarpin, Jorge Muschietti, and José M. Estevez

Abstract

Pollen tubes elongate by tip growth toward the ovule to deliver the sperm cells during fertilization. Since pollen tubes from several species can be grown in vitro maintaining their polarity, pollen tube growth is a suitable model system to study cell polarity and tip growth. *A. thaliana* pollen tubes germinated in vitro for 6 h can reach up to 800 μm. By studying the phenotype of mutants of T-DNA insertion lines, genes involved in pollen tube growth can be identified. Moreover, components involved in the regulation of pollen tube growth such as calcium ions and reactive oxygen species (ROS) can be analyzed.

Key words Pollen tube growth, Cell expansion, Arabidopsis pollen

1 Introduction

In Angiosperms, development of pollen grains (male gametophytes) is carried out inside the anther and is a tightly controlled process because it directly affects fertilization. When Arabidopsis mature pollen grain reaches the stigma surface, and after a positive recognition, starts pollen hydration after which a pollen tube emerges from the pollen grain. Pollen tubes are single cells that elongate within the pistil to deliver the sperm cells into the ovule to achieve fertilization. In this process pollen tubes grow rapidly and they are guided by endogenous signals as well as signals coming from the female tissues, which need to go through the cell wall to reach their targets.

The elongation of the pollen tube is driven by a process known as tip growth, in which all growth is restricted to the apex of the cell and the cytoplasm remains confined to the most proximal region of the tube by the formation of callose plugs. In order to transport materials for the plasma membrane expansion and cell wall assembly, pollen growth requires an active membrane trafficking system

José M. Estevez (ed.), *Plant Cell Expansion: Methods and Protocols*, Methods in Molecular Biology, vol. 1242,
DOI 10.1007/978-1-4939-1902-4_3,

and a dynamic actin cytoskeleton [1, 2]. The organelles and vesicles are transported by the F-actin filaments along the flank of the tube and recycled back along the centre of the tube. This process known as reverse-fountain streaming pattern is typically observed in elongating pollen tubes. As a consequence, four zones can be distinguished inside the pollen tube: an apical zone where the secretory vesicles accumulates, a subapical zone rich in organelles, a nuclear zone, and a vacuolated zone.

During the polarized growth of pollen tubes the cell wall plays a fundamental role not only being the surface of communication between the pollen tube cell and the female tissues (or culture medium) but also in the control of cell shape, in the protection of the sperm cells, and in the resistance against turgor pressure [3]. The later is achieved by a rigorous control of cell wall deposition and remodeling to modify its mechanical properties.

Pollen tubes of many species, including *A. thaliana*, have the capacity to grow in vitro maintaining the polarity and the ability to respond to molecular cues, such as guidance molecules. For this reason in vitro germinated pollen is used as an experimental system to examine the control of cell expansion, directionality of cell growth, and signaling mechanisms. In addition, it can be used to identify mutations in genes involved in pollen tube growth (e.g., genes involved in cell wall biosynthesis, in pollen–pistil interactions, in cell wall remodeling) that could cause an abnormal growth in pollen tubes.

2 Materials

2.1 Plant Material

Seeds of *Arabidopsis thaliana* Col-0 and those from mutants of T-DNA insertion lines which can be obtained from ABRC (Arabidopsis Biological Resource Center) or NASC (Nottingham Arabidopsis Stock Centre).

2.2 Plant Growth Conditions

Sterilized seeds were sown/plate in 0.5× Murashige and Skoog (1962) medium supplemented with 0.8–1 % agar and the corresponding antibiotic. Seeds were cold stratified 2–4 days in the dark at 4 °C and germinated and grown for 10 days at 22 °C under continuous light. Seedlings were then transferred to soil or peat, mixed with vermiculite and perlite (2:1:1), and grown in chamber at 22 °C under long day (16/8 h light/dark) photoperiod and 60 % relative humidity.

2.3 Equipment

1. Plant growth chamber.
2. Bright field microscope.
3. Vortex mixer.

2.4 Reagents Required

1. The following stock solutions must be prepared with MilliQ H_2O:
   (a) 1 M KCl.
   (b) 1 M $CaCl_2$.
   (c) 1 M $MgSO_4$.
   (d) 1 % H_3BO_3.
2. Other reagents:
   (a) Sucrose.
   (b) 1 M KOH (for adjusting pH).
   (c) Low melting agarose.

2.5 Pollen Growth Medium (PGM)

To prepare 30 ml of liquid PGM (*see* **Note 1**):

1. Weigh 3 g of sucrose (final concentration of 10 %). Pour it into a 50 ml Falcon conical tube and add 25 ml of MilliQ H_2O to dissolve the sucrose.
2. Add the necessary volume of each stock solution to the sucrose solution to reach the final desired concentrations of each reagent (1 mM KCl, 1 mM $CaCl_2$, 5 mM $MgSO_4$, and 0.01 % H_3BO_3) (*see* **Note 2**).
3. Add the rest of the MilliQ H_2O to reach the final volume of 30 ml and vortex.
4. If necessary add 0.1 M KOH to adjust the pH 7.5 (*see* **Note 3**).

3 Methods

3.1 Pollen Growth Conditions

1. Put 15–20 flowers of each genotype in a glass vial (*see* **Note 4**).
2. Add 200 µl of PGM and cover the tubes with parafilm.
3. Vortex the tubes for 1–2 min (*see* **Note 5**).
4. Incubate the pollen grains for 4–6 h at 22 °C in light conditions (*see* **Note 6**).

3.2 Pollen Assays

1. Put 15 µl of the liquid PGM (using a cut-off pipette tip) containing the germinated pollen grains (Fig. 1a) on a glass slide and place a cover slip (*see* **Notes 7–9**).
2. Analyze pollen germination and pollen tube length under an Olympus BX43 microscope using bright field (10×, 0.25 NA; 20×, 0.5 NA). Take images of the pollen tubes (*see* **Note 10**).
3. Perform at least three independent experiments with a minimum of three replicates (three samples incubated in different glass tubes under the similar conditions) for each genotype and/or treatment (Fig. 1a, b).

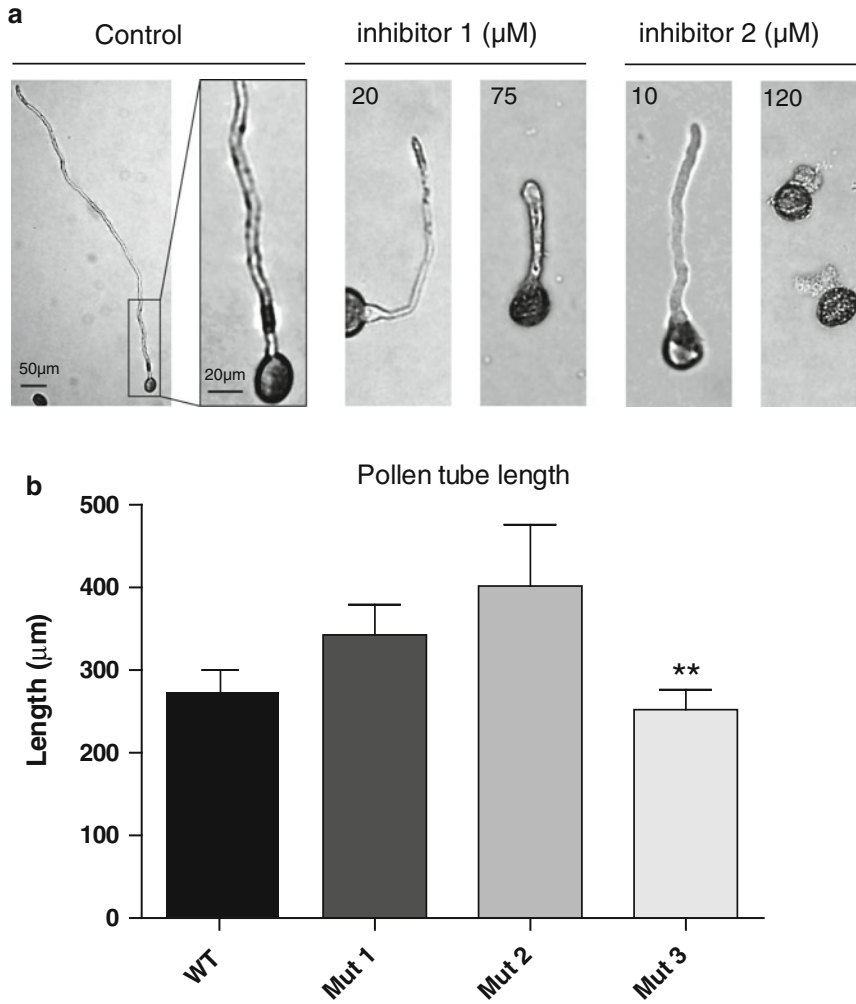

Fig. 1 (**a**) WT Col-0 pollen tube after 4 h in vitro germination (*left*) and in presence of two different inhibitors (*right*). (**b**) Pollen tube length of three different T-DNA mutants compared to WT Col-0. Data are presented as the mean ± SEM from the averages from duplicate samples from one representative experiment; ** statistically significant differences with $p < 0.05$

3.3 Percentage of Germinated Pollen Grains (ImageJ)

1. Open the ImageJ application. In "File," go to "import"-"image sequence" and find the location of the file. Click open (this will open the file using the ImageJ software).
2. Go to "Plugins"-"Analyze"-"Cell Counter".
3. Click on "Initialize" to start the analysis (*see* **Note 11**).
4. Choose a counter of the list for each "cell type" (*see* **Note 12**).
5. Once all pollen grains were classified click on "results" (*see* **Note 13**).
6. Copy and paste the results to an Excel document for analysis.

7. The percentage of geminated pollen grains is calculated for each replicate as (*see* **Note 14**).

$$\frac{\text{no of germinated pollen grains}}{\text{no of pollen grains}} \times 100.$$

3.4 Pollen Tube Length (ImageJ)

1. Open the ImageJ application. In "File", go to "import"-"image sequence" and find the location of the file and open it. Click "ok" on the Sequence Options window.
2. To set the scale:
   (a) In the ImageJ toolbar, right click on the button with the diagonal straight line. Click the option "straight line".
   (b) Trace a line over/upon the scale bar.
   (c) Go to "analyze"-"set scale".
   - Type in the known distance (*see* **Note 15**).
   - Click the "global" button. This will keep the scale bar set while ImageJ is open.
3. Go to the ImageJ toolbar and right click on the button with the diagonal straight line and choose the option "freehand line".
4. Trace the pollen tube from the edge of the pollen grain to the tip of the tube.
5. Press the letter M to measure the length of the pollen tube.
6. All the measurements made on the image sequence will be shown up in a new window called "Results".
7. Copy and paste the results to an Excel document for analysis.

3.5 Statistical Analysis

Statistical analysis of results and further processing can be performed using GraphPad Prism version 5 or a similar program such as Excel. Once the data analysis is finished, a statistical test must be performed to evaluate the differences between the *wild type* and the mutants of interest (Fig. 1b).

4 Notes

1. Agarose is required to prepare solid PGM. When making solid media 1–2 % of low melting agarose is added to PGM containing 20 % sucrose and incubated at 65 °C water bath until all the agarose is completely dissolved. Add the H_3BO_3 after dissolving the agarose. Then, it is poured into small Petri dishes or onto microscope slides and quickly stored in a wet chamber to avoid drying. Once the PGM solidifies take the flowers and gently brush them across the surface of the PGM to transfer the pollen grains. Incubate the Petri dishes or slides in a transparent wet

chamber [4] for 4–6 h at 22 °C in light conditions. To analyze pollen germination using a solid PGM an inverted microscope is recommended.

2. The PGM can be stored at −20 °C without the H_3BO_3. The H_3BO_3 should be added the same day of the experiment.
3. For better results employ younger plants, however the first few flowers of the primary bolt are often infertile. Look for flowers above siliques that have started to lengthen. In general, mature pollen is present in the flower once white petals are visible, coinciding with stage 13 of flower development. If the plants have been grown in a plant growth chamber, then avoid the flowers that have been growing very close to the lights because heat stress can negatively affect pollen development.
4. Vortexing the tubes facilitates the release of pollen grains. Make sure most of the flowers stay submerged in the PGM.
5. Temperature is a determinant factor for pollen tube growth [4]. The glass vials can be incubated in a plant growth chamber under controlled temperature conditions.
6. A cut-off pipette tip is used to avoid the rupture of the pollen tubes.
7. Up to three samples can be placed on the same glass slide.
8. Once the cover slip is placed over the sample it can be sealed with clear nail polish to avoid the evaporation of water. This is recommended if the assay takes too long, otherwise it is not necessary.
9. To take images, choose areas that include the central areas as well as the corners and borders of the cover slip, because the latter are the zones where the germinated pollen grains tend to accumulate.

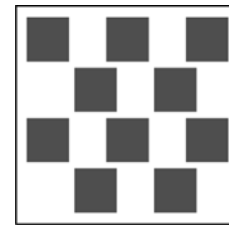

10. Click “Initialize” each time a new set of images is opened.
11. For example, select “type1” each time you click on nongerminated pollen grains and “type2” for germinated pollen grains.
12. A pollen grain is classified as germinated if the pollen tube length was equal to or greater than the pollen grain diameter. A minimum of 100 pollen grains are classified per replicate.
13. No less than 100 pollen grains must be counted. The normal percentage of germination observed for WT pollen grains is

about 70–80 %. Any value below 50 % will cause the assay to be discarded, because no reliable comparison can be done.

14. For example, if your scale bar represents 200 μm, type that in *known distance*, and type in "micrometer" in the *unit of length*.
15. A minimum of 100 pollen tubes are measured for each replicate. The pollen tube length value is obtained by averaging the mean of each replicate. In case that collected data do not fit in a normal distribution then median instead of the mean should be used.

Acknowledgement

This work was supported by PICT2011-0054 (J.M.E.) and PICT2011-1698 and PICT2012-0007 (J.M.).

References

1. Cheung AY, Hen-ming W (2008) Structural and signaling networks for the polar cell growth machinery in pollen tubes. Annu Rev Plant Biol 59:547–572
2. Cole RA, Fowler JE (2006) Polarized growth: maintaining focus on the tip. Curr Opin Plant Biol 9:579–588
3. Chebli Y, Geitmann A (2007) Mechanical principles governing pollen tube growth. Funct Plant Sci Biotechnol 1:232–245
4. Boavida LC, McCormick S (2007) Temperature as a determinant factor for increased and reproducible *in vitro* pollen germination in *Arabidopsis thaliana*. Plant J 52:570–582

Chapter 4

Imaging of Calcium Dynamics in Pollen Tube Cytoplasm

María Laura Barberini and Jorge Muschietti

Abstract

Cytoplasmic calcium [$(Ca^{2+})_{cyt}$] is a central component of cellular signal transduction pathways. In plants, many external and internal stimuli transiently elevate $(Ca^{2+})_{cyt}$, initiating downstream responses that control different features of plant development. In pollen tubes the establishment of an oscillatory gradient of calcium at the tip is essential for polarized growth. Disruption of the cytosolic Ca^{2+} gradient by chelators or channel blockers inhibits pollen tube growth. To quantify the physiological role of $(Ca^{2+})_{cyt}$ in cellular systems, genetically encoded Ca^{2+} indicators such as Yellow Cameleons (YCs) have been developed. The Cameleons are based on a fluorescence resonance energy transfer (FRET) process. Here, we describe a method for imaging cytoplasmic Ca^{2+} dynamics in growing pollen tubes that express the fluorescent calcium indicator Yellow Cameleon 3.6 (YC 3.6), using laser-scanning confocal microscopy.

Key words Pollen, Calcium, Yellow Cameleon 3.6, Ratio imaging, Kymograph

1 Introduction

Tip growth is a specialized form of cell growth associated with cells that direct their growth in response to internal and external signals [1]. Root hairs and pollen tubes are good examples for polarized tip growth. This process requires a highly coordinated pathway that involves many components, such as protein kinases [2], GTPases [3], the actin cytoskeleton [4], and signaling factors such as calcium [5], pH [6], cAMP [7], phosphoinositides [8], and reactive oxygen species [9]. All these factors interact with each other to modulate tip growth, allowing the synthesis of new plasma membrane and cell wall components and their precise targeting to the growing tip.

Calcium (Ca^{2+}) plays essential roles in the control of pollen tip growth [10]. Ion imaging showed that growing pollen tubes possess a cytoplasmic tip-focused Ca^{2+} gradient that range from 10 μM at the tip to 0.2 μM at the base of the tube [11]. The Ca^{2+} gradient oscillates at the same frequency as growth [12, 13],

José M. Estevez (ed.), *Plant Cell Expansion: Methods and Protocols*, Methods in Molecular Biology, vol. 1242,
DOI 10.1007/978-1-4939-1902-4_4,

although not in the same phase [11]. Disruption of the cytosolic Ca^{2+} gradient by calcium channel blockers inhibits pollen tube growth [5, 14].

Measuring intracellular calcium can be done using fluorescent indicators, classified as fluorescent dyes (e.g., Fura-2, Indo-1, Fluo-4) or fluorescent proteins (e.g., yellow cameleons and *aequorin*). Different approaches have been used to load dyes into the cytoplasm of tip-growing plant cells. For example, salt forms dyes are typically loaded into cells by microinjection [4, 11, 15]. The major disadvantages of this technique include low yields, technical difficulties, and cell damage. In contrast, the cell-permeant acetoxymethyl ester dyes [16–18] can be passively loaded into cells, where they are hydrolyzed by intracellular esterases, thus releasing the active Ca^{2+}-sensitive fluorophore. But their major problem is their fast compartmentalization into cellular organelles, mainly vacuoles.

Another way of measuring Ca^{2+} dynamics is the use of genetically encoded Ca^{2+} indicators such as Yellow cameleons (YCs) [19]. These indicators are chimeric proteins consisting of enhanced cyan fluorescent protein (ECFP), calmodulin (CaM), a glycyl–glycine linker, the CaM-binding domain of myosin light chain kinase (M13), and enhanced yellow fluorescent protein (eYFP). They are based on a fluorescence resonance energy transfer (FRET) process; as a consequence the donor emission and acceptor absorption spectra must overlap. The excitation of YFP by CFP emission takes place only when the two fluorophores are within a few nanometers of each other. The binding of calcium ions to the calmodulin domain causes it to associate with the M13 peptide enhancing the efficiency of FRET between the two fluorophores, thus CFP fluorescence decreases and YFP fluorescence increases. YC3.6 was developed as a new YC variant in which the acceptor fluorophore is a circularly permuted version of Venus, yielding a significantly increased dynamic range of the signal [20].

Yellow Cameleons offer the opportunity to monitor calcium dynamics in a noninvasive manner and allow quantitative measurements of Ca^{2+} dynamics by measuring the ratio of acceptor/donor fluorescent intensity in a time course. Another advantage is that recombinant proteins can be targeted to different organelles, so calcium can be measured specifically in endoplasmic reticulum or mitochondria [5, 21, 22]. The YC variant has been used extensively for imaging Ca^{2+} signals in specific plant cell types such as guard cells [23], pollen tubes [14, 24, 25], and root hairs [26–28].

Here we describe the use of YC 3.6 for measuring $(Ca^{2+})_{cyt}$ in growing pollen tubes using laser-scanning confocal microscopy. We also describe a method to analyze how modulators of pollen tube growth could disturb $(Ca^{2+})_{cyt}$ dynamics in pollen tubes that are growing in semisolid pollen germination medium.

2 Materials

2.1 Plant Material

Plants stably expressing YC 3.6 under the control of pollen-specific LAT52 promoter (*see* **Note 1**).

For bleed-through or crosstalk determination (*see* **Note 2**) use pollen tubes that transiently express only CFP-CaM or M13-cpVenus genes (*see* **Note 3**).

Wild type pollen is required for autofluorescence calculation.

2.2 Reagents

Calcium channel modulators.

In vitro calcium calibration requires purified recombinant YC 3.6 protein and a calcium calibration buffer kit (Molecular probes).

2.3 Sample Preparation

Germinate pollen grains from YC3.6-expressing plants in suitable pollen germination medium; the optimum composition of the medium and growing conditions vary between species. Use *Lab-Tek™ Chambered Coverglass* (*Nunc*) for inverted microscope viewing. We used *Solanum lycopersicum* pollen tubes.

In vitro tomato pollen germination:

1. Collect freshly opened flowers of YC3.6-expressing tomato plants.
2. Obtain mature pollen by vibrating anthers of flowers with a biovortex (*BioSpec Products*).
3. Resuspend tomato pollen at a concentration of 0.1 mg/ml (*see* **Note 4**) in an optimized pollen germination medium (PGM_1) (*see* **Note 5**).
4. Place 200 µl of pollen suspension in the four central chambers of a chambered coverslip (*see* **Note 6**).
5. Incubate at 28 °C for 1 h. No agitation.

For calcium channel modulator assays, pollen grains are germinated in semisolid pollen germination medium.

1. Prepare 1.4 % (w/v) low melting point agarose in 1× PGM_2 (*see* **Note 7**).
2. Microwave for approximately 15 s or until agarose is melted.
3. Cool the solution to room temperature.
4. Resuspend pollen grains at a concentration of 0.2 mg/ml in PGM_2.
5. Place one drop (50 µl) of pollen suspension in the four central chambers of a chambered coverslip.
6. Carefully mix with 50 µl of low melting point agarose-PGM_2.
7. Transfer to 4 °C for 30 s.
8. Incubate at 28 °C for 1 h.
9. Add 100 µl of PGM_2.

3 Methods

3.1 Configuration of Confocal Microscope

1. For CFP excitation, select either the 458 nm line of the argon ion laser or the 405 (or 440 nm) emission of a diode laser (*see* **Note 8**). This allows determination of I_{DD} and I_{DA}, where I_{DA} (FRET image) is the intensity of fluorescence upon donor excitation in the acceptor-emission channel and I_{DD} (CFP image) in the donor-emission channel.
2. Photobleaching correction requires cpVenus excitation by the 488 nm line of the argon-ion laser (*see* **Note 9**).
3. Select the proper emission wavelength range, e.g., 480–495 nm for the CFP channel and 535–565 nm for the FRET channel.
4. Select the appropriate dichroic mirror. Generally, the dichroic mirror for confocal microscopy matches the laser line selected (e.g., DM 405/488 nm).
5. Add a transmitted light (bright field) channel to check focus during the time course.

3.2 Parameters for Image Acquisition

The tip-focused intracellular Ca^{2+} gradient oscillates rapidly; as a consequence, set the scanning parameters for fast image acquisition. A compromise between speed and resolution must be determined empirically.

1. Place the chamber with the pollen tubes on the microscope stage and use the 60× objective to focus on the pollen tip using bright-field illumination.
2. Set the scan speed to 10 μs/pixel.
3. Select a pixel resolution that is compatible with fast scan times (e.g., an image size of 512×512).
4. Set the acquisition time to 3–5 s.
5. Confirm that the interval between frames is longer than the time used to scan a single frame.
6. Set Pinhole size to 1 Airy unit.
7. Adjust the laser intensity and detector gain according to the brightness of the sample to assure that the signal from any pixel is not saturated (*see* **Note 10**).

3.3 Data Collection

To compare results between independent samples always use the same confocal configuration and scanning parameters.

1. Place the chamber on the stage of the microscope.
2. In order to verify that the laser is well aligned, perform Köhler alignment of the transmitted light condenser.
3. Use bright field illumination to focus a pollen tube and confirm (using epifluorescence) that is fluorescent.

4. In order to determine the photobleaching coefficient, measure the direct cpVenus intensity ($I_{AA}{}^{0}$) by exciting cpVenus with a 488 nm argon ion laser.
5. Load the previously saved FRET configuration and scanning parameters.
6. Start image acquisition. Acquire 30–50 frames.
7. If needed, prepare the calcium channel modulator buffer at 2× in PGM (*see* **Note 11**).
8. Exchange the PGM and apply treatment.
9. Set up the number of frames to collect in the time course (approximately 100–200).
10. Start the data acquisition. Confirm a stable microscope focus during the time course.
11. Finally, measure the direct cpVenus fluorescent protein intensity ($I_{AA}{}^{t}$) to determine the photobleaching.
12. Measure the fluorescence intensity of wild-type pollen tubes with the same imaging settings to determine the amount of autofluorescence.
13. In vitro *calibration*. To determine the dissociation constant (K_d) with a commercial calcium calibration buffer kit, purify recombinant YC 3.6 protein from *Escherichia coli*. Perform fluorescence measurements of recombinant YC 3.6 in the presence of 11 different Ca^{2+} concentrations under conditions as close as possible to the FRET settings. To determine the background fluorescence value, measure I_{DD} and I_{DA} using a solution that contains no dye.
14. To determine the crosstalk or bleed-through between the donor (CFP) and acceptor (cpVenus) channels, measure I_{DD}, I_{AA}, and I_{DA} using pollen tubes or *E. coli* that transiently express only CFP-CaM, which emits only CFP but no cpVenus signal. Any signal in the FRET channel (I_{DA}) is therefore due to crosstalk of the CFP signal into the FRET channel. Likewise, measure I_{DD}, I_{AA}, and I_{DA} using pollen tubes or *E. coli* that transiently express only M13-cpVenus.

3.4 Data Analysis

Perform postacquisition analyses with the provided confocal software or with open-source software such as ImageJ.

1. *Background correction*. Draw a ROI (region of interest) on the tip of a wild type pollen tube and measure average fluorescence intensity in both I_{DD} and I_{DA} images.
2. *Ratio analysis*. Use ImageJ with the RatioPlus plugin to calculate the ratio between I_{DA} and I_{DD} images. The resulting ratio is calculated as follows:

$$\text{cpVenus} / \text{CFP ratio} = \left(\text{int } I_{DA} - \text{bkg } I_{DA}\right) / \left(\text{int } I_{DD} - \text{bkg } I_{DD}\right)$$

where "int" is the fluorescence intensity and "bkg" corresponds to background intensity (calculated in **step 1**).

Convert the ratio image to pseudocolor to easily see differences between treatments. Use "Image > look-up table (LUT) > e.g. fire" command from the ImageJ software.

3. In vitro *calibration*. To determine the background fluorescence values, select a ROI in I_{DD} and I_{DA} images corresponding to solution with no dye. Obtain cpVenus/CFP ratio for each calcium concentration using the RatioPlus plugin. Calculate K_d of YC 3.6, defined as the concentration at which the half-saturation point is reached. Define R_{max} and R_{min} as the cpVenus/CFP ratio corresponding to the "high Ca^{2+} sample" (10 mM CaEGTA) and the "zero Ca^{2+} sample" (10 mM K_2EGTA), respectively.

   The cpVenus/CFP ratio can be converted into Ca^{2+} concentration, according to the equation:

$$\left[Ca^{2+}\right] = K_{d'} \times \left[\left(R - R_{min}\right) / \left(R_{max} - R\right)\right]^{1/n}$$

   where "K_d'" is the apparent dissociation constant that is 250 nM according to [20].

   "n" represents the Hill coefficient determined as 1.7 for YC3.6 [20].

   R is the background-corrected ratio at a given time.

   R_{max} and R_{min} represent the maximum and minimum ratio values.

4. In order to calculate the growth of pollen tubes use the Template Matching and Slice Alignment plugin for ImageJ in ratio image stack. Select a pollen tube tip as a landmark for aligning. All slices in the stack must be aligned and the displacements for each slice are printed out in a results table. Perform the data analysis in Excel (Microsoft).

5. To measure intracellular calcium, select a ROI in a pollen tube tip in an aligned ratio image stack. Plot the intensity values within a ROI on a stack, using "Image > Stacks > Plot *z*axis" command from ImageJ software.

6. Alternatively, plot a kymograph (also called a "time space plot"), which denotes the fluorescence values along the line for each frame of a time series. Use the Multi-Kymograph plugin for ImageJ and trace a line along the pollen tube in the ratio image stack. The figure shows a typical kymograph of a tomato pollen tube grown in vitro where each horizontal line of the kymograph illustrates the $[Ca^{2+}]_{cyt}$ along a line traced in the middle of the tube at one time point. The *y*-axis of the kymograph corresponds to time axis (seconds) and the unit is the time interval of the sequence. The *x*-axis is the distance along the line ROI (μm) and the unit is the pixel size of the sequence. The slope of the kymograph represents the growth rate of the pollen tube (Fig. 1).

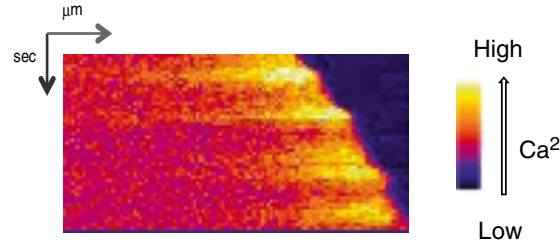

Fig. 1 Kymograph of Ca^{2+} concentrations using YC 3.6 protein sensor in the pollen tube apical zone

7. To correct for photobleaching, multiply the fluorescence intensity of the FRET channel (I_{DA}) by a correction factor. This correction factor is calculated by dividing the intensity of direct cpVenus at the start of the experiment ($I_{AA}{}^{0}$) by the intensity at a given time point ($I_{AA}{}^{t}$).

$$\text{FRET}_{\text{PB correction}} = I_{DA} \times \left(I_{AA}{}^{0} \,/\, I_{AA}{}^{t} \right)$$

8. *Subtract crosstalk*. Determine the crosstalk coefficients ("*a*" and "*d*") using images collected from pollen tubes or *E. coli* expressing either CFP (donor) or cpVenus (acceptor) alone. Obtain the coefficient "*a*" from the ratio of I_{DA} over I_{AA} for the "acceptor only samples" and the coefficient "*d*" from the ratio of I_{DA} over I_{DD} for the "donor only samples".

   To obtain a corrected FRET image,

$$_{\text{Corrected}}\text{FRET} = I_{DA} - a \times I_{AA} - d \times I_{DD}$$

   I_{DA}, I_{AA}, and I_{DD} correspond to YC3.6-expressing pollen tubes; "*a*" and "*d*" represent crosstalk correction coefficients.

4 Notes

1. Alternatively, use biolistic transformation to transiently express YC3.6 in pollen tubes.
2. The bleed-through controls are necessary to determine the amount of donor emission that appears in the FRET signal or vice versa.
3. *Escherichia coli* or onion cells that transiently express CFP-CaM or M13-cpVenus can also be used.
4. Pollen grain concentration must be low enough to observe isolated pollen tubes.
5. Pollen Germination Medium 1 (PGM_1): 20 mM MES, pH 6.0, 2.8 mM $Ca(NO_3)_2$, 1 mM KCl, 0.8 mM $MgSO_4$, 1.6 mM boric acid, 2.5 % (w/v) sucrose, and 24 % (w/v) polyethylene glycol 4000.

6. It is not possible to focus on the peripheral chambers.
7. Pollen Germination Medium 2 (PGM_2): 20 mM MES, pH 6.0, 2.8 mM $Ca(NO_3)_2$, 1 mM KCl, 0.8 mM $MgSO_4$, 1.6 mM boric acid, 7.5 % (w/v) sucrose, and 4 % (w/v) polyethylene glycol 4000.
8. Use as the lowest possible laser power to minimize damage to the pollen tube.
9. cpVenus is less photostable than CFP; photobleaching leads to a steady decrease in the cpVenus/CFP ratio over time.
10. Saturating pixels (shown as red pixels) result in nonquantitative data.
11. Prepare stock solutions of calcium channel modulators in the required solvents (e.g., water, dimethyl sulfoxide, or methanol) and then dilute into germination medium. Perform a control measurement with PGM containing the same volume of solvent alone.

Acknowledgments

We thank Yongfei Wang, Weihua Tang, and Weijie Huang for providing the Cameleon tomato transgenic plants. We thank Sheila McCormick for critical reading of the manuscript. This work was supported by grants to J.M. (UBACyT, PICT2011, and PICT2012).

References

1. Qin Y, Yang Z (2011) Rapid tip growth: insights from pollen tubes. Semin Cell Dev Biol 22:816–824
2. Zhang Y, He J, McCormick S (2009) Two Arabidopsis AGC kinases are critical for the polarized growth of pollen tubes. Plant J 58: 474–484
3. Lee YJ, Szumlanski A, Nielsen E, Yang Z (2008) Rho-GTPase-dependent filamentous actin dynamics coordinate vesicle targeting and exocytosis during tip growth. J Cell Biol 181: 1155–1168
4. Cárdenas L, Lovy-Wheeler A, Kunkel JG, Hepler PK (2008) Pollen tube growth oscillations and intracellular calcium levels are reversibly modulated by actin polymerization. Plant Physiol 146:1611–1621
5. Iwano M, Entani T, Shiba H, Kakita M, Nagai T, Mizuno H, Miyawaki A, Shoji T, Kubo K, Isogai A, Takayama S (2009) Fine-tuning of the cytoplasmic Ca^{2+} concentration is essential for pollen tube growth. Plant Physiol 150: 1322–1334
6. Feijó JA, Sainhas J, Hackett GR, Kunkel JG, Hepler PK (1999) Growing pollen tubes possess a constitutive alkaline band in the clear zone and a growth-dependent acidic tip. J Cell Biol 144:483–496
7. Moutinho A, Hussey PJ, Trewavas AJ, Malhó R (2001) cAMP acts as a second messenger in pollen tube growth and reorientation. Proc Natl Acad Sci U S A 98:10481–10486
8. Dowd PE, Coursol S, Skirpan AL, Kao T-H, Gilroy S (2006) Petunia phospholipase C1 is involved in pollen tube growth. Plant Cell 18:1438–1453
9. Lassig R, Gutermuth T, Bey TD, Konrad KR, Romeis T (2014) Pollen tube NAD(P)H oxidases act as a speed control to dampen growth rate oscillations during polarized cell growth. Plant J 78:94–106
10. Steinhorst L, Kudla J (2013) Calcium—a central regulator of pollen germination and tube growth. Biochim Biophys Acta 7:1573–1581
11. Messerli MA, Creton R, Jaffe LF, Robinson KR (2000) Periodic increases in elongation

rate precede increases in cytosolic Ca^{2+} during pollen tube growth. Dev Cell 222: 84–98

12. Holdaway-Clarke TL, Feijó JA, Hackett GR, Kunkel JG, Hepler PK (1997) Pollen tube growth and the intracellular cytosolic calcium gradient oscillate in phase while extracellular calcium influx is delayed. Plant Cell 9: 1999–2010
13. Messerli M, Robinson KR (1997) Tip localized Ca^{2+} pulses are coincident with peak pulsatile growth rates in pollen tubes of *Lilium longiflorum*. J Cell Sci 110:1269–1278
14. Michard E, Lima PT, Borges F, Silva AC, Portes MT, Carvalho JE, Gilliham M, Liu LH, Obermeyer G, Feijó JA (2011) Glutamate receptor like genes form Ca^{2+} channels in pollen tubes and are regulated by pistil D-serine. Science 332(434):437
15. Pierson ES, Miller DD, Callaham DA, VanAken J, Hackett G, Hepler PK (1996) Tip-localized calcium entry fluctuates during pollen tube growth. Dev Biol 174:160–173
16. Wang YF, Fan LM, Zhang WZ, Zhang W, Wu WH (2004) Ca^{2+}-permeable channels in the plasma membrane of Arabidopsis pollen are regulated by actin microfilaments. Plant Physiol 136:3892–3904
17. Wang Y, Zhu Y, Ling Y, Zhang H, Liu P, Baluška F, Šamaj J, Lin J, Wang Q (2010) Disruption of actin filaments induces mitochondrial Ca^{2+} release to cytoplasm and $[Ca^{2+}]$ c changes in Arabidopsis root hairs. BMC Plant Biol 10:53
18. Wu Y, Xu X, Liu T, Ma L-G, Shang Z-L (2007) Heterotrimeric G-protein participation in Arabidopsis pollen germination through modulation of a plasma membrane hyperpolarization-activated Ca^{2+}-permeable channel. New Phytol 176:550–559
19. Miyawaki A, Llopis J, Heim R, McCaffery JM, Adams JA, Ikura M, Tsien RY (1997) Fluorescent indicators for Ca^{2+} based on green fluorescent proteins and calmodulin. Nature 388:834–835
20. Nagai T, Yamada S, Tominaga T, Ichikawa M, Miyawaki A (2004) Expanded dynamic range of fluorescent indicators for Ca^{2+} by circularly permuted yellow fluorescent proteins. Proc Natl Acad Sci U S A 101:10554–10559
21. Loro G, Drago I, Pozzan T, Schiavo FL, Zottini M, Costa A (2012) Targeting of Cameleons to various subcellular compartments reveals a strict cytoplasmic/mitochondrial Ca^{2+} handling relationship in plant cells. Plant J 71:1–13
22. Bonza MC, Loro G, Behera S, Wong A, Kudla J, Costa A (2013) Analyses of Ca^{2+} accumulation and dynamics in the endoplasmic reticulum of Arabidopsis root cells using a genetically encoded Cameleon sensor. Plant Physiol 163: 1230–1241
23. Allen GJ, Kwak JM, Chu SP, Llopis J, Tsien RY, Harper JF, Schroeder JI (1999) Cameleon calcium indicator reports cytoplasmic calcium dynamics in Arabidopsis guard cells. Plant J 19:735–747
24. Iwano M, Shiba H, Miwa T, Che F-S, Takayama S, Nagai T, Miyawaki A, Isogai A (2004) Ca^{2+} dynamics in a pollen grain and papilla cell during pollination of Arabidopsis. Plant Physiol 136:3562–3571
25. Watahiki MK, Trewavas AJ, Parton RM (2004) Fluctuations in the pollen tube tip-focused calcium gradient are not reflected in nuclear calcium level: a comparative analysis using recombinant yellow cameleon calcium reporter. Sex Plant Reprod 17:125–130
26. Miwa H, Sun J, Oldroyd GE, Downie JA (2006) Analysis of calcium spiking using a cameleon calcium sensor reveals that nodulation gene expression is regulated by calcium spike number and the developmental status of the cell. Plant J 48:883–894
27. Monshausen GB, Messerli MA, Gilroy S (2008) Imaging of the Yellow Cameleon 3.6 indicator reveals that elevations in cytosolic Ca^{2+} follow oscillating increases in growth in root hairs of Arabidopsis. Plant Physiol 147:1690–1698
28. Rincon-Zachary M, Teaster ND, Sparks JA, Valster AH, Motes CM, Blancaflor EB (2010) Fluorescence resonance energy transfer-sensitized emission of yellow cameleon 3.60 reveals root zone-specific calcium signatures in Arabidopsis in response to aluminum and other trivalent cations. Plant Physiol 152:1442–1458

Chapter 5

Live Imaging of Root Hairs

Silvia M. Velasquez, Jose R. Dinneny, and José M. Estevez

Abstract

Root hairs are single cells specialized in the absorption of water and nutrients. Growing root hairs requires intensive cell wall changes to accommodate cell expansion at the apical end by a process known as tip growth. The cell wall of plants is a very rigid structure comprised largely of polysaccharides and hydroxyproline-rich *O*-glycoproteins. The importance of root hairs stems from their capacity to expand the surface of interaction between the root and the environment, in search for the necessary nutrients and water to allow plant growth. Therefore, it becomes crucial to deepen our knowledge of them, particularly in the light of the applicability in agriculture by allowing the expansion of croplands. Root hair growth is an extremely fast process, reaching growth rates of up to 1 μm/min and it also is a dynamic process; there can be situations in which the final length might not be affected but the growth rate is. Consequently, in this chapter we focus on a method for studying growth dynamics and rates during a time course. This method is versatile allowing for it to be used in other plant organs such as lateral root, hypocotyl, etc., and also in various conditions.

Key words Roots hairs, Tip growth, Growth rate, Arabidopsis

1 Introduction

Plant root hairs, just like pollen tubes, are single tubular cells and their cell walls are typically comprised of low-crystalline cellulose, xyloglucans, and pectins, together with hydroxyproline-rich *O*-glycoproteins such as extensins and proline-rich proteins [1]. Both the root hairs and the pollen tubes develop by polar cell expansion (tip or polarized growth). This type of growth involves turgor pressure, cell wall loosening at the tip, new cell wall materials synthesis, and their subsequent deposition at the root hair tip by vesicular transport from the endomembrane system [2, 3]. After the fusion of these vesicles with the plasma membrane comes the next step which is the stiffening of the cell wall. Afterwards, the turgor pressure will build again and a new growth cycle will start.

The signaling accompanying these growth pulses involves Reactive Oxygen Species (ROS) [4] which in turn activates Ca^{2+} channels that result in a local apical Ca^{2+} gradient. The Ca^{2+}gradient

José M. Estevez (ed.), *Plant Cell Expansion: Methods and Protocols*, Methods in Molecular Biology, vol. 1242,
DOI 10.1007/978-1-4939-1902-4_5,

is necessary for the exocytosis of the vesicles [5, 6]. Both ROS and Ca2+, as well as pH, present cycling patterns just like the root hair growth [7–9]. Because vesicular transport is a fundamental part of polarized growth, consequently actin microfilaments are fundamental too [10]. Inhibition of their polymerization impairs elongation of both root hairs and pollen tubes [10, 11]. Root hair growth is an extremely fast process, reaching growth rates of up to 1 μm/min [12, 13].

The root is involved in water, nutrient uptake, nitrogen fixation [8, 14], and plant anchorage to the soil. Given that the plant is a sessile organism, depending only on the root for the uptake and absorption would result in a very limited area available for interaction with the environment. Therefore, the root hairs can expand the surface of interaction, in search for the necessary nutrients and water that allow plant growth. For example, in rye (*Secale cereale* L.) root hairs can represent an interaction surface of 400 m^2 in 50 L of soil [15].

There are various factors, exogenous and endogenous, that can affect the length of the root hair and therefore have a potential impact on agricultural applications by allowing the extension of croplands. Phosphate starvation triggers a set of plant adaptive responses that involve a combination of growth, developmental, and metabolic changes [16–19]. A similar effect is observed upon starvation of nitrate [20]. Among the endogenous factors, auxin is known to have an effect on root hair elongation. Addition of exogenous auxin increases root hair length, whereas inhibition of auxin signaling or disruption of auxin transport results in a decrease in root hair length [21, 22].

Knowing the importance of root hairs in water and nutrient absorption, it becomes highly relevant to be able to fully understand the process by which they grow and the different factors that can affect this process. It is also relevant to see these effects in a live cell context because using measurements of growth at a specific end point can have the negative consequence of missing changes in growth dynamics [23] such as changes in growth rate that perhaps do not have an effect in the final growth length.

In the present chapter, we propose a method for analyzing the root hair growth through a live imaging approach. The current method allows you to determine growth dynamics and rates during a time course, in standard conditions and modified conditions, such as the exogenous addition of auxin.

2 Materials

2.1 Plant Growth

1. *Plant material. Arabidopsis thaliana* Columbia-0 seeds which can be obtained from the Nottingham Arabidopsis Stock Center or Arabidopsis Biological Resource Center.

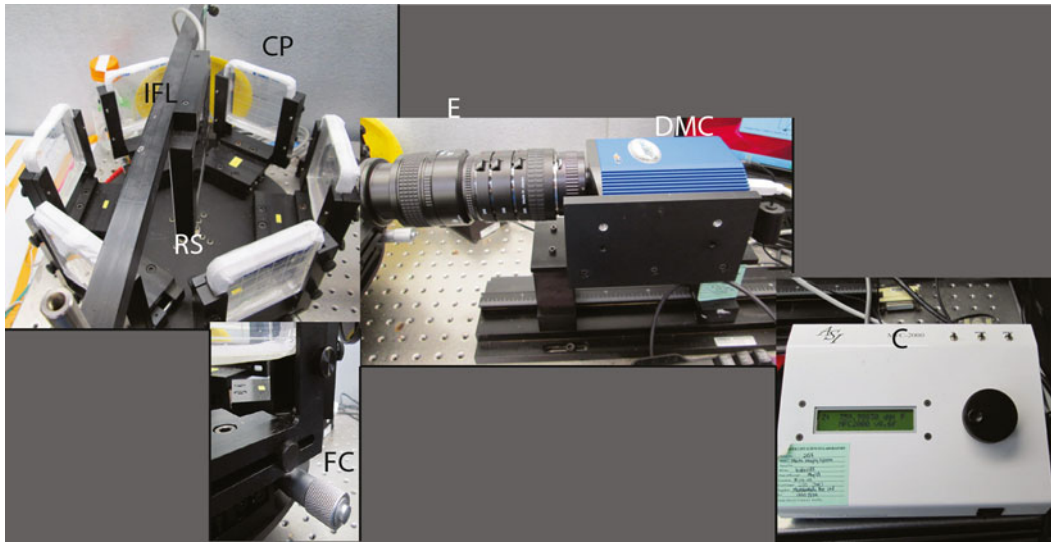

Fig. 1 Custom live-imaging system. *IFL* infrared light, *CP* circular platform, *RS* rotating stage, *E* extension tube, *DMC* digital monochrome camera, *C* controller, *FC* focus controller

2. *Plant growth*. Plants were grown in 0.5× MS medium (Caisson) supplemented with 0.7 % GelRight (Gelzan Sigma) at 21 °C under long day conditions (16 h light/8 h dark) for 7 days in vertical plates of 90 mm × 90 mm.
3. *Auxin treatment*. In the case of the auxin experiments, plants were grown in the same conditions as the standard ones, but supplementing the media with 1 μM Indol Acetic Acid (IAA). The auxin was added after the media had cooled and then poured all together into the plates.

2.2 Equipment

Custom live-imaging system [24] consisting of (Fig. 1):

1. Circular platform with six tissue-culture plate holders.
2. Automated Theta/360° rotary stage.
3. MFC-2000 controller (Applied Scientific Instrumentation).
4. Infrared light-emitting diode panel.
5. Digital monochrome camera (CoolSnap) fitted with a NF Micro-Nikon 60 mm lens (Nikon) and infrared filter.
6. Auto extension tube set DG (Kenko).

Software used to control de equipment:

Micro-Manager Software (Vale Lab, University of California, San Francisco) that allowed to control the stage and automate image acquisition [25].

2.3 Software Used for Image Analysis

The following plug-ins for ImageJ [26] software will be used to analyze the stack of images:

1. StackReg.
2. RootTipPrecalculate [27].
3. Manual Tracking.

3 Methods

3.1 Preparation of Seedlings Plates

1. 90 mm × 90 mm, half-strength MS, 1 % GelRight vertical plates were left to dry in a laminar flow hood for 20 min (*see* **Notes 1** and **2**).
2. 7-day-old seedlings were transferred with the help of forceps to the vertical plates. Up to 4 seedlings per plate were transferred (*see* **Note 3**). The seedlings were placed at the center bottom of the plate (2.6 cm from the bottom of the plate and 3.5 cm from each border, respectively) (Fig. 2).
3. A slice of 10 μl pipette tip was placed in between the roots of 2 seedlings as a reference point (*see* **Note 4**) (Fig. 2).
4. The plates need to be sealed at the bottom with parafilm so as to avoid leaking of water onto the equipment and then sealed all around with micropore tape.

3.2 Setting of the Plates on the Platform

1. The plate was set and secured in each plate holder (*see* **Note 5**).
2. Have the Micro-Manager software open on Live Snap.

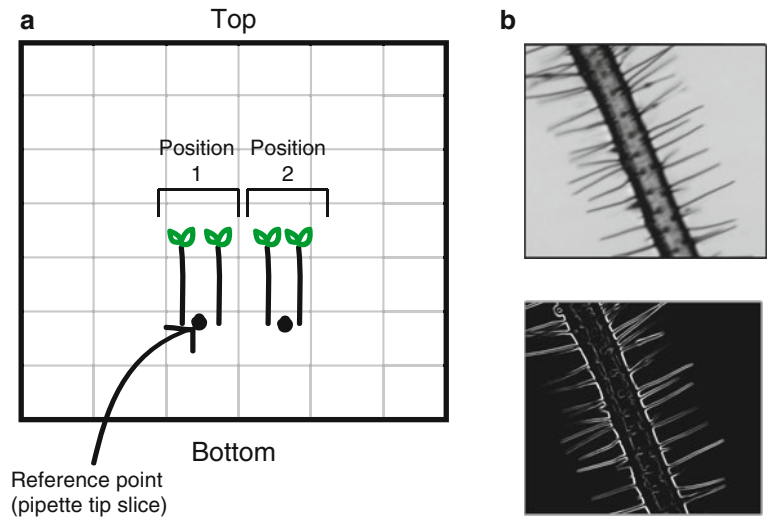

Fig. 2 (**a**) Schematic illustration of vertical plate for the live imaging set up. (**b**) Example of processed imaged ready for measurement

3. The focus was set for each plate individually with the aid of the micro-actuator focus control located at the bottom of each plate holder (Fig. 1). The focus is one for the entire plate so if you have several positions, it might happen that one or more of the positions are not in focus.

3.3 Setting of the Acquisition Parameters

1. For root hair imaging the exposition was set at 100 μs and the binning at 1.
2. When imaging more than one seedling, then the Multi-Dimensional Acquisition must be set up.
3. Up to two positions for imaging can be set up per plate (Fig. 2). To determine the positions one must go the Edit positions submenu, at the Multi-Dimensional Acquisitions panel.
4. Set up the zero position.
5. With the help of the platform controller place yourself on each position you want to acquire and mark it twice (*see* **Note 6**).
6. For root hairs, the images are taken every 5 min and for a time course of 24 h. That adds up to a total of 284 number of time points (*see* **Note 7**).
7. Create a folder to store the acquired images.
8. Press Acquire.

3.4 Processing of Images and Data Acquisition

1. Sequential images have to be imported to ImageJ as a stack.
2. The stack of images is aligned using the StackReg plug-in.
3. The RootTip Precalculate plug-in is used to enhance the contrast between the background and the root (Fig. 3).

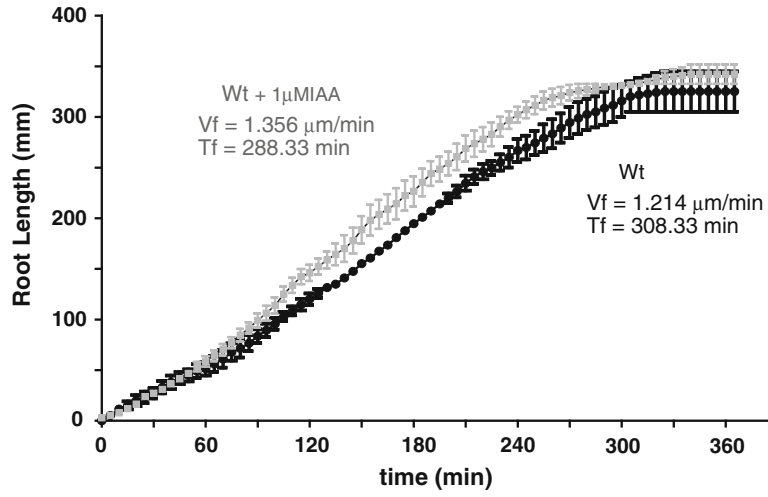

Fig. 3 Example of root hair length vs. time graph for Wt Col-0, in standard conditions and when 1 μM IAA had been added to the media. Total time of growth and growth rate are also included in this graph

4. A 200 % zoom was done on the areas where the root hairs were longer (which would be an indicative of a mature root hair) and where the entire development could be observed.
5. Quantification of the root hair growth is done with the Manual Tracking plug-in.
6. You must set the following parameters: time interval between the frames, *x/y* calibration (the inverse of the number of pixel per unit distance) (*see* **Note 8**).
7. The growth of the root hair is tracked manually from frame to frame, from its initiation to its completion (*see* **Note 9**). To start a new track, click on "Add Track." This will turn the tracking mode on.
8. To record *x/y* coordinates of a structure of interest, simply click on it on the image window. The results table will appear, showing recorded *x/y* coordinates, as well as the distance travelled by the root hair tip during the time interval between two successive images, and velocity of movement. The intensity of the corresponding pixel will also be recorded.

3.5 Data Analysis

1. In the table of measurements generated by ImageJ, each track is marked by a –1.
2. With the values of distance travelled by the root hair tip between each frame, you can calculate the total distance for each time point by adding the increments of travelled distance (e.g., for the time point 10 min, you must add the distance travelled between 0 and 5 min plus the distance between 5 and 10 min); the last value calculated being that of the total length of the root hair.
3. With the distances calculated above, you can generate a graph of root hair length vs. time. This graph will show you the growth dynamics of the root hair (Fig. 3) (*see* **Note 10**).
4. By adding all the time points, you can calculate the total time of growth and afterwards generate the corresponding graph.
5. By diving the total root hair length with the total time of growth, you can calculate the growth rate (*see* **Note 11**).

4 Notes

1. The preparation of the seedling plates to be imaged was all done in sterile conditions. 50 ml of media was added for every plate used.
2. The media can be supplemented with other compounds such as NaCl, hormones, chemical compounds, etc., so as to try other growth conditions other than the standard.

3. The seedlings selected for transfer had all the same root length.
4. Two reference points (=two slices of pipette tips) will be needed if there are 4 seedlings in the plate.
5. Up to 6 plates can be set up simultaneously (one for each plate holder available). Make sure the plates are properly secured as they may slide during the movement of the platform and you can lose the focus on the root.
6. Each position must be entered twice because due to the movement of the platform, the first set of images will probably be shaky. For each plate, if you have placed four seedlings you will end up with 4 sets of images.
7. You must set up the number of time positions manually based on the time course and the frequency of the acquisition of the images.
8. Remember to set the scale for each stack of images if you want the distances travelled to be expressed in units of length instead of pixels.
9. The initiation of the root hair was determined as the frame prior to the emergence of the root hair. Only root hairs that were growing in contact with the agar surface and at a 90° angle from the primary root were measured.
10. When representing the data for various mutant lines, that do not have the same final growth time, more time points can be added for the lines that end sooner but maintaining their final root hair length. In this way, the graphs will be more consistent.
11. Since the root hairs presented an initial lag phase in their growth, the growth rate was calculated for the constant growth phase.

Acknowledgement

This work was supported by PICT2011-0054 (J.M.E.), Fulbright Fellowship (S.M.V.), and Mizutani Grant (J.M.E.).

References

1. Nothnagel EA (1997) Proteoglycans and related components in plant cells. Int Rev Cytol 174:195–291.
2. Ishida T, Kurata T, Okada K, Wada T (2008) Annu Rev Plant Biol 59:365–386
3. Galway M, Heckman J Jr, Schiefelbein J (1997) Planta 201:209–218
4. Carol, Rachel J., et al. "A RhoGDP dissociation inhibitor spatially regulates growth in root hair cells." Nature 438.7070 (2005): 1013–1016.
5. Pierson ES, Miller DD, Callaham DA, van Aken J, Hackett G, Hepler PK (1996) Dev Biol 174:160–173
6. Schiefelbein JW, Shipley A, Rowse P (1992) Planta 187:455–459
7. Monshausen G, Bibikova T, Messerli M, Shi C, Gilroy S (2007) Proc Natl Acad Sci U S A 104:20996–21001
8. Gilroy S, Jones DL (2000) Trends Plant Sci 5:56–60

9. Feijó J, Sainhas J, Hackett G, Kunkel J, Hepler P (1999) J Cell Biol 144:483–496
10. Vidali L, Hepler P (2001) Protoplasma 215: 64–76
11. Miller DD, De Ruijter NC, Bisseling T (1999) Plant J 17:141–154
12. Hwang J-U, Gu Y, Lee Y-J, Yang Z (2005) Mol Biol Cell 16:5385–5399
13. Chen CY, Wong EI, Vidali L, Estavillo A, Hepler PK, Wu H-M, Cheung AY (2002) Plant Cell 14:2175–2190
14. Oldroyd GE, Murray JD, Poole PS, Downie JA (2011) Annu Rev Genet 45:119–144
15. Dittmer HJ (1937) Am J Bot: 417–420
16. Ticconi CA, Abel S (2004) Trends Plant Sci 9:548–555
17. Desnos T (2008) Curr Opin Plant Biol 11:82–87
18. Lin W-Y, Lin S-I, Chiou T-J (2009) J Exp Bot 60:1427–1438
19. Rouached H, Arpat AB, Poirier Y (2010) Mol Plant 3:288–299
20. Foehse D, Jungk A (1983) Plant Soil 74: 359–368
21. Pitts RJ, Cernac A, Estelle M (1998) Plant J 16:553–560
22. Rahman A, Hosokawa S, Oono Y, Amakawa T, Goto N, Tsurumi S (2002) Plant Physiol 130:1908–1917
23. Reddy GV, Gordon SP, Meyerowitz EM (2007) Nat Rev Mol Cell Biol 8:491–501
24. Duan L, Dietrich D, Ng CH, Chan PMY, Bhalerao R, Bennett MJ, Dinneny JR (2013) Plant Cell 25:324–341
25. Edelstein A, Amodaj N, Hoover K, Vale R, Stuurman N (2010) Curr Protoc Mol Biol 14.20.11–14.20.17
26. Abràmoff MD, Magalhães PJ, Ram SJ (2004) Biophotonics International 11: 36–42
27. Geng Y, Wu R, Wee CW, Xie F, Wei X, Chan PM, Tham C, Duan L, Dinneny JR (2013) Plant Cell 25:2132–2154

Chapter 6

Improved ROS Measurement in Root Hair Cells

Silvina Paola Denita Juárez*, Silvina Mangano*, and José M. Estevez

Abstract

Reactive oxygen species (ROS) are recognized as important signaling components in various processes in plants. ROS are produced for NADPH oxidase in different subcellular compartments and they are involved for a wide range of stimuli, such as cell cycle, growth, plant defenses, abiotic stress responses, and abscisic acid signaling in guard cells. In Arabidopsis, root hairs ROS also play a key role in root hair growth and they control the activity of calcium channels required for polar growth (Takeda et al. Science 319:1241–1244, 2008). The production of reactive oxygen species is under a specific molecular control in order to avoid detrimental side effects. Here we describe a protocol to detect ROS by oxidation of a derivative of fluorescein: 2′,7-dihidro dicloro fluorescein (H2DCFDA).

Key words ROS, Root hair, 2′,7-Dihidro dicloro fluorescein

1 Introduction

Reactive oxygen species (ROS) play a key signal transduction role in cells. They are involved in different physiological process like growing, development, homeostasis, and survival of plants [1]. The level of ROS in cells is determined by interplay between ROS producing pathways and ROS scavenging mechanisms, part of the ROS gene network of plants. Key players are NADPH oxidases (NADPHox). These catalyze the production of superoxides, a type of reactive oxygen species (ROS) which is rapidly converted to hydrogen peroxide [2].

In plant NADPH oxidase regulates developmental programs such as polarized cell expansion in root hair formation [3] and pollen tip growth [4]. In Arabidopsis, the Root Hair Defective 2 (RHD2) or AtrbohC protein is required for root elongation. The roots of plants homozygous for loss-of-function rhd2 mutations have decreased levels of ROS and are shorter than the wild type, indicating that cell expansion is defective in these plants [3, 5] and the ROS production is crucial for tip growth of root hair.

*Both the authors contributed equally for this chapter.

José M. Estevez (ed.), *Plant Cell Expansion: Methods and Protocols*, Methods in Molecular Biology, vol. 1242,
DOI 10.1007/978-1-4939-1902-4_6,

Fluorophores typically change their emission properties due to the interaction with ROS [5]. The addition of exogenous fluorescence probes, which penetrate into the cell and change their fluorescence properties due to reaction with ROS. In principle, the permeability across membranes and the ROS specificity are necessary for the applicability of the exogenous ROS-sensing fluorophores. However, for a quantitative analysis, it is necessary to know the reaction mechanism in detail, as well as possible interfering side effects and the cellular localization of these dyes. Some of these ROS probes can be turned regarding their properties inside the cell by enzymatic reactions. For example, 2′,7′-Dichlorofluorescin diacetate is a nonfluorescent probe in the reduced state and diffuses passively through the cellular membrane. Into the cytosol it is rapidly cleaved by unspecific esterases. The resulting molecule emits green fluorescence when it is oxidized and it is excited with blue light [6]. It could be oxidized by different ROS like anion superoxide, hydrogen peroxide, or nitrogen monoxide. This technique does not differ between the different ROS. We describe here an optimized technique by which to measure ROS specifically in the root hair.

2 Materials

1. *Arabidopsis thaliana* seeds.
   Arabidopsis thaliana Col-0 ecotype and mutants seeds can be obtained from the Arabidopsis Biological Resource Center. All mutants in this work are T-DNA insertions lines.
2. Agar 1 %.
3. H2DCFDA 50 mM (Sigma).
4. Sterilized water.
5. Slide and coverslip.

2.1 Equipment

1. Biological Control Camera (Bio-Control).
2. Confocal Microscopy (Olympus FV300/BX61).

3 Method

3.1 Plant Growth

Plants were grown in Agar 1 % (Chemit) at 22 °C under continuous light conditions for 10 days.

3.2 ROS Measurements

1. Grow sterilized Arabidopsis seed in plate with agar 1 % sterile for 8 days in chamber at 25 °C with a continuous light.
2. Remove seedlings from sterile culture and incubate in darkness in a slide for 10 min with the H2DCFDA 50 μM at room temperature (*see* **Note 1**).
3. Wash the seedling with Milli Q water.

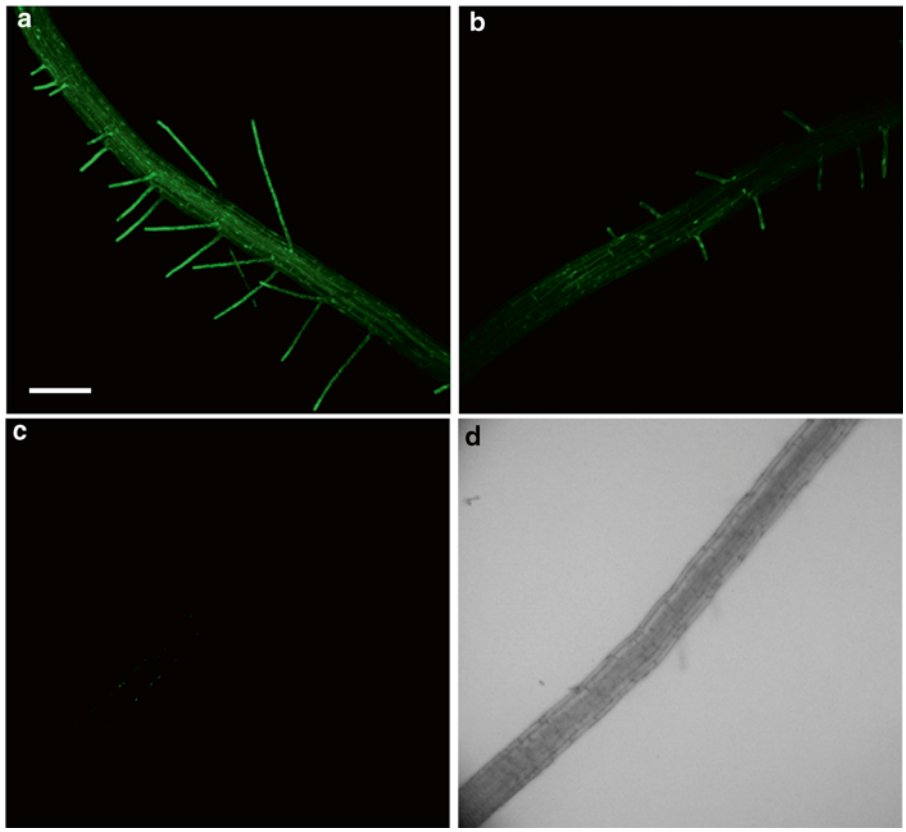

Fig. 1 Images that obtained with this technique. (**a**) ROS in a wild type root hair. (**b**) ROS in a rbohc, a insertional mutant. This mutant has been described with short root hair, which is a product of decrease in ROS levels [3]. (**c**) Wild type root with 140 nM of DPI. DPI is an inhibitor of NADPH oxidases [1]. (**d**) Wild type root with Bright field view

4. Mount seedlings in water and cover the sample with a cover slip for direct microscopic observation.
5. Examine the samples (*see* **Note 2**) using a confocal microscope equipped with the 488 nm argon laser and BA510IF filter sets. Use 10× objective and 0.30 NA (*see* **Note 3**).
6. Take the image scanning XZY with a 2 μm between the focal planes. Take all the optical sections necessary to get a clearly image of the root (Fig. 1).
7. Transfer the large data files to a computer (Fig. 2). Images were taken in different root hair developmental stages in order to measure ROS levels during cell expansion process.

3.3 Analyze the Images with ImageJ

1. Open the *Stack* in ImageJ.
2. Integrate the slices. Click on *Image—Stacks—Z project*: Projection type: Max Intensity.
3. Select an area including the root hair (*see* **Note 4**).

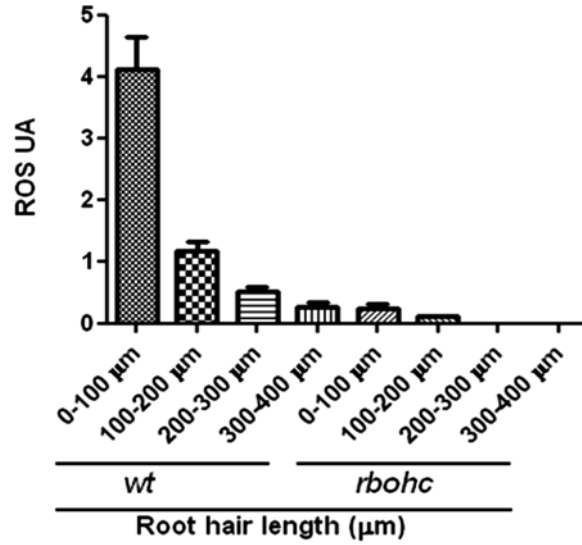

Fig. 2 Example of the experience. We examine the root hairs in different states of development. Measure ROS in different stages of root hair is important because levels can oscillate during the development

4. Quantify the intensity. Click on *Analyze—Set Measurement*, select Mean gray value. Click on *Analyze—Measure* (*see* **Note 5**).
5. Measure length.
6. Create a table to upload data.

4 Notes

1. H2DCFDA is highly sensitive to light.
2. As a negative control it was used a WT seedling incubated in a slide for 10 minutes in water (without the H2DCFDA) at room temperature in darkness. Another negative control was root hairs treated with 140 nM DPI (Fig. 1).
3. Parameters used were laser: 4.7, PMT: 503, gain: 1.1, off set: 3 %, exposure time: fast. This condition was set so as not to detect autofluorescence from root.
4. For quantification with Image J, only include the area of the root hair, be careful you do not include background.
5. Another option is to click on the letter M in the keyboard.

References

1. Suzuki N, Miller G, Morales J, Shulaev V, Torres M, Mittler R (2011) Respiratory burst oxidases: the engines of ROS signaling. Plant Biol 14:691–699
2. Roppolo D, De Rybel B, Tendon V, Pfister A, Alassimone J, Vermeer J, Yamazaki M, Stierhof Y, Beeckman T, Geldner N (2011) A novel protein

family mediates Casparian strip formation in the endodermis. Nature 473:380–384

3. Takeda S, Gapper C, Kaya H, Bell E, Kuchitsu K, Dolan L (2008) Local positive feedback regulation determines cell shape in root hair cells. Science 319:1241–1244
4. Potocký M, Jones M, Bezvoda R, Smirnoff N, Zársky V (2007) Reactive oxygen species produced by NADPH oxidase are involved in pollen tube growth. New Phytol 174:742–751
5. Foreman J, Demidchik V, Bothwell J, Mylona P, Miedema H, Torres M, Linstead P, Costa S, Brownlee C, Jones J (2003) Reactive oxygen species produced by NADPH oxidase regulate plant cell growth. Nature 422: 442–446
6. Karlsson M, Kurz T, Brunk U, Nilsson S, Frennesson C (2010) What does the commonly used DCF test for oxidative stress really show? Biochem J 428:183–190

Chapter 7

A Root Hair Assay to Expedite Cell Death Research

Joanna Kacprzyk and Paul F. McCabe

Abstract

Programmed cell death can be defined as an organized cellular destruction and can be activated throughout plant development, as a defense response against invading pathogens or during environmental stress. The root hair assay presented herein enables in vivo quantitative measurements of programmed cell death based on the morphological changes of dying root hairs. Application of this novel, simple technique eliminates the need for establishing cell suspension cultures, resulting in a significant reduction in time, cost, and labor input. Here, we present a detailed root hair assay protocol for the dicotyledonous model plant *Arabidopsis thaliana*, where results from germination to scoring of cell death can be obtained within 7 days. We also suggest and present a panel of cell death inducing treatments which can be used to study abiotic stress- and mycotoxin-induced programmed cell death in the root hair system in Arabidopsis. A root hair assay protocol for the monocotyledonous model species *Brachypodium distachyon* is also included.

Key words Programmed cell death, Root hair assay, Arabidopsis, Apoptosis-like

1 Introduction

Programmed cell death (PCD) describes a number of processes that result in a highly controlled and organized form of cellular destruction, activated in every part of the plant, throughout its entire life cycle [1]. It is an indispensable facet of plant development, senescence, defense responses, and architecture [2–4]. In the last 20 years research has increased our understanding of several facets relating to the induction and destruction of cells undergoing PCD, however its central execution mechanisms are still relatively poorly understood compared to animal cell death programs. Plant PCD can often be characterized by a specific morphology: the condensation of cell contents and retraction of plasma membrane from the cell wall, resulting in a visible gap, and this type of death has been named apoptosis-like PCD (AL-PCD) [5, 6]. This morphological hallmark feature has been commonly observed following PCD events occurring in response to abiotic stress and pathogen attack [7], during developmental PCD, such as during leaf morphogenesis in

José M. Estevez (ed.), *Plant Cell Expansion: Methods and Protocols*, Methods in Molecular Biology, vol. 1242,
DOI 10.1007/978-1-4939-1902-4_7,

Monstera [8] and lace plant leaves [9], the culmination of senescence [10, 11], and in embryogenic associated suspensor cells [4].

PCD research in plants has been hindered to some extent by a lack of convenient and reliable methods which facilitate quantitative measurement of rates of in vivo cell death as cells undergoing PCD are often buried within living tissue, which impedes large-scale visual scoring of living and dead cells. Several methods have recently been used to monitor in vivo rates of PCD, for example, the lace plant (*Aponogeton madagascariensis*) facilitates studies of developmental PCD in real time in vivo [12]. Another method is the root hair assay, which allows quantitative measurements of stress-induced AL-PCD in vivo [13]. Root hairs, already considered a classic system for studying plant cell growth [14], also provide a robust tool for determination of PCD rates in whole plants. In order to expand the scope of potential applications of the root hair assay, the technique has subsequently been optimized for high-throughput performance and a panel of cell death inducing treatments has been developed for use with the assay. To date, the root hair assay has proved useful in several research contexts. For example, the assay has been used to demonstrate a reduction in stress-induced PCD levels in Arabidopsis plants overexpressing the Defender Against Apoptotic Death-1 (DAD1) protein [13]. This result was in accordance with earlier in vitro results obtained using a protoplast system [15]. Obviously the root hair assay is technically simpler and often quicker than protoplast isolation and this is one of the major advantages of using root hairs, indeed the root hair assay can also be used as an alternative to establishing cell suspension cultures and therefore is a convenient tool for rapid determination of changes in stress-induced PCD in transgenic or mutant lines. Root hairs can also be used to study the role of genes and gene products in cell death, for example, Blanvillain et al., [16] used this technique to characterize two mutant alleles of the Kiss of Death peptide coding gene to demonstrate there was a reduced PCD phenotype after a 55 °C heat treatment. The root hair assay is therefore a promising tool for the rapid screening of mutant populations in order to identify novel genes involved in AL-PCD regulation. Additionally the root hair system is also a convenient tool to investigate potential modulators of AL-PCD, for example, caspase inhibitors [13]. Root hairs are easily accessible for chemical manipulations, as the cells are exposed on the root surface. Their natural function is absorption of water and nutrients and therefore the uptake of chemicals that are potential cell death modulators is facilitated. A combination of pharmacological and genetic approaches also means the root hair assay is a suitable technique for dissecting more complex cell signaling processes. For example, it has been recently used to identify components of salicylic acid induced programmed cell death and autophagy [17].

2 Materials

2.1 Growth of Plant Material

2.1.1 Growth of Arabidopsis Seedlings

1. 1.5 ml microfuge tubes.
2. Growth medium: MS half-strength basal salt mixture (Duchefa), 1 % (w/v) sucrose, adjust pH to 5.8 with KOH, add 1.5 % agar (w/v) and autoclave. Pour into 12×12 cm^2 sterile Petri dishes (approximately 25 ml of growth medium per plate).
3. Sterilizing solution: 20 % (v/v) commercial bleach (final concentration of sodium hypochlorite ~1 % v/v).
4. Sterile deionized water.
5. 1,000 μl pipettes and pipette tips.
6. 200 μl pipettes and pipette tips with ends cut-off.

2.1.2 Growth of Brachypodium distachyon Seedlings

1. Forceps, sterilized in autoclave.
2. Sterile deionized water.
3. Sterilizing solution: 20 % (v/v) commercial bleach (final concentration of sodium hypochlorite ~1 % v/v).
4. Filter paper (90 mm Ø discs), sterilized in autoclave.
5. Sterile Petri dishes (90 mm Ø).

2.2 Induction of PCD in Root Hairs of Arabidopsis

1. Forceps.
2. 24-well plates (e.g., Cellstar multiwell culture plates, Greiner Bio-One GmbH).
3. Sterile deionized water.
4. For heat treatment: waterbath (not shaking) (Grant OLS200), Leucopore tape.
5. For NaCl treatment: 100 mM NaCl solution in deionized water, prepared beforehand and stored at 4 °C.
6. For hydrogen peroxide treatment: 30 % w/v H_2O_2 stock solution (Sigma-Aldrich).
7. For SA treatment: 0.1 M SA stock solution in ethanol, prepare directly prior to use.
8. For fumonisin B1 (FB1) treatment: 1 mM stock solution in deionized water, prepare beforehand and store at −20 °C.

2.3 Induction of PCD in Root Hairs of Brachypodium distachyon by Heat Treatment

1. Forceps.
2. 24-well plates (e.g., Cellstar multiwell culture plates, Greiner Bio-One GmbH).
3. Sterile deionized water.
4. Waterbath with no stirring (Grant OLS200), Leucopore tape.

2.4 Root Hair Assay

1. Forceps.
2. Razors (optional).
3. Fluorescein diacetate (FDA) stock solution in acetone (0.1 %, w/v). Store at –20 °C and dilute to 0.001 % w/v in deionized water directly prior to use.
4. Standard microscope slides and cover slips.
5. White and fluorescent light microscope (e.g., Olympus BX60).
6. Three mechanical counters.

3 Methods

3.1 Growth of Plant Material

The root hair assay is a technique based on the examination of the morphology of individual cells. Relatively short root hairs and moderately dense root hair distribution facilitates observation of single cells and also reduces mechanical damage during handling of the plant material. The preliminary optimization of species specific growth protocols that result in these short dense root hairs will be of significant benefit in facilitating subsequent root hair scoring assays in different species (*see* **Note 1**). Herein, we present growth protocols that work well for us for two model species, *Arabidopsis thaliana* and *Brachypodium distachyon*.

3.1.1 Growth of Arabidopsis Seedlings

1. This method is adapted from ref. [13].
2. Place Arabidopsis seeds in the labeled 1.5 ml microfuge tube. All subsequent steps should be performed using sterile techniques in a laminar flow hood.
3. Add 1 ml of sterilizing solution and mix by inverting the tube a few times. Sterilize for 20 min with mixing every 5 min.
4. Remove the sterilizing solution by pipetting and wash seeds with 1 ml of sterile deionized water 4 times.
5. Sow seeds in 2–3 lines on solid growth medium using 200 μl cut-off pipette tips. Preferably, individual seeds should be separated by 0.5 cm. Seal Petri dishes with Parafilm and vernalize in the dark, at 4 °C for 1 day.
6. Place Petri dishes at 22 °C, in constant light, in a vertical position, so that the seeds are germinating in horizontal lines, to allow the roots to grow down the surface. Seedlings should be used for experiments when 5–6 days old.

3.1.2 Growth of Brachypodium distachyon Seedlings

1. Soak mature *Brachypodium distachyon* seeds in sterile deionized water at room temperature for 3 h in a Petri dish.
2. Using fingers, carefully remove lemma from the seeds. Collect the seeds in deionized water in a Petri dish.

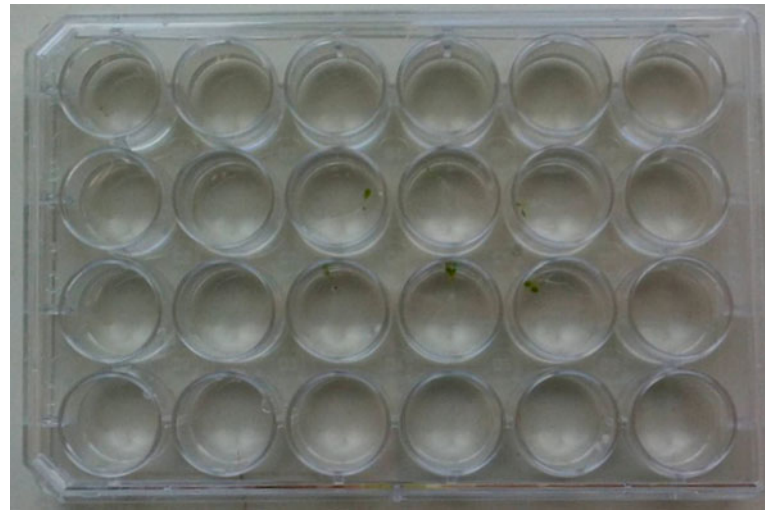

Fig. 1 24-well culture plate used for AL-PCD cell death inducing treatments with Arabidopsis seedlings

3. In the sterile flow cabinet, drain seeds from water and add sterilizing solution. Gently shake for 4 min. Rinse 4 times with sterile deionized water. Place seeds in a sterile Petri dish on two layers of filter paper soaked with sterile deionized water. Seal the Petri dish with Parafilm.
4. Vernalize for 4 days in the dark at 4 °C to synchronize germination and transfer to 25 °C with a 16-h photoperiod.
5. Seedlings can be used as soon as the emerging radicle is approximately 1 cm long (typically after 1–2 days).

3.2 Induction of PCD in Root Hairs of Arabidopsis

Twenty-four-well culture plates (Fig. 1) provide a convenient system for simultaneous treatment of up to 24 seedlings, making the root hair assay a promising tool for high-throughput screening of mutant or transgenic lines (*see* **Note 2**). A panel of cell death inducing treatments, including temperature, NaCl, hydrogen peroxide, salicylic acid, and mycotoxin fumonisin B1 is presented and can be expanded to suit the purpose of planned experiments (*see* **Note 3**).

1. Heat treatment: Fill each well of a 24-well culture plate with 1 ml of sterile deionized water. Using forceps, transfer Arabidopsis seedlings to individual wells. Seal the lid of multiwell plate with Leucopore tape. Set the waterbath (with shaking switched off) to the desired temperature. Perform the heat treatment by allowing the culture plate to float on the surface of water. Following the heat shock incubate seedlings in the light at 22 °C until scoring for PCD rates. Typically, a 10 min heat shock at temperatures between 49 and 51 °C results in induction of 30–60 % AL-PCD within 24 h.

2. NaCl treatment: warm 100 mM NaCl solution to room temperature. Fill wells of multiwell plates with 1 ml of NaCl solution or 1 ml of deionized water. Perform the stress treatment by incubating seedlings in NaCl for 5 min followed by transfer to deionized water. Following the treatment incubate seedlings in the light at 22 °C until scoring for PCD rates. Typically, treatment results in induction of 50–60 % AL-PCD within 24 h.
3. H_2O_2 treatment: Dilute 30 % w/v H_2O_2 stock in deionized water. Fill wells of multiwell plates with 1 ml of H_2O_2 solution or 1 ml of deionized water. Perform the stress treatment by incubating seedlings in H_2O_2 for 5 min followed by transfer to deionized water. Following the treatment incubate seedlings in the light at 22 °C until scoring for PCD rates. Typically, treatment with 15 mM H_2O_2 results in induction of 30–40 % of AL-PCD within 24 h.
4. SA treatment: Dilute SA stock in deionized water. Fill wells of multiwell plates with 1 ml of SA solution. Perform the stress treatment by incubating seedlings in SA solution in the light at 22 °C until scoring for PCD rates. Typically, treatment with 60–75 μM SA results in induction of 30–70 % AL-PCD within 24 h.
5. FB1 treatment: Dilute mycotoxin stock solution in deionized water. Fill wells of multiwell plates with 1 ml of FB1 solution. Perform the stress treatment by incubating seedlings in FB1 solution in the light at 22 °C until scoring for PCD rates. Typically, treatment with 50 μM FB1 results in induction of 30–40 % of AL-PCD within 24 h.

3.3 Induction of PCD in Root Hairs of Brachypodium by Heat Treatment

Perform the heat treatment according to protocol recommended for Arabidopsis seedlings. Typically, 10 min heat shock at temperature between 49 and 51 °C results in induction of 40–60 % AL-PCD within 24 h.

3.4 Root Hair Assay

1. This method is adapted from ref. [13].
2. Select the time point after cell death induction when the root hair assay will be performed (*see* **Note 4**).
3. Prepare 0.001 % w/v FDA solution directly prior to use. Whole Arabidopsis seedlings can be stained directly on the microscope slide and immediately examined under white and fluorescent light. For Brachypodium seedlings, carefully cut off the radicle with a razor blade before FDA staining and placing the cover slip on (*see* **Note 5**).
4. Examine root hairs under fluorescent and white light, starting from the root tip (*see* **Note 6**). The root hair assay is based on observation of root hairs morphology and result of FDA staining (Fig. 2). Score root hairs positive for FDA staining

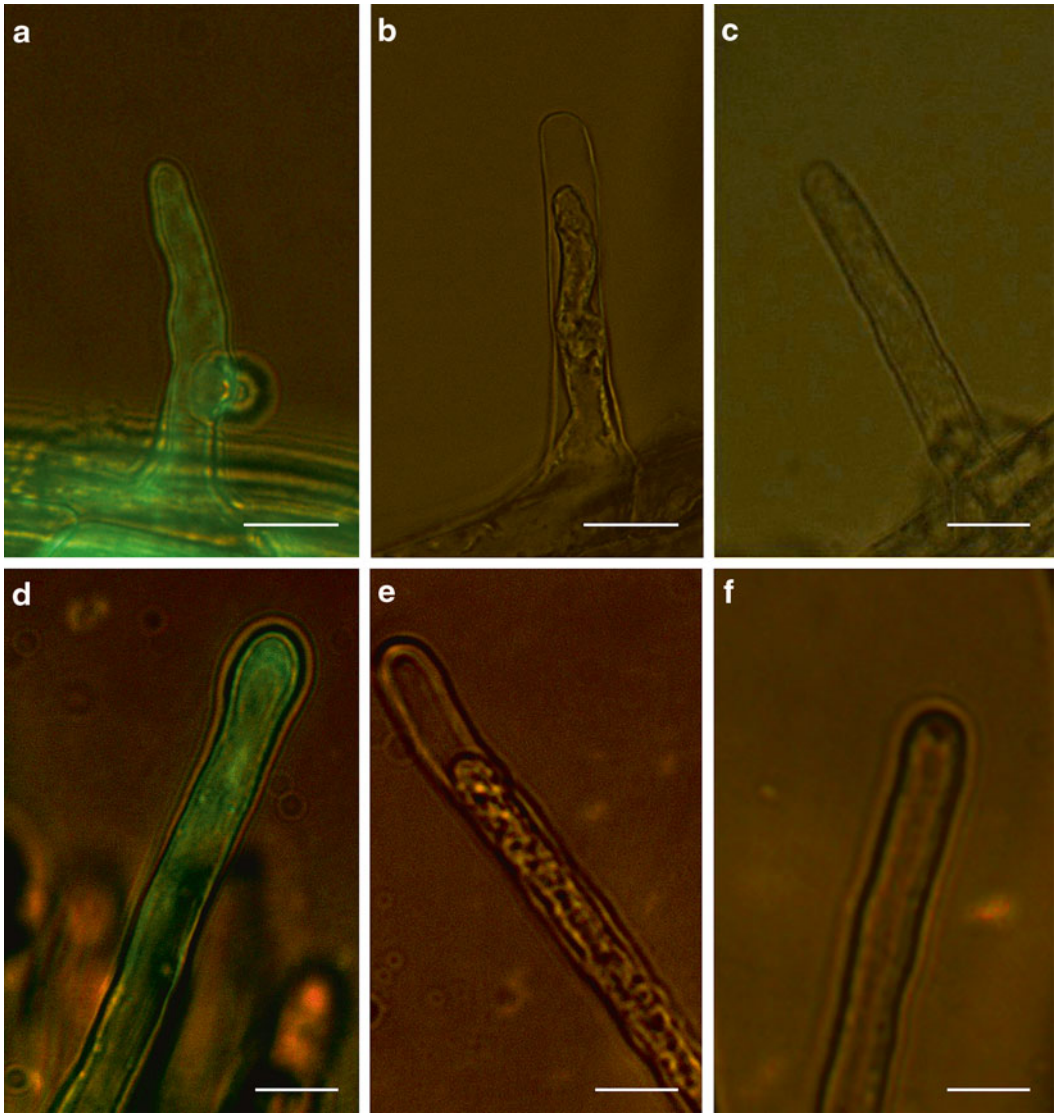

Fig. 2 AL-PCD morphology in root hairs of *Arabidopsis thaliana* (**a**–**c**) and *Brachypodium distachyon* (**d**–**f**). (**a**, **d**) Living root hair stained with FDA and viewed under both white and fluorescent light. (**b**, **e**) Root hair 24 h after a 10-min heat shock at 51 °C. The root hair shows condensation of the cytoplasm and no FDA staining, indicating it has undergone AL-PCD. (**c**, **f**) Root hair 24 h after a 10-min heat shock at 75 °C. No FDA staining and no retraction of the cytoplasm can be observed. Scalebar: 10 μm

(exhibiting green fluorescence) as alive. Examine the morphology of FDA-negative root hairs and score them as AL-PCD, if they exhibit cytoplasm condensation and retraction of protoplast away from the cell wall (*see* **Note 7**). If the root hair is FDA negative and does not exhibit AL-PCD morphology, score it as necrotic (*see* **Note 8**). Record your results using mechanical counters until you score at least 100 root hairs.

4 Notes

1. Root hair length and density can be varied and optimized for scoring by changing factors such as light regime, growth system type (e.g., solid medium or hydroponic culture), growth medium type, composition (concentration of salts), and hardness (concentration of gelling agent). Testing different growth conditions can facilitate identification of conditions producing seedlings with root hair characteristics for optimized cell death type scoring.
2. To prevent high background cell death rates due to mechanical damage, seedlings should be handled very carefully with forceps during transfer from the growth medium to the cell death inducing treatment solution.
3. While establishing a protocol for cell death induction in the root hair system with a novel chemical agent, it may be useful to test a wide range of concentrations. From our experience, concentrations of chemical agents which induce AL-PCD in Arabidopsis root hairs are often significantly lower than in cell suspension culture, possibly due to absorptive function of root hairs, favoring uptake of chemicals.
4. AL-PCD morphology takes several hours/days to develop, depending on the type and intensity of the cell death inducing stimuli. Typically, 24 h after the cell death induction, AL-PCD in root hairs is fully developed and significant condensation of the cell content can be clearly recognized. However, we have used the root hair assay to investigate AL-PCD at earlier time points in *Arabidopsis thaliana*, characterized by less advanced, although still recognizable, levels of cytoplasm condensation and a smaller gap between the cell wall and retracted protoplast.
5. If the background FDA staining is excessive, seedlings can be washed and mounted on the microscope slide in deionized water.
6. In order to correctly identify root hairs as viable it is often useful to adjust the focus on the individual cell under fluorescent light with the white light switched-off.
7. AL-PCD morphology is characterized by a gap between the protoplast and cell wall, usually being readily recognizable at the tip of the root hair. However, occasionally, cytoplasm condensation leaves a clearly identifiable gap between the cell wall and retracted protoplast only in the middle part of the root hair or close to its base (Fig. 3a, b). In certain root hairs, the cytoplasm does not retract as a complete unit and splitting of the cell content into two or more parts can be observed (Fig. 3c, d). Occasionally, especially in case of the relatively short root hairs the cytoplasm retracts almost completely to the root hair base cell (Fig. 3d, e).

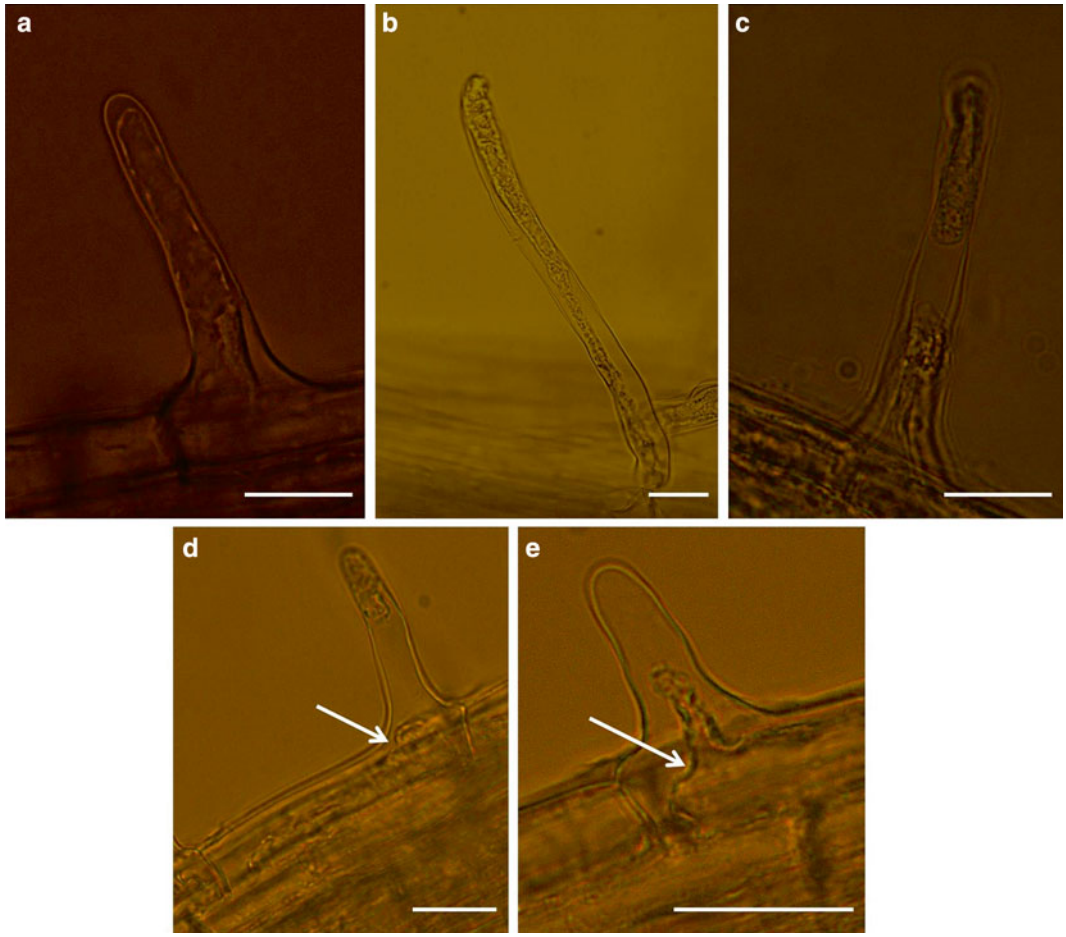

Fig. 3 Different appearances of AL-PCD morphology in the root hairs of *Arabidopsis thaliana*. Cytoplasm condensation leaving a clearly identifiable gap between the cell wall and retracted protoplast in the middle part of the root hair or close to its base (**a**, **b**). Condensed cell content split into two parts (**c**, **d**). Condensed cell content almost completely retracted to the base cell (**d**, **e**)

8. Necrosis is a rapid cell death that usually takes place in case of overwhelming stress on injury and is not associated with cytoplasm retraction. For example, in the case of heat treatment, the percentage of AL-PCD in root hairs increases with temperature increases up to 65 °C, whereas further increases of temperature cause root hairs to die by necrosis rather than AL-PCD [13].

Acknowledgments

J.K. was supported by IRCSET postgraduate scholarship scheme. Dr. Ali Behpouri is acknowledged for useful tips concerning germination of *Brachypodium distachyon*.

References

1. Kacprzyk J, Daly CT, McCabe PF (2011) The botanical dance of death: programmed cell death in plants. In: Kader JC, Delseny M (eds) Advances in botanical research, vol 60. Academic Press, UK, pp 169–261
2. Greenberg J (1996) Programmed cell death: a way of life for plants. Proc Natl Acad Sci U S A 93:12094–12097
3. Heath MC (2000) Hypersensitive response-related death. Plant Mol Biol 44:321–334
4. McCabe PF, Levine A, Meijer P-J, Tapon NA, Pennell RI (1997) A programmed cell death pathway activated in carrot cells cultured at low cell density. Plant J 12:267–280
5. Danon A, Delorme V, Mailhac N, Gallois P (2000) Plant programmed cell death: a common way to die. Plant Physiol Biochem 38:647–655
6. Reape TJ, McCabe PF (2013) Commentary: the cellular condensation of dying plant cells: programmed retraction or necrotic collapse? Plant Sci 207:135–139
7. van Doorn WG, Beers EP, Dangl JL, Franklin-Tong VE, Gallois P, Hara-Nishimura I, Jones AM, Kawai-Yamada M, Lam E, Mundy J, Mur LAJ, Petersen M, Smertenko A, Taliansky M, Van Breusegem F, Wolpert T, Woltering E, Zhivotovsky B, Bozhkov PV (2011) Morphological classification of plant cell deaths. Cell Death Differ 18:1241–1246
8. Gunawardena AHLAN, Sault K, Donnelly P, Greenwood JS, Dengler NG (2005) Programmed cell death and leaf morphogenesis in *Monstera obliqua* (Araceae). Planta 221: 607–618
9. Gunawardena AHLAN, Greenwood JS, Dengler NG (2004) Programmed cell death remodels lace plant leaf shape during development. Plant Cell 16:60–73
10. Delorme VGR, McCabe PF, Kim D-J, Leaver CJ (2000) A matrix metalloproteinase gene is expressed at the boundary of senescence and programmed cell death in cucumber. Plant Physiol 123:917–928
11. Swidzinski JA, Sweetlove LJ, Leaver CJ (2002) A custom microarray analysis of gene expression during programmed cell death in *Arabidopsis thaliana*. Plant J 30:431–446
12. Wright H, van Doorn WG, Gunawardena AHLAN (2009) *In vivo* study of developmental programmed cell death using the lace plant (*Aponogeton madagascariensis*; Aponogetonaceae) leaf model system. Am J Bot 96:865–876
13. Hogg BV, Kacprzyk J, Molony E, O'Reilly C, Gallagher T, Gallois P, McCabe PF (2011) An *in vivo* root hair assay for determining rates of apoptotic-like programmed cell death in plants. Plant Methods 7:45
14. Foreman J, Dolan L (2001) Root hairs as a model system for studying plant cell growth. Ann Bot 88:1–7
15. Danon A, Rotari VI, Gordon A, Mailhac N, Gallois P (2004) Ultraviolet-C overexposure induces programmed cell death in Arabidopsis, which is mediated by caspase-like activities and which can be suppressed by caspase inhibitors, p35 and defender against apoptotic death. J Biol Chem 279:779–787
16. Blanvillain R, Young B, Cai Y-M, Hecht V, Varoquaux F, Delorme V, Lancelin J-M, Delseny M, Gallois P (2011) The Arabidopsis peptide kiss of death is an inducer of programmed cell death. EMBO J 30: 1173–1183
17. Kacprzyk J, Devine A, McCabe PF (2014) The root hair assay facilitates the use of genetic and pharmacological tools in order to dissect multiple signalling pathways that lead to programmed cell death. PLoS One 9:e94898

Chapter 8

Vacuolar Staining Methods in Plant Cells

David Scheuring, Maria Schöller, Jürgen Kleine-Vehn, and Christian Löfke

Abstract

Commercially available fluorescent dyes enable the fast and specific visualization of plant vacuoles, allowing for investigation of membrane dynamics and vacuolar biogenesis in living cells. Here, we describe different approaches tinting the tonoplast or the vacuolar lumen with a range of dyes, and illustrate its utilization with established fluorescent-tagged marker lines.

Key words Tonoplast, Vacuole, Membrane staining, BCECF-AM, FM4-64, MDY-64, VAMP711, PIN-FORMED (PIN) *Arabidopsis thaliana*, Bright Yellow-2 (BY-2)

1 Introduction

The vacuole large size and multifunctional contribution to cellular survival evoke it to one of the most prominent organelles in plant cells. Even very simple microscopes of more than a century ago were sufficient to discover plant cell vacuoles. In this regard, the vacuole was an early focal point for cell biology, and, owing to its cellular importance, remains under extensive investigation. Vacuoles function predominantly as lytic compartments and storage reservoirs (e.g., for ions, pigments, proteins), but are also involved in a variety of other important cellular processes, such as osmoregulation and defensive reactions to pathogens (reviewed in ref. 1).

Structurally, vacuoles, which can occupy up to 90 % of the cellular volume, are surrounded by a single membrane known as the tonoplast (reviewed in ref. 2). Within the endomembrane system these compartments represent the endpoint of several transport processes. Vacuoles are functionally divided into protein storage vacuoles (PSV) and lytic vacuoles (LV). The accumulation of PSV and protein bodies in seeds is of great importance as a contributory food source for animals and humans (reviewed in ref. 3). Many plants, such as soybeans (*Glycine max*), peas (*Pisum sativum*), lentils (*Lens culinaris*), and common beans (*Phaseolus vulgaris*),

José M. Estevez (ed.), *Plant Cell Expansion: Methods and Protocols*, Methods in Molecular Biology, vol. 1242,
DOI 10.1007/978-1-4939-1902-4_8,

store a remarkably large amount of proteins in their vacuoles. In contrast, LVs contain smaller amounts of proteins, but have a major role in breaking down cellular material destined for degradation. Defined vesicle trafficking to the lytic vacuole allows, for instance, the conditional degradation of transmembrane proteins, such as transporters, at the plasma membrane (reviewed in ref. 4).

Fluorescent-based detection techniques, using either specific dyes or fluorescent-tagged proteins, are fast and convenient methods for visualizing vacuolar dynamics in living organisms. Here, we describe different vacuolar staining methods, focusing on three commonly used dyes that we favor for application in the laboratory (Fig. 1):

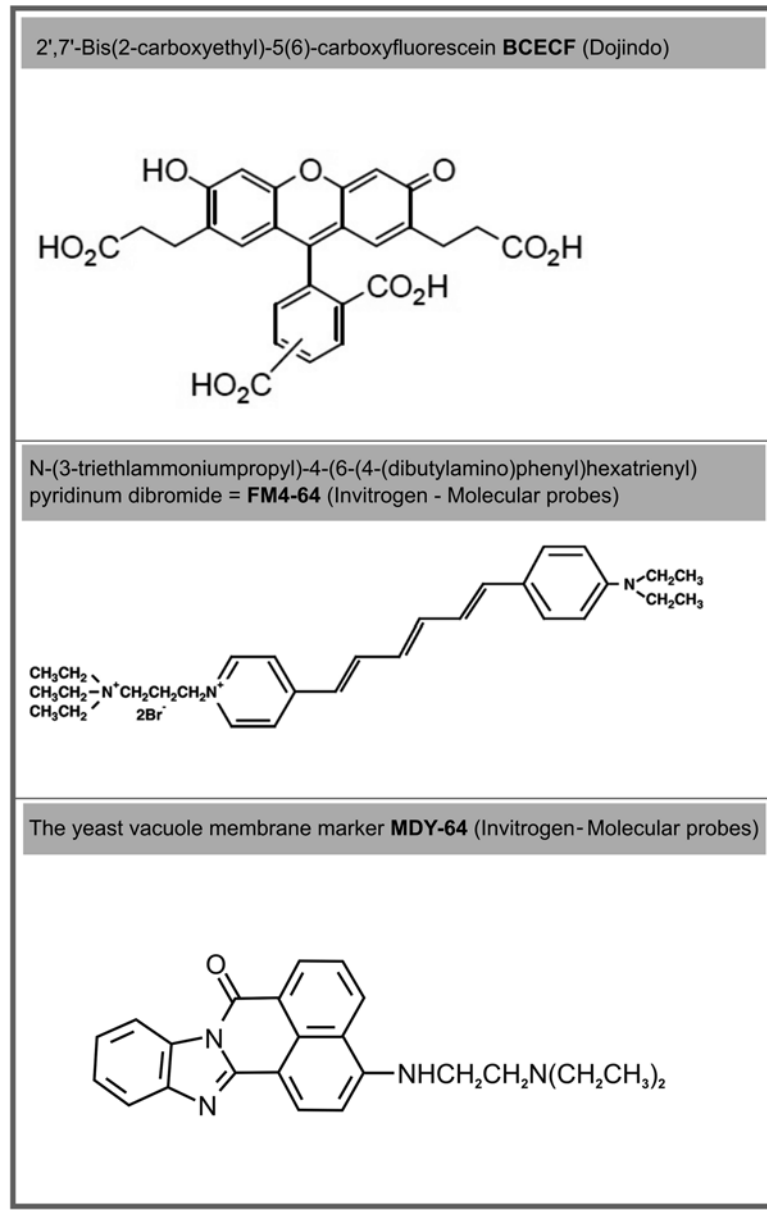

Fig. 1 Molecular structure of the dyes used

1.1 BCECF

BCECF is reasonably membrane permeable at a neutral pH, but acidification reduces its permeability and ultimately leads to its distinct accumulation in the vacuolar lumen (Figs. 2a, d, and 3g). BCECF-AM, the widely used ester of BCECF, improves the cellular uptake of the dye. Recommended as a highly specialized dye for vacuolar lumens, BCECF might also label other acidic compartments, such as the prevacuolar compartments. Beside its usage as vacuolar stain, BCECF is an extensively applied reporter to measure intracellular pH [5]. Depending on the pH and the excitation wavelength (458 and 488 nm), the emission wavelength varies between 520 and 540 nm (Table 1).

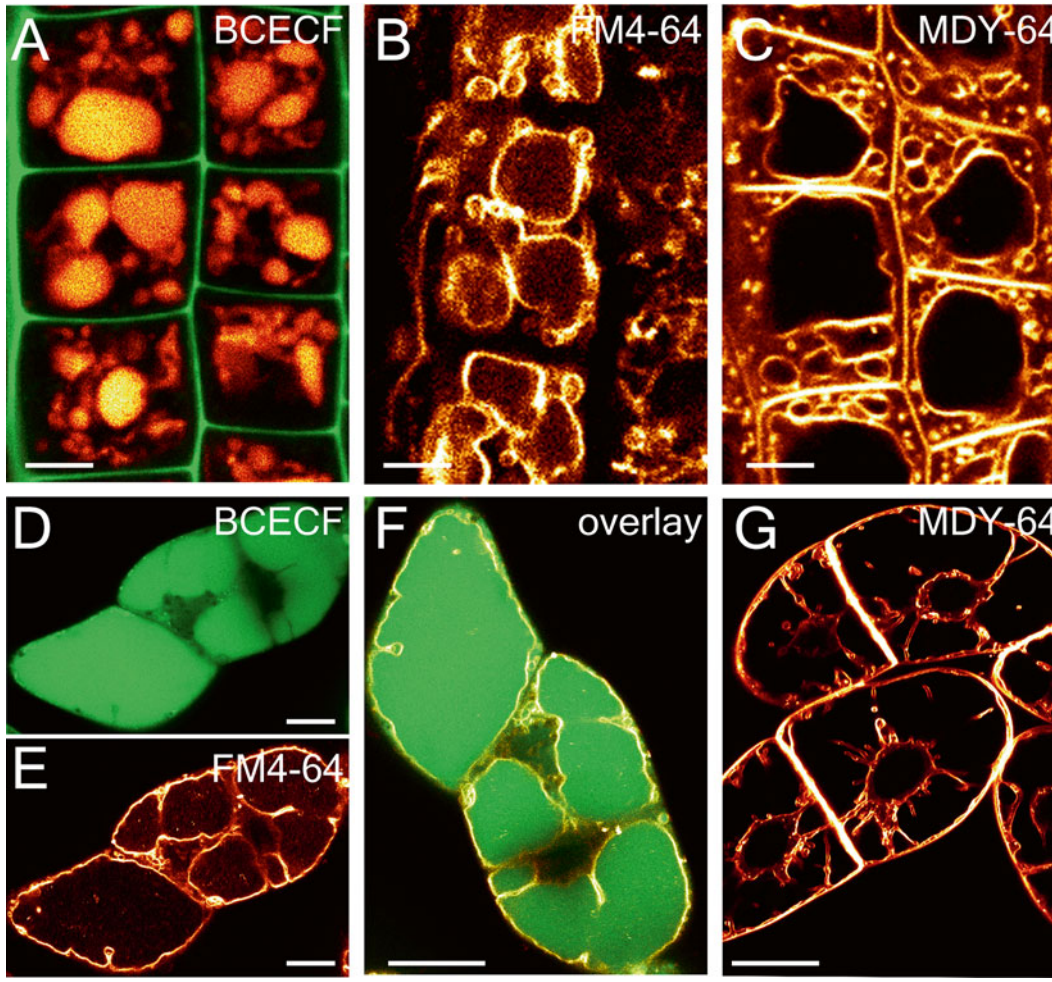

Fig. 2 Staining of the tonoplast and vacuolar lumen in *Arabidopsis* roots or BY-2 cells by BCECF-AM, FM4-64, and MDY-64. (**a**–**c**) Shows staining of epidermal *Arabidopsis* root cells. (**d**–**g**) Shows staining of BY-2 cells. (**a**) BCECF-AM (*orange*) labels the acidic lumen of the vacuole; propidium iodine was used as a counterstain (*green*). (**b**) Long-term uptake of the endocytotic tracer FM4-64 led to integration into the tonoplast. (**c**) MDY-64 labeling of the tonoplast membrane. (**d**) Staining of the vacuolar lumen in BY-2 cells with BCECF-AM. (**e**) FM4-64 labeled tonoplast and in (**f**) colocalization of BCECF-AM and FM4-64. (**g**) Shows staining of the tonoplast with MDY-64. Scale bar: (**a**–**c**) 7 μm; (**d**–**g**) 20 μm

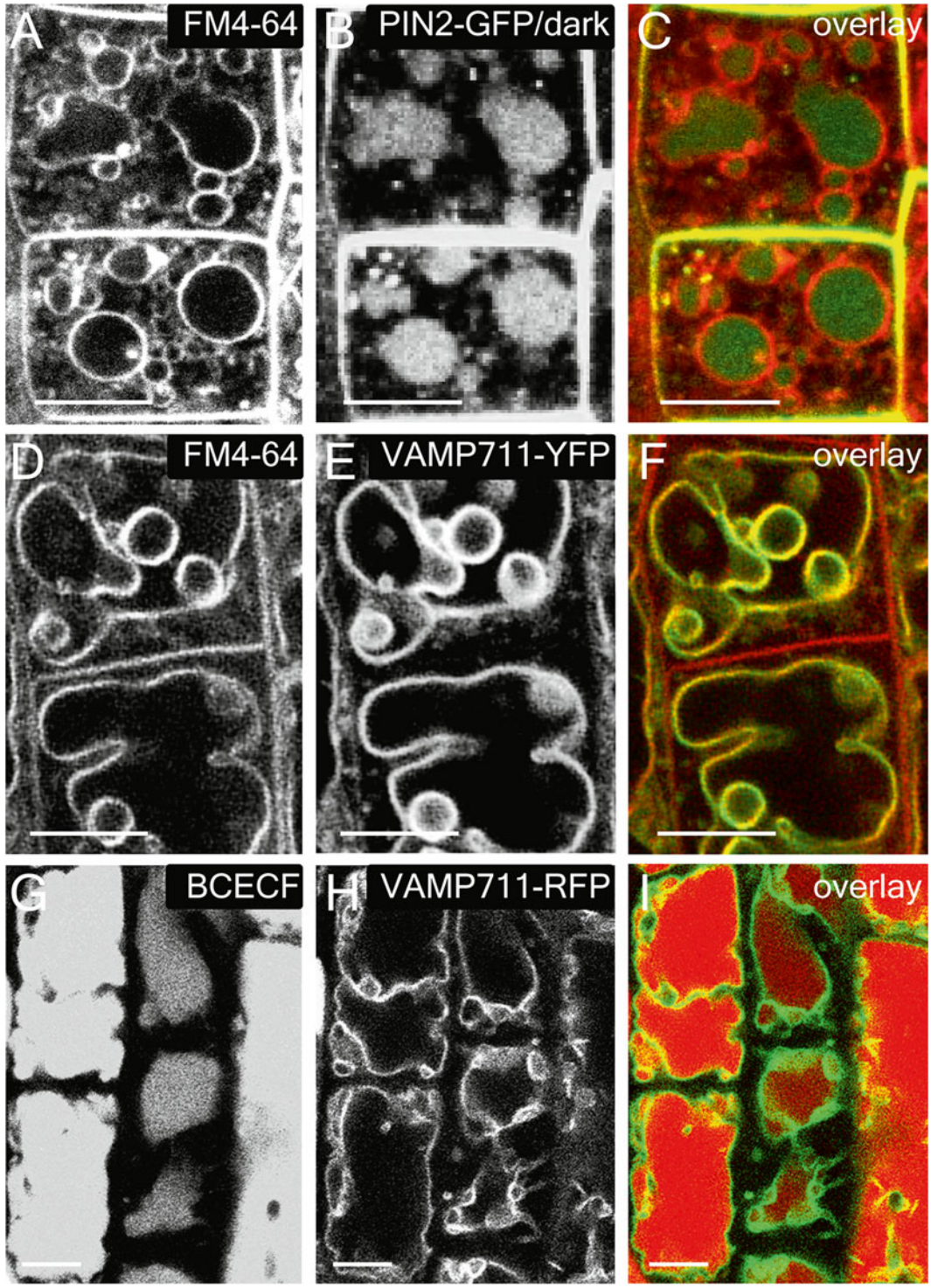

Fig. 3 Colabeling of the respective dyes with established fluorescent marker lines in epidermal *Arabidopsis* root cells. (**a**–**c**) Colocalization of FM4-64 long-term uptake with vacuolar targeted PIN2-GFP (**b**); *PIN2::PIN2-GFP* plants were kept in the dark for 2.5 h and subsequently stained for 30 min with FM4-64 (**a**) followed by a 3 h washout in darkness. (**c**) Overlay of (**a**) (FM4-64; *red*) and (**b**) (PIN2-GFP; *green*). FM4-64 (**d**) colocalization with VAMP711-YFP (**e**). (**f**) Overlay of (**d**) (FM4-64; *red*) and (**e**) (VAMP711-YFP; *green*). (**g**) BCECF-AM uptake in the acidic lumen of the vacuole. (**h**) VAMP711-RFP decorates tonoplast. (**i**) Overlay of (**g**) (BCECF-AM; *red*) and (**h**) (VAMP711-RFP; *green*). Scale bar: (**a**–**i**) 7 μm

Table 1
Dye preparation and characteristics

Stain	Solvent	Stock concentration (mM)	Working concentration	Excitation (nm)	Emission (nm)
BCECF-AM	DMSO	10	1:1,000	488	520
FM4-64	DMSO	4/20[a]	1:1,000	515	734
MDY-64	DMSO	0.25	1:1,000	451	497

[a]For BY-2 cell culture usage

1.2 FM4-64

The styryl dye FM4-64 (FM = Fei Mao) binds to the outer lipid leaflet of the plasma membrane and enters cells specifically via endocytosis. Following its internalization, the dye reaches the endosomal compartments [6] and eventually the endocytic journey ends at the tonoplast [7]. Hence, FM4-64 does not label the tonoplast alone. However, relative specific labeling is possible in a time-dependent manner: Long-term uptake (starting 2–3 h after application) will lead to a high accumulation of the dye at the tonoplast (Figs. 2b, e and 3a, d). The lipophilic dye has its excitation and emission maxima at 515 nm and 640 nm, respectively (Table 1).

1.3 MDY-64

The yeast vacuolar membrane stain MDY-64 [8] is used in various plant species and labels the cell wall/apoplast and the tonoplast [9–11] (Fig. 2). MDY-64 is also a hydrophobic styryl dye (Fig. 1), showing excitation and emission maxima of 451 nm and 497 nm, respectively (Table 1). One of the major advantages of using MDY-64 is the fast and reliable staining, giving a strong fluorescent signal 5 min after application. The dye appears reasonably specific for the tonoplast; however, in addition it colors the cell exterior and some smaller compartments, possibly related to prevacuolar compartments (Fig. 2c).

The specificity of dyes remains a critical issue; however, the morphology of the vacuole helps to clearly distinguish it from other cellular compartments. We would like to mention that a range of other vacuolar stains is available, such as neutral red (reviewed in ref. 12), lucifer yellow [13], lysotracker, and acridine orange (here used to follow stomata dynamics [14]). In addition to dyes, fluorescent fusion proteins can also be used to label the tonoplast (e.g., using VAMP711-YFP) or the lumen of the vacuole (e.g., through PIN2-GFP dark treatments [15]). These markers can be applied in combination with vacuolar staining methods (Fig. 3a–i). For an overview of *Arabidopsis* marker lines and fluorescent probes currently available, we refer to the chapter about vacuoles on the "illuminated plant cell" webpage (http://www.illuminatedcell.com/Vacuolarsystem.html).

2 Materials

2.1 Plant Growth

Cultivation media and growth conditions of *Arabidopsis thaliana* seedlings and the Bright Yellow-2 (BY-2) cell line.

1. Prepare *Arabidopsis* half strength (½) Murashige and Skoog (MS) medium using 2.15 g/L MS salts (Duchefa, NL), 1 % sucrose, and 0.5 g/L MES. Adjust the media pH with KOH to 5.7. For solid media preparation, add 0.8 % plant agar (Duchefa, NL) before autoclaving.
2. Prepare liquid BY-2 medium using 3 % sucrose, 4.3 g/L Murashige and Skoog salts (Duchefa, NL), 100 mg/L inositol, 1 mg/L thiamin, 0.2 mg/L 2,4-dichlorophenoxacetic acid (2,4-D), and 200 mg/L KH_2PO_4. Adjust the media pH with KOH to 5.8.
3. Grow seedlings at 22 °C on vertically oriented plates (Greiner bio-one, D, No. 688161), sealed with Leucopore (Duchefa, NL). Use a long day regime of 16-h light and 8-h darkness.
4. Cultivate BY-2 cells at 25 °C in darkness on an orbital incubator at 150 rpm in 100 mL Erlenmeyer flasks supplemented with liquid medium. Subculture the cells weekly (50× dilution).

2.2 Preparation of Dye Solution

1. BCECF-AM (Life Technology, Molecular Probes, CA, USA) stock solution preparation. Solution of 10 mM in DMSO. To avoid frequent freezing and thawing, divide the stock solution into aliquots and store frozen at −20 °C. Protect the solution from light to ensure compound stability (*see* **Note 1**). The stock solution should be stable for at least 6 months (Table 1).
2. FM4-64 (Life Technology, Molecular Probes, CA, USA) stock solution preparation. Solution of 4 mM and/or 20 mM in DMSO. To avoid frequent freezing and thawing divide the stock solution into aliquots and store frozen at −20 °C or at 4 °C. Protect the solution from light to ensure compound stability. The stock solution should be stable for at least 6 months (Table 1).
3. MDY-64 (Life Technology, Molecular Probes, CA, USA) stock solution preparation. Solution of 0.25 mM in DMSO. To avoid frequent freezing and thawing divide the stock solution into aliquots and store frozen at −20 °C. Protect the solution from light to ensure compound stability. The stock solution should be stable for at least 6 months (Table 1).

2.3 Used Transgenic Arabidopsis Lines

pUBQ10::VAMP711-YFP/RFP [16] and *PIN2::PIN2-GFP* [17] (described previously).

2.4 Microscope

For live cell imaging, mount the roots in liquid ½ MS medium and record—here with a Leica DM6000 CS, TCS AOBS confocal laser scanning microscope (SP5) using an HCX PL APO CS 63.0×1.20 WATER objective. Set the emission bandwidth of the PMT to the indicated nm range of each dye and use a laser for excitation—here the Argon or the DPSS 561.

3 Methods

Carry out all procedures at room temperature (22 °C).

3.1 Probing Arabidopsis Roots with BCECF-AM

1. Prepare a multiwell plate (we suggest a 12-well plate; Greiner bio-one, No. 665180) by adding 1–1.5 mL of liquid ½ MS medium to each well.
2. Supplement the medium with BCECF-AM to a final concentration of 10 μM (1:1,000 dilution) (*see* **Note 2**). Mix gently to ensure dye dispersion in the medium.
3. Carefully transfer the seedling into the dye-complemented liquid medium (*see* **Note 3**) and incubate for 1 h in darkness (wrap the well plate in aluminum foil).
4. Wash the seedlings by replacing the staining solution with ½ MS medium and incubate them on an orbital shaker (80 rpm) for 5 min. The orbital shaker step is optional, but will lead to consistent staining.
5. Transfer the seedlings to fresh ½ MS medium to preserve vitality until imaging. Immediate imaging is advisable.
6. Visualize the stained roots by fluorescent or confocal microscopy (Table 1).

3.2 Probing Arabidopsis Roots with FM4-64

1. Prepare a multiwell plate (we suggest a 12-well plate; Greiner bio-one, No. 665180) by adding 1–1.5 mL of liquid ½ MS medium to each well.
2. Supplement the medium with FM4-64 to a final concentration of 4 μM (1:1,000 dilution). Mix gently to ensure dye dispersion in the medium.
3. Carefully transfer the seedlings into the dye-complemented liquid medium (*see* **Note 3**) and incubate for 30 min in darkness (wrap the well plate in aluminum foil).
4. Place the seedlings in fresh ½ MS medium and incubate them on an orbital shaker (80 rpm) for 3–4 h (*see* **Note 4**), again in darkness (*see* **Note 5**), to allow the transportation of the stain to the tonoplast membrane before imaging. The orbital shaker step is optional, but will lead to consistent staining. Immediate imaging is advisable.
5. Visualize the stained roots by fluorescent or confocal microscopy (Table 1).

3.3 Probing Arabidopsis Roots with MDY-64

1. Prepare a multiwell plate (we suggest a 12 well plate; Greiner bio-one, No. 665180) by adding 1–1.5 mL of liquid ½ MS medium to each well.
2. Supplement the medium with MDY-64 to a final concentration of 0.25 μM (1:1,000 dilution). Mix gently to ensure dye dispersion in the medium.
3. Carefully transfer the seedlings into the dye-complemented liquid medium (*see* **Note 3**) and incubate for up to 5 min (*see* **Note 6**).
4. Place the seedlings in fresh ½ MS medium to preserve the vitality until imaging. Immediate imaging is advisable.
5. Visualize the stained roots by fluorescent or confocal microscopy (Table 1).

3.4 Probing BY-2 Cells with BCECF-AM

1. Transfer 1.5 mL of a 3-day-old BY-2 suspension culture in a 2 mL reaction tube. Use trimmed (3–4 mm) 1 mL pipet tips.
2. Add BCECF-AM (final concentration of 10 μM; 1:1,000 dilution; *see* **Note 2**) to the cells and incubate for 10 min on an orbital shaker (100 rpm).
3. Pellet the cells by centrifugation (800 rcf) and replace the staining solution with liquid BY-2 MS medium. Resuspend the cells carefully with a trimmed 1 mL tip. Repeat this step once.
4. Use a trimmed 200 μL pipet tip to transfer some of the stained BY2 cells onto a microscope slide (*see* **Note 7**).
5. Visualize the stained cells by fluorescent or confocal microscopy (Table 1).

3.5 Probing BY-2 Cells with FM4-64

1. Transfer 1.5 mL of a 3-day-old BY-2 suspension culture in a 2 mL reaction tube. Use trimmed (3–4 mm) 1 mL pipet tips.
2. Add FM4-64 (final concentration of 20 μM; 1:1,000 dilution) to the cells and incubate for 5 min on an orbital shaker (100 rpm).
3. Pellet the cells by centrifugation (800 rcf) and replace the staining solution with liquid BY-2 MS medium. Resuspend the cells carefully with a trimmed 1 mL tip.
4. Incubate the cells on an orbital shaker (100 rpm) for 3–4 h (*see* **Note 4**) in darkness (*see* **Note 5**) to allow the transportation of the stain to the tonoplast membrane before imaging.
5. Use a trimmed 200 μL tip to pipet/transfer some of the stained BY2 cells onto a microscope slide (*see* **Note 7**).
6. Visualize the stained cells by fluorescent or confocal microscopy (Table 1).

3.6 Probing BY-2 Cells with MDY-64

1. Transfer 1.5 mL of a 3-day-old BY-2 suspension culture in a 2 mL reaction tube. Use trimmed (3–4 mm) 1 mL pipet tips.

2. Add MDY-64 (final concentration of 0.25 μM; 1:1,000 dilution) to the cells and incubate for max 5 min on an orbital shaker (100 rpm) (*see* **Note 6**).
3. Pellet the cells by centrifugation (800 rcf) and replace the staining solution with liquid BY-2 MS medium. Resuspend the cells carefully with a trimmed 1 mL tip.
4. Use a trimmed 200 μL tip to pipet/transfer some of the stained BY2 cells onto a microscope slide (*see* **Note 7**).
5. Visualize the stained cells by fluorescent microscopy (Table 1).

4 Notes

1. BCECF-AM is normally colorless and nonfluorescent (although faint color and fluorescence are tolerable). If the solution exhibits strong fluorescence and coloration (indicated by absorbance at >400 nm), it probably contains a significant amount of hydrolyzed material and should be discarded.
2. To improve the BCECF-AM uptake into the cells, supplement the staining solution with 0.02 % pluronic acid (Pluronic F-127 solution, Life Technology, Molecular Probes, CA, USA).
3. To prevent the seedlings from floating on the staining solution, carefully spray the plates/seedlings with water before placing them into the ½ MS medium.
4. To shift the plasma membrane signal toward the tonoplast, increase the incubation time in (FM4-64 unsupplemented) liquid medium.
5. Long-term dark incubations may affect the vacuolar pH and biogenesis. If necessary, the experiment can be also carried out in light.
6. If the 5-min incubation step is extended, MDY-64 will unspecifically label other intracellular compartments.
7. To protect the cells from the high pressure of the cover slip, use tape as a spacer between the coverslip and microscope slide.

Acknowledgement

We are grateful to N. Geldner and C. Luschnig for providing material, D. Whittaker for help in preparing the manuscript, and the BOKU-VIBT Imaging Center for access and expertise. This work was supported by the Vienna Science and Technology Fund (WWTF) (to J.K.-V.) and the Deutsche Forschungsgemeinschaft (DFG) (personal postdoctoral research grant to C.L. and D.S.).

References

1. Wink M (1993) The plant vacuole: a multifunctional compartment. J Exp Bot 44:231–246
2. Marty F (1999) Plant vacuoles. Plant Cell 11(4): 587–600
3. Herman EM, Larkins BA (1999) Protein storage bodies and vacuoles. Plant Cell 11(4):601–614
4. Löfke C, Luschnig C, Kleine-Vehn J (2013) Posttranslational modification and trafficking of PIN auxin efflux carriers. Mech Dev 130(1): 82–94
5. Ozkan P, Mutharasan R (2002) A rapid method for measuring intracellular pH using BCECF-AM. Biochim Biophys Acta 1572(1):143–148
6. Jelinkova A et al (2010) Probing plant membranes with FM dyes: tracking, dragging or blocking? Plant J 61(5):883–892
7. Löfke C, Dünser K, Kleine-Vehn J (2013) Epidermal patterning genes impose non-cell autonomous cell size determination and have additional roles in root meristem size control. J Integr Plant Biol 55(9):864–875
8. Cole L, Orlovich DA, Ashford AE (1998) Structure, function, and motility of vacuoles in filamentous fungi. Fungal Genet Biol 24(1–2): 86–100
9. Wiltshire EJ, Collings DA (2009) New dynamics in an old friend: dynamic tubular vacuoles radiate through the cortical cytoplasm of red onion epidermal cells. Plant Cell Physiol 50(10):1826–1839
10. Abrahams S et al (2003) The Arabidopsis TDS4 gene encodes leucoanthocyanidin dioxygenase (LDOX) and is essential for proanthocyanidin synthesis and vacuole development. Plant J 35(5):624–636
11. Jackson MA et al (2007) A bioinformatic approach to the identification of a conserved domain in a sugarcane legumain that directs GFP to the lytic vacuole. Funct Plant Biol 34(7):633–644
12. Schwab B, Hulskamp M (2010) Neutral red staining for plant vacuoles. Cold Spring Harb Protoc 2010(6):pdb prot4953
13. Hillmer S, Quader H, Robert-Nicoud M, Robinson DG (1989) Lucifer yellow uptake in cells and protoplasts of Daucas carota visualized by laser scanning microscopy. J Exp Bot 40(4):417–423
14. Gao XQ et al (2005) The dynamic changes of tonoplasts in guard cells are important for stomatal movement in Vicia faba. Plant Physiol 139(3):1207–1216
15. Löfke C et al (2013) Asymmetric gibberellin signaling regulates vacuolar trafficking of PIN auxin transporters during root gravitropism. Proc Natl Acad Sci U S A 110(9):3627–3632
16. Geldner N et al (2009) Rapid, combinatorial analysis of membrane compartments in intact plants with a multicolor marker set. Plant J 59(1):169–178
17. Abas L et al (2006) Intracellular trafficking and proteolysis of the Arabidopsis auxin-efflux facilitator PIN2 are involved in root gravitropism. Nat Cell Biol 8(3):249–256

Chapter 9

Live Cell Imaging of FM4-64, a Tool for Tracing the Endocytic Pathways in *Arabidopsis* Root Cells

Adeline Rigal, Siamsa M. Doyle, and Stéphanie Robert

Abstract

Confocal live imaging of the amphiphilic styryl dye FM4-64 is a valuable technique to monitor organelle dynamics and in particular endocytic pathways. After application in plants, FM4-64 immediately stains the plasma membrane and is then integrated on vesicles following endomembrane system-dependent internalization processes. Over time, FM4-64 becomes distributed throughout the full vesicular network from the plasma membrane to the vacuole, including the components of the secretory pathways. Here we provide succinct examples of the many important developmental processes in plants that rely on endocytosis and describe two suitable methods to trace the endocytic pathways in *Arabidopsis thaliana* root cells based on the uptake of FM4-64.

Key words Endocytosis, FM4-64, Confocal microscopy, Root, Epidermal cells

1 Introduction and Minireview

Because of the presence of the rigid cell wall and high turgor pressure, the existence of endocytosis in higher plants was controversial for some time [1–3]. However, recent technological advances such as the use of styryl and filipin dyes, the fluid phase marker Luciferase Yellow, fluorescent protein tagging, and pharmacological approaches have demonstrated the existence of endocytosis in plants [4–7]. In this book chapter, we provide some examples of the many developmental processes in plants for which endocytosis events are essential, before focusing on the use of the styryl dye *N*-(3-triethylammoniumpropyl)-4-(6-(4-(diethylamino) phenyl) hexatrienyl) pyridinium dibromide (FM4-64) to image the endocytosis process.

FM4-64 was first developed to follow endocytosis events in animal nerve cells [8]. Due to its amphiphilic nature, FM4-64 becomes anchored in the outer leaflets of lipid bilayers and only emits strong fluorescence in hydrophobic environments, such as lipid-rich membranes [9]. When exogenously applied, FM4-64 immediately stains the plasma membrane (PM) and starts to be

José M. Estevez (ed.), *Plant Cell Expansion: Methods and Protocols*, Methods in Molecular Biology, vol. 1242,
DOI 10.1007/978-1-4939-1902-4_9,

internalized by the invagination of endocytic vesicles. Due to the highly dynamic nature of the endomembrane system, its different components are marked within minutes following FM4-64 treatment. FM4-64 uptake has now also widely been used to trace endocytic pathways in cells of fungi and plants [10–17]. To perform FM4-64 staining of *Arabidopsis* epidermal root cells, we recommend to label young in vitro-grown seedlings in liquid medium containing 2 μM FM4-64 for 5 min before washing out the dye with dye-free liquid medium [18–20]. These consecutive steps are best performed on ice (at 4 °C) to inhibit the process of endocytosis before imaging [21]. After removing the seedlings from the wash (time 0), the seedlings can be mounted on slides in dye-free liquid medium at room temperature, FM4-64 uptake imaged with a confocal laser scanning microscope (CLSM), and the kinetics of internalization analyzed. The excitation maximum for FM4-64 is 515 nm, consequently either the 488 or 514 nm argon ion laser lines of a CLSM should be used to image FM4-64 localization.

Here, we recommend monitoring the kinetics of FM4-64 staining in the epidermal cell layer of *Arabidopsis* roots by recording the uptake every minute after time 0 (starting as soon as the seedlings are mounted) for 30 min to follow the dynamic process of endocytosis.

All organisms possess the ability to receive environmental and internal signals and to respond in ways that enhance their survival and reproductive success. Because of their sessile life style, plants have acquired the capacity to grow continuously, adapting their architecture in response to signals. The endomembrane trafficking network is essential for mediating rapid responses to external and endogenous stimuli. Within this tightly regulated and highly dynamic network, endocytosis is the cellular process whereby the PM invaginates to form membrane-bounded vesicles, allowing the transport of PM and extracellular components into the cell [22, 23]. The internalized vesicles are either recycled back to the PM via early endosomal *trans*-Golgi network (TGN) compartments or targeted to late endosomal compartments, prevacuolar compartments (PVC)/multivesicular bodies (MVB), and the lytic vacuole [24–27]. Endocytosis is well conserved within the eukaryotic kingdom and is essential for many different cellular functions. In plants, these functions include regulation of cell polarity, PM-localized protein recycling, cell-to-cell communication, transduction and degradation of signaling molecules, and nutrient uptake [28–34].

Most aspects of plant development are controlled by the spatio-regulation of the phytohormone auxin, with the most abundant endogenous auxin being indole acetic acid (IAA; [35, 36]). Local auxin biosynthesis, metabolism, and directional transport contribute to the generation of auxin maxima and gradients [37–44]. Polarized auxin transport occurs in a cell-to-cell manner and is mediated by auxin efflux and influx carriers [45, 46]. Among them,

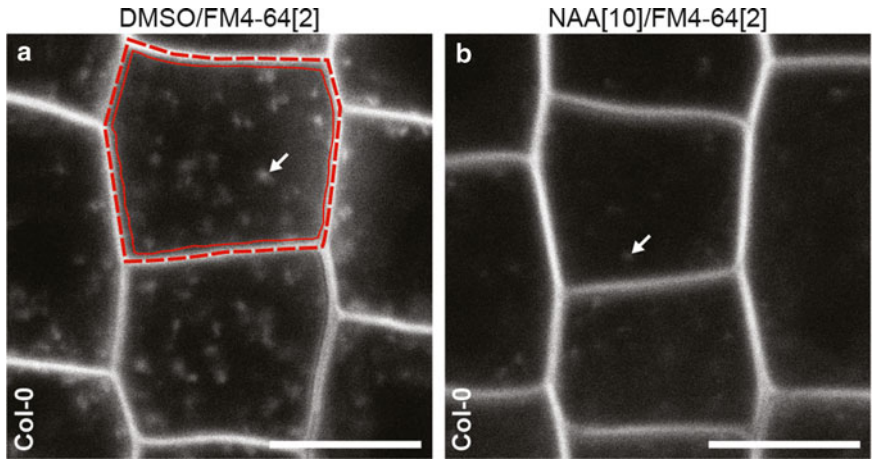

Fig. 1 Root epidermal cells of *Arabidopsis thaliana* ecotype Columbia-0 (Col-0) seedlings labeled with 2 μM FM4-64, 5 min after endocytosis was restarted (*see* Subheading 3). Before labeling, the seedlings were treated for 30 min with (**a**) solvent only (DMSO) or (**b**) 10 μM of the synthetic auxin 1-*naphthaleneacetic acid* (NAA), demonstrating that auxin inhibits endocytosis. *Red dotted* and *continuous lines* represent lines that should be drawn in ImageJ to measure the fluorescence intensity of the plasma membrane and cell, respectively. *White arrows* mark endocytic early endosomal compartments labeled with FM4-64. Scale bars represent 10 μm (Color figure online)

the PIN-FORMED (PIN) auxin efflux carriers are polarly localized at the PM and are sufficient for the establishment of an auxin gradient [47]. PIN subcellular localization is dynamically regulated by endocytosis at the PM [45]. Hence, genetic interference with important regulators of endocytic trafficking, such as the ADP-ribosylation factor-guanine nucleotide exchange factors (ARF-GEFs) GNOM and BEN1 and the Rab GTPase RAB5, leads to PIN mislocalization and auxin-related developmental defects [6, 18, 30]. To date, the best-characterized endocytic pathway in plants, and indeed all eukaryotes, is mediated by clathrin proteins [48, 49], which play a major role in the formation of coated vesicles [22]. It has been shown that clathrin-mediated endocytosis is the most important endocytic pathway by which PIN localization is regulated; hence, a disruption of clathrin machinery by pharmacological and genetic approaches impairs PIN localization and polarity [31, 48, 50, 51], leading to auxin transport problems and developmental defects such as altered gravitropism, embryogenic patterning, and organogenesis [50, 52].

It has been shown that auxin itself promotes the retention of PIN proteins at the PM by inhibiting endocytosis (Fig. 1; [51, 53]), thereby regulating its own transport at the PM. Furthermore, endocytosis regulates changes in auxin distribution and flow within tissues in response to environmental stimuli such as gravity and light [54–58]. For example, gravistimulation induces differential auxin levels in the root partially via endocytosis mechanisms. In

response to the gravitropic stimulus, endocytic vacuolar targeting of PIN2 is enhanced in the upper side of the root, leading to decreased PIN2 at the PM, while endocytosis of PIN2 is inhibited in the lower side of the root, leading to increased PIN2 at the PM [15, 53, 59]. This asymmetry of PIN2 across the root establishes the differential auxin flux required for gravitropic bending [60].

Endocytosis is also involved in regulating intracellular levels of micronutrients, such as boron, which is essential for plant development [61]. Boron deficiency affects many physiological processes and is a widespread agricultural problem [62, 63]; however, boron is toxic when present in excess [64]. Characterization of the *Arabidopsis* mutant *bor1-1* (*high boron requiring1-1*) which requires a high level of boron to grow normally [65] led to the identification of the BOR boron efflux transporters. Among them, BOR1, a boron efflux transporter for xylem loading, is mainly expressed in root pericycle, allowing the translocation of boron from the root to the shoot under boron limitation [66]. Under boron deficiency BOR1 is PM localized and is constantly recycled between the PM and early endosomes, while under high levels of boron BOR1 is targeted to the vacuole for degradation [64].

The presence and importance of endocytosis in plant cells is now beyond dispute. The endocytosis process, essential for protein turnover (targeting, recycling, and degradation), is of fundamental importance for many processes during plant development, organ differentiation, and defense responses. Increased knowledge of the mechanisms regulating endomembrane trafficking has been facilitated by technological advances, including the use of FM4-64 dyes, which is one of the most useful techniques for monitoring and understanding endocytosis pathways.

2 Materials

1. Fine balance.
2. Autoclave.
3. Opaque microcentrifuge tubes.
4. 24-well plates.
5. Ice.
6. Curved tip forceps or straight microdissection forceps.
7. Aluminum foil.
8. Glass slides (76 × 26 mm).
9. Coverslips (24 × 50 mm).
10. Timer with count-up function.
11. Confocal laser scanning microscope (CLSM) system equipped with an argon ion laser with lines at 488 and/or 514 nm.

12. Image J software (http://rsbweb.nih.gov/ij/).
13. Liquid ½ Murashige and Skoog (MS) medium: MS medium, distilled water, sucrose, 10 M potassium hydroxide (*see* **Note 1**). Dissolve 2.2 g/l MS medium in distilled water. Adjust the pH to 5.6 using 10 M potassium hydroxide. For medium supplemented with 1 % sucrose, add 10 g/l sucrose before adjusting the pH. Autoclave before use.
14. Plant material: 4- to 6-day-old *Arabidopsis* seedlings. Growing seedlings on vertically orientated agar plates is recommended (*see* **Notes 1** and **2**).
15. Dimethyl sulfoxide (DMSO)
    CAUTION: DMSO is harmful, personal protective equipment is needed.
16. *N*-(3-triethylammoniumpropyl)-4-(6-(4-(diethylamino) phenyl) hexatrienyl) pyridinium dibromide (FM4-64) stock solution (2 mM): FM4-64, DMSO. At room temperature, dissolve 12.15 mg FM4-64 in DMSO until the total volume is 10 ml. To avoid repeated defrosting and refreezing, aliquot to smaller volumes (20 µl) in opaque tubes and store at −20 °C (*see* **Note 3**).
    CAUTION: FM4-64 is harmful, personal protective equipment is needed. FM4-64 is light sensitive and should be kept in a dry, cool, and well-ventilated place.
17. Brefeldin A (BFA) stock solution (50 mM): BFA, DMSO. At room temperature, dissolve 14 mg of BFA in DMSO until the total volume is 1 ml. Aliquot to smaller volumes (10 µl) to avoid repeated defrosting and refreezing. Store at −20 °C.

3 Methods

3.1 FM4-64 Staining

Before starting the experiment, place one aliquot of FM4-64 solution (2 mM) at room temperature for approximately 15 min.

1. Set up the staining solution by mixing 1 µl of FM4-64 stock solution (2 mM) and 1 ml of liquid medium (working concentration 2 µM, *see* **Note 4**) directly in one well of a 24-well plate. Pipette the liquid up and down a few times to homogenize the staining solution.
2. Place 1 ml of dye-free liquid medium in each of two other wells for use as washing solutions.
3. Place the multiwell plate (just prepared) on ice for 15–30 min before the following steps, to ensure that the staining and washing solutions are cooled down to 4 °C (*see* **Note 5**).
4. Gently transfer seedlings to the staining solution (*see* **Notes 2** and **6**), wrap the multiwell plate in aluminum foil and incubate for precisely 5 min on ice (*see* **Notes 3** and **5**).

5. Transfer the seedlings consecutively to each of the two cold fresh washing solutions to remove free FM4-64. Keep working on ice.
6. Pipette 100 µl of liquid medium onto a glass slide. Use the same medium as used throughout the protocol. Gently transfer, orientate, and align the seedlings on the slide (*see* **Note 6**). Cover with a coverslip and press it down gently along its sides with the forceps (*see* **Note 7**). As soon as the seedlings are placed on the slide at room temperature, the endocytosis process starts. Therefore, this time point is considered as 0 and the timer should be started in count-up mode at precisely this moment.
7. Observe the fluorescence using confocal laser microscopy. FM4-64 is excited at 488 or 514 nm (excitation maximum 515 nm) and detected at 640 nm (emission maximum 640 nm). The laser intensity should be adjusted and the same settings maintained during the entire experiment (*see* **Note 8**).
8. Focus on the epidermal cell layer of each root. Adjust the focus to directly underneath the PM in order to visualize a focal plane through the cytoplasm above the vacuole. To acquire the images, we recommend the use of a 40× water immersion lens with an additional digital magnification of 2 or 4.
9. Take an image every minute for 30 min to monitor the endocytosis process (*see* **Notes 9** and **10**).
10. Perform at least three biological replicates, using at least ten seedlings in total per replicate (*see* **Note 11**).

3.2 Alternative Method Using BFA

In *Arabidopsis* roots, BFA inhibits trafficking pathways from the endosomes to the PM but is not effective in modifying trafficking from the PM to the endosomes [6]. This differential effect leads to the agglomeration of membrane material in so-called BFA bodies. Consequently, BFA is a nice pharmacological tool to monitor trafficking from the PM to endosomal compartments in *Arabidopsis* roots.

Place one aliquot of FM4-64 solution (2 mM) at room temperature for approximately 15 min before starting the staining (**step 5** below).

1. Prepare BFA solution (working concentration 25 µM) by mixing 0.5 µl of BFA (50 mM) per ml of liquid medium (4 ml needed in total).
2. To pretreat the seedlings with BFA, add 1 ml of the BFA solution to a well of a 24-well plate and gently transfer the seedlings to the solution (*see* **Notes 2** and **6**). Incubate for 60 min at room temperature.
3. Add 1 ml of BFA solution to each of three different wells of a new 24-well plate.

4. Put this newly prepared plate on ice for 15–30 min before the following steps, to ensure that the experiment will be performed at 4 °C (*see* **Note 5**).
5. Set up the staining solution by mixing 1 μl of FM4-64 stock solution (2 mM) (working concentration 2 μM, *see* **Note 4**) directly into one well containing 1 ml of BFA solution in the 24-well plate. Pipette the liquid up and down a few times to homogenize the staining solution. Keep working on ice.
6. Gently transfer seedlings to the staining solution, wrap the multiwell plate in aluminum foil and incubate for precisely 5 min on ice (*see* **Notes 3** and **5**).
7. Transfer the seedlings consecutively to each of the two wells containing cold fresh dye-free BFA solution to remove free FM4-64. Keep working on ice.
8. Pipette 100 μl of dye-free BFA solution onto a glass slide. Gently transfer, orientate, and align the seedlings onto the slide (*see* **Note 6**). Cover with a coverslip and press it down gently along its sides with the forceps (*see* **Note 7**). As soon as the seedlings are placed on the slide at room temperature, the endocytosis process starts. Therefore, this time point is considered as 0 and the timer should be started in count-up mode at precisely this moment.
9. Observe the fluorescence using confocal laser microscopy. Start the observation after a maximum of 10 min at room temperature. The fluorescence of FM4-64 is excited at 488 or 514 nm (excitation maximum 515 nm) and detected at 640 nm (emission maximum 640 nm). The laser intensity should be adjusted and the same settings maintained during the entire experiment (*see* **Note 8**).
10. Focus on the epidermal cell layer of each root. Adjust the focus to directly underneath the PM in order to visualize a focal plane through cytoplasm above the vacuole. To acquire the images, we recommend the use of a 40× water immersion lens with an additional digital magnification of 2 or 4.
11. Take images at regular intervals such as every 3 min for 30 min to record the endocytosis process (*see* **Notes 9** and **10**).
12. Perform at least three biological replicates, using at least ten seedlings in total per replicate (*see* **Note 11**).

3.3 Quantification of FM4-64 Uptake

Measure the fluorescence intensity of the PM (the red dotted line in Fig. 1) and inside the cell (the red continuous line in Fig. 1) separately for a total of ten cells per root for each biological replicate using ImageJ software (National Institutes of Health, http://rsb.info.nih.gov/ij).

Before starting the measurements, adjust the line width to 3. To measure fluorescence, select the parameter *Mean Gray Value* in

the *Set Measurements* tab of the *Analyze* menu. To quantify the fluorescence at the PM, use the *Segmented Line* tool to draw along the PM and select *Measure*. To quantify the fluorescence intensity inside the cell, use the *Polygon Selection* tool to draw a polygon inside the PM and select *Measure*. Copy and paste the measurements to a Microsoft Excel table.

Calculate the ratio of intracellular and PM fluorescence intensities for each cell. The values should be normalized to the corresponding control for each experiment.

3.4 Quantification of FM4-64 Uptake for the Alternative Method Using BFA

The same quantifications of FM4-64 uptake as described in Subheading 3.3 can be performed. Additionally, the number of BFA bodies per cell, as well as their size, can also be quantified. To measure BFA body size, select the parameter *Area* in the *Set Measurements* tab of the *Analyze* menu. Use either the *Freehand* or *Oval Selection* tool to draw a circle around the BFA body and select *Measure*.

4 Notes

1. It is important to use the same liquid medium for treatments as used in solid form (with the addition of agar) for growth, to avoid stress on the seedlings.
2. Growing seedlings vertically allows easier transfer of the seedlings into liquid medium without damaging the roots.
3. The dye FM4-64 is unstable at room temperature and is sensitive to light.
4. This concentration of FM4-64 is thought to have no effect on the endocytic pathways in *Arabidopsis* root epidermal cells [21].
5. The staining of the PM by FM4-64 is immediate and the endocytosis process is very fast and highly dynamic. Working on ice inhibits endocytosis [21].
6. Use forceps to transfer seedlings from solid medium into liquid medium or onto a slide. Gently lift each seedling just under the cotyledons to avoid damage to the root.
7. At this step, make sure not to press too hard to avoid damage to the root. The root should be as flat as possible for a homogeneous longitudinal focal plane in your images.
8. Do not change the laser intensity parameters between image acquisitions throughout the entire experiment. This is extremely important for normalizing to the control and to compare the different time points during the endocytosis process.
9. When the seedlings are mounted on slides at room temperature, endocytosis restarts immediately. Start taking images as quickly

as possible (no more than 3 or 4 min after time 0). Make sure to change the root observed between each image to obtain a better representative sampling.

10. Image the FM4-64 fluorescence with gray scale settings instead of false color to ease visualization.
11. Due to biological variation, repetition is extremely important. Biological replicates should be performed on different days. We also recommend performing at least two technical replicates per biological replicate, meaning performing the experiment twice consecutively per biological replicate, using five different seedlings each time for a total of ten seedlings.

Acknowledgements

This work was supported by The Kempe Foundation (A.R.), The Knut and Alice Wallenberg Foundation (S.D.), and Vetenskapsrådet and VINNOVA (S.R., S.D.).

References

1. Cram WJ (1980) Pinocytosis in plants. New Phytol 84:1–17
2. Gradmann D, Robinson DG (1989) Does turgor prevent endocytosis in plant cells? Plant Cell Environ 12:151–154
3. Hawes C, Crooks K, Coleman J, Satiat-Jeunemaitre B (1995) Endocytosis in plants: fact or artefact? Plant Cell Environ 18: 1245–1252
4. Geldner N, Friml J, Stierhof Y-D, Jürgens G, Palme K (2001) Auxin transport inhibitors block PIN1 cycling and vesicle trafficking. Nature 413:425–428
5. Baluška F, Šamaj J, Hlavacka A, Kendrick-Jones J, Volkmann D (2004) Actin-dependent fluid-phase endocytosis in inner cortex cells of maize root apices. J Exp Bot 55:463–473
6. Geldner N, Anders N, Wolters H, Keicher J, Kornberger W, Muller P et al (2003) The *Arabidopsis* GNOM ARF-GEF mediates endosomal recycling, auxin transport, and auxin-dependent plant growth. Cell 112:219–230
7. Grebe M, Xu J, Möbius W, Ueda T, Nakano A, Geuze HJ et al (2003) Arabidopsis sterol endocytosis involves actin-mediated trafficking via ARA6-positive early endosomes. Curr Biol 13: 1378–1387
8. Betz WJ, Mao F, Smith CB (1996) Imaging exocytosis and endocytosis. Curr Opin Neurobiol 6:365–371
9. Bolte S, Talbot C, Boutte Y, Catrice O, Read ND, Satiat-Jeunemaitre B (2004) FM-dyes as experimental probes for dissecting vesicle trafficking in living plant cells. J Microsc 214: 159–173
10. Vida TA, Emr SD (1995) A new vital stain for visualizing vacuolar membrane dynamics and endocytosis in yeast. J Cell Biol 128:779–792
11. Hoffmann J, Mendgen K (1998) Endocytosis and membrane turnover in the germ tube of *Uromyces fabae*. Fungal Genet Biol 24:77–85
12. Belanger KD, Quatrano RS (2000) Membrane recycling occurs during asymmetric tip growth and cell plate formation in *Fucus distichus* zygotes. Protoplasma 212:24–37
13. Meckel T, Hurst AC, Thiel G, Homann U (2004) Endocytosis against high turgor: intact guard cells of *Vicia faba* constitutively endocytose fluorescently labelled plasma membrane and GFP-tagged K^+-channel KAT1. Plant J 39: 182–193
14. Ueda T, Yamaguchi M, Uchimiya H, Nakano A (2001) Ara6, a plant-unique novel type Rab GTPase, functions in the endocytic pathway of *Arabidopsis thaliana*. EMBO J 20:4730–4741
15. Kleine-Vehn J, Leitner J, Zwiewka M, Sauer M, Abas L, Luschnig C et al (2008) Differential degradation of PIN2 auxin efflux carrier by retromer-dependent vacuolar targeting. Proc Natl Acad Sci U S A 105:17812–17817

16. Kakar K, Zhang H, Scheres B, Dhonukshe P (2013) CLASP-mediated cortical microtubule organization guides PIN polarization axis. Nature 495:529–533
17. Jaillais Y, Fobis-Loisy I, Miège C, Rollin C, Gaude T (2006) AtSNX1 defines an endosome for auxin-carrier trafficking in *Arabidopsis*. Nature 443:106–109
18. Tanaka H, Kitakura S, De Rycke R, De Groodt R, Friml J (2009) Fluorescence imaging-based screen identifies ARF GEF component of early endosomal trafficking. Curr Biol 19:391–397
19. Nodzyński T, Feraru MI, Hirsch S, De Rycke R, Niculaes C, Boerjan W et al (2013) Retromer subunits VPS35A and VPS29 mediate prevacuolar compartment (PVC) function in *Arabidopsis*. Mol Plant 6(6):1849–1862
20. Naramoto S, Kleine-Vehn J, Robert S, Fujimoto M, Dainobu T, Paciorek T et al (2010) ADP-ribosylation factor machinery mediates endocytosis in plant cells. Proc Natl Acad Sci U S A 107:21890–21895
21. Jelínková A, Malínská K, Simon S, Kleine-Vehn J, Pařezová M, Pejchar P et al (2010) Probing plant membranes with FM dyes: tracking, dragging or blocking? Plant J 61:883–892
22. Low PS, Chandra S (1994) Endocytosis in plants. Annu Rev Plant Physiol Plant Mol Biol 45:609–631
23. Robinson DG, Jiang L, Schumacher K (2008) The endosomal system of plants: charting new and familiar territories. Plant Physiol 147: 1482–1492
24. Jürgens G (2004) Membrane trafficking in plants. Annu Rev Cell Dev Biol 20:481–504
25. Šamaj J, Read ND, Volkmann D, Menzel D, Baluška F (2005) The endocytic network in plants. Trends Cell Biol 15:425–433
26. Hicks GR, Raikhel NV (2010) Advances in dissecting endomembrane trafficking with small molecules. Curr Opin Plant Biol 13:706–713
27. Reyes FC, Buono R, Otegui MS (2011) Plant endosomal trafficking pathways. Curr Opin Plant Biol 14:666–673
28. Šamaj J, Baluška F, Voigt B, Schlicht M, Volkmann D, Menzel D (2004) Endocytosis, actin cytoskeleton, and signaling. Plant Physiol 135:1150–1161
29. Sharfman M, Bar M, Ehrlich M, Schuster S, Melech-Bonfil S, Ezer R et al (2011) Endosomal signaling of the tomato leucine-rich repeat receptor-like protein LeEix2. Plant J 68:413–423
30. Dhonukshe P, Tanaka H, Goh T, Ebine K, Mähönen AP, Prasad K et al (2008) Generation of cell polarity in plants links endocytosis, auxin distribution and cell fate decisions. Nature 456:962–966
31. Kleine-Vehn J, Wabnik K, Martinière A, Łangowski L, Willig K, Naramoto S et al (2011) Recycling, clustering, and endocytosis jointly maintain PIN auxin carrier polarity at the plasma membrane. Mol Syst Biol 7:540
32. Etxeberria E, Baroja-Fernandez E, Muñoz FJ, Pozueta-Romero J (2005) Sucrose-inducible endocytosis as a mechanism for nutrient uptake in heterotrophic plant cells. Plant Cell Physiol 46:474–481
33. Surpin M, Raikhel N (2004) Traffic jams affect plant development and signal transduction. Nat Rev Mol Cell Biol 5:100–109
34. Robatzek S, Chinchilla D, Boller T (2006) Ligand-induced endocytosis of the pattern recognition receptor FLS2 in *Arabidopsis*. Genes Dev 20:537–542
35. Vanneste S, Friml J (2009) Auxin: a trigger for change in plant development. Cell 136: 1005–1016
36. Tanaka H, Dhonukshe P, Brewer PB, Friml J (2006) Spatiotemporal asymmetric auxin distribution: a means to coordinate plant development. Cell Mol Life Sci 63: 2738–2754
37. Cheng Y, Dai X, Zhao Y (2006) Auxin biosynthesis by the YUCCA flavin monooxygenases controls the formation of floral organs and vascular tissues in *Arabidopsis*. Genes Dev 20:1790–1799
38. Stepanova AN, Robertson-Hoyt J, Yun J, Benavente LM, Xie DY, Doležal K et al (2008) TAA1-mediated auxin biosynthesis is essential for hormone crosstalk and plant development. Cell 133:177–191
39. Tao Y, Ferrer J-L, Ljung K, Pojer F, Hong F, Long JA et al (2008) Rapid synthesis of auxin via a new tryptophan-dependent pathway is required for shade avoidance in plants. Cell 133:164–176
40. Ruiz Rosquete M, Barbez E, Kleine-Vehn J (2012) Cellular auxin homeostasis: gatekeeping is housekeeping. Mol Plant 5:772–786
41. Peer WA, Blakeslee JJ, Yang H, Murphy AS (2011) Seven things we think we know about auxin transport. Mol Plant 4:487–504
42. Friml J, Benková E, Blilou I, Wisniewska J, Hamann T, Ljung K et al (2002) AtPIN4 mediates sink-driven auxin gradients and root patterning in *Arabidopsis*. Cell 108:661–673
43. Blilou I, Xu J, Wildwater M, Willemsen V, Paponov I, Friml J et al (2005) The PIN auxin efflux facilitator network controls growth and patterning in *Arabidopsis* roots. Nature 433: 39–44
44. Benková E, Michniewicz M, Sauer M, Teichmann T, Seifertová D, Jürgens G et al (2003) Local, efflux-dependent auxin gradients

as a common module for plant organ formation. Cell 115:591–602

45. Grunewald W, Friml J (2010) The march of the PINs: developmental plasticity by dynamic polar targeting in plant cells. EMBO J 29: 2700–2714
46. Kleine-Vehn J, Friml J (2008) Polar targeting and endocytic recycling in auxin-dependent plant development. Annu Rev Cell Dev Biol 24:447–473
47. Wiśniewska J, Xu J, Seifertová D, Brewer PB, Růžička K, Blilou I et al (2006) Polar PIN localization directs auxin flow in plants. Science 312:883
48. Dhonukshe P, Aniento F, Hwang I, Robinson DG, Mravec J, Stierhof YD et al (2007) Clathrin-mediated constitutive endocytosis of PIN auxin efflux carriers in *Arabidopsis*. Curr Biol 17:520–527
49. Ito E, Fujimoto M, Ebine K, Uemura T, Ueda T, Nakano A (2012) Dynamic behavior of clathrin in *Arabidopsis thaliana* unveiled by live imaging. Plant J 69:204–216
50. Kitakura S, Vanneste S, Robert S, Löfke C, Teichmann T, Tanaka H et al (2011) Clathrin mediates endocytosis and polar distribution of PIN auxin transporters in *Arabidopsis*. Plant Cell 23:1920–1931
51. Robert S, Kleine-Vehn J, Barbez E, Sauer M, Paciorek T, Baster P et al (2010) ABP1 mediates auxin inhibition of clathrin-dependent endocytosis in *Arabidopsis*. Cell 143:111–121
52. Wang C, Yan X, Chen Q, Jiang N, Fu W, Ma B et al (2013) Clathrin light chains regulate clathrin-mediated trafficking, auxin signaling, and development in *Arabidopsis*. Plant Cell 25:499–516
53. Paciorek T, Zažímalová E, Ruthardt N, Petrášek J, Stierhof Y-D, Kleine-Vehn J et al (2005) Auxin inhibits endocytosis and promotes its own efflux from cells. Nature 435: 1251–1256
54. Friml J, Wiśniewska J, Benková E, Mendgen K, Palme K (2002) Lateral relocation of auxin efflux regulator PIN3 mediates tropism in *Arabidopsis*. Nature 415:806–809
55. Kleine-Vehn J, Ding Z, Jones AR, Tasaka M, Morita MT, Friml J (2010) Gravity-induced PIN transcytosis for polarization of auxin fluxes in gravity-sensing root cells. Proc Natl Acad Sci 107:22344–22349
56. Ding Z, Galván-Ampudia CS, Demarsy E, Łangowski L, Kleine-Vehn J, Fan Y et al (2011) Light-mediated polarization of the PIN3 auxin transporter for the phototropic response in *Arabidopsis*. Nat Cell Biol 13:447–452
57. Zhang KX, Xu HH, Yuan TT, Zhang L, Lu YT (2013) Blue-light-induced PIN3 polarization for root negative phototropic response in *Arabidopsis*. Plant J 76:308–321
58. Rakusová H, Gallego-Bartolomé J, Vanstraelen M, Robert HS, Alabadí D, Blázquez MA et al (2011) Polarization of PIN3-dependent auxin transport for hypocotyl gravitropic response in *Arabidopsis thaliana*. Plant J 67:817–826
59. Abas L, Benjamins R, Malenica N, Paciorek T, Wiśniewska J, Moulinier-Anzola JC et al (2006) Intracellular trafficking and proteolysis of the *Arabidopsis* auxin-efflux facilitator PIN2 are involved in root gravitropism. Nat Cell Biol 8:249–256
60. Baster P, Robert S, Kleine-Vehn J, Vanneste S, Kania U, Grunewald W et al (2013) $SCF^{TIR1/AFB}$-auxin signalling regulates PIN vacuolar trafficking and auxin fluxes during root gravitropism. EMBO J 32:260–274
61. Broadley M, Brown P, Cakmak I, Rengel Z, Zhao F (2012) Function of nutrients: micronutrients. In: Marschner P (ed) Marschner's mineral nutrition of higher plants. Academic, New York
62. González-Fontes A, Rexach J, Navarro-Gochicoa MT, Herrera-Rodríguez MB, Beato VM, Maldonado JM et al (2008) Is boron involved solely in structural roles in vascular plants? Plant Signal Behav 3:24–26
63. Shorrocks VM (1997) The occurrence and correction of boron deficiency. Plant and Soil 193:121–148
64. Takano J, Miwa K, Yuan L, von Wirén N, Fujiwara T (2005) Endocytosis and degradation of BOR1, a boron transporter of *Arabidopsis thaliana*, regulated by boron availability. Proc Natl Acad Sci U S A 102:12276–12281
65. Noguchi K, Yasumori M, Imai T, Naito S, Matsunaga T, Oda H et al (1997) *bor1-1*, an *Arabidopsis thaliana* mutant that requires a high level of boron. Plant Physiol 115:901–906
66. Takano J, Noguchi K, Yasumori M, Kobayashi M, Gajdos Z, Miwa K et al (2002) *Arabidopsis* boron transporter for xylem loading. Nature 420:337–340

Chapter 10

Salt-Stress Regulation of Root System Growth and Architecture in *Arabidopsis* Seedlings

Lina Duan, Jose Sebastian, and Jose R. Dinneny

Abstract

In order to acclimate to the soil environment, plants need to constantly optimize their root system architecture for efficient resource uptake. Roots are highly sensitive to changes in their surrounding environment and root system responses to a stress such as salinity and drought can be very dynamic and complex in nature. These responses can be manifested differentially at the cellular, tissue, or organ level and between the types of roots in a root system. Therefore, various approaches must be taken to quantify and characterize these responses. In this chapter, we review methods to study basic root growth traits, such as root length, cell cycle activity and meristem size, cell shape and size that form the basis for the emergent properties of the root system. Methods for the detailed analysis of lateral root initiation and postemergence growth are described. Finally, several live-imaging systems, which allow for dynamic imaging of the root, will be explored. Together these tools provide insight into the regulatory steps that sculpt the root system upon environmental change and can be used as the basis for the evaluation of genetic variation affecting these pathways.

Key words Root systems, Salt stress, Growth traits, Root imaging

1 Introduction

Roots have evolved the ability to sense a myriad of environmental factors and use this information to drive changes in growth activities. As a model organ, *Arabidopsis* roots have a very simple and rotationally symmetric structure with a stereotypical tissue organization [1] (Fig. 1a). In the root apical meristem (RAM), the quiescent center (QC), a group of four to six cells with low mitotic activity sustains a pool of stem cells. These stem cells, which surround the QC, produce daughter cells that divide, expand, and subsequently differentiate and form the different cell types present in the adult root [2]. Unlike much of animal development, plants have evolved mechanisms to incorporate a variety of environmental cues to affect developmental decisions. Therefore, these exogenous signals have a unique role in determining the final architecture and morphology of the plant. Among the multitude of abiotic stresses that a

José M. Estevez (ed.), *Plant Cell Expansion: Methods and Protocols*, Methods in Molecular Biology, vol. 1242,
DOI 10.1007/978-1-4939-1902-4_10,

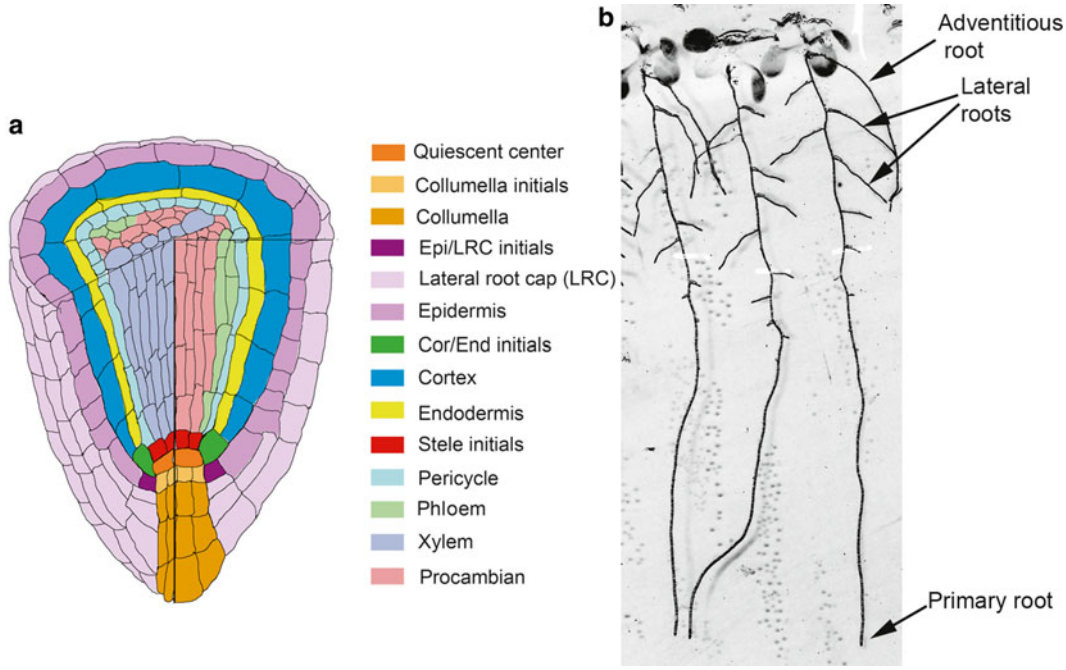

Fig. 1 *Arabidopsis* root structure. (**a**) Color-coded diagram of the cellular structure of *Arabidopsis* root tip. (**b**) Scanned image of *Arabidopsis* roots grown on Standard MS medium for 10 days. Different root types are marked by *arrows*

plant might face during its life cycle, drought and salinity represent some of the most challenging. Like many other environmental factors, they affect the plant's internal regulatory circuits controlling growth and development.

Drought and salinity affect plant growth and development mainly by causing cellular damage and disrupting the osmotic balance of the cell [3]. When water becomes limiting or contains more soluble molecules, like NaCl, the osmotic potential in the environment decreases, which restricts the movement of water into the plant roots causing osmotic stress [4]. Osmotic stress can impinge on cellular water balance and disrupts various cellular activities or in severe cases leads to plant death [5]. A hyper-osmotic environment can cause the plant cell to lose water, which reduces the turgor pressure of cells, thus affecting their ability to elongate [6]. Under hyper-osmotic stress conditions (NaCl concentrations above 150 mM), plasmolysis (separation of the plasma membrane from the cell wall accompanied with reduction in protoplast volume) may also occur eventually leading to cell death [7, 8].

Owing to their importance in water uptake from the soil, roots play a central role in initiating plant responses to water deficit conditions. Among the different root traits, root growth and architecture are particularly sensitive to changing environmental conditions. The root system of higher plants is often composed of different root types. In monocot plants such as maize, there are

embryonic-born primary and seminal roots, postembryonic-born lateral roots, and shoot born roots such as brace and crown roots [9]. In *Arabidopsis*, a eudicot model plant, the root system has a relatively simple structure consisting of a primary root that originates during embryogenesis and lateral roots that develop from the primary root. Adventitious roots also develop in *Arabidopsis* and originate from the shoot–root junction (Fig. 1b). These root types have different developmental programs and unique functions; thus, it is important to understand whether these root types respond to environmental changes differently and what is the relevance of these differences in a natural soil context. In this chapter, we give an overview of various developmental responses of roots to drought and salt stress and discuss the tools currently available to study these processes.

1.1 Drought Stress and Root System Responses

Broadly, drought mediated root responses can be categorized into developmental, physiological, and metabolic acclimatory mechanisms. A well-studied developmental response of roots to drought involves the spatial regulation of expansive growth. A process in which the root sustains cell elongation activities at the apical few millimeters (apical 3 mm in maize primary roots), while it is gradually suppressed further away from the root tip [10–13]. Even under severe drought conditions (0.4 MPa below the permanent wilting point of −1.5 MPa), maize primary roots maintain this apical most region of cell growth and elongation. Drought triggers accumulation of the phytohormone abscisic acid (ABA), and modifications in cell wall properties and rapid osmotic adjustments contribute to this growth maintenance [14]. Cell division activities in the root meristem region are suppressed under severe drought [15, 16]. Drought-treated roots also appear thinner due to a decrease in the rate of radial expansion [10]. In *Arabidopsis*, under severe water deficit, the primary root tip ceases meristematic activities and growth. Reactive oxygen species mediate programmed cell death in the meristematic region, which leads to root growth arrest [17]. The cessation of primary root growth subsequently promotes increased lateral root production. Jupp and Newman have shown that in *Lolium perenne* under low water potential conditions lateral root initiation and growth were enhanced [18]. However, others have reported that in *Arabidopsis* an osmotic stress treatment with mannitol (50 or 75 mM) resulted in an inhibition of lateral root growth [19]. Thus, it is plausible that there is variation in lateral root response depending on the type and severity of water stress.

Change in the distribution of roots within the soil column is another important adaptive response plants use to guard against water deficit. Studies in many plant species have demonstrated the capability of plants to sense and alter their root architecture so as to best suit growing conditions [20–24]. For example, after the exhaustion of top soil moisture, plants with a deep root system are able to access water present deep in the soil and thus evade drought.

1.2 Root Growth Regulation During Salt Stress

High soil salinity is one of the most pressing global agricultural stresses and often co-occurs with drought resulting in a serious challenge to root growth and development [25]. High salinity can be caused by excessive amounts of dissolved salts such as sodium chloride (NaCl) in the soil. Accumulation of other ions like K^+, Ca^{2+}, or Mg^{2+} can also contribute to high soil salinity. Accumulation of NaCl in cells leads to osmotic and ionic stresses, which results in toxicity and cell death as a consequence. For example, the excessive amount of NaCl in the environment will lead to a competition between Na^+ and K^+ transportation into the cells due to their similar chemical properties, and causes potassium deficiency [26]. K^+ is important in maintaining the activities of enzymes inside the cell, while the excessive Na^+ inhibits their activity [27, 28].

High salinity represses root growth by suppressing cell division and elongation [29, 30]. Cyclins, a group of protein that controls progress through cell cycle are transiently suppressed by salt stress in the root meristem. These changes in cyclin levels are associated with reduced meristem size and root growth [31, 32]. The reduced activity of cell division markers (CYCB1;2, CYCA2;1, as well as the cyclin-activated kinase, CDC2) in the root stele, especially pericycle cells is also associated with reduced lateral root initiation [31, 32]. Proper protein folding and endoplasmic reticulum stress regulation are involved in salt-stress mediated cell-cycle progression [33].

To shape plant cells, cell walls need to be synthesized to suit a particular form. The elasticity of the cell and the cell-expansion direction can be controlled by modifying the composition of the cell wall and synthesizing new wall materials. Under high salinity, cell expansion increases along the radial axis in the epidermis and cortex [31]. Mutants such as *sos5*, which have a defective cell wall structure, are more sensitive to salt stress in radial cell expansion [34]. These findings indicate the importance of proper cell wall structure in cell shape regulation under salt stress. Results from studies on the *SPR1* gene suggest that the cytoskeletal structure can be directly regulated by salt stress to affect cell shape and overall growth in roots [35, 36].

1.3 Cell-Type-Specific Responses Are Induced During Salt Stress

Distinct transcriptional and phenotypic changes have been found in different root cell types [37]. Cell-type-specific transcriptional profiling has also found that the majority of salt-stress regulated genes are regulated in a cell-type-specific manner. Interestingly, these unique transcriptional changes are well correlated with cell-type-specific phenotypic changes. For example, Dinneny et al. have shown that the radial expansion of the outer tissue layers under salt stress correlates with the down-regulation of cell wall biogenesis and tubulin genes [38]. As a common stress-induced secondary signal, changes in cytosolic Ca^{2+} concentration were also found to be regulated differently in each cell type during the salt stress response [39]. The cytoplasmic Ca^{2+} content is rapidly

induced by salt treatment in all tissue layers, however fluctuations are maintained only in the endodermis and pericycle [39], which suggests the presence of tissue-specific mechanisms for the induction and function of calcium signaling during salt stress.

ABA related transcriptional components have been found to be induced by salt stress in all cell types in the root [38]; however, it was not known whether it has different effects in each layer. Recently, it was shown that ABA has a similar effect on root system architecture as salt stress, both of which suppress lateral root growth by inducing a "growth quiescent phase" for 2–3 days [40, 41]. ABA signaling is the most important signal that mediates the salt response and it acts primarily in the endodermis in regulating lateral root growth under salt stress [41]. Salt stress also induces a brief growth quiescent phase at concentrations of NaCl above 140 mM in primary root, which is then followed by rapid growth recovery [42]. Interestingly, ABA signaling in the endodermis is found to play a positive role in promoting this growth recovery phase [42]. In these studies, instead of an end-point measurement, the growth dynamics of the *Arabidopsis* root is continuously monitored by automated time-lapse imaging, which gives more information about the dynamic nature of root growth regulation under stress.

Root systems are the result of many different developmental processes, differentially regulated across the root types and dynamically controlled by internal and external information. Developmental and environmental pathways may cause changes in the emergent properties of root system architecture through very specific and highly localized changes in cell division rates and cell elongation. Thus, to fully capture all the diverse root system responses to a stress in a meaningful way, one needs to employ different techniques that monitor various root system parameters. In the following sections, we describe the prominent tools that are currently available to study important aspects of root and root system response to drought and salinity.

2 Materials

2.1 Seed Sterilization

1. 95 % Ethanol.
2. 20 % Bleach with 0.1 % Tween-20 (prepare fresh each time of use).
3. Autoclaved distilled water.

2.2 Plant Growth Medium and Necessary Supplies

1. Agar (Fisher Scientific Cat. No. DF0145-17-0) or Gelzan (Sigma Cat. No. G1910).
2. Murashige and Skoog salts (MSP01-50LT, Caisson).
3. Sucrose (Sigma Cat. No. S0389).

4. MES hydrate (Sigma Cat. No. M2933).
5. KOH (Sigma Cat. No. P5958).
6. NaCl (Sigma Cat. No. S7653) for salt treatment.
7. Polyethylene glycol 8000 (Sigma Cat. No. P2139) for water deficit treatment.
8. D-Mannitol (Sigma Cat. No. M1902) for water deficit treatment.
9. Square tissue culture plates with dimension of 120 × 120 × 17 mm (USA Scientific Cat. No. 5668-8102) or 100 × 100 × 15 mm (VWR Cat. No. 60872-310).
10. Parafilm (52858-000, VWR).
11. Micropore tape (3M, Cat. No. 19-027-761).
12. Percival CU41L4 incubator with a setting of constant temperature of 22 °C with long-day lighting conditions (16 h light and 8 h dark).

2.3 Root Imaging

1. Revised Hoyer's solution: 80 % chloral hydrate, 10 % glycerol.
2. Propidium iodide (Life Tech. Cat. No. P1304MP) X-gluc solution: 0.2 mM 5-bromo-4-chloro-3-indolyl-β-D-glucuronide, 1 mM potassium ferricyanide, 1 mM potassium ferrocyanide, 10 mM EDTA, and 0.1 M sodium phosphate buffer (pH 7).
3. Compound DIC microscope (Leica).
4. Confocal Laser scanning microscope with 488 nm laser (Leica).
5. Flatbed document scanner or mounted camera.
6. Glass sides (25 × 75 mm, 1.0 mm thick, Fisher Scientific (Cat. No. 12-544-2)).
7. Coverslips (22 × 40 mm, 0.16–0.19 mm thick, Fisher Scientific (Cat. No. 12-544-B)).

2.4 Marker Lines to Study Lateral Root Patterning

For the purpose of monitoring temporal progression of lateral root development, or quickly counting the total number of lateral root primordia, several markers lines can be used.

1. High auxin accumulation occurs prior to lateral root initiation. To monitor the accumulation of auxin along the primary root and identify the positions where lateral roots are likely to initiate, the *DR5:luciferase+* reporter [43] can be used. Sites of sustained auxin response are termed as prebranch sites (PBSs) and correlate well with the position of future lateral roots. In comparison, *DR5:3xVenus-N7* [44, 45] marks the first lateral root initiation stage; it offers more spatial resolution but less temporal resolution.
2. The initiation of lateral root morphogenesis starts with the migration of two nuclei toward the shared cell wall from two

adjacent pericycle cells at the xylem pole. This event is followed by asymmetric cell divisions in the two cells. To monitor this unique event, nuclear markers can be used, such as *proGATA23:GUS:GFP* [46], which is an auxin responsive transcription factor that regulates the first early asymmetric division.

3. LBD16, which was found to be the direct target of ARF7/19 [47], also shows specific localization (*LBD16:GFP*) during the processes of nuclei migration and the first asymmetric cell divisions [48].
4. The *miRNA390a:GUS:GFP* [49] can be used to monitor the early lateral root initiation process, and is expressed during the initiation stage, while after stage 2, the expression is only prominent at the flanking cells of the primordium.
5. *ProSCARCROW:GFP* [50] is expressed strongly in the outer layer one (OL1) in the stage 2 lateral root primordium and becomes restricted to the endodermis when the lateral root reaches developmental stage 7.

3 Methods

3.1 Growing Arabidopsis Seedlings

Over the years many techniques have been proposed to study the dynamics of root growth [10, 51–54]. The choice of the method depends largely on the plant species and the questions being addressed in the study. For plants with a relatively small, slow growing root system like *Arabidopsis*, the method of choice can be a simple technique of growing the plants on the surface of agar media in a petri dish and monitoring root growth over time using transmitted or reflected light and a microscope, digital camera, or flat-bed document scanner.

1. *Arabidopsis* seeds are washed in 95 % ethanol for 5 min in a 1.5 ml centrifuge tube, followed by a wash in 20 % bleach + 0.1 % tween-20 for 5 min. Wash seeds in sterilized distilled water four times. Add 500 μl water to the seeds and stratify seeds at 4 °C for 2 days to promote uniform germination.
2. Growth medium is prepared and autoclaved (121 °C for 30 min) beforehand. The quantity of different media components needs to be controlled depending on the purpose of the experiment. For example, sucrose is often added to the medium as a carbon source, which promotes root growth and developmental uniformity between seedlings, however it has also been shown to influence root system development [55, 56]. Similarly, the concentration of nutrients such as phosphate and nitrate in the medium also may impact development of the root system [57, 58]. Thus, it is important to test varying strengths of Murashige and Skoog salts (MS salts) to standardize

the best conditions for the given experimental purpose. Our "standard medium" for root growth is composed of 1× MS salts, 1 % sucrose, 0.5 g/l MES, adjusted to pH 5.7 with 1 M KOH and solidified with 1 % agar or 0.7 % Gelzan.

3. Stratified seeds are sown on the surface of the medium in petri plates in a row using sterile tweezers or pipettes. Plates are then sealed with parafilm at the bottom half to prevent water from leaking out and the top half is sealed with micropore tape to allow for gas exchange. Plates are placed vertically in the growth chamber to facilitate downward root growth along the surface of the medium and root growth activities monitored on a regular basis. Alternatively, a customized black plastic shield can be used to cover the petri dish to promote a dark growth environment for the roots while the shoots are still illuminated. This technique allows studying root growth under more natural conditions [59].
4. To study root system development under high salinity or drought, transferring seedlings from standard media plates to plates containing medium supplemented with NaCl or polyethylene glycol (PEG)/mannitol is recommended as these are known to suppress seed germination in *Arabidopsis* [60]. The 5–6-day-old seedlings germinated and grown on standard medium can be gently transferred individually to experimental plates using sterile forceps. To simplify the transfer process, a sterile nylon mesh (100 μm pore size) can be placed on top of the media before sowing and seedlings grown vertically along the surface [61]. At the time of transfer, the sheet of nylon and seedlings is transferred to the treatment media. Mark the position of the root tip (transfer point) soon after transfer for later reference.

3.2 Analysis of Root Growth Characteristics

Growth is almost entirely confined to the tip of a root where the meristem produces new cells that subsequently elongate and differentiate. Along the longitudinal axis this one-dimensional growth zone can be subdivided into an apical-most meristematic region, which is a zone of rapid cell division, a transition zone where cells prepare to elongate, an elongation zone, which is an area where cells elongate rapidly, and the differentiation/maturation zone where cells attain their final form and function [62]. The growth activities can be monitored based on alterations in either the root length or meristem size. Such changes in cellular or growth properties can then be used to interpret the effect of the particular stress regime on root growth and development.

1. Seeds are grown and treated with the stress of interest as described in Subheading 3.1.
2. For root length measurements, images of the seedlings are taken at regular intervals with optimum zoom and resolution using either a document scanner or mounted camera. For scaling purposes, a ruler is imaged alongside the sample. Image resolution of 600 dpi is sufficient for later applications.

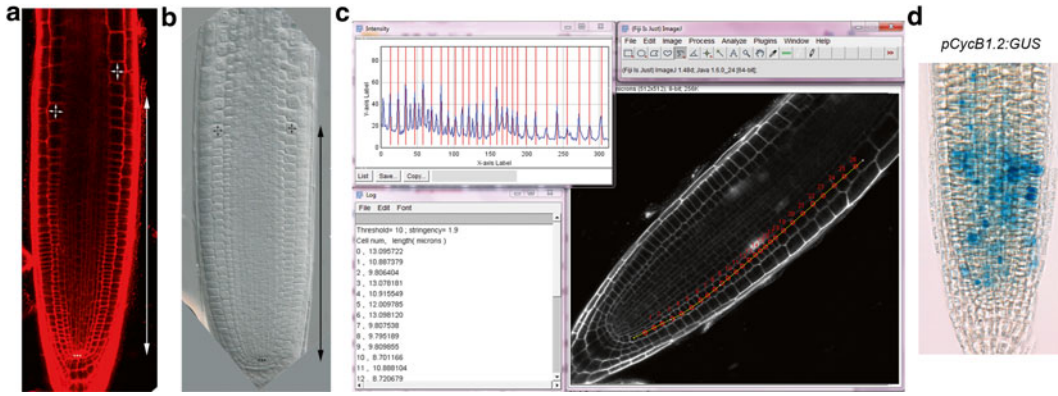

Fig. 2 Root meristem size and cell shape measurements in *Arabidopsis*. (**a**) Confocal image of an *Arabidopsis* root tip stained with propidium iodide. (**b**) DIC image of an *Arabidopsis* root tip fixed with revised Hoyer's solution. *Asterisks* mark the quiescent center (QC). *Short arrow lines* mark the cortex cells which have length/width ratio larger than 1. *Long arrow lines* roughly label the whole size of the meristem. (**c**) Semiautomated measurements of cell length by using Cell-o-Tape in ImageJ. (**d**) GUS-stained sample expressing the *pCYCB1.2:GUS* reporter in the primary root tip

3. Acquired images are analyzed using the ImageJ software [63, 64] to measure root length and the rate of root growth between time points. Root length is measured from the tip of the root to the hypocotyl region or the transfer point. Rate of root growth can be inferred from this data as the increase in root length or displacement of the position of the root tip per time point, usually 24 h later.
4. Root meristem size can be determined by counting the number of meristematic cortical cells in a file starting from the cell closest to the QC till the first elongated cell (cell showing an increase in length relative to its width). This can be done with the help of a microscope and roots that are either cleared in chloral hydrate solution (can be imaged using a differential interference contrast (DIC) microscope) or stained with propidium iodide (imaged using a confocal laser scanning microscope; Fig. 2a, b).
5. Length and diameter of individual cells in a file or group can be measured using the software Cell-o-Tape; a Fiji (an image processing software, [63, 64]) macro tool [65]. To successfully use this technique, cell walls must be well defined in the captured images. Images of roots stained with propidium iodide and captured using a confocal laser-scanning microscope are the most ideal (Fig. 2c). For analysis, the user has to first manually set a linear line through the intended area of measurement in each image using Fiji's "segmented line" tool. Once this region of interest is set, the software takes measurements automatically and gives the outputs (Fig. 2c).
6. Cell division activities in the meristem region can be monitored using the G_2-M cell-cycle marker, *pCycB1.2:GUS* [66].

Transgenic roots carrying this visual marker can be stained with X-gluc solution for 5–7 h at 37 °C. After several washes in phosphate buffer, these roots can then be cleared in revised Hoyer's solution and imaged using a compound microscope fitted with DIC optics (Fig. 2d).

3.3 Live-Imaging Techniques

Time-lapse imaging allows one to continuously monitor the growth dynamics of roots after treatment with environmental stimuli such as salinity. As mentioned above, such a system of continuous monitoring/imaging is advantageous over end-point analysis in understanding a dynamic and complex process like root growth response to a stress/environmental stimulus. For the purpose of monitoring root growth rate and changes in root system architecture, plants can be grown on transparent media, and digital cameras can be used to capture images over time. Here, we will introduce a few examples of studies utilizing live-imaging techniques to study root development and their responses to environmental stimuli.

1. To monitor root growth rates under salt stress, the Dinneny lab has developed a customized live-imaging system [41, 42]. Here, a motorized stage is set up to hold six square petri dishes, a digital camera with macro lens, and infrared filter and infrared light source are used to capture images over time (Fig. 3a). Images are usually taken every 15 min for 24 h to examine primary root growth dynamics, while for lateral roots, images are taken every 20 min for 7 days. Sequential images are collated as a stack for further analysis using ImageJ. Quantification of data from the time-lapse movies is conducted using the Manual Tracking plug-in for ImageJ (Fig. 3b), or using a semi-automated image analysis algorithm written as a macro in ImageJ [42, 67]. These growth rate data can provide information on regulatory events that occur in the root in response to stress. This design was modified from imaging systems developed by the lab of Edgar Spalding to monitor root gravitropic responses [68].
2. To visualize the three-dimensional structure of the root system, researchers have developed a gel-based imaging system to monitor the root system architecture of rice plant over time [69, 70]. Here, a turntable platform is controlled by computer, which supports the transparent gel cylinder system for growing plants. Forty sequential images are taken by a digital camera as the cylinder is rotated 360°, and these sets of images can be taken as many times as desired per day for time-course analysis. For 3-D image reconstruction and multiple root traits extraction, RootReader3D [70] or other customized software can be used. Common image analysis software like ImageJ and Photoshop can also be used for manually extracting some root features.

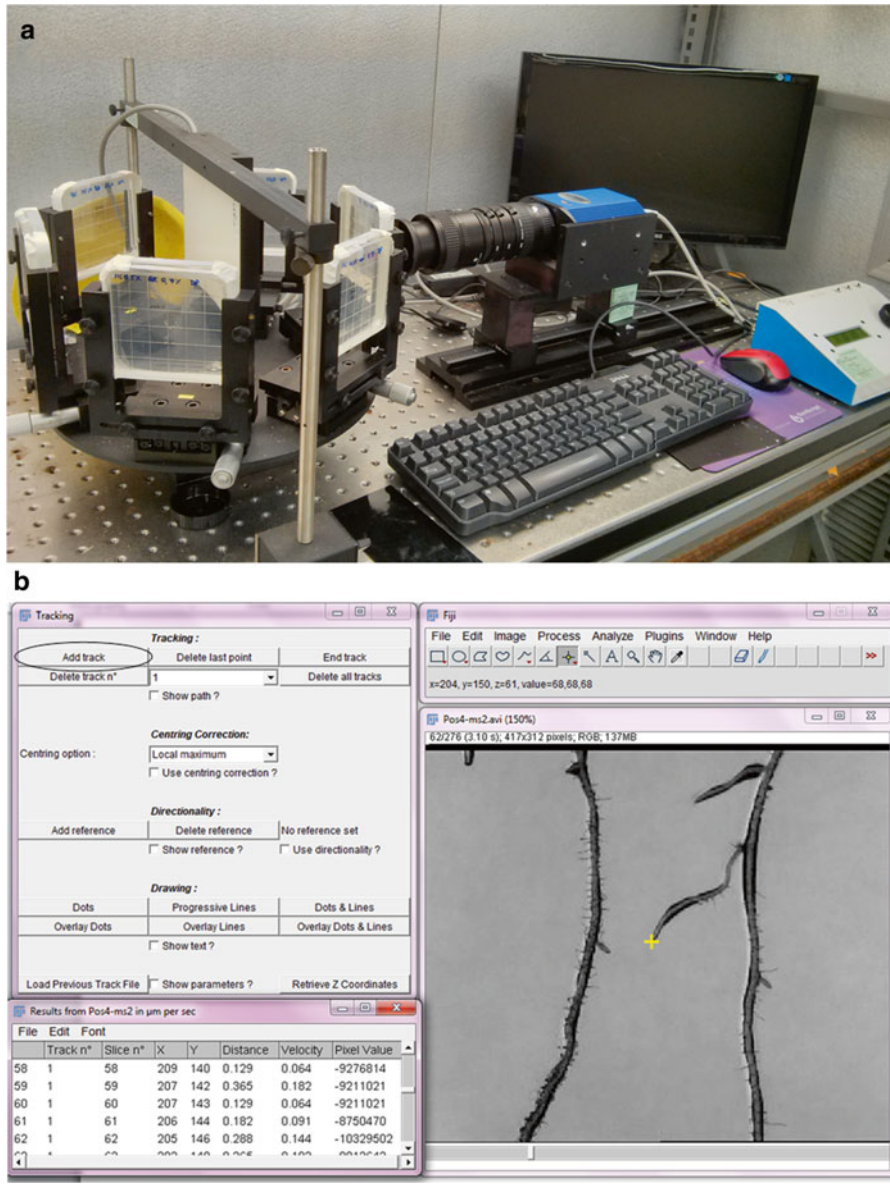

Fig. 3 Live-imaging system for root growth and data analysis. (**a**) Photo of the customized live-imaging system. (**b**) Manual quantification of root growth rate in Fiji (ImageJ)

3. For the purpose of visualizing rapid changes in gene expression or the activity of FRET-based metabolite sensors in response to highly controlled changes in the environment, a microfluidic chip platform has been developed to carry out live cell imaging in *Arabidopsis* roots [71]. Here, individual *Arabidopsis* roots expressing fluorescence-based reporters are grown in separate chambers filled with liquid medium. Once the roots grow into the observation chambers, pressure lines with a valve

system controlled by computer are used to adjust the fluid that baths the root. The platform is installed on a microscope or confocal system for live observation. This technique allows observations of very rapid changes induced in the root cells by environmental perturbations, such as the glucose/galactose sensor, FLII^{12}Pglu700μ-t which reflects the rapid changes in cytosolic Glc level [71, 72].

3.4 Lateral Root Development (Root Branching)

Lateral roots are important constituents of the root system and their growth is highly sensitive to changes in the surrounding environment. Processes including lateral root patterning, rate of initiation, pre-emergent development, and outgrowth rate influence root system architecture. Thus, it is important to systematically monitor changes in these specific processes to elucidate their effect on the emergent properties of the root system. Here we describe methods to quantify each of these aspects of lateral root development.

1. As described in Moreno-Risueno et al., the position of future lateral roots is marked by a sustained increase in the expression of the auxin reporter, *ProDR5:LUC+*. To monitoring this predetermination process of branching under stress conditions, *Arabidopsis* plants carrying the *ProDR5:LUC+* are grown and treated with stress as described in Subheading 3.1. For imaging luciferase expression, 5 mM potassium D-luciferin solution is sprayed onto seedlings before being loaded into a Chemiluminescence imaging system such as Bertold's Nightowl or Nightshade. ImageJ is used to analyze the images and quantify features such as the number of auxin maxima, brightness, and localization.
2. To examine the process of lateral root initiation and development of preemergent primordia, transgenic lines mentioned in Subheading 2.4 can be used. To track lateral root initiation rates under stressful environments, plants expressing these fluorescence reporters are grown on plates that can be directly imaged using a fluorescence dissection microscope over time. If only an end-point measurement is required, higher resolution imaging methods such as confocal microscopy can be used for better quantitation of the fluorescence level and lateral root anatomy.
3. Root tissue can be fixed and cleared in Hoyer's solution before imaging to observe lateral root primordia using DIC optics on a compound microscope. Detailed lateral root stages can be scored as previously described [50]. Compared with the method described in the previous section, tissue clearing may provide a more accurate estimate of lateral root stages present in a seedling; however, this is an end-point analysis method and seedlings cannot be analyzed over time.
4. Postemergence lateral root growth can be quantified by performing an end-point analysis using images (Subheading 3.2) captured with a flat-bed scanner and average or total lateral

root length quantified using ImageJ. When the temporal dynamics of lateral root growth is of interest, live-imaging methods mentioned in Subheading 3.3, Sect. 1 can be used.

3.5 Root System Architecture Analysis Using RootScape

RootScape [73] is a landmark-based method to quantify root system architecture based on allometric parameters (allometry is the study of the relative growth of a part of an organism in relation to an entire organism or to a standard). The technique uses a 20-point landmark template (with 6 primary landmarks recognizable by developmental features such as the position of the first and last lateral root, apex of primary root, etc. and associated 14 secondary landmarks), which will represent the primary root as a line and lateral roots as a polygon. Alterations in root system architecture detected as a response to a particular stress regime using this technique can then be utilized to interpret the effect of that stress regime.

1. Plants are grown till 7 days postgermination and imaged as mentioned earlier (Subheading 3.2).
2. Captured images are analyzed using the 20-point allometric template of the RootScape consisting of primary and secondary landmark points [73]. These points are manually placed on each captured root image (Fig. 4).

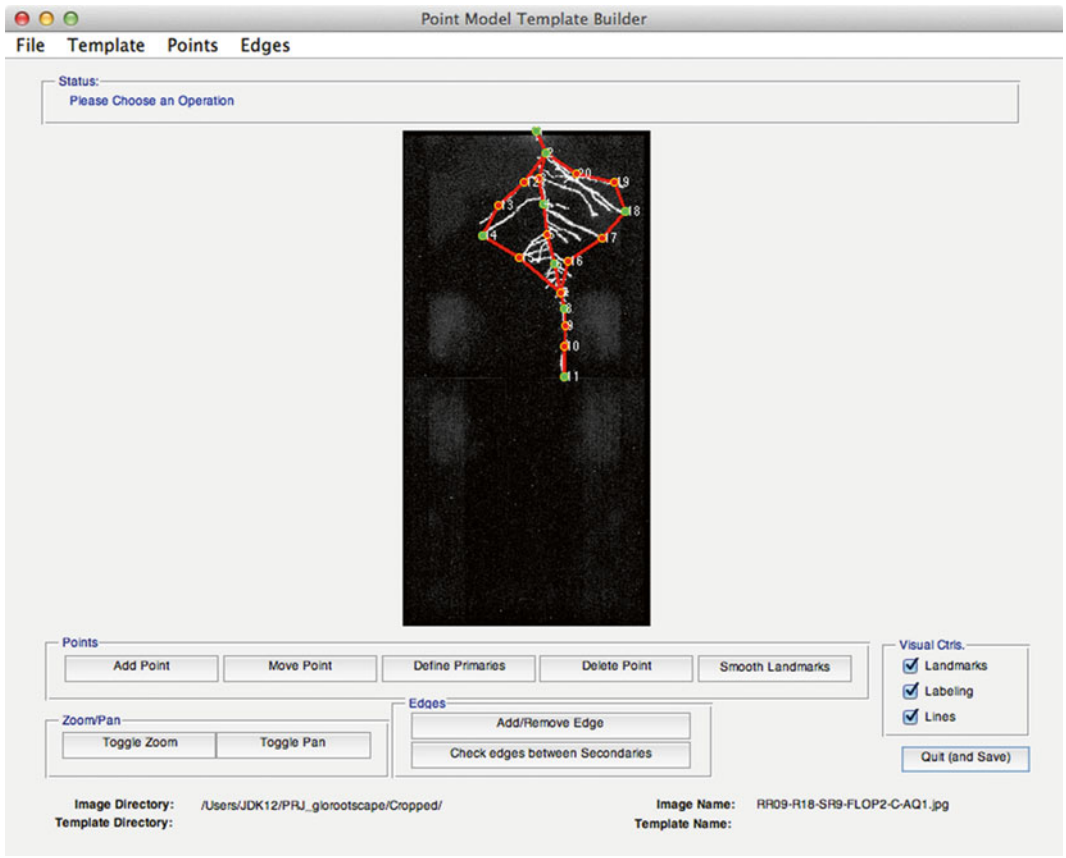

Fig. 4 The analysis interface of root system architecture in RootScape

3. Generate a root system architecture morphospace called allometric plasticity space based on the 20-point landmark assay.
4. Estimate the main trends of variation in root system architecture between the control and treatments based on these data, which can be processed using publically available AAMToolbox software (a MATLAB plugin) (http://cmpdartsvr1.cmp.uea.ac.uk/wiki/BanghamLab/index.php/Software) and principal component analysis.

4 Notes

4.1 Considerations for Experimental Design

1. Different gelling agents can be tested for hardness and clarity. We use agar and Gelzan in the lab and both work for most purposes. Addition of NaCl may decrease the ability of Gelzan to melt, and accelerate gel solidification after autoclaving.
2. Although other plate sealing methods have been described, in our experimental setup, the sealing method of half parafilm and half micropore tape was found most effective. Parafilm at the bottom half of the plate stops liquid leakage to the growth chamber. Micropore tape allows gas exchange, which is necessary for lateral root growth.
3. While handling seedlings, proper care should be taken to ensure that no tissue damage is caused to the roots. Young seedlings can be handled using tweezers, holding gently on the cotyledons. For transfers using nylon mesh, a pore size of 100 μm is sufficient to prevent most roots growing through the mesh. However, if growing mutants with thinner roots such as *shortroot*, a mesh with a smaller pore size (50 μm) is recommended.
4. Both propidium iodide (stains cell walls) and FM-464 (stains cell membrane) can be used to stain the roots before confocal microscopic imaging. Propidium iodide is generally able to penetrate better into the inner root tissues than FM-464 for standard grown roots. However, we recommend using FM-464 to stain salt treated roots as propidium iodide enters the cells in salt treated roots and causes difficulty in defining cell boundaries.
5. Transferring seedlings to a new environmental condition post-germination creates two distinct regions along the length of the primary root that should be considered distinct in a phenotypic analysis. Regions of the primary root that developed first under standard conditions will have already patterned the position of prebranch sites, thus effects of density may be minimal while the regulation of lateral root initiation, outgrowth, and post-emergence development may be affected. Parts of the primary

root that form in the new environmental condition may be affected at the earliest stages of lateral root development.

6. Care needs to be taken to avoid the effects of circadian rhythm while characterizing root responses to an environmental stimulus. Collecting and analyzing samples at the same time of the day may help in avoiding many of the circadian rhythm associated effects.

Acknowledgments

We would like to acknowledge Ruben Rellan Alvarez for providing images for Figure 4. We thanks members of the Dinneny lab for helpful suggests to improve the manuscript. Work in the DInneny lab on salt stress responses in roots is provided by the Carnegie Institution for Science Endowment and a grant from NSF MCB (Award Number MCB-1157895.

References

1. Dolan L, Janmaat K, Willemsen V, Linstead P, Poethig S, Roberts K, Scheres B (1993) Cellular organisation of the *Arabidopsis thaliana* root. Development 119:71–84
2. Scheres B, Benfey P, Dolan L (2002) Root development. In: Somerville CR, Meyerowitz EM (eds) The Arabidopsis book. American Society of Plant Biologists, Rockville, MD
3. Mahajan S, Tuteja N (2005) Cold, salinity and drought stresses: an overview. Arch Biochem Biophys 444:139–158
4. Zhu JK, Hasegawa PM, Bressan RA, Bohnert PHJ (1997) Molecular aspects of osmotic stress in plants. Crit Rev Plant Sci 16:253–277
5. Xiong L, Schumaker KS, Zhu J-K (2002) Cell signaling during cold, drought, and salt stress. Plant Cell 14:S165–S183
6. Iraki NM, Bressan RA, Hasegawa P, Carpita NC (1989) Alteration of the physical and chemical structure of the primary cell wall of growth-limited plant cells adapted to osmotic stress. Plant Physiol 91:39
7. Cho MH, Shears SB, Boss WF (1993) Changes in phosphatidylinositol metabolism in response to hyperosmotic stress in *Daucus carota L.* cells grown in suspension culture. Plant Physiol 103:637–647
8. Slayman CL (1982) Charge-transport characteristics of a plasma membrane proton pump. In: Martonosi AN (ed) Membranes and transport. Springer, New York, pp 485–490
9. Smith S, De Smet I (2012) Root system architecture: insights from Arabidopsis and cereal crops. Philos Trans R Soc Lond B Biol Sci 367: 1441–1452
10. Sharp RE, Silk WK, Hsiao TC (1988) Growth of the maize primary root at low water potentials: I. Spatial distribution of expansive growth. Plant Physiol 87:50–57
11. Liang BM, Sharp RE, Baskin TI (1997) Regulation of growth anisotropy in well-watered and water-stressed maize roots (I. Spatial distribution of longitudinal, radial, and tangential expansion rates). Plant Physiol 115: 101–111
12. Yamaguchi M, Valliyodan B, Zhang J, Lenoble ME, Yu O, Rogers EE, Nguyen HT, Sharp RE (2010) Regulation of growth response to water stress in the soybean primary root. I. Proteomic analysis reveals region-specific regulation of phenylpropanoid metabolism and control of free iron in the elongation zone. Plant Cell Environ 33:223–243
13. Westgate M, Boyer J (1985) Osmotic adjustment and the inhibition of leaf, root, stem and silk growth at low water potentials in maize. Planta 164:540–549
14. Hsiao TC, Xu LK (2000) Sensitivity of growth of roots versus leaves to water stress: biophysical analysis and relation to water transport. J Exp Bot 51:1595–1616
15. Saab IN, Sharp RE, Pritchard J (1992) Effect of inhibition of abscisic acid accumulation on the spatial distribution of elongation in the primary root and mesocotyl of maize at low water potentials. Plant Physiol 99:26–33

16. Sacks MM, Silk WK, Burman P (1997) Effect of water stress on cortical cell division rates within the apical meristem of primary roots of maize. Plant Physiol 114:519–527
17. Duan Y, Zhang W, Li B, Wang Y, Li K, Sodmergen, Han C, Zhang Y, Li X (2010) An endoplasmic reticulum response pathway mediates programmed cell death of root tip induced by water stress in *Arabidopsis*. New Phytol 186:681–695
18. Jupp A, Newman E (1987) Morphological and anatomical effects of severe drought on the roots of *Lolium perenne L.* New Phytol 105: 393–402
19. Xiong L, Wang R-G, Mao G, Koczan JM (2006) Identification of drought tolerance determinants by genetic analysis of root response to drought stress and abscisic acid. Plant Physiol 142:1065–1074
20. Matsui T, Singh B (2003) Root characteristics in cowpea related to drought tolerance at the seedling stage. Exp Agric 39:29–38
21. Songsri P, Jogloy S, Vorasoot N, Akkasaeng C, Patanothai A, Holbrook C (2008) Root distribution of drought-resistant peanut genotypes in response to drought. J Agron Crop Sci 194:92–103
22. Ali A, Xu J, Ismail A, Fu B, Vijaykumar C, Gao Y, Domingo J, Maghirang R, Yu S, Gregorio G (2006) Hidden diversity for abiotic and biotic stress tolerances in the primary gene pool of rice revealed by a large backcross breeding program. Field Crop Res 97:66–76
23. Annicchiarico P, Piano E (2005) Use of artificial environments to reproduce and exploit genotype × location interaction for lucerne in northern Italy. Theor Appl Genet 110: 219–227
24. Folkard AM (2005) Hydrodynamics of model Posidonia oceanica patches in shallow water. Limnol Oceanogr 50:1592
25. Munns R (2002) Comparative physiology of salt and water stress. Plant Cell Environ 25:239–250
26. Rubio F, Gassmann W, Schroeder JI (1995) Sodium-driven potassium uptake by the plant potassium transporter HKT1 and mutations conferring salt tolerance. Science 270:1660–1663
27. Luan S, Lan W, Chul Lee S (2009) Potassium nutrition, sodium toxicity, and calcium signaling: connections through the CBL-CIPK network. Curr Opin Plant Biol 12:339–346
28. Shabala S, Cuin TA (2008) Potassium transport and plant salt tolerance. Physiol Plant 133: 651–669
29. Kurth E, Cramer GR, Läuchli A, Epstein E (1986) Effects of NaCl and $CaCl_2$ on cell enlargement and cell production in cotton roots. Plant Physiol 82:1102–1106
30. Samarajeewa P, Barrero R, Umeda-Hara C, Kawai M, Uchimiya H (1999) Cortical cell death, cell proliferation, macromolecular movements and rTip1 expression pattern in roots of rice (*Oryza sativa L.*) under NaCl stress. Planta 207:354–361
31. Burssens S, Himanen K, van de Cotte B, Beeckman T, Van Montagu M, Inzé D, Verbruggen N (2000) Expression of cell cycle regulatory genes and morphological alterations in response to salt stress in *Arabidopsis thaliana*. Planta 211:632–640
32. West G, Inzé D, Beemster GT (2004) Cell cycle modulation in the response of the primary root of *Arabidopsis* to salt stress. Plant Physiol 135:1050–1058
33. Koiwa H, Li F, McCully MG, Mendoza I, Koizumi N, Manabe Y, Nakagawa Y, Zhu J, Rus A, Pardo JM (2003) The STT3a subunit isoform of the *Arabidopsis* oligosaccharyltransferase controls adaptive responses to salt/osmotic stress. Plant Cell 15:2273–2284
34. Shi H, Kim Y, Guo Y, Stevenson B, Zhu J-K (2003) The *Arabidopsis SOS5* locus encodes a putative cell surface adhesion protein and is required for normal cell expansion. Plant Cell 15:19–32
35. Shoji T, Suzuki K, Abe T, Kaneko Y, Shi H, Zhu J-K, Rus A, Hasegawa PM, Hashimoto T (2006) Salt stress affects cortical microtubule organization and helical growth in *Arabidopsis*. Plant Cell Physiol 47:1158–1168
36. Furutani I, Watanabe Y, Prieto R, Masukawa M, Suzuki K, Naoi K, Thitamadee S, Shikanai T, Hashimoto T (2000) The SPIRAL genes are required for directional control of cell elongation in *Arabidopsis thaliana*. Development 127:4443–4453
37. Brady SM, Orlando DA, Lee JY, Wang JY, Koch J, Dinneny JR, Mace D, Ohler U, Benfey PN (2007) A high-resolution root spatiotemporal map reveals dominant expression patterns. Science 318:801
38. Dinneny JR, Long TA, Wang JY, Jung JW, Mace D, Pointer S, Barron C, Brady SM, Schiefelbein J, Benfey PN (2008) Cell identity mediates the response of *Arabidopsis* roots to abiotic stress. Science 320:942
39. Kiegle E, Moore CA, Haseloff J, Tester MA, Knight MR (2001) Cell-type-specific calcium responses to drought, salt and cold in the *Arabidopsis* root. Plant J 23:267–278
40. De Smet I, Signora L, Beeckman T, Inzé D, Foyer CH, Zhang H (2003) An abscisic acid-sensitive checkpoint in lateral root development of *Arabidopsis*. Plant J 33:543–555

41. Duan L, Dietrich D, Ng CH, Chan PMY, Bhalerao R, Bennett MJ, Dinneny JR (2013) Endodermal ABA signaling promotes lateral root quiescence during salt stress in *Arabidopsis* seedlings. Plant Cell 25:324–341
42. Geng Y, Wu R, Wee CW, Xie F, Wei X, Chan PMY, Tham C, Duan L, Dinneny JR (2013) A spatio-temporal understanding of growth regulation during the salt stress response in *Arabidopsis*. Plant Cell 25:2132–2154
43. Moreno-Risueno MA, Van Norman JM, Moreno A, Zhang J, Ahnert SE, Benfey PN (2010) Oscillating gene expression determines competence for periodic *Arabidopsis* root branching. Science 329:1306
44. Heisler MG, Ohno C, Das P, Sieber P, Reddy GV, Long JA, Meyerowitz EM (2005) Patterns of auxin transport and gene expression during primordium development revealed by live imaging of the *Arabidopsis* inflorescence meristem. Curr Biol 15:1899–1911
45. Bielach A, Podlešáková K, Marhavý P, Duclercq J, Cuesta C, Müller B, Grunewald W, Tarkowski P, Benková E (2012) Spatiotemporal regulation of lateral root organogenesis in *Arabidopsis* by cytokinin. Plant Cell 24:3967–3981
46. De Rybel B, Vassileva V, Parizot B, Demeulenaere M, Grunewald W, Audenaert D, Van Campenhout J, Overvoorde P, Jansen L, Vanneste S (2010) A novel aux/IAA28 signaling cascade activates GATA23-dependent specification of lateral root founder cell identity. Curr Biol 20:1697–1706
47. Okushima Y, Fukaki H, Onoda M, Theologis A, Tasaka M (2007) ARF7 and ARF19 regulate lateral root formation via direct activation of LBD/ASL genes in *Arabidopsis*. Plant Cell 19:118–130
48. Goh T, Joi S, Mimura T, Fukaki H (2012) The establishment of asymmetry in *Arabidopsis* lateral root founder cells is regulated by LBD16/ASL18 and related LBD/ASL proteins. Development 139:883–893
49. Marin E, Jouannet V, Herz A, Lokerse AS, Weijers D, Vaucheret H, Nussaume L, Crespi MD, Maizel A (2010) miR390, *Arabidopsis* TAS3 tasiRNAs, and their AUXIN RESPONSE FACTOR targets define an autoregulatory network quantitatively regulating lateral root growth. Plant Cell 22:1104–1117
50. Malamy JE, Benfey PN (1997) Organization and cell differentiation in lateral roots of *Arabidopsis thaliana*. Development 124:33–44
51. Doerner P (2008) Phenotypic analysis of *Arabidopsis* mutants: quantitative analysis of root growth. *CSH Protoc* 2008:pdb prot4960
52. Yazdanbakhsh N, Fisahn J (2010) Analysis of *Arabidopsis thaliana* root growth kinetics with high temporal and spatial resolution. Ann Bot 105:783–791
53. Yazdanbakhsh N, Fisahn J (2012) High-throughput phenotyping of root growth dynamics. Methods Mol Biol 918:21–40
54. French A, Ubeda-Tomas S, Holman TJ, Bennett MJ, Pridmore T (2009) High-throughput quantification of root growth using a novel image-analysis tool. Plant Physiol 150:1784–1795
55. Jain A, Poling MD, Karthikeyan AS, Blakeslee JJ, Peer WA, Titapiwatanakun B, Murphy AS, Raghothama KG (2007) Differential effects of sucrose and auxin on localized phosphate deficiency-induced modulation of different traits of root system architecture in *Arabidopsis*. Plant Physiol 144:232–247
56. Malamy JE, Ryan KS (2001) Environmental regulation of lateral root initiation in *Arabidopsis*. Plant Physiol 127:899–909
57. Zhang H, Forde BG (2000) Regulation of *Arabidopsis* root development by nitrate availability. J Exp Bot 51:51–59
58. Linkohr BI, Williamson LC, Fitter AH, Leyser H (2002) Nitrate and phosphate availability and distribution have different effects on root system architecture of *Arabidopsis*. Plant J 29:751–760
59. Xu W, Ding G, Yokawa K, Baluška F, Li Q-F, Liu Y, Shi W, Liang J, Zhang J (2013) An improved agar-plate method for studying root growth and response of *Arabidopsis thaliana*. Sci Rep 3, 1273
60. Vallejo AJ, Yanovsky MJ, Botto JF (2010) Germination variation in *Arabidopsis thaliana* accessions under moderate osmotic and salt stresses. Ann Bot 106:833–842
61. Murphy A, Taiz L (1995) A new vertical mesh transfer technique for metal-tolerance studies in *Arabidopsis* (ecotypic variation and copper-sensitive mutants). Plant Physiol 108:29–38
62. Sebastian J, Lee J-Y (2013) Root apical meristems. In: ELS. John Wiley & Sons Ltd, Chichester. doi:10.1002/9780470015902.a0020121.pub2
63. Schindelin J, Arganda-Carreras I, Frise E, Kaynig V, Longair M, Pietzsch T, Preibisch S, Rueden C, Saalfeld S, Schmid B (2012) Fiji: an open-source platform for biological-image analysis. Nat Methods 9:676–682
64. Schindelin J (2008) Fiji is just ImageJ-Batteries included. In: Proceedings of the ImageJ User and Developer Conference, Luxembourg
65. French AP, Wilson MH, Kenobi K, Dietrich D, Voß U, Ubeda-Tomás S, Pridmore TP, Wells DM (2012) Identifying biological landmarks

using a novel cell measuring image analysis tool: Cell-o-Tape. Plant Methods 8:7

66. Ingouff M, Jullien PE, Berger F (2006) The female gametophyte and the endosperm control cell proliferation and differentiation of the seed coat in *Arabidopsis*. Plant Cell 18: 3491–3501
67. Abràmoff MD, Magalhães PJ, Ram SJ (2004) Image processing with ImageJ. Biophotonics Int 11:36–42
68. Miller ND, Brooks TLD, Assadi AH, Spalding EP (2010) Detection of a gravitropism phenotype in glutamate receptor-like 3.3 mutants of *Arabidopsis thaliana* using machine vision and computation. Genetics 186:585–593
69. Iyer-Pascuzzi AS, Zurek PR, Benfey PN (2013) High-throughput, noninvasive imaging of root systems. In: De Smet I (ed) Plant organogenesis. Springer, New York, pp 177–187
70. Clark RT, MacCurdy RB, Jung JK, Shaff JE, McCouch SR, Aneshansley DJ, Kochian LV (2011) Three-dimensional root phenotyping with a novel imaging and software platform. Plant Physiol 156:455–465
71. Grossmann G, Guo W-J, Ehrhardt DW, Frommer WB, Sit RV, Quake SR, Meier M (2011) The RootChip: an integrated microfluidic chip for plant science. Plant Cell 23:4234–4240
72. Takanaga H, Chaudhuri B, Frommer WB (2008) GLUT1 and GLUT9 as major contributors to glucose influx in HepG2 cells identified by a high sensitivity intramolecular FRET glucose sensor. Biochim Biophys Acta 1778:1091–1099
73. Ristova D, Rosas U, Krouk G, Ruffel S, Birnbaum KD, Coruzzi GM (2013) RootScape: a landmark-based system for rapid screening of root architecture in *Arabidopsis*. Plant Physiol 161:1086–1096

Chapter 11

Quantification of Fluorescent Reporters in Plant Cells

Michael Pound, Andrew P. French, and Darren M. Wells

Abstract

Fluorescent reporters are powerful tools for plant research. Many studies require accurate determination of fluorescence intensity and localization. Here, we describe protocols for the quantification of fluorescence intensity in plant cells from confocal laser scanning microscope images using semiautomated software and image analysis techniques.

Key words Fluorescent reporters, Image analysis, CellSeT, DII-VENUS

1 Introduction

Fluorescent reporters represent powerful tools for plant research, allowing spatial monitoring of dynamic expression patterns at the subcellular, cellular, and tissue scale [1]. There are several reasons, detailed in refs. 2 and 3, why quantitative analysis of confocal images can be problematic. Modeling approaches, such as those employed to quantify the phytohormone auxin using the DII-VENUS reporter [4], rely on accurate determination of fluorescence at the cellular level. Manual determination of cellular and tissue geometry from images is both labor-intensive and prone to subjective errors, and localization of, for example, asymmetrically localized membrane proteins also requires an unbiased method of quantification.

Plant tissues are composed of a cellular network which can be visualized using dyes or genetically encoded markers. Semiautomatic segmentation of images of this network provides an unbiased quantification of tissue anatomy. Once segmented, this cellular structure can be exploited to direct image analysis techniques to local regions, improving accuracy. In this chapter, we describe a protocol for imaging fluorescent reporters in *Arabidopsis* root tips and the subsequent extraction of anatomical and fluorescence data via the CellSeT software package [5], using as an example the nuclear-localized fluorescent auxin reporter DII-VENUS.

José M. Estevez (ed.), *Plant Cell Expansion: Methods and Protocols*, Methods in Molecular Biology, vol. 1242,
DOI 10.1007/978-1-4939-1902-4_11,

2 Materials

Follow all waste disposal regulations when disposing of transgenic *Arabidopsis* seeds and seedlings.

2.1 *Arabidopsis thaliana* Germination and Growth Medium Composition

1. Half-strength Murashige and Skoog (MS) medium: dissolve 2.15 g of MS salts (Sigma, UK), in approximately 900 mL of double-distilled water and adjust the pH to 5.8 using 1 M KOH. Top up solution to 1 L and dispense into a suitable bottle and add 10 g bacto-agar (Appleton Woods, UK). Autoclave for 11 min at 121 °C, 20 psi. Plates can be poured once the medium has cooled to ~50 °C. Autoclaved MS medium can be stored for up to 1 month at room temperature and remelted when required using a steamer.
2. *Arabidopsis thaliana* seed surface sterilization solution: 5 % sodium hypochlorite (w/v). Protect from light and store at room temperature.
3. Petri dishes.
4. Propidium iodide stock solution: 1 mg/mL in water. Protect from light and store at 4–6 °C.

2.2 Image Acquisition and Analysis

1. Confocal laser scanning microscope. The measurements presented here were made using an inverted Leica TCS SP5.
2. Computer suitable for running CellSeT (http://sourceforge.net/projects/cellset/) and, optionally, Fiji software (http://fiji.sc/Fiji).

3 Methods

3.1 Seed Germination

1. Perform procedure in a laminar flow hood. Transfer 50–100 seeds to a 1.5 mL microfuge tube and add 1 mL of surface sterilization solution. Mix by inverting and incubate at room temperature for 5 min (*see* **Note 1**). Rinse five times in sterile double-distilled water. Seeds can be stored at 4 °C in sterile water in darkness for up to 1 week.
2. Prepare half-strength MS plates (use 60 mL of medium for 120 mm square Petri dishes or 25 mL of medium for 60 mm diameter round dishes).
3. Sow the sterilized seeds using a pipette onto solidified half-strength MS medium plates and seal the plates with gas-permeable tape, e.g., Micropore™ (3M Co., USA). If not already stored in water and stratified at 4 °C, transfer the plates to 4 °C and maintain in darkness for 2 days. Transfer the plates to a controlled environment chamber for 5–7 days (typical conditions: 12 h photoperiod or continuous light, 22 °C, 100 μE light intensity).

3.2 Sample Handling

1. Mount seedlings under a coverslip on glass slides in sterile water.
2. If the seedling does not have a fluorescent marker for the plasma membrane or cell wall (*see* **Note 2**), the seedling can be counterstained with propidium iodide (PI). Dilute stock solution to 5 μL/mL with sterile water and transfer 1–3 mL to a suitable container (e.g., multiwell plates or weighing boats). Transfer seedlings to the staining container and incubate for 60 s to 3 min. Wash seedlings by dipping briefly in sterile water before mounting to remove excess PI and minimize the risk of contamination of the microscope (*see* **Note 3**).

3.3 Image Acquisition

1. Image seedlings using appropriate microscope settings for individual fluorophores to optimize the signal-to-noise ratio, taking care not to saturate the signal (*see* **Note 4**). Select an appropriate image size and magnification (*see* **Note 5**). Sequential scanning may be necessary to reduce crosstalk if employing multiple fluorophores. The cell wall/plasma membrane marker should always be imaged in a separate color channel from the other features to be quantified (Fig. 1a). If features of interest are not in the same plane of focus, a z-stack of images can be taken and a surface projected through the stack (*see* **Note 6**).
2. Separate the various color channels of the image into individual image files. This function is usually available in the microscope operating software but can easily be performed later using open-source software such as Fiji [6]. Suitable image formats are *.bmp, *.png, *.jpg, and *.gif.

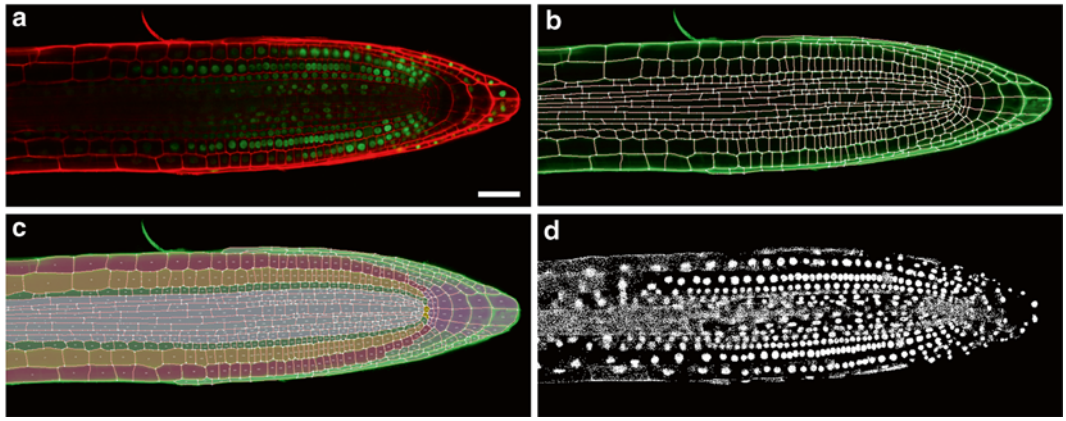

Fig. 1 Extraction of information from root images. (**a**) Confocal micrograph of an *Arabidopsis* root tip expressing DII-VENUS (*green channel*). Cell walls stained with propidium iodide (*red channel*). (**b**) Automatic network refinement of the cell wall channel in (**a**). Note that the wall channel is displayed in *green*. Snake parameters in this case were as follows: node spacing, 3; curvature, 1; continuity, 16; image weight, 1. (**c**) Manually tagged image map with cells and cell file identity labeled. (**d**) Detection of nuclei using targeted local thresholding on a per cell basis using the CellSeT Nuclei Plugin. Scale bar: 50 μm

3.4 Image Analysis Using CellSeT

1. Extract the CellSeT software into a directory, including any additional files that are supplied with the installation. Running Cellset.exe will begin the software.
2. Before loading images in to CellSeT, check that the cells and features of interest in the image are all in the correct image plane, i.e., they do not disappear out of the plane of focus (*see* **Note 6**).
3. Click in the main window to load images for quantification (one of which must be an image representing the cell wall), or click on the File Menu, and select New Image. A file dialog will appear, highlight one or more images and click Open.
4. The CellSeT processing pipeline begins with the selection of the image representing the cell wall marker channel. Use the left and right arrow buttons to highlight the appropriate image, and select the corresponding color channel. If the image is grayscale, then selecting *Any* is appropriate.
5. The loaded image will be shown within the main window in CellSeT (note that whatever the color of the original channel, cell walls are shown in green for clarity, Fig. 1b). The view can be zoomed with the mouse wheel, and scrolled by clicking and dragging with the right mouse button.
6. Once an image is loaded options will appear to apply various noise-reduction filters. Images will usually require filtering before they are processed. The quantity and nature of the filtering required will depend on the quality and resolution of the input image. However, a reasonable starting point is to apply a Median filter, followed by a Gaussian filter (*see* **Note 7**). To achieve this, ensure that the 3×3 Kernel size is selected (this determines the size of the filter; with 3×3 being a sensible default value), then toggle the Median option, before clicking Filter. Then select the Gaussian option, and click filter for a second time. Once the image is filtered, and noise has been adequately reduced, click Accept Filters to proceed to image segmentation.
7. The default segmentation mode in CellSeT is a two-level watershed segmentation algorithm using a threshold of 10. Immediately click Segment, and examine the results. An appropriate threshold level will segment the maximum possible number of cells automatically. If too few cells are observed using the default threshold level of 10, reduce this threshold using the slider, and click segment again. If the image is over-segmented (numerous cells split into multiple segments), raise the threshold and click segment. The aim is to extract as many cells as possible, to reduce the manual refinement required at the next stage. Once the image is segmented satisfactorily, click Accept Segmentation. If a reasonable segmentation cannot

be found it may be that the image filtering stage should adjusted (*see* **Note 8**).

8. Once segmentation has been accepted, the cell walls are converted into a graph structure, where walls can be removed or added by the user. If one or more cells have been oversegmented, toggle the Remove Segments button, and then click on individual walls to remove them. Walls that are positioned incorrectly can also be removed and replaced this way. To add walls, toggle the Add Segments button, and then click on an existing wall. A line will appear from that position to the mouse cursor, and subsequent clicks will add a new wall between these locations. To complete a wall, either click on the edge of the image (for a cell that intersects the image edge) or an existing wall or junction point. High accuracy during this stage is not required (*see* **Note 9**).
9. The goal of the refinement stage is to reconstruct any missing walls, completing the cell network. Only cells that require quantification need be completed in this manner (*see* **Note 10**). Once the geometry of all cells is complete, click Accept Refinement to proceed to the next step. Refinement data can be saved or loaded for convenience (*see* **Note 11**).
10. Accepting a refinement will load a series of active contours ("network snakes" [7]) onto the cell network, and refine the position of each wall based on the image data. The parameters of these snakes can be altered before clicking Accept Refinement, the value of which will affect the outcome of the tracking procedure. In many cases altering these values will not be necessary, however for more details *see* **Note 12**.
11. After refinement, CellSeT converts the cell wall structure into a network of cell objects that can be highlighted and measured (Fig. 1b). Before any measurements are taken, the cells of interest must be highlighted, and can optionally be tagged with semantic information, such as "Epidermis" for epidermal cells (Fig. 1c). To highlight cells, toggle the Add Cells button, and then click cells in the image. Cells will be tagged with the information selected in the drop down menu above, the value of which is defaulted to "General." For example, to highlight a cell in the Cortex, select the drop down list, and click "Cortex." Then toggle add cells, and click the cortex cells. Multiple cells in files or blocks can be highlighted using the File and Area options, and then clicking and dragging on the image. Cell highlighting can be removed using the Remove Cells toggle button, before clicking on the cell. Note that this does not permanently remove the cell walls, but will prevent the cell from being measured.
12. The same highlighting process can be used for cell walls, which are also quantified during the measurement stage.

Only cells or walls that are highlighted will be measured. If all cells and walls should be measured, it may be quicker to click Tag All (*see* **Note 13**).

13. Once all relevant cells and walls have been highlighted, clicking Export XML will output all information on the geometry of these objects to an XML file, which can be imported into other software (*see* **Note 14**). If this is not necessary, skip to the next step.
14. CellSet measurements are split into two forms, a general measurement set, and specific measurements provided by external plug-ins. Each available plug-in is listed, and is disabled by default, followed by an Export Measurements button that computes all internal and plug-ins measurements simultaneously. If no plug-in measurements, such as nuclear fluorescence, are required, then click Export Measurements to quantify all highlighted objects and output this information to a table. An optional Tag can be added at this point when requested. If plug-in measurements are required, *see* **step 16**.
15. Once measurements are computed a table of data will appear. The rows of the table hold all measurements taken regarding the cell network, and can be highlighted by dragging the left mouse button, or all using the Ctrl + A shortcut. The information can be exported to Microsoft Excel or another analysis program by first copying it, using the Ctrl + C shortcut, and then pasting (Ctrl + V).
16. Additional quantification using targeted image analysis algorithms is provided by a series of specially programmed procedures, or "plug-ins." These plug-ins perform measurements with more specific requirements than the standard measurements within CellSeT. For example, nuclear fluorescence can be measured, but only in cases where fluorescent or stained nuclei are available in a separate image channel. To use a plug-in, check the Enabled checkbox under the plug-in's title, and alter any other parameters as required. The Assign Image buttons are used to point the plug-in toward other image channels that were not required for CellSeT's cell geometry reconstruction. For example, the Nuclei Plugin requires at least one image assigned to the Nuclei channel to use for the detection of nuclei and fluorescence measurement within each cell (Fig. 1a, d). Assign an image by clicking the relevant button, at which point the image load dialog is provided in the same way as when the cell wall image was loaded. Select the nuclei image, and select the appropriate color channel that it uses. Any plug-in that is enabled and has the necessary images assigned will be executed at the same time as the standard CellSeT measurement set, and results will be combined into the output table.

17. Once all measurements are completed, a new image can be loaded by clicking File, then New image. All loaded data will be erased, and CellSeT will start again with the new image as a wall reference.

4 Notes

1. If using media supplemented with sucrose, increase incubation time to 10 min.
2. *Arabidopsis* lines with well-defined plasma membrane markers include Lti6a-GFP [8] and Wave line 131 (available in EYFP, mCherry, and mCerulean variants [9]).
3. PI is potentially mutagenic—always wear suitable protective clothing and gloves. PI degrades in light and stocks and incubation solutions are thus best kept in opaque containers. Cover the incubation chamber at all times. Only living cells are impermeant to PI, so care must be taken when handling seedlings as any damaged cells will quickly accumulate PI and fluoresce strongly, obscuring anatomical details.
4. Care at the imaging stage is essential to produce images amenable for segmentation and subsequent analysis. To determine if background pixels are set to zero and those corresponding to the fluorophore are not saturated, use a suitable lookup table in which zero and the upper limit of intensity are mapped to contrasting colors.
5. Select an image size and magnification that ensures cells can be easily distinguished with reasonable contrast between the cell wall/plasma membrane and internal contents. For *Arabidopsis* root tips, a suitable compromise between cellular and tissue detail is to use an image resolution of 1024 by 512 pixels using a 20× objective with a 1.5 zoom factor. The resulting image covers 500 μm of the root tip with enough resolution to segment the smallest cells in the meristem in a manageable file size (*see* Fig. 1a).
6. CellSeT requires 2D images. If a 3D stack has been taken, it is necessary to extract the plane of interest as a 2D image. If this plane does not lie flat or parallel with the default stack slices, another tool can be used to export a surface through the stack as a 2D image (e.g., Surface Project [10] or MorphoGraphX [11]).
7. Confocal images, as with all digital images, are affected by noise. This is erroneous data which affects the real data and is derived both from the properties of the sensor and the biological sample itself. Noise has different statistical properties, which is why different filtering methods are used (for more details *see* refs. 12, 13).

8. If segmentation of the cell network within CellSet leads to poor results regardless of the threshold chosen, it may be that the amount of filtering at the previous stage should be adjusted. Too much filtering will reduce image clarity and cause undersegmentation, with many cells being omitted. Too little filtering will result in oversegmentation, with many cells segmented multiple times. To redo the filtering stage, click the back arrow, and then click Undo Filters. The image can then be refiltered as required.
9. While it may seem that manually added walls must be carefully placed exactly over the corresponding region of the image, this is not necessary. CellSet uses a series of Active Contours to refine these wall positions automatically, which will pull them towards the walls in the underlying image. For this reason, walls need only be placed approximately over the image, but sufficiently close to the actual locations.
10. It may be necessary to reconstruct every single cell in a confocal image for a given experiment. However, where an experiment focuses on a single type of cell, cell file, or a small section of tissue, then only those cells need be reconstructed. Any cells not required for quantification can be ignored, and will not affect results.
11. Any cell refinement can be saved by clicking File, then Save Refinement. Saved refinements are useful if quantification is likely to be repeated, or if this data should be preserved for reference at a later date. Previously saved refinements (stored in .crf files) can be loaded, significantly speeding up processing. Previous stages such as image filtering and segmentation can be skipped if a refinement file exists.
12. Values in the section labeled Snake Parameters will affect how the active contours track the image and the resulting geometry. The node spacing alters how far apart control points on each active contour are created. Decreasing this value will produce more control points, resulting in a snake that is more accurate, but possible more susceptible to image noise. Altering the parameters of Curvature, Continuity, and Image Weight will alter how much snakes respond attempt to remain straight, remain evenly spaced, and remain attracted to image information.
13. The Tag All button highlights every nonhighlighted cell and wall in an image with a General tag. This is a quick way of highlighting all objects, such that all objects are quantified during the measurement stage. No semantic information will be included, but this might not be required in some experiments.
14. The data held in the XML files can be imported into vertex-based modeling frameworks such as OpenAlea and VirtualLeaf [14, 15].

Acknowledgments

The authors wish to acknowledge the support of the Biotechnology and Biological Sciences Research Council (BBSRC) and Engineering and Physical Sciences Research Council (EPSRC) funding to the Centre for Plant Integrative Biology (CPIB) and BBSRC responsive mode grant support to M.P.

References

1. Vos U, Larrieu A, Wells DM (2013) From jellyfish to biosensors: the use of fluorescent proteins in plants. Int J Dev Biol 57:525–533
2. French AP, Mills S, Swarup R, Bennet MJ, Pridmore TP (2008) Colocalization of fluorescent markers in confocal microscope images of plant cells. Nat Protoc 4:619–628
3. Pawley J (2000) The 39 steps: a cautionary tale of quantitative 3-D fluorescence microscopy. Biotechniques 5:884–889
4. Band LR, Wells DM, Larrieu A, Sun J, Middleton AM, French AP, Brunoud G, Sato EM, Wilson MH, Peret B, Oliva M, Swarup R, Sairanen I, Parry G, Ljung K, Beeckman T, Garibaldi JM, Estelle M, Owen MR, Vissenberg K, Hodgman TC, Pridmore TP, King JR, Vernoux T, Bennett MJ (2012) Root gravitropism is regulated by a transient lateral auxin gradient controlled by a tipping-point mechanism. Proc Natl Acad Sci U S A 109:4668–4673
5. Pound MP, French AP, Wells DM, Bennett MJ, Pridmore TP (2012) CellSeT: novel software to extract and analyze structured networks of plant cells from confocal images. Plant Cell 24:1353–1361
6. Schindelin J, Arganda-Carreras I, Frise E, Kaynig V, Longair M, Pietzsch T, Preibisch S, Rueden C, Saalfeld S, Schmid B, Tinevez JY, White DJ, Hartenstein V, Eliceiri K, Tomancak P, Cardona A (2012) Fiji: an open-source platform for biological-image analysis. Nat Methods 9:676–682
7. Sethuraman V, French A, Wells D, Kenobi K, Pridmore T (2012) Tissue-level segmentation and tracking of cells in growing plant roots. Mach Vis Appl 23:639–658
8. Cutler SR, Ehrhardt DW, Griffitts JS, Somerville CR (2000) Random GFP::cDNA fusions enable visualization of subcellular structures in cells of *Arabidopsis* at a high frequency. Proc Natl Acad Sci U S A 97:3718–3723
9. Geldner N, Dénervaud-Tendon V, Hyman DL, Mayer U, Stierhof Y-D, Chory J (2009) Rapid, combinatorial analysis of membrane compartments in intact plants with a multicolor marker set. Plant J 59:169–178
10. Band L, Wells D, Fozard J, Ghetiu T, French A, Pound M, Wilson M, Yu L, Li W, Hijazi H, Oh J, Pearce S, Perez-Amador M, Yun J, Kramer E, Alonso J, Godin C, Vernoux T, Hodgman TC, Pridmore T, Swarup R, King J, Bennett MJ (2014) Systems analysis of auxin transport in the Arabidopsis root apex. Plant Cell 26(3):862–875
11. Kierzkowski D, Nakayama N, Routier-Kierzkowska A-L, Weber A, Bayer E, Schorderet M, Reinhardt D, Kuhlemeier C, Smith RS (2012) Elastic domains regulate growth and organogenesis in the plant shoot apical meristem. Science 335(6072):1096–1099
12. Roberts TJ, McKenna SJ, Du C-J, Wuyts N, Valentine TA, Bengough AG (2009) Estimating the motion of plant root cells from in vivo confocal laser scanning microscopy images. Mach Vis Appl 21:921–939
13. Pawley J (2006) Handbook of biological confocal microscopy, 3rd edn. Springer, New York
14. Pradal C, Dufour-Kowalski S, Boudon F, Fournier C, Godin C (2008) OpenAlea: a visual programming and component-based software platform for plant modeling. Funct Plant Biol 35:751–760
15. Merks RM, Guravage M, Inzé D, Beemster GTS (2011) VirtualLeaf: an open-source framework for cell-based modeling of plant tissue growth and development. Plant Physiol 155: 656–666

Chapter 12

Live Cell Imaging of the Cytoskeleton and Cell Wall Enzymes in Plant Cells

Arun Sampathkumar and Raymond Wightman

Abstract

The use of live imaging techniques to visualize the dynamic changes and interactions within plant cells has given us detailed information on the function and organization of the cytoskeleton and cell wall associated proteins. This information has grown with the constant improvement in imaging hardware and molecular tools. In this chapter, we describe the procedure for the preparation and live visualization of fluorescent protein fusions associated with the cytoskeleton and the cell wall in *Arabidopsis*.

Key words Live cell imaging, Microtubules, Actin filaments, Cell wall, Point scanning confocal microscopy, Spinning disc microscopy, Hypocotyls, Xylem vessels

1 Introduction

Studies using fixed plant tissue have given us important insights into the organization of the actin filament (AF) and microtubule (MT) networks, but gives no or limited information on the dynamic behavior of these cytoskeletal components and their associated proteins and cargo. Initial live cell imaging of AFs and MTs was carried out by microinjection of actin-binding dyes or actin-binding components and tubulin, respectively, into plant cells [1]. However, microinjection of such substances in living cells is very challenging, and has been successful only in specific cell types. An alternative strategy is to transiently or stably transform plant cells with actin or MT reporters, which consists of a fluorescent protein fused to an actin- or MT-binding domain. Several different actin- and MT-binding reporters have been developed in the last decade. The first reported use of such an AF marker was the fusion of the actin-binding domain of mouse talin to a green fluorescent protein (GFP) for observations in pollen tubes [2]. Fusion of GFP to the microtubule binding domain of MAP4, a mammalian MT associated protein, and subsequent transient expression of the

José M. Estevez (ed.), *Plant Cell Expansion: Methods and Protocols*, Methods in Molecular Biology, vol. 1242,
DOI 10.1007/978-1-4939-1902-4_12,

protein in epidermal cells of fava bean lead to the visualization of dynamic MTs [3]. These experiments were followed by production of stably transformed *Arabidopsis* plants expressing several actin and microtubule reporter proteins. The most commonly used actin reporter is the GFP fusion of the second actin-binding domain of a protein fimbrin1 (GFP-FABD2). Stably transformed plants of this construct exhibited "normal" actin organization and did not cause any visible changes in plant growth and development [4, 5]. *Arabidopsis* plants expressing MT reporters have made use of direct fusion of GFP to tubulin subunits such as TUA6 [6]. Several variants of fluorescent fusion proteins to different tubulin genes are now available.

Accompanying the first report describing MTs using improved preparations for electron microscopy, was the presence of fibrillar cellulose structures that followed the orientation of MTs [7]. The particles that synthesize these cellulose microfibrils were later observed through freeze fracture preparations of corn and mung bean plants as rosette like complexes in the plasma membrane [8] and such complexes were postulated to move through the plasma membrane as the cellulose chain elongates [9]. Identification of the genes encoding cellulose synthases (CESA), coupled with the construction of functional fluorescent protein fusions to the CESA protein subunits, has enabled the tracking of these complexes in living cells [10–12].

The use of epifluorescent- and conventional confocal-based microscopes for visualizing these probes has greatly increased our understanding of these cell components. This has also been applied to imaging of interacting factors and other cell wall enzymes. Some of these components, for example, the Golgi and other smaller cytoskeleton interacting compartments, move and interact at speeds in the range of milliseconds along with changes in cytoskeletal structure. This requires the application of high speed imaging techniques such as variable angle epifluorescence and spinning disc microscopes. These platforms have allowed the visualization of more rapid and dynamic changes in plant cells [13, 14]. These techniques further allow monitoring of the complex interplay between the cell wall and the cytoskeleton structures, as well as between both the cytoskeleton in living cells [10, 15, 16]. While these high acquisition, low bleaching techniques are applicable for imaging epidermal cells of *Arabidopsis* when studying processes that occur during primary wall deposition, the study of secondary wall deposition *in planta* is much more challenging and the emphasis is upon achieving optimum focal distance whilst retaining, where possible, the ability to see individual structures within the developing vessels of the xylem [17].

2 Materials

2.1 Plant Materials and Growth Conditions

1. *Arabidopsis* seeds are surfaced sterilized using either 70 % (v/v) ethanol or a mixture of sodium hypochlorite (30 % v/v) and triton X-100 (1 % v/v) for 8–10 min, rinsed with sterile water three to five times, and stratified for 3 days at 4 °C.
2. Murashige and Skoog media: 1× Murashige and Skoog salts, 8 g/L agar, 1× B5 vitamins, and 10.8 g/L sugar.
3. Half the quantities of Murashige and Skoog media with 1.5 g/L agar and omitting the sugar.
4. The plates are coved in aluminum foil and placed vertically at 22 °C for 3 days for hypocotyl growth and imaging. For imaging developing xylem tissue stratified seeds are plated and placed vertically at 22 °C in the light for 5–6 days.

2.2 Imaging Chamber for Hypocotyls

1. Dark-grown hypocotyls are imaged in a simple custom designed imaging chamber. A conventional glass side or a metal slide of 75 × 25 mm dimension is modified by drilling a hole of 22 mm diameter in the center. A cover glass of 24 × 32 mm of thickness NO. 1.5 is fixed to the slides using silicone grease dispensed from a syringe fitted with a large diameter blunt ended needle.
2. 1 % agarose pad to prevent mechanical damage and drying of seedlings. Circular cover glass of 18 mm diameter is required for preparation.

2.3 Tools and Microscopes

1. General tools required for sample mounting include sterile wooden toothpicks, 20–200 μL pipettes, kimwipes, petri dish, and sterile water.
2. A basic stereo fluorescence microscope is required to rapidly screen the dark-grown seedlings to confirm the presence of the fluorescent signal if the lines are segregating.
3. Confocal microscopes
   (a) Hypocotyl Imaging: Spinning disc microscope are usually inverted microscopes (NIKON Ti-E), however upright versions are also available (*see* **Note 1**). The major components of the microscope are the Yokogawa spinning disc head, an EMCCD camera, solid state lasers 491 nm for GFP or yellow fluorescent protein (YFP) and 561 nm for mCherry or red fluorescent protein excitation (RFP), band pass emission filters 525/550 nm for GFP and YFP, 595/650 nm for mCherry and RFP (CHROMA TECHNOLOGY). High numerical aperture objective CFI

APO TIRF 100× N.A. 1.49 oil immersion NIKON lens was used for imaging. However, lower N.A. objectives can also be used but a magnification of 60× or greater is ideal for imaging CESA particles.

(b) Developing protoxylem vessels of root: The emphasis for successfully imaging the root protoxylem is more upon the optical hardware rather than the light source or detector. A water immersion Leica HCX PL APO CS ×63 NA 1.2 objective (part no. 506220) has been used successfully for visualizing the actin, microtubules, and secondary wall CESAs for both standard epifluorescent and confocal laser scanning systems. Other manufacturers supply equivalent objective lenses. For standard epifluorescence, small improvements have been obtained with an oil immersion objective fitted with a coverslip correction collar (Leica HCX PL APO ×100 part no. 506220).

3 Methods

3.1 Hypocotyl Sample Preparation and Mounting

1. After 3 days of growth, dark-grown hypocotyls are typically 10 mm in length in 1× Murashige and Skoog media. Seedlings are rapidly screened under the stereo-fluorescence microscope without opening the petri dishes and selected based on the expression of the fluorescence protein and wrapped immediately with the foil (*see* **Note 2**).
2. 1 % agarose solution in water is prepared and cooled to bearable warmth. Circular cover glasses are placed on a clean bench and 100 μL of agarose solution is dispensed on it. This is allowed to cool for not more than 10 s and a second cover glass is placed on it gently, which spreads the agar uniformly along the cover slip and allowed to solidify (*see* **Note 3**).
3. A cover glass of 24 × 32 mm of thickness NO. 1.5 is affixed on one side of the custom designed slide using silicone grease applied along the entire length along the borders. Grease can be applied using a syringe fitted with a blunt tip needle, by gently squeezing the syringe and gradually moving it along the border (Fig. 1a).
4. A small droplet of sterile water is placed on the inner side of the chamber and seedlings are lifted with wooden toothpicks and placed on the water droplet.
5. One side of the circular cover slips of the agarose pad is removed, exposing the solidified agar pad. The pad is now lifted using forceps with the other face still having the coverslip attached. This is now inverted and the exposed agar side is placed on top of the seedling gently.

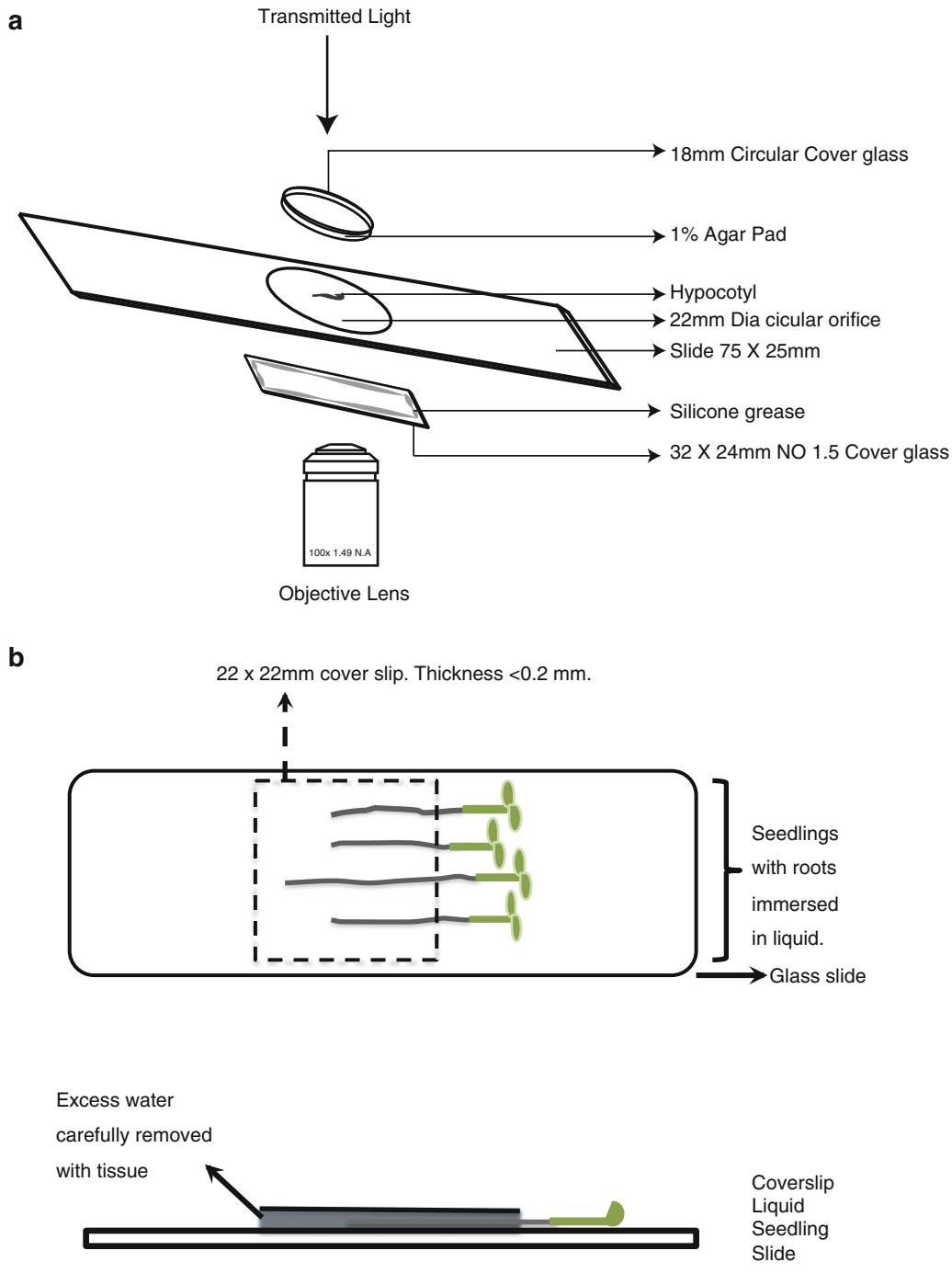

Fig. 1 Illustration representing imaging setup for (**a**) hypocotyl imaging on an inverted spinning disc microscope, (**b**) xylem vessels on an upright point scanning confocal microscope

6. Using pipette water is now added to the sides of the agar pad till the entire region of the circular agar pad is filled with water. This will prevent the sample from mechanical damage as well as drying (*see* **Note 4**).

3.2 Imaging of Hypocotyls

1. The slide is now mounted on the inverted microscope with the rectangular cover glass in contact with the objective and the sample is allowed to settle on the microscope stage for at least 5 min before imaging.
2. Using the transmitted light the hook of the hypocotyl consisting of actively expanding cells is brought into the field of view. This region is ideal for imaging dynamics of cytoskeletal as well as CESA complexes in expanding cells. Whereas, the lower files of cells are already expanded cells and would have less dense cytoskeletal arrays and CESA complexes.
3. Now the sample is viewed through the camera and the first plane that comes in focus along the *Z*-axis is usually the cortical plane. Exposure time of 100–200 ms is used to scan for the region of interest, which makes it easier to move the sample and observe in the microscope software user interface. A relatively flat cortical region is most favorable for doing time series imaging, this focal plane is then maintained for acquisition. This process should be very brief and unwanted exposure to laser light should be avoided.
4. Based on the intensity of the fluorescent markers the exposure times for acquisition are set; this might vary between 200 and 800 ms (*see* **Note 5**). Single-channel MT imaging can be done for a period lasting up to 5 min or longer based on the amount of photo-bleaching with a 5-s time interval between each frame. Actin dynamics on the other hand is much faster and a lower time interval ranging not more than 1 s should be used during acquisition. Dual-channel imaging of AF and MT dynamics is done with a time interval of 2 s or less between each acquired frame of fluorophores.
5. CESA imaging is carried at a focal point around 0.5 μm higher than the cortical MT array. Similar to the cytoskeleton imaging the exposure time might vary depending on the line used for imaging. A time interval of 5 s is maintained during the period of acquisition between each frame for single-channel CESA imaging. Dual imaging between microtubule and CESA is done with a time interval of 5 s between each time point. However dual imaging of AFs along with CESAs is carried out with a time interval of not more than 2 s for at least 5 min (*see* **Note 6**).

3.3 Imaging of Developing Xylem Vessels in Planta

1. Seedlings grown on half the concentration of Murashige and Skoog media are taken from plates and placed on a glass slide so that the root is lying completely flat. Two to four seedlings are arranged side by side and drops of water applied immediately and directly to the roots to prevent drying.
2. A cover slip (either 25 × 25 mm or 50 × 25 mm) is placed over the roots but does not cover the hypocotyls. This results in a slide

with the roots beneath the cover slip with the hypocotyls all emanating from one edge (Fig. 1b).

3. Excess water is removed with tissue paper such that distance between the cover slip and the top of the root is minimized. No pressure should be applied to the coverslip.
4. (Optional) Slides can be sealed along three edges leaving the side containing the hypocotyls untouched.
5. YFP-IRX3 (CESA7) fusion proteins and actin, microtubule, endoplasmic reticulum, and Golgi reporters placed under the control of the *IRX3* promoter can be visualized using lower power objectives in order to find the region for imaging. Behind the root tip fluorescence can be observed at the two poles and becomes more intense within the region of active secondary wall deposition. Where one pole is higher up in the sample, then this can give better results due to the reduced focal distance required for imaging.
6. After switching to the higher power objective lens, focus upon the top of the uppermost vessel and then rotate the correction collar to provide the optimum focal depth. Newly formed protoxylem vessels will possess YFP-IRX3 in intracellular compartments. Moving away from the root tip YFP-IRX3 will be additionally found at cortical sites of secondary wall deposition arranged in spirals or complete hoops. Where secondary walls have undergone a great deal of thickening, diffraction of the signal will likely become a problem. The best images are obtained in regions devoid or exhibiting minimal secondary thickening.
7. Imaging of the vessels has been successfully carried out using both epifluorescence (*see* **Note 7** and equipped with both water and oil immersion objectives) and confocal systems (equipped with water immersion objectives). For modern confocal systems, optimum signal to noise is found when the airy diameter is set to approx 1.5 units (*see* **Note 8**).
8. During time lapse acquisition complete and sudden disappearance of YFP signal is attributed to the onset of programmed cell death (PCD) and a new region or sample will need to be found (*see* **Note 9**).

4 Notes

1. Upright spinning disc microscopes with the spinning disc head fitted on top of the microscope body can cause minor vibration during acquisition due to the rotation of the spinning disc as well as the cooling fan in the EMCCD camera.
2. Care should be taken not to expose the etiolated seedlings to light, and to maintain the correct orientation of the seedlings. These factors are known to affect the physiology of the plant

thereby causing changes to dynamic behavior of the system under study.

3. After preparation of the agarose pad, they should be stored in an airtight container with a moist tissue paper to prevent drying of agarose pads.
4. After adding water to the circular agarose pad, excess water is removed by dabbing tissue papers on the side of the agarose pad. Excess water will cause the sample to drift during the acquisition process.
5. Laser powers needed for imaging are determined in such a way, that at the set value an output of 3–3.5 mW is achieved out of the optical cable before entry into the spinning disc head and an output of 250–300 μW is obtained at the back end of the objective. This is done periodically by checking the laser power using a power meter. The set values of the different lasers would differ based on the different solid-state lasers used in the setup.
6. Seedlings should be imaged for not more than 30 min, after which fresh seedlings should be prepared.
7. Filter sets (Chroma) used are YFP (part no. 41028), CFP (part no. 31044v2), mCherry (part no. 41043), and for systems fitted with a color camera a YFP/mCherry dual filter set (part no. 51019).
8. For fast acquisition coupled with bleaching analysis [18], the airy disk was opened to 5.5 airy units for a Leica SP2 confocal system.
9. Disappearance of YFP signal has been attributed to the pH change that occurs within the cytoplasm at the onset of PCD [19]. During rapid time lapse imaging disappearance of YFP can appear as a "wave" beginning at one end of the vessel and ending at the opposite end.

Acknowledgements

We would like to thank Dr. Staffan Persson at the Max Planck Institute of Molecular Plant Physiology for his comments on the chapter.

References

1. Hepler PK et al (1993) Cytoskeletal dynamics in living plant cells. Cell Biol Int 17(2):127–142
2. Kost B, Spielhofer P, Chua NH (1998) A GFP-mouse talin fusion protein labels plant actin filaments in vivo and visualizes the actin cytoskeleton in growing pollen tubes. Plant J 16(3):393–401
3. Marc J et al (1998) A GFP-MAP4 reporter gene for visualizing cortical microtubule rearrangements in living epidermal cells. Plant Cell 10(11):1927–1940
4. Ketelaar T, Anthony RG, Hussey PJ (2004) Green fluorescent protein-mTalin causes defects in actin organization and cell expansion in Arabidopsis and inhibits actin depolymeriz-

ing factor's actin depolymerizing activity in vitro. Plant Physiol 136(4):3990–3998

5. Sheahan MB et al (2004) A green fluorescent protein fusion to actin-binding domain 2 of Arabidopsis fimbrin highlights new features of a dynamic actin cytoskeleton in live plant cells. Plant Physiol 136(4):3968–3978
6. Ueda K, Matsuyama T, Hashimoto T (1999) Visualization of microtubules in living cells of transgenic Arabidopsis thaliana. Protoplasma 206(1–3):201–206
7. Ledbetter MC, Porter KR (1963) A "microtubule" in plant cell fine structure. J Cell Biol 19(1):239–250
8. Mueller SC, Brown RM (1980) Evidence for an intramembrane component associated with a cellulose microfibril-synthesizing complex in higher plants. J Cell Biol 84(2):315–326
9. Delmer DP, Amor Y (1995) Cellulose biosynthesis. Plant Cell 7(7):987–1000
10. Paredez AR, Somerville CR, Ehrhardt DW (2006) Visualization of cellulose synthase demonstrates functional association with microtubules. Science 312(5779):1491–1495
11. Bischoff V et al (2011) Phytochrome regulation of cellulose synthesis in Arabidopsis. Curr Biol 21(21):1822–1827
12. Desprez T et al (2007) Organization of cellulose synthase complexes involved in primary cell wall synthesis in Arabidopsis thaliana. Proc Natl Acad Sci U S A 104(39):15572–15577
13. Staiger CJ et al (2009) Actin filament dynamics are dominated by rapid growth and severing activity in the Arabidopsis cortical array. J Cell Biol 184(2):269–280
14. Shaw SL, Kamyar R, Ehrhardt DW (2003) Sustained microtubule treadmilling in Arabidopsis cortical arrays. Science 300(5626): 1715–1718
15. Sampathkumar A et al (2011) Live cell imaging reveals structural associations between the actin and microtubule cytoskeleton in Arabidopsis. Plant Cell 23(6):2302–2313
16. Sampathkumar A et al (2013) Patterning and lifetime of plasma membrane-localized cellulose synthase is dependent on actin organization in Arabidopsis interphase cells. Plant Physiol 162(2):675–688
17. Wightman R, Turner SR (2008) The roles of the cytoskeleton during cellulose deposition at the secondary cell wall. Plant J 54(5):794–805
18. Wightman R, Marshall R, Turner SR (2009) A cellulose synthase-containing compartment moves rapidly beneath sites of secondary wall synthesis. Plant Cell Physiol 50(3):584–594
19. Young B et al (2010) pH-sensitivity of YFP provides an intracellular indicator of programmed cell death. Plant Methods 6:27

Chapter 13

Using the Split-Ubiquitin Yeast Two-Hybrid System to Test Protein–Protein Interactions of Transmembrane Proteins

Logan Bashline and Ying Gu

Abstract

Proteins are responsible for many biological processes within living organisms. Many proteins have the ability to specifically interact with other proteins in order to function properly. The identification of protein–protein interactions (PPIs) can provide useful information about the function of a protein of interest. Historically, the properties of transmembrane proteins have caused difficulty in analyzing PPIs among transmembrane proteins. The development of an assay that is capable of analyzing PPIs involving transmembrane proteins, the split-ubiquitin yeast two-hybrid (SU-Y2H) assay, has provided a method to probe pairwise PPIs between two proteins of interest or to screen a single protein of interest for interaction partners. The following protocol explains how to use the SU-Y2H assay, which is compatible with the use of transmembrane proteins, to investigate PPIs between two proteins of interest and also briefly describes how to adjust the system to be used as a high-throughput screen for interaction partners of a particular protein of interest.

Key words Split-ubiquitin, Yeast two-hybrid, Protein–protein interaction, Transmembrane protein, Yeast

Abbreviations

3-AT	3-Amino-1,2,4-triazole
ADE2	Phosphoribosylaminoimidazole carboxylase gene in the adenine biosynthesis pathway
ADHp	Promoter of yeast alcohol dehydrogenase 1
AmpR	Ampicillin resistance gene
ccdb	Gene encoding cytotoxic gene
CmR	Chloramphenicol resistance gene
Cub	C-terminal half of ubiquitin
ddH_2O	Double distilled water
DMF	Dimethylformamide
DMSO	Dimethyl sulfoxide
H or His	Histidine
HIS3	Imidazoleglycerol-phosphate dehydratase gene in the histidine biosynthesis pathway
L or Leu	Leucine
LacZ	β-Galactosidase gene

José M. Estevez (ed.), *Plant Cell Expansion: Methods and Protocols*, Methods in Molecular Biology, vol. 1242,
DOI 10.1007/978-1-4939-1902-4_13,

LEU2	Beta-isopropylmalate dehydrogenase gene in the leucine biosynthesis pathway
Met	Methionine
Met25p	Methionine repressive promoter
NaCl	Sodium chloride
Nub	N-terminal half of ubiquitin
NubG	Mutated N-terminal half of ubiquitin with reduced Cub binding affinity
PEG	Polyethylene glycol
PLV	ProteinA-LexA-VP16 reporter module
PPI	Protein–protein interaction
SD	Synthetic dropout
SpecR	Spectinomycin resistance gene
ssDNA	Salmon sperm DNA
SU-Y2H	Split-ubiquitin yeast two-hybrid
TE	Tris–HCl and EDTA buffer
TOPO	Topoisomerase
TRP	Tryptophan
TRP1	Phosphoribosylanthranilate isomerase gene of the tryptophan biosynthesis pathway
USP	Ubiquitin-specific protease
W	Tryptophan
X-Gal	5-bromo-4-chloro-3-indolyl-β-D-galactopyranoside
Y2H	Yeast two-hybrid

1 Introduction

The molecular machinery of living cells is predominantly comprised of proteins, which provide a majority of the biological functions that are required to begin, develop, and sustain the life of cells and organisms. One quality possessed by proteins that is essential for proper function is the ability of certain proteins to specifically and coordinately form noncovalent interactions with other proteins. The identification of protein–protein interactions (PPIs) can significantly aid in the characterization of the function of a protein of interest, and the establishment of large-scale protein–protein interactomes can provide a more comprehensive understanding of complex biological processes.

On account of the importance of analyzing PPIs, several techniques have been developed to detect PPIs [1]. One popular method by which PPIs have been tested or screened is the traditional yeast two-hybrid (Y2H) assay [2]. In the traditional Y2H, one protein of interest, referred to as the bait protein, is fused to the DNA-binding domain of a transcription factor (GAL4) while a second protein of interest, referred to as the prey protein, is fused to the activation domain of GAL4. If an interaction occurs between the bait and prey proteins when coexpressed in yeast, the GAL4 transcription factor becomes reconstituted and triggers the expression of reporter genes that signify the bait and prey protein interaction in yeast (Fig. 1a). One limitation of the traditional Y2H is the

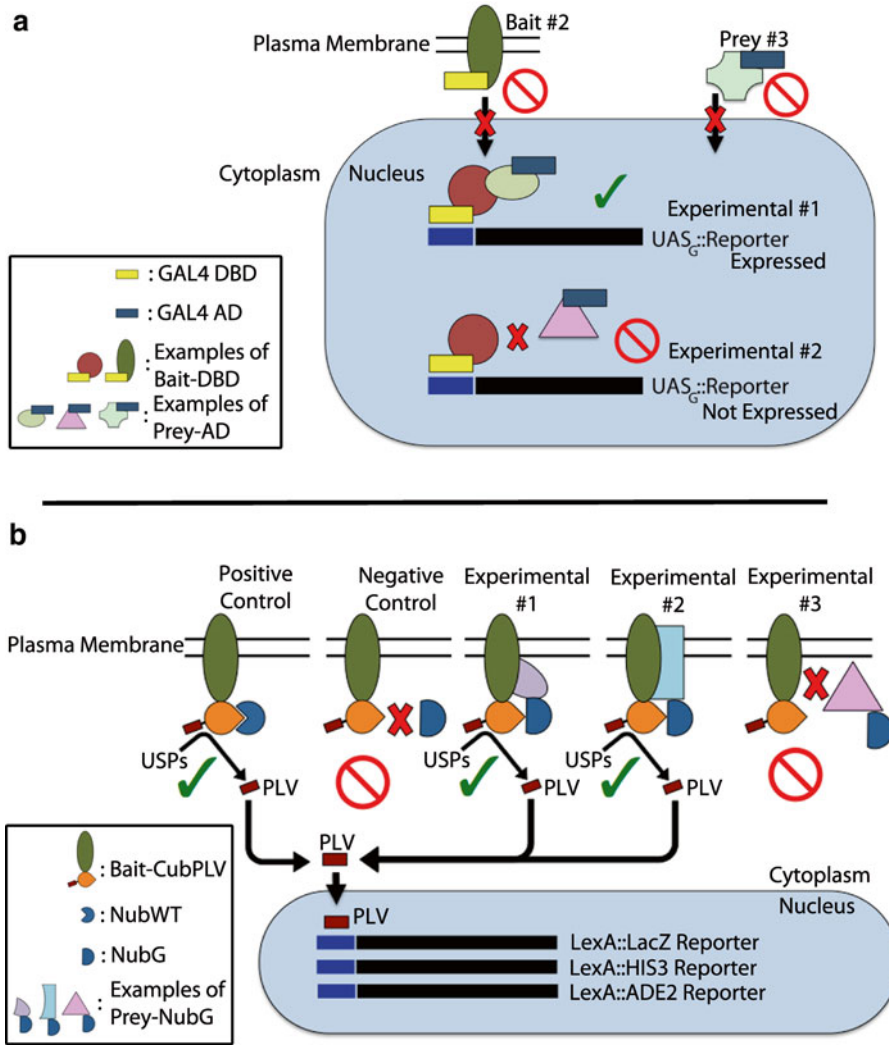

Fig. 1 Schematic representations of the traditional yeast two-hybrid (Y2H) assay (**a**) and the split-ubiquitin yeast two-hybrid (SU-Y2H) assay (**b**). (**a**) In the traditional Y2H, the bait protein is fused with the DNA-binding domain (DBD) of the GAL4 transcription factor and the prey protein is fused to the activation domain (AD) of GAL4. A positive bait–prey interaction in the nucleus of the yeast reconstitutes a functional GAL4 transcription factor, which triggers the expression of UAS_G regulated reporter genes (Experimental #1). If the bait and prey do not interact, no reporter expression occurs (Experimental #2). If either the bait protein (bait #2) or the prey protein (prey #3) is unable to enter the nucleus, the traditional Y2H assay is not suitable for detecting PPIs. (**b**) In the SU-Y2H, the bait protein is fused with the C-terminal half of ubiquitin (Cub), which is in turn fused with a Protein A-LexA-VP16 (PLV) reporter module to create bait-CubPLV. The prey protein is fused with a mutated N-terminal half of ubiquitin (NubG), which has a reduced binding affinity with Cub, to create NubG-prey or prey-NubG. NubG and Cub will reconstitute a functional ubiquitin molecule only if the bait and prey proteins interact (Experimental #1 and #2). The reconstituted ubiquitin is recognized by ubiquitin specific proteases (USPs) in the yeast that release the PLV reporter module, which activates the transcription of LexA-driven reporter genes. As a positive control, NubWT binds to Cub of the bait-CubPLV chimeric protein to mimic a positive interaction in the system. As a negative control, NubG lacking a prey protein is unable to bind to bait-CubPLV in the absence of a prey protein and should not elicit a reporter response. Experimental #1 shows an interaction between a transmembrane bait protein and a cytoplasmic prey protein. Experimental #2 shows an interaction between two transmembrane proteins. Experimental #3 shows a negative result in which the bait and prey proteins do not interact and therefore do not trigger reporter expression

requirement that the bait–prey protein interaction must occur in the yeast nucleus, the site of GAL4 function. Therefore, the traditional Y2H is incapable of analyzing PPIs of proteins that cannot gain access to the nucleus, such as transmembrane proteins. Likewise, many biochemical techniques for analyzing PPIs, such as coimmunoprecipitation or in vitro pull down assays, have difficulty in the analysis of transmembrane proteins due to the limited solubility exhibited by many transmembrane proteins. In order to circumvent the limitations of existing assays in analyzing PPIs of transmembrane proteins, a membrane-based variation of the Y2H assay, the split-ubiquitin yeast two-hybrid (SU-Y2H) assay, was developed [3, 4]. In the SU-Y2H assay, the bait protein is fused to the C-terminal half of ubiquitin (Cub) that has an attached ProteinA-LexA-VP16 (PLV) reporter module to create a bait-CubPLV chimeric protein, and the prey protein is fused with a mutated version of the N-terminus of ubiquitin (NubG) to create a prey-NubG (XN21_GW) or NubG-prey (NX32_GW) chimeric protein (Fig. 1b). The mutation in NubG causes a significant reduction in the binding affinity between Nub and Cub compared to the wild type Nub (NubWT), thereby preventing spontaneous reconstitution of a functional ubiquitin molecule. However, if the bait and prey proteins interact in yeast, the NubG of the prey construct and the Cub of the bait construct will reconstitute a functional ubiquitin protein, which is then recognized by ubiquitin-specific proteases (USPs) that cleave and release the PLV module from the bait-CubPLV. The PLV module is then free to migrate to the nucleus to activate the transcription of reporter genes (Fig. 1b). The reporter genes in the SU-Y2H assay are LacZ, which is used for blue/white screening in the presence of X-Gal, HIS3, which is a histidine auxotrophy marker, and ADE2, which is an adenine auxotrophy marker.

As with other types of Y2H assays, false positive and false negative results are possible, so proper positive and negative controls must be in place. As a positive control, bait-CubPLV constructs should be tested with NubWT to ensure that the CubPLV is properly translated and displayed in the yeast when fused with the bait protein of interest. As a negative control, bait-CubPLV constructs should also be tested with NubG that lacks a prey protein to ensure that nonspecific activation of the reporter does not occur in the absence of a prey protein. Additional strategies can be taken to increase the stringency of the reporter system that is used to detect the PPIs. First, the transcription of bait-CubPLV is controlled by a Met25 promoter and can be repressed by the addition of methionine to the yeast growth medium (Fig. 2). Therefore, increasing the concentration of methionine suppresses the expression of bait-CubPLV and attenuates the reporter system. Second, 3-amino-1,2,4-triazole (3-AT) acts as a competitive inhibitor of

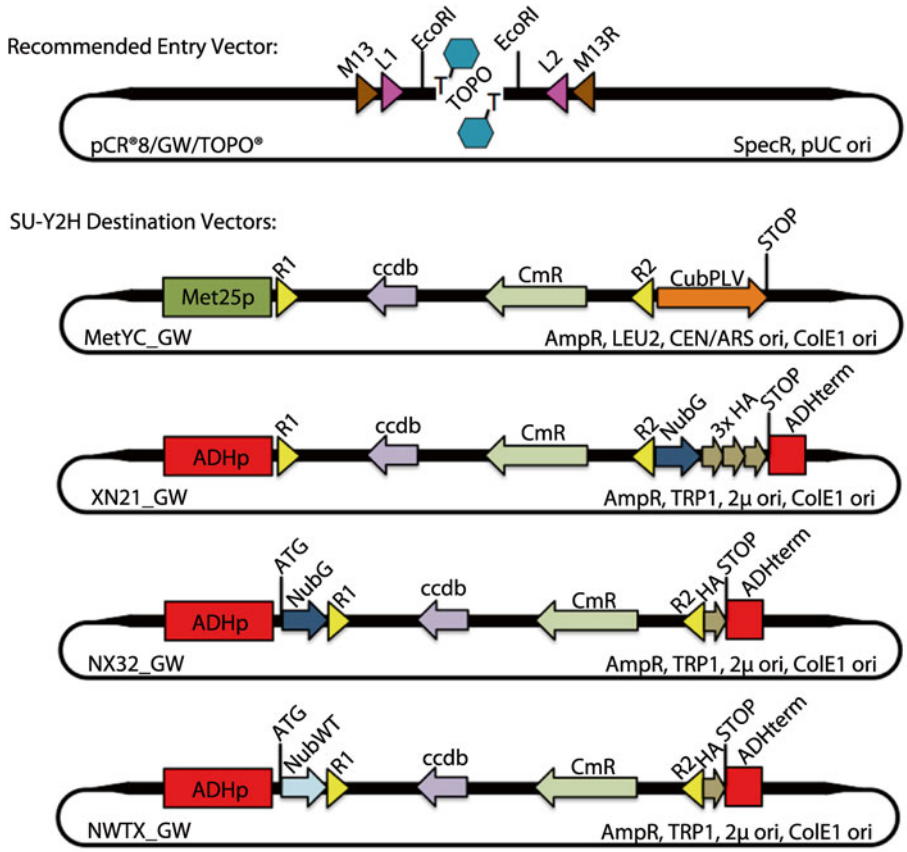

Fig. 2 Vector information for the recommended entry vector, pCR®8/GW/TOPO® vector (Invitrogen), and the SU-Y2H destination vectors, MetYC_GW (GenBank #HQ646605 and ABRC stock # CD3-1740), XN21_GW (GenBank #HQ700951 and ABRC stock # CD3-1734), NX32_GW (GenBank #HQ700952 and ABRC stock # CD3-1737), NWTX_GW (GenBank #HQ700954 and ABRC stock # CD3-1739)

imidazoleglycerol-phosphate dehydratase, the gene product of HIS3 [5]. The addition of 3-AT can be used to increase the stringency of the HIS3 auxotrophy selection.

The SU-Y2H protocol highlighted below provides a detailed, step-by-step, robust procedure for testing the pairwise interaction between two proteins of interest via cotransformation of yeast with bait-CubPLV and prey-Nub vectors. The SU-Y2H bait and prey vectors have been modified for use with Gateway® recombination-based cloning for rapid, easy, and high-throughput cloning (Fig. 2) [6, 7]. Although this protocol focuses on testing for an interaction between two proteins of interest, high-throughput screening of putative interaction partners of a single protein of interest is also possible with this system by making a few adjustments (*see* **Note 31**) [7].

2 Materials

All stock solutions and media are prepared using double distilled water (ddH_2O) unless otherwise noted.

2.1 Vectors and Cloning Supplies

1. Entry vectors containing the genes of interest flanked by 5′ attL1 and 3′ attL2 Gateway® recombination sites (Fig. 2) (*see* **Note 1**).
2. SU-Y2H destination vectors: MetYC_GW (HQ646605), NWTX_GW (HQ700954), XN21_GW (HQ700951), NX32_GW (HQ700952) (Fig. 2).
3. Gateway® LR Clonase™ II enzyme mix kit (Invitrogen).
4. Chemically competent *E. coli* cells.
5. 1.5-mL microcentrifuge tubes, *autoclaved*.
6. 0.2-mL plastic PCR tubes.
7. Sterile petri dishes.
8. LB bacterial growth media: 10 g/L tryptone, 5 g/L yeast extract, 10 g/L NaCL, *autoclaved*.
9. LB bacterial growth plates: 10 g/L tryptone, 5 g/L yeast extract, 10 g/L NaCL, 15 g/L bacto agar, *autoclaved*.
10. Ampicillin (100 mg/mL stock solution).
11. Glass test tubes, *autoclaved*.
12. GeneJET Plasmid Miniprep Kit (Thermo) or the equivalent.

2.2 Yeast Transformation Reagents and Supplies

1. Yeast strain THY.AP4 [MATa *ura3*⁻ *leu2*⁻ *trp1*⁻ *his3*⁻ *ade2*⁻ lexA::lacZ::trp1 lexA::HIS3 lexA::ADE2] (*see* **Note 2**).
2. 40 % glucose stock solution, *autoclaved*.
3. 2 g/L adenine hemisulfate stock solution, *autoclaved*.
4. YPAD yeast growth medium: 10 g/L yeast extract, 20 g/L peptone, 2 % glucose (50 mL/L of 40 % stock), 0.004 % adenine (20 mL/L of 2 g/L stock), *autoclaved*.
5. 1 M Tris–HCl pH 7.5 stock solution, *autoclaved*.
6. 0.5 M EDTA stock solution, *autoclaved*.
7. 10× TE buffer: 0.1 M Tris–HCl pH 7.5 (100 mL/L of 1 M Tris–HCl pH 7.5 stock), 0.01 M EDTA (20 mL/L of 0.5 M EDTA stock), *autoclaved*.
8. 1 M lithium acetate (LiOAc) stock solution, *filter sterilized*.
9. 50 % polyethylene glycol (PEG; average molecular weight 3,350) stock solution, *filter sterilized*.
10. Double distilled water (ddH_2O), *autoclaved*.
11. 50-mL sterile plastic conical tubes.

12. 15-mL sterile plastic conical tubes.
13. 250-mL and 500-mL Erlenmeyer flasks, *autoclaved*.
14. Spectrophotometer or cell density meter.
15. Centrifuge.
16. Salmon sperm DNA (ssDNA) type III sodium salt (Sigma).
17. Dimethyl Sulfoxide (DMSO).
18. 0.9 % sodium chloride (NaCl) solution, *autoclaved*.
19. 10× phosphate buffer: 37 g/L sodium phosphate dibasic anhydrous (Na_2HPO_4), 30 g/L sodium phosphate monobasic anhydrous (NaH_2PO_4), *autoclaved*.
20. 10 g/L histidine stock solution, *autoclaved*.
21. Synthetic dropout (SD) yeast growth plates (-LW SD plates): 1.7 g/L yeast nitrogen base without amino acids or ammonium sulfate (Becton, Dickinson and Co.), 5 g/L ammonium sulfate, 0.6 g/L -Ade -Leu -Trp -His dropout supplement (Clontech), 20 g/L bacto agar, 100 mL/L of 10× phosphate buffer, 2 % glucose (50 mL/L of 40 % stock), 0.004 % adenine (20 mL/L of 2 g/L stock), 0.002 % histidine (2 mL/L of 10 g/L stock) (*see* **Note 3**).

2.3 Supplies for the Detection of Interactions

1. 20 mg/mL X-Gal stock solution in dimethylformamide (DMF).
2. 0.1 M Methionine stock solution, *autoclaved*.
3. 1 M 3-amino-1,2,4-triazole (3-AT), *filter sterilized*.

3 Methods

3.1 Cloning Your Genes of Interest into the SU-Y2H Destination Vectors

1. Start by preparing entry vector constructs that contain the coding sequences of the genes of interest flanked by a 5′ attL1 and a 3′ attL2 Gateway® recombination site (Fig. 1) (*see* **Note 1**).
2. At room temperature, mix 50–150 ng of the attL1/gene-of-interest/attL2 entry vector and 150 ng of the desired SU-Y2H destination vector (Fig. 2) in a 0.2-mL PCR tube and adjust the volume of the mixture to 8 μL with 1× TE buffer or water (*see* **Note 4**).
3. Add 2 μL of LR Clonase™ II enzyme mix, vortex, and microcentrifuge briefly (*see* **Note 5**).
4. Incubate the reaction for 1 h at room temperature (*see* **Note 6**).
5. Add 1 μL of Proteinase K solution to each reaction and incubate at 37 °C for 10 min to terminate the reaction (*see* **Note 5**).
6. Prepare LB bacterial growth plates: 10 g tryptone, 5 g yeast extract, 10 g NaCL, 15 g bacto agar, *autoclaved*. After autoclaving,

allow the media to cool to 45–55 °C before adding a 1:1,000 dilution of the 100 mg/mL Ampicillin stock solution. Swirl the media to mix before pouring plates.

7. Transform chemically competent *E. coli* cells with the LR reaction mixture by (1) incubating the cells on ice in a 1.5-mL microfuge tube with 2–4 μL of each LR reaction for 30 min, (2) heat shocking the cells by incubating the mixture at 42 °C for 30–45 s, (3) adding 450 μL of LB, and (4) incubating the cells at 37 °C for 1 h (*see* **Note 7**).
8. Spread 20–100 μL of the transformed *E. coli* cells on ampicillin-containing LB bacterial growth plates (*see* **Note 8**).
9. Incubate plates at 37 °C overnight.
10. Prepare LB bacterial growth media: 10 g tryptone, 5 g yeast extract, 10 g NaCL, *autoclaved*. After autoclaving, allow the media to cool to ≤ 55 °C before adding a 1:1,000 dilution of the 100 mg/mL ampicillin stock solution.
11. Propagate several colonies from each plate in 2–3 mL of ampicillin-containing liquid LB media at 37 °C in autoclaved test tubes with agitation until a dense culture grows.
12. Isolate the plasmid DNA using a miniprep kit (*see* **Note 9**).
13. Verify that your genes of interest have been successfully inserted into the destination vectors using a diagnostic restriction enzyme digest and/or by sequencing the plasmids (*see* **Note 10**).

3.2 Cotransformation of Yeast with Bait and Prey Vectors for a Pairwise Protein–Protein Interaction Assay

1. Prepare YPAD yeast growth medium: 10 g/L yeast extract, 20 g/L peptone, 2 % glucose (50 mL/L of 40 % stock), 0.002 % adenine (20 mL/L of 2 g/L stock), *autoclaved* (*see* **Note 11**).
2. Prepare -LW SD plates: 1.7 g/L yeast nitrogen base without amino acids or ammonium sulfate (Becton, Dickinson and Co.), 5 g/L ammonium sulfate, 0.6 g/L -Ade -Leu -Trp -His dropout supplement (Clontech), 20 g/L bacto agar, 100 mL/L of 10× phosphate buffer, 2 % glucose (50 mL/L of 40 % stock), 0.004 % adenine (20 mL/L of 2 g/L stock), 0.002 % histidine (2 mL/L of 10 g/L stock) (*see* **Note 3**).
3. Prepare ssDNA solution by mixing 200 mg of ssDNA into 100 mL of autoclaved ddH_2O (*see* **Note 12**). Once dissolved, aliquot the ssDNA into autoclaved 1.5-mL microfuge tubes, boil for 5 min, and store at –20 °C.
4. In an autoclaved 250-mL Erlenmeyer flask, inoculate 50 mL of YPAD medium with THY.AP4 yeast and incubate at 28–30 °C overnight with shaking to propagate a dense culture (*see* **Note 2**).
5. Prepare LiOAc/TE solution by mixing 1.1 mL of 1 M LiOAc stock solution, 1.1 mL of 10× TE pH 7.5 stock solution, and 7.8 mL of autoclaved ddH_2O in a sterile 15-mL plastic conical tube (*see* **Note 13**).

6. Prepare LiOAc/PEG solution by mixing 1.5 mL of 1 M LiOAc stock solution, 1.5 mL of 10× TE pH 7.5 stock solution, and 12 mL of 50 % PEG stock solution in a sterile 15-mL plastic conical tube (*see* **Note 13**).
7. In an autoclaved 500-mL Erlenmeyer flask, inoculate 150 mL of YPAD medium with 10–20 mL of the fresh overnight THY. AP4 culture (*see* **Notes 13** and **14**).
8. Using a spectrophotometer or cell density meter, record the cell density (OD_{600}) of the inoculated culture as the starting OD_{600}. A starting OD_{600} of 0.2–0.3 is desired (*see* **Note 14**).
9. Incubate the culture at 28–30 °C with shaking until the OD_{600} approximately triples in value (*see* **Note 15**).
10. Boil ssDNA for 10 min and immediately transfer to ice. Keep on ice until needed.
11. Decant 50 mL of the culture into each of two sterile 50-mL plastic conical tubes and centrifuge at about 4,000 × *g* for 1 min to pellet the cells (*see* **Note 16**). Decant and discard supernatant.
12. Decant the remaining yeast culture evenly between the two 50-mL tubes that contain the yeast pellets from **step 11**. Centrifuge at about 4,000 × *g* for 1 min to pellet the cells. Decant and discard the supernatant.
13. Resuspend each of the pellets in 50 mL of autoclaved ddH_2O and vortex to wash the cells free of YPAD medium. Centrifuge at about 4,000 × *g* for 1 min to pellet the cells. Decant and discard the supernatant.
14. Resuspend each of the pellets in 2 mL of LiOAc/TE solution and transfer all of the resuspended yeast (approximately 4 mL) to a sterile 15-mL plastic conical tube. Centrifuge at about 4,000 × *g* for 1 min to pellet the cells (*see* **Note 17**). Decant and discard the supernatant.
15. Resuspend the yeast pellet in 4 mL of LiOAc/TE solution (*see* **Note 18**).
16. For each cotransformation, gently mix the following components in the order listed in autoclaved 1.5-mL microcentrifuge tubes: 200 µL of LiOAc/TE/yeast solution, 200 ng of bait-CubPLV plasmid DNA, 200 ng of prey plasmid DNA (NubG-prey, prey-NubG, NWT_GW, or NX32_GW), 10 µL of ssDNA, 700 µL of LiOAc/PEG solution (*see* **Notes 19** and **20**).
17. Incubate the mixture at 28–30 °C for 30 min.
18. Add 55 µL of DMSO to each transformation, gently mix, and heat shock at 42 °C for 15 min (*see* **Note 20**).
19. Centrifuge each transformation tube for 1 min to form a yeast pellet. Decant and discard the supernatant (*see* **Note 21**).

20. Resuspend each pellet with 500 μL of 0.9 % NaCl solution. Centrifuge each tube for 1 min to form a yeast pellet. Decant and discard the supernatant.
21. Resuspend each pellet with 300 μL of 0.9 % NaCl solution (*see* **Note 22**).
22. Plate 100–200 μL of the yeast on -LW SD plates and allow to dry (*see* **Notes 23** and **24**).
23. Incubate plates at 28–30 °C for several days (*see* **Note 25**).

3.3 Detection of Interaction on Growth Plates

1. Prepare -LW + X-Gal SD plates: 1.7 g/L yeast nitrogen base without amino acids or ammonium sulfate (Becton, Dickinson and Co.), 5 g/L ammonium sulfate, 0.6 g/L -Ade -Leu -Trp -His dropout supplement (Clontech), 20 g/L bacto agar, 100 mL/L of 10× phosphate buffer, 2 % glucose (50 mL/L of 40 % stock), 0.004 % adenine (20 mL/L of 2 g/L stock), 0.002 % histidine (2 mL/L of 10 g/L stock), 0.008 % X-Gal (4 mL/L of 20 mg/mL X-Gal stock solution) (*see* **Notes 3**, **26**, and **27**).
2. Prepare -LWH + Met SD plates with varying methionine concentrations: 1.7 g/L yeast nitrogen base without amino acids or ammonium sulfate (Becton, Dickinson and Co.), 5 g/L ammonium sulfate, 0.6 g/L -Ade -Leu -Trp -His dropout supplement (Clontech), 20 g/L bacto agar, 100 mL/L of 10× phosphate buffer, 2 % glucose (50 mL/L of 40 % stock), 0.004 % adenine (20 mL/L of 2 g/L stock), 0.15–1 mM methionine (0.15–1 mL/L of 1 M stock) (*see* **Notes 3** and **26**).
3. Prepare -LWH +3-AT plates with varying 3-AT concentrations: 1.7 g/L yeast nitrogen base without amino acids or ammonium sulfate (Becton, Dickinson and Co.), 5 g/L ammonium sulfate, 0.6 g/L -Ade -Leu -Trp -His dropout supplement (Clontech), 20 g/L bacto agar, 100 mL/L of 10× phosphate buffer, 2 % glucose (50 mL/L of 40 % stock), 0.004 % adenine (20 mL/L of 2 g/L stock), 5–50 mM 3-AT (5–50 mL/L of 1 M stock) (*see* **Notes 3**, **26**, and **27**).
4. Pick a positive cotransformed yeast colony from a -LW SD plate using an autoclaved pipet tip and resuspend the yeast in 50–100 μL of autoclaved ddH_2O in an autoclaved 1.5-mL microcentrifuge tube.
5. Spot 5 μL of resuspended yeast onto each type of SD plate (-LW + X-Gal, -LWH + Met of each concentration, -LWH +3-AT of each concentration) and allow to dry (*see* **Note 28**).
6. Repeat **steps 4** and **5** using several colonies from each transformation -LW SD plate. When dry, incubate plates at 28–30 °C for 2–3 days until significant growth is apparent (*see* **Notes 29** and **30**).

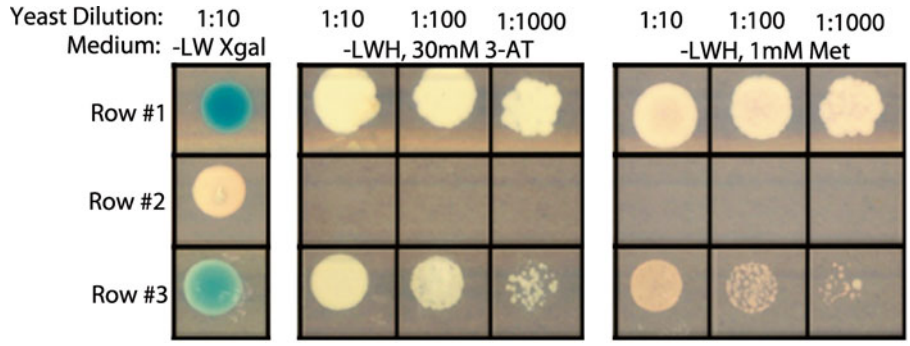

Fig. 3 A representative SU-Y2H assay modified from [8] (www.plantphysiol.org, Copyright American Society of Plant Biologists). The positive control (Row #1) shows a positive interaction between bait-CubPLV and NubWT. The negative control (Row #2) has no indication of reporter gene expression, which indicates that there is not an interaction between bait-CubPLV and NubG lacking a fused prey protein. The experimental interaction test between bait-CubPLV and prey-NubG (Row #3) shows reporter gene expression, which is indicative of a positive interaction. In this assay, -LW + X-Gal SD plates were used for blue/white screening and -LWH SD plates were used for histidine auxotrophy selection. Either 30 mM 3-AT or 1 mM Met was added to the -LWH SD plates to increase the stringency of the assay

7. Blue color on -LW + X-Gal SD plates is indicative of a positive interaction. Growth on -LWH SD plates is also indicative of a positive interaction. Increasing concentrations of 3-AT or Met causes the interaction assay to be more stringent. In all cases, the interaction is only positive if the corresponding negative control remains white (-LW + X-Gal SD plates) or does not grow (-LWH SD plates) on plates that are under the equivalent conditions (Fig. 3). If neither the experimental nor the positive control colonies show indications of an interaction, the bait-CubPLV protein is not suitable for use in the SU-Y2H system.

4 Notes

1. The pCR®8/GW/TOPO® vector (Invitrogen) is a great choice for an entry vector in this system for multiple reasons. The pCR®8/GW/TOPO® vector allows for easy insertion of genes of interest through TOPO cloning techniques and easy sequencing with M13F/M13R sites. The attL1 and attL2 sites that flank the gene insertion site are compatible with the attR1 and attR2 sites of the destination vectors of the SU-Y2H system (Fig. 2). Lastly, pCR®8/GW/TOPO® contains SpecR for selection while the destination vectors contain AmpR, which prevents pCR®8/GW/TOPO®-gene-of-interest colonies from growing in later stages when screening for destination vector-gene-of-interest colonies.
2. The genetic background of THY.AP4 is specifically designed for this protocol. MATa *ura3*$^-$ *leu2*$^-$ *trp1*$^-$ *his3*$^-$ *ade2*$^-$ lexA::lacZ::trp1

lexA::HIS3 lexA::ADE2 The *leu2*$^-$ *trp1*$^-$ lesions are necessary for selection of positive Cub and Nub transformants. The *his3*$^-$ *ade2*$^-$ lexA::lacZ::trp1 lexA::HIS3 lexA::ADE2 modifications are required for the reporter system. The culture can be inoculated from a glycerol stock of THY.AP4 or by 2–3 fresh THY.AP4 colonies from a YPAD plate.

3. SD media is prone to boiling over during autoclaving. To avoid boiling over, it is recommended to add 10× phosphate buffer, glucose, adenine, and amino acid (histidine or methionine) stock solutions after autoclaving and to prepare the medium in a container that has a volume multiple times larger than the volume of medium being prepared (e.g., 500 mL of media in a 2 L flask).
4. Genes to be used as bait should be cloned into the MetYC_GW vector and genes to be used as prey should be cloned into the NX32_GW and the XN21_GW vector. It is recommended to use both vectors because detection of some interactions has been observed to depend on whether NubG is fused to the N-terminus or C-terminus of the prey protein.
5. Efficient LR reactions have been performed using half of the suggested amount of LR Clonase™ II enzyme mix (1 μL) and Proteinase K (0.5 μL). LR Clonase™ II enzyme mix should be kept at −80 °C and distributed into multiple aliquots to avoid excessive freeze/thaw cycles.
6. In our hands, the efficiency of the LR reaction has been increased significantly by incubating at room temperature overnight instead of for 1 h.
7. If using commercially purchased competent cells, refer to the instruction manual. If using competent cells that were prepared on site, familiar heat shock procedures should be successful.
8. The desired amount of bacteria to plate is contingent on the transformation efficiency. It is desirable to plate a volume that provides a large number of well-spaced colonies. Left over transformed bacteria can be stored at 4 °C and plated several days later if required to provide a suitable number of colonies.
9. Several plasmid miniprep kits are commercially available (e.g., GeneJET Plasmid Miniprep Kit by Thermo Scientific) and can be used to isolate and purify the plasmid DNA.
10. The complete SU-Y2H destination vector sequences are available through GenBank [MetYC_GW (HQ646605), NWTX_GW (HQ700954), XN21_GW (HQ700951), NX32_GW (HQ700952)] and can be used to locate restriction enzyme sites and/or to design sequencing primers that can be used to determine that the genes of interest have been properly cloned into the SU-Y2H vectors. Met25pF primer (TCTATTACCCCCATCCATAC) can be used to sequence

the 5′ end of genes that are inserted in MetYC_GW and ADHpF primer (CAAGCTATACCAAGCATAC) can be used to sequence the 5′ end of genes that are inserted in NWTX_GW, XN21_GW, or NX32_GW.

11. Adding glucose stock solution and adenine stock solution to the medium after autoclaving is recommended to prevent the medium from becoming discolored or boiling over during autoclaving.
12. ssDNA may be difficult to dissolve into solution. It may be necessary to leave on a stir plate or shaker overnight to completely dissolve the ssDNA.
13. This protocol prepares enough competent yeast cells, LiOAc/TE solution, and LiOAc/PEG solution for approximately 20 transformations, but can be scaled up to accommodate additional transformations.
14. The target OD_{600} cell density at the time of inoculation is 0.2–0.3. Since the density of the overnight culture can vary, the amount of inoculum required to obtain the target cell density can also vary. Ten to fifteen milliliters of inoculum is usually sufficient to obtain the target cell density, but it is possible that more or less inoculum is required to match the target cell density.
15. It usually takes the culture 2–4 h to triple in density (e.g., if the starting OD_{600} is 0.25, the final OD_{600} should be approximately 0.75).
16. Any speed that efficiently causes the cells to form a pellet is sufficient.
17. Always be sure to balance the centrifuge with a counterbalancing tube of water when needed.
18. The cells are stable at this step for several hours if required.
19. For each protein–protein interaction test with the bait-CubPLV and NubG-prey or prey-NubG, two control cotransformations must be done in addition to the experimental cotransformations (Fig. 3). In this case, the experimental cotransformations are bait-CubPLV plus NubG-prey and bait-CubPLV plus prey-NubG. As a positive control, the yeast should be cotransformed with bait-CubPLV and NWTX_GW. As a negative control, the yeast should be cotransformed with bait-CubPLV and NX32_GW.
20. Do not mix by pipetting. Mix by gently tapping/flicking the tube. DMSO has been shown to improve the transformation efficiency but it can be skipped if transformation efficiency is not a concern.
21. The addition of an optional step between **steps 19** and **20** in Subheading 3.2 might improve transformation efficiency, which may be especially helpful if performing high-throughput

screening (*see* **Note 31**). *Optional*: Resuspend each pellet in 1 mL of YPAD medium and incubate at 28–30 °C for 90 min. Centrifuge each tube for 1 min to form a yeast pellet. Decant and discard the supernatant.

22. Resuspending twice in 0.9 % NaCl solution has a dual role. First, these steps act as a washing step. The washes are intended to rid the yeast of potentially harmful reagents from the transformation protocol and to remove any contaminating nutrients (e.g., YPAD medium from **Note 21**) from interfering with auxotrophy selection. Second, the 0.9 % NaCl solution acts as a favorable osmotic environment for the yeast cells to recuperate from the transformation procedure.
23. The amount of yeast to plate varies depending on the transformation efficiency. If the efficiency is low, all of the yeast can be plated on a single plate. Any yeast remaining after plating can be stored at 4 °C and plated days later if required.
24. -LW SD plates will be selective for colonies that were successfully cotransformed with at least one copy of each of the bait plasmid and the prey plasmid.
25. Colonies are typically visible after 2–3 days. Plates can be incubated until colonies reach a desirable size (2–3 mm diameter).
26. Other ingredients may be supplemented to or retracted from the -LW SD media recipe to make different varieties of SD media. -LW + X-Gal SD media includes the addition of 0.008 % X-Gal (4 mL/L of 20 mg/mL X-Gal stock solution), which allows for blue/white screening of colonies to assay protein–protein interactions. -LWH SD media, which is selective for colonies exhibiting a positive protein–protein interaction, is made by withholding histidine from the recipe. Either 5–50 mM 3-Amino-1,2,4,-triazole (3-AT) or 0.15–1 mM methionine (Met) should be added to -LWH SD media in order to increase the stringency of selection.
27. X-Gal and 3-AT stock solutions are heat labile and should only be added to medium after autoclaving and after cooling to ≤ 55 °C.
28. To organize and label spotted colonies, draw a grid pattern on the underside of all SD plates and properly label each cell prior to the spotting of colonies.
29. It is common for only a certain percentage of cotransformed colonies to show indications of a positive interaction. Therefore, it is recommended to test many colonies from each cotransformation.
30. Alternatively, yeast from the cotransformation procedure can be plated directly on -LW + X-Gal SD plates in **step 22** of Subheading 3.2 to select for positive cotransformants and to screen for positive interacting colonies in a single step. If using

this approach, colonies may take longer to show blue color. Store plates at 4 °C after they grow to a desirable size. Blue color may not develop significantly until several days after being placed at 4 °C.

31. A protocol for the high-throughput screening for putative interaction partners of a protein of interest is beyond the scope of this protocol, but with the construction of a cDNA prey library and a slight modification of the protocol above, high-throughput screening becomes possible. First, the protein of interest (bait protein) should be cloned into the pMetCY_GW vector and transformed into yeast as described in Subheadings 3.1 and 3.2 to create a stable yeast strain that contains the bait-CubPLV vector. This yeast strain should be grown on -L SD plates [-LW SD medium with the addition of 0.002 % tryptophan (2 mL/L of 10 g/L stock)]. A prey library can be prepared from the organism of interest by isolating mRNA, performing reverse transcription to convert the mRNA into complementary DNA (cDNA), and by inserting the cDNA clones into an entry vector that has attL1 and attL2 sites as in **step 1** of Subheading 3.1 (*see* **Note 1**). This attL1-cDNA-attL2 entry vector library can then be cloned into the XN21_GW or NX32_GW vector as described in Subheading 3.1 and transformed into the yeast that already contains the bait-CubPLV and plated on -LW SD plates as described in Subheading 3.2. Colonies can be tested for positive interactions as described in Subheading 3.3. For each positive colony, propagate the yeast in liquid -LW SD medium, isolate the plasmid DNA from the yeast, sequence the plasmids using ADHpF (CAAGCTATACCAAGCATAC), and BLAST the obtained sequence to identify the putative interaction partner of your bait protein of interest. The cDNA clone likely only contains a piece of a prey gene and should be checked to ensure that the sequence is in frame with NubG. As a follow-up to the high-throughput screen, the full-length sequence of each positive cDNA prey should be tested pairwise with the bait-CubPLV in the SU-Y2H as described in Subheadings 3.1–3.3.

5 Concluding Remarks and Applications

The pairwise SU-Y2H assay described above has been integral to the investigation of several PPIs in plants (Fig. 3) [6–12] and the high-throughput SU-Y2H screen (*see* **Note 31**) has provided several leads for future research endeavors. The SU-Y2H is a useful tool in investigating the biological role of proteins by examining the PPIs shared among proteins that work cooperatively in biological processes. The SU-Y2H has several advantages over alternative PPI techniques including: the ability to investigate PPIs among

transmembrane proteins, the capability to test PPIs in both a pairwise and a high-throughput manner, cloning procedures that are quick and easy via Gateway® recombination, and easy accessibility of the vectors through the Arabidopsis Biological Resource Center (ABRC).

Acknowledgment

We thank Sylvie Lalonde and Wolf Frommer for providing MetYC_GW, XN21_GW, NX32_GW, and NWTX_GW vectors. This work was primarily supported by the Center for LignoCellulose Structure and Formation, an Energy Frontier Research Center funded by the U.S. Department of Energy, Office of Science, Office of Basic Sciences under Award Number DE-SC0001090 and in part by grant from National Science Foundation (1121375).

References

1. Syafrizayanti BC, Hoheisel JD, Kastelic D (2014) Methods for analyzing and quantifying protein-protein interaction. Expert Rev Proteomics 11:107
2. Fields S, Song O (1989) A novel genetic system to detect protein-protein interactions. Nature 340(6230):245–246
3. Stagljar I, Korostensky C, Johnsson N, te Heesen S (1998) A genetic system based on split-ubiquitin for the analysis of interactions between membrane proteins in vivo. Proc Natl Acad Sci U S A 95(9):5187–5192
4. Johnsson N, Varshavsky A (1994) Split ubiquitin as a sensor of protein interactions in vivo. Proc Natl Acad Sci U S A 91(22):10340–10344
5. Joung JK, Ramm EI, Pabo CO (2000) A bacterial two-hybrid selection system for studying protein-DNA and protein-protein interactions. Proc Natl Acad Sci U S A 97(13):7382–7387
6. Obrdlik P, El-Bakkoury M, Hamacher T, Cappellaro C, Vilarino C, Fleischer C, Ellerbrok H, Kamuzinzi R, Ledent V, Blaudez D, Sanders D, Revuelta JL, Boles E, Andre B, Frommer WB (2004) K+ channel interactions detected by a genetic system optimized for systematic studies of membrane protein interactions. Proc Natl Acad Sci U S A 101(33):12242–12247
7. Lalonde S, Sero A, Pratelli R, Pilot G, Chen J, Sardi MI, Parsa SA, Kim DY, Acharya BR, Stein EV, Hu HC, Villiers F, Takeda K, Yang Y, Han YS, Schwacke R, Chiang W, Kato N, Loque D, Assmann SM, Kwak JM, Schroeder JI, Rhee SY, Frommer WB (2010) A membrane protein/signaling protein interaction network for Arabidopsis version AMPv2. Front Physiol 1:24
8. Bashline L, Li S, Anderson CT, Lei L, Gu Y (2013) The endocytosis of cellulose synthase in Arabidopsis is dependent on mu2, a clathrin-mediated endocytosis adaptin. Plant Physiol 163(1):150–160
9. Lei L, Li S, Du J, Bashline L, Gu Y (2013) Cellulose synthase INTERACTIVE3 regulates cellulose biosynthesis in both a microtubule-dependent and microtubule-independent manner in arabidopsis. Plant Cell 25:4912
10. Li S, Lei L, Gu Y (2013) Functional analysis of complexes with mixed primary and secondary cellulose synthases. Plant Signal Behav 8(3):e23179
11. Reinders A, Schulze W, Thaminy S, Stagljar I, Frommer WB, Ward JM (2002) Intra- and intermolecular interactions in sucrose transporters at the plasma membrane detected by the split-ubiquitin system and functional assays. Structure 10(6):763–772
12. Xuan YH, Hu YB, Chen LQ, Sosso D, Ducat DC, Hou BH, Frommer WB (2013) Functional role of oligomerization for bacterial and plant SWEET sugar transporter family. Proc Natl Acad Sci U S A 110(39):E3685–E3694

Chapter 14

Activation Tag Screening for Cell Expansion Genes in *Arabidopsis thaliana*

Chaowen Xiao and Charles T. Anderson

Abstract

Forward genetic screens for growth-deficient loss-of-function mutants have uncovered a wide array of genes involved in cell expansion. However, the centrality of cell growth to plant survival means that null mutations in many genes involved in this process are likely to be lethal early in development, making phenotypic analysis difficult. Additionally, the phenotypes of loss-of-function mutations in genes that are members of large gene families might be masked by functional redundancy with other family members. Activation tagging provides a method of screening for dominant overexpression phenotypes in an arbitrarily large collection of transgenic individuals, allowing for functional genomic identification of genes related to cell growth and expansion. In this chapter, we discuss the advantages and limitations of activation tag screening and describe a protocol for identifying activation tag lines with enhanced cell expansion, using dark-grown *Arabidopsis thaliana* seedlings as an experimental system. We also describe secondary screens to identify candidate genes for further cell biological and genetic characterization. These protocols can be adapted to any process or species of interest, as long as a suitable activation-tagged population and a genome sequence are available.

Key words Activation tagging, Forward genetics, Genetic redundancy, Overexpression, Cell expansion, Arabidopsis

1 Introduction

For most plant cells, growth and expansion involve the synthesis and delivery of cell wall components, establishment of internal turgor pressure, and controlled yielding of the plant cell wall [1]. The putative proteins involved in these processes include carbohydrate biosynthetic enzymes, cytoskeletal and membrane trafficking elements, ion transporters, and wall-remodeling proteins, and classical forward genetic loss-of-function approaches, such as EMS and insertional mutagenesis, have been used to identify many mutants with defects in cell expansion [1–3]. However, the likely early lethality caused by genetically ablating genes required for cell growth, along with the potential for redundancy among closely

José M. Estevez (ed.), *Plant Cell Expansion: Methods and Protocols*, Methods in Molecular Biology, vol. 1242,
DOI 10.1007/978-1-4939-1902-4_14,

related genes, limits the capacity of loss-of-function screening to reveal the entire suite of growth and expansion-related genes.

Activation tagging, in which enhancer elements are inserted randomly into the genome to drive overexpression of nearby genes, has been recognized for over two decades as a complementary functional genomics approach that allows for the identification of genes involved in a process by detection of overexpression phenotypes [4, 5]. In searching for cell growth and expansion genes, this approach has the distinct advantage of allowing researchers to identify plants that are larger than average instead of plants that are smaller than average, allowing for easy detection in large populations of mutants. In addition, activation tagging is usually expected to have a dominant effect on plant phenotype, allowing for phenotypic screening in heterozygous T1 plants, thus reducing the screening population by 75 % as compared with recessive loss-of-function screens. Activation tagging collections exist for the model plant species *Arabidopsis thaliana* and *Oryza sativa* [4, 6, 7], but have also been developed for newer model species such as *Brachypodium distachyon* and *Populus trichocarpa* [8, 9]. In addition, the identification of activation tag insertion points is simple and efficient for sequenced plant species, since the activation tag cassette provides a unique molecular "handle" with which to amplify and sequence the insert-genome boundary by methods such as TAIL PCR [10] or adapter ligation PCR [11], followed by alignment of the junction sequence with the plant genome. Finally, because it maintains the integrity of endogenous promoter binding sites, activation tagging has the potential to amplify endogenous developmental expression patterns, as opposed to ubiquitous overexpression, driven for example by the CaMV 35S promoter, which can lead to aberrant expression patterns and artifactual phenotypes.

There are a few caveats associated with activation tag screening: multiple insertion events in a single line can complicate genetic analysis of hits from screens, and an activation tag can potentially drive the overexpression of multiple genes in the vicinity of the insertion, requiring careful validation of candidate genes by measuring gene expression levels in activation-tagged and control lines and/or recapitulation of the overexpression phenotype by specific transgenic overexpression of single candidate genes [4]. Recently, we have performed an activation tag screen for genes involved in cell expansion using dark-grown *Arabidopsis* hypocotyls, which provide several experimental advantages in that they carry out little cell division and display rapid, uniform, anisotropic growth [12, 13]. The protocol for this screening approach follows and can be readily adapted to any plant species for which there is sufficient genomic data to allow for alignment of insertion-genome boundaries.

2 Materials (*See* Note 1)

2.1 Primary Screening Materials

1. Set of pools of *Arabidopsis thaliana* activation tag seeds transformed with pSKI015 containing a tetramerized 35S enhancer [4] (Arabidopsis Biological Resource Center stock CS31100).
2. 15 mL conical tubes (VWR 21008-931).
3. Bleach sterilization solution: 30 % (v/v) bleach + 0.1 % (w/v) SDS in MilliQ water; store in dark at room temperature for up to 1 month.
4. Sterile autoclaved MilliQ water.
5. Sterile autoclaved 0.15 % (w/v) agar-agar (Research Organics) in MilliQ water.
6. Murashige and Skoog salts (Caisson Laboratories MSP01).
7. MES, monohydrate (2-(*N*-Morpholino)ethanesulfonic acid) (Research Organics 0113M).
8. Agar-agar (Research Organics 10020).
9. 1 M KOH (VWR BDH0262) in MilliQ water.
10. Small transparent plastic boxes (e.g., autoclaved empty pipette tip boxes).
11. Laminar flow biohood.
12. 14.6 cm Pasteur pipettes (VWR 14673-010).
13. Pasteur pipette bulbs (VWR 56311-049).
14. Light-tight box (can be made using a thick cardboard box sealed with lightproof foil tape).
15. 22 °C plant growth chamber.
16. Nitrile gloves.
17. 70 % (v/v) ethanol in MilliQ water.
18. 40 % sucrose (w/v) in MilliQ water, filter-sterilized through an 0.45 μm vacuum filtration unit (VWR 97066-204) and aliquoted into sterile 50 mL conical tubes.
19. Gridded square Petri plates (VWR 60872-310).
20. Micropore surgical tape (3M 1530.0).
21. 3C forceps (VWR 37692-930).
22. Fafard C2 mix soil.
23. 6.35 cm square pots (Hummert 1212501).
24. Plastic flats with holes (Hummert 1130001).
25. Plastic flats without holes (Hummert 1130501).
26. Transparent plastic domes (Hummert 1270661).
27. Wooden stakes (Griffin Greenhouse 74-100150).

28. 5 cm twist ties.
29. 20 cm diameter metal sieve, number 35 (500 μm) openings (VWR 57331-584).

2.2 Secondary Screening for Hypocotyl Length Materials

1. 1.7 mL microcentrifuge tubes (Denville C2170).
2. 20 μL micropipette.
3. Sterile 20–200 μL micropipette tips.
4. Single edge razor blade.
5. HP Scanjet 8300 scanner.
6. Aluminum foil.
7. ImageJ software (http://imagej.nih.gov/ij/).

2.3 Secondary Screening for Insertion Copy Number Materials

1. L-methionine sulfoximine (Sigma M5379).

2.4 Cell Length Measurement Materials

1. Transmitted light microscope with brightfield illumination, 10× air objective, and digital camera.
2. 1 × 3 in. microscope slides (VWR 48312-057).
3. #1.5 thickness 24 × 40 mm coverslips (VWR 48393-230).

2.5 Adapter Ligation PCR Materials

1. Liquid N_2.
2. GenElute™ Plant Genomic DNA isolation kit (Sigma G2N70-1KT).
3. Adapter ligation and PCR primers (*see* [11] and Table 1).
4. 1 M Tris-HCl pH 8.3.
5. Vortexer.
6. Heat block or water bath for microcentrifuge tubes.
7. T4 ligase (NEB M0202).
8. HindIII (NEB R0104).
9. EcoRI (NEB R0101).
10. AseI (NEB R0526).
11. 10 mM ATP (NEB P0756).
12. ExTaq and buffer (Takara TAK RR001A).
13. 10 mM dNTPs (NEB N0446).
14. Thermocycler (Applied Biosystems Veriti).
15. Agarose (VWR 97062-246).
16. 1× TAE buffer.
17. DNA gel electrophoresis equipment.
18. Ethidium bromide (Sigma E7637).

Table 1
Primer sequences for adapter ligation PCR and *ACT2* qPCR. Note that 5′ phosphate and 3′ C7 amino modifications are required for Short Strand Adapters

Short Strand Adapter Hind	5′ phosphate-AGCTGCAGCCCG-3′ C7 amino
Short Strand Adapter Eco	5′ phosphate-AATTGCAGCCCG-3′ C7 amino
Short Strand Adapter Ase	5′ phosphate-TAGCACAGCCCG-3′ C7 amino
Long Strand Adapter 1	GTAATACGACTCACTTAGGGCACGCGTGGTCGACGGCCCGG GCTGC
Long Strand Adapter 2	GTAATACGACTCACTATAGGGCACGCGTGGTCGACGGCCCGG GCTGTGC
AP1	GTAATACGACTCACTATAGGGC
AP2	TGGTCGACGGCCCGGGCTGC
pSKI015_LB_278-304rc	GAAGTTTCTCATCTAAGCCCCCATTTG
pSKI015_LB_136-159rc	TATAATAACGCTGCGGACATCTAC
ACT2-qF	CTTGCACCAAGCAGCATGAA
ACT2-qR	CCGATCCAGACACTGTACTTCCTT

19. UV trans-illuminator.
20. Spectrophotometer (NanoDrop 2000C).
21. Gel Extraction kit (Omega Bio-Tek D2500).
22. PCR purification kit (Omega Bio-Tek D6493).

2.6 qPCR Materials

1. E.Z.N.A. Plant RNA isolation kit (Omega Bio-Tek R6827-02).
2. RNase-free DNase I (NEB M0303L).
3. qScript cDNA SuperMix (Quanta Biosciences 95048-100).
4. Quanta PerfeCTa SYBR Fastmix ROX (Quanta Biosciences 95073-012).
5. Gene-specific primers for candidate genes and Actin2 (*AtACT2*, At3g18780) as a reference (*see* Table 1).
6. 37 °C incubator.
7. RNase-free water (Life Technologies 10977015).
8. Ice bucket.
9. Microcentrifuge (Eppendorf 5424 or similar).
10. StepOne Plus Real-Time PCR machine (Applied Biosystems).
11. 96-well optical reaction plates (Applied Biosystems 4366932).
12. Optical adhesive covers (Applied Biosystems 4311971).
13. StepOne software v 2.2.2 (Applied Biosystems; http://www.appliedbiosystems.com/absite/us/en/home/support/software/real-time-pcr/stepone.html).

3 Methods

Perform all sterile procedures in a laminar flow biohood.

3.1 Primary Screening

1. Place ~2 mL activation tag seeds in a 15 mL conical tube, add 13 mL bleach sterilization solution, vortex; invert tube every 5 min for 20 min total to surface sterilize seeds.
2. Aspirate bleach solution, add 13 mL sterile MilliQ water, invert to wash seeds, allow seeds to settle, aspirate supernatant; repeat 4 times.
3. Suspend seeds in 0.15 % (w/v) sterile agar-agar solution, store at 4 °C in dark for 3 days to stratify.
4. Prepare 0 % sucrose MS medium: add 2.2 g/L Murashige and Skoog salts, 0.6 g/L MES, 8 g/L agar-agar to 1 L MilliQ water, pH to 5.6 using 1 M KOH, autoclave.
5. Pour molten 0 % sucrose MS medium to a depth of 3 mm in pre-autoclaved transparent plastic boxes.
6. Sow sterilized, stratified seeds on 0 % sucrose MS medium using a Pasteur pipette, dispensing seeds at high density in closely spaced rows across the medium (there should be approximately 1,000 seeds per box).
7. Leave boxes open in biohood for 1 h to allow seed solution to dry, close boxes, leave in biohood with lights on for an additional 3 h to stimulate germination, place boxes in a light-tight box, incubate in 22 °C growth chamber for 6 days (*see* **Note 2**).
8. Prepare 1 % sucrose MS plates: add 2.2 g/L Murashige and Skoog salts, 0.6 g/L MES, 8 g/L agar-agar to 975 mL MilliQ water, pH to 5.6 using 1 M KOH, autoclave, transfer to biohood, add 25 mL sterile 40 % sucrose solution, pour into square gridded Petri plates, allow plates to cool in biohood with lids off for 30 min, cover, wrap in sterile plastic bags, store at 4 °C.
9. Transfer transparent boxes containing "lawns" of dark-grown seedlings from light-tight box to biohood.
10. Wearing nitrile gloves sterilized with 70 % ethanol, hold a transparent box at eye level to identify seedlings that have grown taller than surrounding seedlings (*see* **Note 3**).
11. Using thumb and forefinger, gently pluck taller seedlings from "lawn" of dark-grown seedlings, transfer to a 1 % sucrose MS plate.
12. Seal 1 % sucrose MS plate with micropore tape and place vertically in 22 °C growth chamber under continuous light for 10 days to allow seedlings to undergo photomorphogenesis.

13. Using sterilized 3C forceps, transfer seedlings to thoroughly soaked soil in 6.35 cm square pots that are arranged in a plastic flat with holes inside a plastic flat without holes.
14. Cover flat with a transparent plastic dome, incubate in 22 °C 16 h light/8 h dark growth chamber for 3 days, shift dome so that a 1 cm gap exists between dome and flat, continue growth for 3 days, remove dome.
15. Grow plants until they reach senescence, watering as needed to keep soil moist (*see* **Note 4**).
16. Stop watering plants, transfer plants to a low-humidity room for 1–2 weeks to allow them to dry.
17. Harvest seeds from each plant individually using a metal sieve; these represent initial hit lines from screen.

3.2 Secondary Screening for Heritability of the Long Hypocotyl Phenotype

1. Sterilize Col and activation tag line seeds (~50 μL of each line), resuspend in 0.15 % agar-agar solution, incubate at 4 °C for 2–4 days.
2. Sow seeds using 20 μL micropipette with cutoff 20 μL tip (*see* **Note 5**) on 0 % sucrose MS plates (*see* **Note 6**).
3. Keep plates in biohood with lids off for 30–45 min to dry.
4. Place lids on plates, place under light for 2–4 h to induce seed germination.
5. Wrap plates in two layers of aluminum foil, grow in dark in a 22 °C growth chamber for 6 days.
6. Remove foil, dry off any condensation, scan plates at 600 dpi on a flatbed scanner.
7. Open images in ImageJ, set scale (*see* **Note 7**).
8. Choose Freehand Line tool to measure the distance between the apical hook and the hypocotyl–root junction.
9. Use Student's *t*-test to test whether activation tag line seedlings are significantly longer than Col controls (*see* Fig. 1a), with $p < 0.01$ as a statistical cutoff.

3.3 Secondary Screening for Segregation of the Activation Tag Selectable Marker

1. Sterilize Col and activation tag line seeds (~50 μL of each line), resuspend in 0.15 % agar-agar solution, incubate at 4 °C for 2–4 days.
2. Sow seeds using 20 μL micropipette with cutoff 20 μL tip on 1 % sucrose MS plates containing 5 μM methionine sulfoximine.
3. Keep plates in biohood with lids off for 30–45 min to dry.
4. Incubate in a 22 °C, 24 h light growth chamber for 5 days.
5. Dry off any condensation, scan plates at 600 dpi on a flatbed scanner.

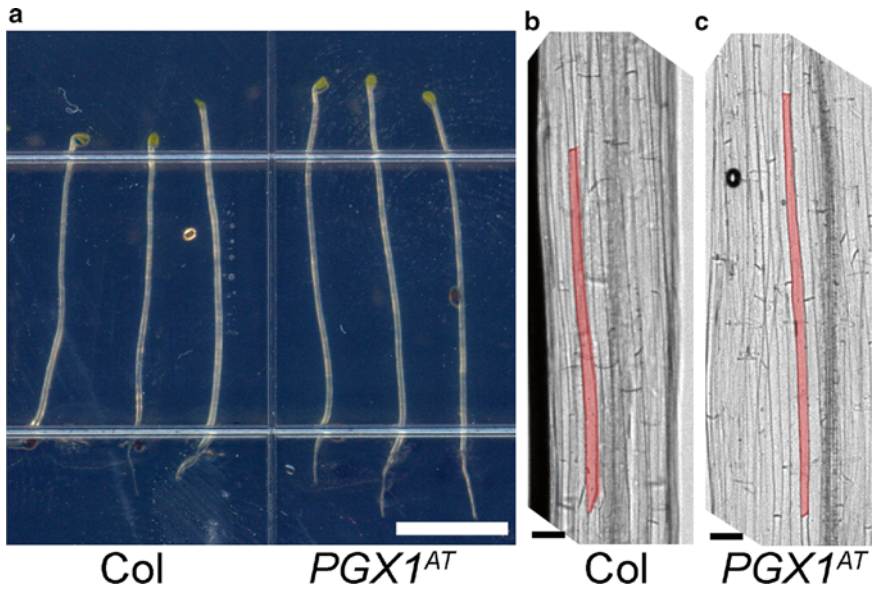

Fig. 1 Enhanced hypocotyl elongation and cell length in an activation tag line. (**a**) 6-day-old dark-grown activation tag seedlings (*PGX1*^{AT}) display longer hypocotyls than Col controls. Scale bar = 500 mm. (**b**, **c**) Cell lengths at the base of 6-day-old dark-grown Col (**b**) and *PGX1*^{AT} hypocotyls (**c**). Scale bars = 50 μm. See Reference 14 for details

6. Score seedlings for methionine sulfoximine resistance (*see* **Note 8**).
7. Use chi-squared analysis to calculate whether the line is likely to contain a single heterozygous insertion (expected 3:1 segregation ratio of methionine sulfoximine resistance), with $p > 0.1$ as a statistical cutoff.

3.4 Cell Length Measurements

1. Sterilize Col and activation tag line seeds (~50 μL of each line), resuspend in 0.15 % agar-agar solution, incubate at 4 °C for 2–4 days.
2. Sow seeds using 20 μL micropipette with cutoff 20 μL tip on 0 % sucrose MS plates.
3. Keep plates in biohood with lids off for 30–45 min to dry.
4. Place lids on plates, place under light for 2–4 h to induce seed germination.
5. Wrap plates in two layers of aluminum foil, grow in dark in a 22 °C growth chamber for 6 days.
6. Mount seedlings with water on slides, record images with clearly visible cell outlines at base of hypocotyls using a 10× air objective.
7. Use ImageJ to measure cell length based on cell outlines in recorded images (*see* Fig. 1b, c) (*see* **Note 9**).
8. Calculate and compare cell lengths from activation tag lines and Col controls using a Student's *t*-test, with $p < 0.01$ as a statistical cutoff.

3.5 Adapter Ligation PCR to Identify Activation Tag Insertion Points (See Note 10)

1. Grind 7-day-old seedlings grown on 1 % sucrose MS plates in 24 h light for 7 days in liquid N_2, extract genomic DNA using Genelute Plant DNA isolation kit. Store at –20 °C up to 6 months.
2. Prepare 10× Hind, Eco adapters: add 20 μL 5 μM Long Strand Adapter 1, 20 μL 5 μM Short Strand Adapter (Hind or Eco) in 1,210 μL 1 mM Tris-HCl pH 8.3 in a 1.7 mL microcentrifuge tube. Vortex tube, place on heat block set to 96 °C for 2 min. Turn off block, let cool to 25 °C. Store at –20 °C up to 6 months.
3. Prepare 10× Ase adapter: add 10 μL 5 μM Long Strand Adapter 2 and 20 μL 5 μM Short Strand Adapter Ase in 1,220 μL 1 mM Tris-HCl pH 8.3 in 1.7 mL microcentrifuge tube. Anneal as above, store at –20 °C up to 6 months.
4. Digestion/ligation of gDNA with Eco, Hind adapters (can be done together): for each reaction, mix 3 μL gDNA, 5.2 μL MilliQ water, 1 μL 10× T4 ligase buffer, 0.25 μL 10× Hind adapter, 0.25 μL 10× Eco adapter, 0.1 μL NEB HindIII, 0.1 μL NEB EcoRI, 0.05 μL NEB T4 ligase, 0.05 μL 10 mM ATP; incubate overnight at 25 °C.
5. Digestion, ligation with Ase adapter (digestion and ligation done separately): for each reaction, mix 3 μL gDNA, 2.65 μL MilliQ water, 0.65 μL 10× T4 ligase buffer, 0.2 μL NEB AseI; incubate 4 h to overnight at 37 °C. To ligate, add: 1 μL 10× Ase adapter, 1 μL MilliQ water, 1 μL 10× T4 ligase buffer, 0.3 μL 10 mM ATP, 0.2 μL T4 ligase; incubate 8 h to overnight at 20 °C.
6. Transfer 1 μL of each adapter-ligated gDNA to a new well/tube.
7. Perform PCR with adapter primer pairs: for each reaction, mix 14.15 μL MilliQ water, 2 μL 10× ExTaq buffer, 0.8 μL 10 mM dNTPs, 1 μL pSKI015_LB_278-304rc (5 μM), 1 μL AP1 primer (5 μM), 0.05 μL ExTaq (5 U/μL); cover, load onto PCR machine paused at first 96 °C step: Cycle 1–10: 96 °C 20 s, 72 °C 140 s; Cycle 11–25: 96 °C 20 s, 67 °C 140 s.
8. Perform second PCR: for each reaction, mix 0.5 μL first PCR product, 16.55 μL MilliQ water, 2 μL 10× ExTaq buffer, 0.8 μL 10 mM dNTPs, 0.025 μL pSKI015_LB_136-159rc (200 μM), 0.025 μL AP2 primer (200 μM), 0.1 μL ExTaq; cover, load onto PCR machine paused at first 96 °C step: Cycle 1–5: 96 °C 30 s, 94 °C 20 s, 72 °C 140 s; Cycle 6–28: 96 °C 20 s, 67 °C 20 s, 72 °C 130 s.
9. Separate PCR products on 1.5 % agarose TAE gel, cut out bands.
10. Extract DNA from bands using Gel Extraction kit into 10 μL water, perform amplification PCR: for each reaction, mix 5 μL DNA, 2 μL 10× ExTaq buffer, 1.6 μL dNTPs, 0.2 μL pSKI015_LB_136-159rc (200 μM), 0.2 μL AP2 primer (200 μM),

0.2 μL ExTaq, 10.8 μL MilliQ water; run PCR reaction: (1) 95 °C 3 min; (2) 95 °C 30 s; (3) 55 °C 30 s; (4) 72 °C 150 s; repeat **steps 2–4** 34 times; (5) 72 °C 7 min; (6) 4 °C forever.

11. Purify DNA using PCR purification kit into 30 μL MilliQ water, measure concentration using a NanoDrop 2000C spectrophotometer (*see* **Note 11**).
12. Sequence PCR product using pSKI015_LB_136-159rc primer.
13. Perform a BLAST search of the resulting sequence in NCBI to identify alignment with the *Arabidopsis* genome (*see* **Note 12**).
14. For sequence alignment, use Seqviewer tool (http://tairvm09.tacc.utexas.edu/servlets/sv) to align sequence to Arabidopsis genome.

3.6 Gene Expression Analysis by qPCR

1. Grow at least 50 6-day-old dark-grown seedlings of activation tag lines and Col controls (*see* Subheading 3.2).
2. Isolate RNA from activation tag line and Col plants using an RNA isolation kit.
3. Remove any contaminating DNA by adding RNase-free DNase I and incubating at 37 °C for 30 min.
4. Measure total RNA concentration using NanoDrop 2000C spectrophotometer.
5. Synthesize first-strand cDNA using qScript cDNA SuperMix from 500 ng DNase I-treated template RNA: mix components including template RNA, 4 μL qScript cDNA SuperMix, and DEPC-treated water to a total of 20 μL, incubate at 25 °C for 5 min, 42 °C for 30 min, 80 °C for 5 min, incubate for 5 min on ice; store at −20 °C until use.
6. Prepare 20 μL PCR reaction: mix 1 μL cDNA (diluted tenfold), 10 μL SYBR Green mix with ROX (2×), 0.3 μL Forward primer (20 μM) (*see* **Note 13**), 0.3 μL Reverse primer (20 μM), add MilliQ water up to 20 μL.
7. Set up the following protocol in a qPCR machine (e.g., Applied Biosystems StepOne Plus): (95 °C 2 min, 95 °C 10 s, 60 °C 30 s) for 40 cycles.
8. Use StepOne Plus software and Excel to determine relative expression levels with *ACT2* as the invariant gene, using the ΔΔCT method (*see* **Note 14**).

4 Notes

1. Materials also used in subsequent protocols are only listed for the first protocol in which they are used.
2. Occasionally a transparent box will become contaminated—discard all seedlings from this box.

3. Some seedlings can be elevated above the medium by sticking to the sides of other seedlings; only taller seedlings that are growing from the level of the medium should be chosen.
4. Avoid over-watering, as this can encourage the proliferation of pests.
5. Use a razor blade sterilized with 70 % ethanol to cut ~1 mm off of pipette tip on a sterilized surface.
6. It is preferable to sow the Col and activation tag seeds on the same plate.
7. For square gridded plates, draw a line across three grid squares; this equals 4 cm.
8. We use 0.67 cm as a cutoff for root length; all Col seedlings should be susceptible to methionine sulfoximine.
9. Be sure to set the scale properly for the 10× objective magnification; this can be measured directly using a stage micrometer.
10. This protocol is modified from [11].
11. Concentration range should be 10–120 ng/μL.
12. The 5′ portion of each sequence should align with pSKI015, and the 3′ portion should align with an *Arabidopsis* genomic sequence. We have obtained a 75 % success rate for adapter ligation PCR-based insertion point identification; additional restriction enzymes or optimization of PCR conditions might be necessary for samples that do not result in a single band in the first round of experiments.
13. Use Primer 3 website (http://primer3.ut.ee/) to design qPCR primers; ideally, at least one primer should span multiple exons.
14. Using this activation tag screen strategy, we have identified over 600 activation tag lines that display enhanced growth in dark-grown hypocotyls, and have performed detailed characterization of one of these lines, which overexpresses a polygalacturonase [14]. An increasing number of genes have been discovered in *Arabidopsis* by activation tag screening [15–20]. This technique is also being used in diverse plant species including rice [6, 7], tomato [21], and petunia [22]. Transposon-based activation tagging has also been developed for gene function discovery in *Arabidopsis* [23, 24], aspen [25], and tobacco [26], and a new GAL4-based activation tagging system for inducible overexpression in specific *Arabidopsis* tissues or developmental stages has recently been constructed [27]. In addition to its utility in identifying overexpression phenotypes, activation tagging can also identify loss-of-function mutants when the tag disrupts a gene involved in the process of interest [28]. The potential of activation tag screening in the genomic age is substantial, given the ease with which activation tags can be mapped to the sequenced genomes of an

increasing number of plant species. As a complementary approach to such genomics-enabled loss-of-function genetic tools as TILLING and genome editing technologies involving TALENs and the CRISPR/Cas9 system, forward genetic-style overexpression strategies such as activation tag screening will retain their usefulness in identifying new genes involved in plant growth, development, and environmental responses, providing a richer picture of how plants accomplish these processes by transcriptional regulation and protein function.

Acknowledgments

Thanks to Chris Somerville and members of the Somerville lab for helpful discussions on this topic, to Wenting Xi for technical assistance with primary and secondary screening, and to William Barnes for critical reading. The writing of this chapter was supported as part of the Center for Lignocellulose Structure and Formation, an Energy Frontier Research Center funded by the U.S. Department of Energy, Office of Science, Basic Energy Sciences under Award # DE-SC0001090.

References

1. Cosgrove DJ (2005) Growth of the plant cell wall. Nat Rev Mol Cell Biol 6(11):850–861
2. Baskin TI (2005) Anisotropic expansion of the plant cell wall. Annu Rev Cell Dev Biol 21: 203–222
3. Dolan L, Davies J (2004) Cell expansion in roots. Curr Opin Plant Biol 7(1):33–39
4. Weigel D et al (2000) Activation tagging in Arabidopsis. Plant Physiol 122(4):1003–1013
5. Walden R et al (1994) Activation tagging: a means of isolating genes implicated as playing a role in plant growth and development. Plant Mol Biol 26(5):1521–1528
6. Jeong DH et al (2002) T-DNA insertional mutagenesis for activation tagging in rice. Plant Physiol 130(4):1636–1644
7. Wan S et al (2009) Activation tagging, an efficient tool for functional analysis of the rice genome. Plant Mol Biol 69(1–2):69–80
8. Mur LA et al (2011) Exploiting the Brachypodium Tool Box in cereal and grass research. New Phytol 191(2):334–347
9. Busov VB et al (2003) Activation tagging of a dominant gibberellin catabolism gene (GA 2-oxidase) from poplar that regulates tree stature. Plant Physiol 132(3):1283–1291
10. Liu YG, Mitsukawa N, Oosumi T, Whittier RF (1995) Efficient isolation and mapping of Arabidopsis thaliana T-DNA insert junctions by thermal asymmetric interlaced PCR. Plant J 8(3):457–463
11. O'Malley RC, Alonso JM, Kim CJ, Leisse TJ, Ecker JR (2007) An adapter ligation-mediated PCR method for high-throughput mapping of T-DNA inserts in the Arabidopsis genome. Nat Protoc 2(11):2910–2917
12. Gendreau E et al (1997) Cellular basis of hypocotyl growth in Arabidopsis thaliana. Plant Physiol 114(1):295–305
13. Boron AK, Vissenberg K (2014) The Arabidopsis thaliana hypocotyl, a model to identify and study control mechanisms of cellular expansion. Plant Cell Rep 33:697
14. Xiao C, Somerville C, Anderson CT (2014) Polygalacturonase involved in cell expansion 1 functions in cell elongation and flower development in *Arabidopsis thaliana*. Plant Cell 26(3):1018–1035
15. Kardailsky I et al (1999) Activation tagging of the floral inducer FT. Science 286(5446): 1962–1965
16. van der Graaff E, Dulk-Ras AD, Hooykaas PJ, Keller B (2000) Activation tagging of the

LEAFY PETIOLE gene affects leaf petiole development in Arabidopsis thaliana. Development 127(22):4971–4980

17. van der Graaff E, Hooykaas PJ, Keller B (2002) Activation tagging of the two closely linked genes LEP and VAS independently affects vascular cell number. Plant J 32(5):819–830
18. Borevitz JO, Xia Y, Blount J, Dixon RA, Lamb C (2000) Activation tagging identifies a conserved MYB regulator of phenylpropanoid biosynthesis. Plant Cell 12(12):2383–2394
19. Woodward C et al (2005) Interaction of auxin and ERECTA in elaborating Arabidopsis inflorescence architecture revealed by the activation tagging of a new member of the YUCCA family putative flavin monooxygenases. Plant Physiol 139(1):192–203
20. Xiao C, Chen F, Yu X, Lin C, Fu YF (2009) Over-expression of an AT-hook gene, AHL22, delays flowering and inhibits the elongation of the hypocotyl in Arabidopsis thaliana. Plant Mol Biol 71(1–2):39–50
21. Mathews H et al (2003) Activation tagging in tomato identifies a transcriptional regulator of anthocyanin biosynthesis, modification, and transport. Plant Cell 15(8):1689–1703
22. Zubko E et al (2002) Activation tagging identifies a gene from Petunia hybrida responsible for the production of active cytokinins in plants. Plant J 29(6):797–808
23. Marsch-Martinez N (2011) A transposon-based activation tagging system for gene function discovery in Arabidopsis. Methods Mol Biol 754:67–83
24. Harb A, Pereira A (2013) Activation tagging using the maize En-I transposon system for the identification of abiotic stress resistance genes in Arabidopsis. Methods Mol Biol 1057:193–204
25. Fladung M, Ahuja MR (1997) Excision of the maize transposable element Ac in periclinal chimeric leaves of 35S-Ac-rolC transgenic aspen-Populus. Plant Mol Biol 33(6):1097–1103
26. Spena A, Aalen RB, Schulze SC (1989) Cell-autonomous behavior of the rolC gene of Agrobacterium rhizogenes during leaf development: a visual assay for transposon excision in transgenic plants. Plant Cell 1(12):1157–1164
27. Waki T et al (2013) A GAL4-based targeted activation tagging system in Arabidopsis thaliana. Plant J 73(3):357–367
28. Sedbrook JC, Ehrhardt DW, Fisher SE, Scheible WR, Somerville CR (2004) The Arabidopsis sku6/spiral1 gene encodes a plus end-localized microtubule-interacting protein involved in directional cell expansion. Plant Cell 16(6): 1506–1520

Chapter 15

BiFC for Protein–Protein Interactions and Protein Topology: Discussing an Integrative Approach for an Old Technique

Giovanni Stefano, Luciana Renna, and Federica Brandizzi

Abstract

BiFC (*Bi*molecular *F*luorescence *C*omplementation) is one of the most widely used techniques to study protein–protein interactions as well as protein topology in living cells. This method allows the visualization of protein interactions or the analysis of their topology in the cell compartments where the proteins belong, without changing their chemical properties, as often occurs after mixing the content of different cellular compartments in cell extracts. Several laboratories use this method because it is relatively easy to perform; however, sometimes a positive protein–protein interaction BiFC signal (i.e., reconstitution of fluorescence of interacting protein pairs) does not necessarily mean that the tested proteins are actually interacting in vivo in a specific way. Here we describe the BiFC approach for assessing protein–protein interactions and for establishing protein topology and we discuss how to best perform this method to avoid false positive results when studying protein interactions in plant cells.

Key words Bimolecular fluorescence complementation, BiFC, Tobacco, Protein–protein interactions, YFP, Fluorescent protein

1 Introduction

Theoretically, BiFC is a useful technique that can be used to investigate different protein properties. The method is based on splitting the yellow fluorescent protein (YFP) or other fluorescent proteins in half and then monitoring for the reconstitution of fluorescence when expressed in live cells. Indeed, if two proteins interact, the two halves of the fluorescent protein are close enough together to reconstitute the full protein that can be excited and produce fluorescence (Fig. 1).

Commonly, BiFC approach relies on splitting the YFP into a first portion from amino acid position 1–154 (YN), and a second portion from amino acid 155–239 (YC) [1]. This is not the only arrangement feasible. Another possibility is to split the fluorescent protein in half at a different position between amino acid 174 and 175 [2].

José M. Estevez (ed.), *Plant Cell Expansion: Methods and Protocols*, Methods in Molecular Biology, vol. 1242,
DOI 10.1007/978-1-4939-1902-4_15,

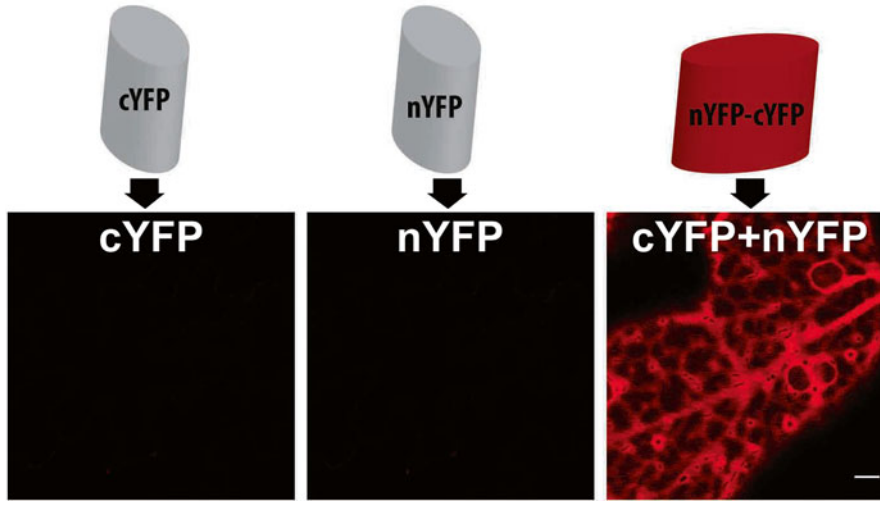

Fig. 1 BiFC principle. Confocal microscopy image demonstrating BiFC of YFP using untagged cYFP and nYFP in the cytoplasm of a tobacco leaf epidermal cell. Fluorescence is detected only when the two halves are coexpressed. Scale bar = 5 μm

Because false-positive results are very frequently obtained with BiFC, it has been proposed to remove the amino acids from position 153–155 to lower the rate of nonspecific results. This change positively influences the stability of the protein without interfering with the protein interaction [3]. This specific modification is highly recommended when protein–protein interactions need to be monitored in enclosed cell compartments with high protein crowding such as the endoplasmic reticulum (ER), where often the constricted volume of tubules increases the chances of nonspecific interactions.

The presence of nonspecific BiFC fluorescence signal mostly affects results if we are looking for protein interaction partners. To determine accurately if two proteins interact, a statistical analysis to establish the significance in the given BiFC signals appears to be fundamental. This analysis is extremely important, especially if you are working with a gene controlled by the CaMV35S promoter. Indeed, the CaMV35S promoter leads to constitutive overexpression of proteins, which in turn may lead to a nonspecific interaction due the fact that the cellular environment becomes oversaturated with the protein of interest.

BiFC has also been successfully used to visualize interactions between three proteins in the same cell compartment [4], defined as a multicolor BiFC assay. This method is based on the fusion of multiple proteins, herein indicated as ProteinA, ProteinB, and ProteinC, where ProteinA is fused to the N-terminal of YFP half, ProteinB is fused to the N-terminal CFP half, and ProteinC is fused to the C-terminal half of CFP. If interaction among the three proteins occurs then fluorescence due to ProteinA–ProteinB and

ProteinB–ProteinC interaction will be observed. This will result in well-separated fluorescence signals from ProteinA–ProteinB and ProteinB–ProteinC interaction, respectively.

Remarkably, the possibility to produce nonspecific signal with the BiFC approach has revealed a useful strategy for establishing topology of membrane proteins. Thanks to the presence of membrane boundaries in the cell, overexpression of the protein is not a problem. For this kind of approach, BiFC analyses are based on the interaction of a protein fused to either the C- or the N-terminal half of YFP coexpressed in cells with the complementary half of the fluorescent protein. If the proteins are in the same compartment, they can interact, giving a clear indication of protein orientation with respect to the membrane (Fig. 2). Recently, this approach has been successfully used as a fast technique to assess topology of ER membrane proteins, using the half-YFPs targeted to the ER lumen in virtue of the ER retention signal HDEL, where the negative control was a half-YFP facing the cytosol [5–7]. Here we describe an approach commonly used in our lab to establish protein–protein interactions or protein topology with BiFC in transient expression in plant cells.

2 Materials

2.1 Plant Plasmids

Various plant binary vectors with the -N- or C-terminal half of the YFP can be used for the subcloning of the gene of interest. Alternatively, any binary vector without YFP sequences can also be used. In this case, the half YFP portions can be spliced to the cDNA of interest by overlapping PCR technique [8, 9].

2.2 Agrobacterium Culture and Infiltration Medium

1. Agrobacterium strain GV3101::mp90 transformed with the binary vector (e.g., pVKH18En6) containing a nYFP or cYFP fusion construct of interest.
2. Appropriate antibiotics for agrobacterium selection.
3. LB medium: yeast extract (5.0 g/1 L), peptone (10.0 g/1 L), sodium chloride (10.0 g/1 L), pH 7.0.
4. Infiltration medium: 0.5 % D-glucose, 50 mM MES, 2 mM $Na_3PO_4{\cdot}12H_2O$, 0.2 mM acetosyringone.

2.3 Plants

Three–four weeks old *Nicotiana tabacum* plants should be used. They should be grown in a controlled growth chamber with a cycle of 23 °C for 18 h light and 18 °C for 6 h night.

2.4 Fluorescence or Confocal Laser Scanning Microscope

Fluorescence or confocal microscope equipped with a 10× and 40× objective.

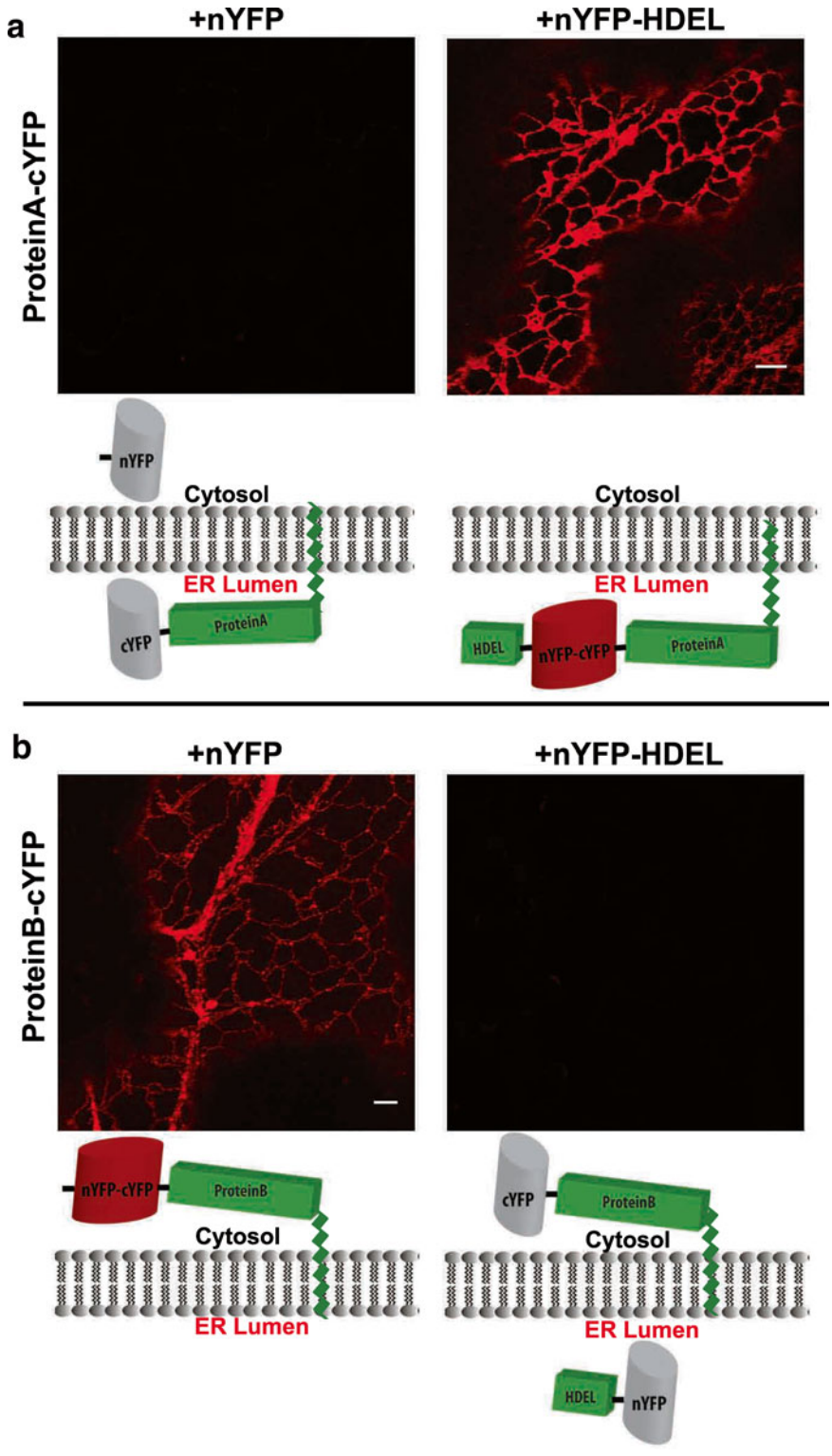

Fig. 2 BIFC as a tool to investigate membrane protein topology. (**a**) Example of protein with N-terminal region localized to the ER lumen. To map the N-terminal region of the protein coexpression analysis was done with nYFP (cytosolic localization) or with an ER-targeted and retained nYFP (nYFP-HDEL). The same approach can be used to map the C-terminal region of the unknown protein. (**b**) Example of protein with N-terminal region facing the cytosol. In this case, coexpression analysis with nYFP or nYFP-HDEL established that the N-terminal region of ProteinB is facing the cytosol. The same approach can be used to map the C-terminal region of this protein

3 Methods

3.1 Plant Binary Vectors

Plant binary vector such as pVKH18En6 with the N- or C-terminal half of YFP has been used successfully for BiFC experiments [5, 10]. pVKH18En6-based BiFC expression plasmids contain the CaMV35S promoter. The pVKH18En6-nYFP and pVKH18En6-cYFP vectors contain amino acids 1–155 and amino acids 156–239 of YFP, respectively. The gene of interest is subcloned into the multiple cloning site (MCS) in correct orientation and reading frame to generate a translational fusion with nYFP or cYFP. Other plasmids have been used for BiFC analysis in plant cells [11, 12]. In alternative to the CaMV35S promoter, the ubiquitin-10 gene promoter (PUBQ10) of Arabidopsis can also be used (*see* **Notes 1–4**).

The fusion of either half YFP portion can be performed at the N- or C-terminus of the protein of interest. In alternative, coding sequence of the half fluorescent protein can be spliced inside the coding sequence of the protein of interest (Fig. 3). The latter strategy is useful when fusion at the terminal regions of the proteins somehow alter their behavior. The choice of the fusion of the half YFP should depend on prior knowledge of protein targeting determinants and/or function so that the fusions will not affect protein distribution and behavior. Furthermore, the half YFP should be placed in the protein of interest where it may be accessible by the complementary half YFP.

3.2 Gene Sequencing and Agrobacterium Transformation

Once the subcloning into the plant binary vectors is completed, checking the sequence of the cloned DNA is necessary to ensure the region of overlapping between the half-fluorescent protein and your gene of interest is in frame. If the clone is correct, you can transform the agrobacteria as follows:

1. Add 50–100 ng of plasmid DNA to 40 μL of competent agrobacteria in a 1.5-mL Eppendorf tube.
2. Put competent cells on ice for 10 min.
3. Freeze tubes in liquid nitrogen for 5 min.
4. Remove the tube from liquid nitrogen and heat-shock the cells at 37 °C for 5 min in water bath or suitable incubator.

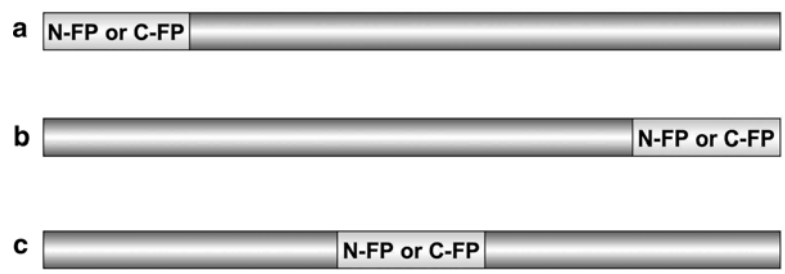

Fig. 3 Fusion protein strategy. Half-fluorescent protein fusion at N-terminal region (**a**), C-terminal region (**b**), or inside the gene of interest (**c**)

5. Add 750 µl of LB medium and incubate in a shaker at 200 rpm, 28 °C for 2 h.
6. Spread on plates (LB medium with 0.8 % agar) containing the appropriate antibiotics according to the bacterial resistance encoded in the vector of choice, and incubate the plates at 28 °C for 2 days.

3.3 Infiltration Medium and Tobacco Infiltration

Because in the BiFC the reconstitution of the fluorescent protein is generally irreversible, BiFC interactions induce stable interaction of proteins. While this is not a problem when the fluorescence reconstitution is analyzed for topology analyses that are based on the interaction of an unfused half YFP with the complementary half YFP fused to a protein, BiFC interactions can affect the behavior of the interacting pairs in protein–protein interaction analyses. This may cause problems in generating stable transformants expressing protein interacting pairs fused to complementary YFP halves. Therefore, for protein–protein interaction analyses, transient expression experiments are generally preferred over stable transformations. Here we describe a BiFC protocol for transient transformation in tobacco leaf epidermis, which is an established approach for successfully conducting quantitative and qualitative images analyses in living plant cells.

Prepare infiltration medium from stock solutions. A minimum of 5 mL of medium is necessary for each clone that needs to be transformed. The preparation of 10 mL infiltration buffer requires:

1. 50 mg of D-glucose.
2. 1 mL from a stock solution of 500 mM MES.
3. 1 mL from a stock solution of 20 mM $Na_3PO_4{\cdot}12H_2O$. MES and $Na_3PO_4{\cdot}12H_2O$ Stock should be sterilized by filtration and stored at 4 °C.
4. 10 µL from a stock 200 mM of acetosyringone. Acetosyringone stock solution is prepared in DMSO and aliquoted in an Eppendorf tube and stored at −20 °C until use.

Agrobacterium infiltration in tobacco leaf epidermis can be performed as described previously [13] and generally the transformed samples are observed 2–3 days after bacterial inoculation. Here we suggest a modification that can help avoid false positive results in BiFC analyses. Specifically, a preliminary BiFC experiment should be conducted with dilutions of agrobacteria based on the absorbance at 600 nm (optical density O.D. at 600 nm) to establish the lowest bacterial working dilution that can be used to avoid false positive results (*see* below). BiFC experiments have been successfully performed using pVKH18En6 at an O.D. of 0.0025–0.005 to avoid nonspecific results.

3.4 Microscope Observations and Fluorescence Analysis

YFP fluorescence can be analyzed by fluorescence or confocal microscope (*see* **Notes 5** and **6**). Prepare a sample for imaging by sectioning the infiltrated section of a tobacco leaf with a razor blade (usually, 25 mm^2 leaf sections). Place the section on a microscope slide and cover with water and a coverslip. Start your experiment observing first the negative control sample with a 10× objective. The negative control should be based on coexpression of your protein of interest fused to a half YFP with either a protein that is known not to interact with the protein of interest fused to the complementary YFP half or with the complementary YFP half alone. It is critical that the negative control is based on YFP half that is targeted to the same compartment as the protein of interest. If the protein of interest is a membrane protein then the complementary YFP half control should be targeted to the same membrane with the same orientation of the YFP half in the fusion with the protein of interest with respect to the membrane. In your confocal observations, the optimal situation is reached when the bacterial OD_{600} used for the infiltration of the negative control is clear, i.e., no fluorescence reconstitution should be observed, due to the fact that the half-fluorescent fused proteins are sufficiently far apart in the environment where they are present to reconstitute the whole fluorescent protein.

The next step is to observe the sample, which contains the possible interactors. The 10× view will give an idea how well the experiment is working and you may wish to do statistical analyses (Fig. 4; *see* **Note 7–8**). Namely, you should acquire images (at least 20–30) of multiple 10× field of view (at least 10) within the same sample, using settings for YFP (excitation 514 nm, emission 530–600 nm) as well as for differential interference contrast (DIC). The DIC settings will allow you to distinguish the perimeter of the epidermal cells. This is necessary to count the cells that populate each image sector. Count the number of fluorescent and nonfluorescent cells within the imaged sectors. With this approach, you can easily estimate the percentage of fluorescent cells over a large population of cells.

Using the 40× objective it is possible to acquire information about the nature of the compartment where the BiFC-based interaction occurs.

4 Notes

1. Use of fluorescent protein with a faster folding time (such as venus YFP) is preferred to perform the BiFC experiments.
2. Different amino acids can be used as linkers between your gene and the half-fluorescent protein to provide good flexibility. This approach will offer the best opportunity for the interacting

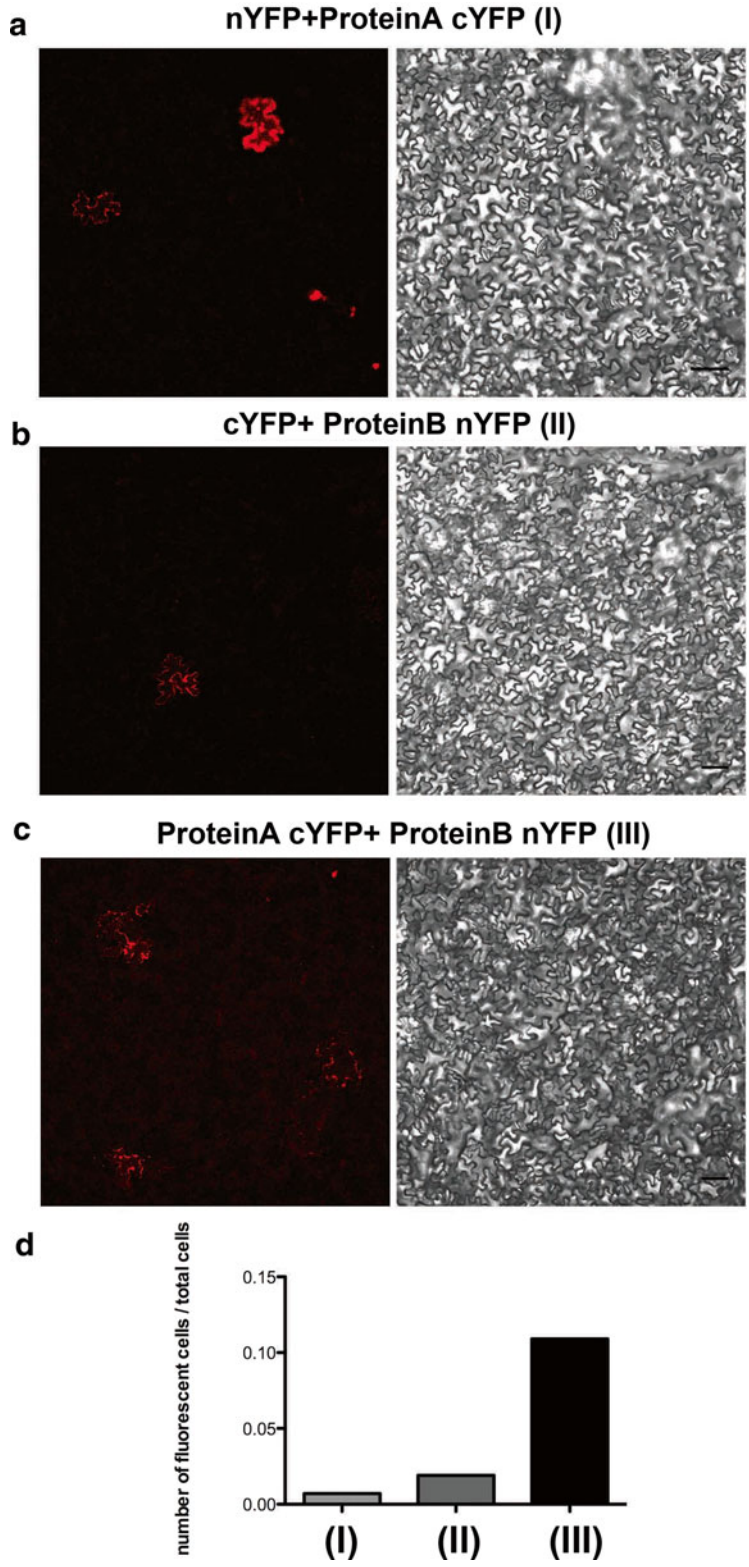
a
nYFP+ProteinA cYFP (I)
b
cYFP+ ProteinB nYFP (II)
c
ProteinA cYFP+ ProteinB nYFP (III)
d
number of fluorescent cells / total cells
0.15
0.10
0.05
0.00
(I)
(II)
(III)

proteins and the two YFP halves to interact properly. For details, *see* refs. 14, 15.

3. It is not recommended to perform the BiFC experiment using candidate interacting proteins encoded in different plant vectors, as each plasmid can have a different linker amino acid sequence.
4. Organelles of the plant secretory pathway have different pH and fluorescent proteins such as CFP and YFP are sensitive to the environmental pH. Therefore, to ensure that it is possible to visualize the protein of interest, an analysis should be performed using the protein of interest fused to full-length YFP. The presence of YFP signal in the expected compartment can increase the confidence in the BiFC approach. This step can also be very useful to establish whether the fluorescent protein fusion based on the half YFP is likely to affect the targeting and/or trafficking of the protein of interest to the expected secretory compartment.
5. It is recommended to ensure that in the BiFC experiment both YFP halves are expressed. This can be achieved by Western blot analyses on protein extracts from leaf tissues transformed with individual YFP halves using commercial GFP antibodies which generally also recognize YFP. In alternative, fluorescence reconstitution between the protein fused with half YFP and unfused complementary YFP targeted to the same compartment can be used as evidence that the protein of interest is expressed.
6. Coexpression of two interacting proteins may exert negative effects on the biology of the cell even in transient expression experiments.
7. As explained in this chapter, although seemingly powerful, relatively inexpensive and fast, BiFC can be easily prone to artifacts. We have experienced that for certain membrane proteins

Fig. 4 A statistical analysis can help distinguish false positive from positive BiFC results. Here secretory proteins forming interacting pairs (ProteinA and ProteinB; panel **c**) have been fused to complementary YFP halves, expressed in tobacco leaf epidermal cells and imaged with a EC Plan-Neofluar 10×/0.30 M27 objective at Zeiss LSM510 META confocal microscope using YFP settings. Images in panel (**a**) and (**b**) represent controls based on the interaction of ProteinA fused to the C-terminal half of YFP [nYFP + ProteinA cYFP (I) and cYFP + ProteinB nYFP(II)]. Panel (**d**) shows an example of graph obtained after estimating the number of fluorescent cells per total cells acquiring at least 25 images for each sample (area of each image was 1,273 × 1,273 μm). Although for this experiment the bacterial OD was low, we verified nonspecific interactions (panels **a** and **b**). The analysis of a large number of cells however has revealed that the number of cells that were positive for BiFC signal was higher than that of the negative controls providing a degree of confidence in the interaction between ProteinA and ProteinB

positive results can be obscured by false positives. This may be due to the fact that some proteins may segregate in crowded membrane micro-compartments, rendering the BiFC approach unsuccessful.

8. As for any protein–protein interaction analysis, BiFC should be considered as one proof of evidence for protein–protein interaction analyses and additional independent approaches are likely to increase the confidence of the results.

Acknowledgements

We acknowledge support by the Chemical Sciences, Geosciences and Biosciences Division, Office of Basic Energy Sciences, Office of Science, U.S. Department of Energy (award number DE-FG02-91ER20021) for infrastructure support and National Science Foundation (MCB 1243792).

References

1. Hu CD, Chinenov Y, Kerppola TK (2002) Mol Cell 9:789–798
2. Citovsky V, Lee LY, Vyas S, Glick E, Chen MH, Vainstein A, Gafni Y, Gelvin SB, Tzfira T (2006) J Mol Biol 362:1120–1131
3. Schutze K, Harter K, Chaban C (2009) Methods Mol Biol 479:189–202
4. Hu CD, Kerppola TK (2003) Nat Biotechnol 21:539–545
5. Mehrshahi P, Stefano G, Andaloro JM, Brandizzi F, Froehlich JE, Dellapenna D (2013) Proc Natl Acad Sci U S A 110: 12126–12131
6. Zamyatnin AA Jr, Solovyev AG, Bozhkov PV, Valkonen JP, Morozov SY, Savenkov EI (2006) Plant J 46:145–154
7. Sparkes I, Brandizzi F (2012) Plant J 70: 96–107
8. Ho SN, Hunt HD, Horton RM, Pullen JK, Pease LR (1989) Gene 77:51–59
9. Higuchi R, Krummel B, Saiki RK (1988) Nucleic Acids Res 16:7351–7367
10. Slabaugh E, Held M, Brandizzi F (2011) Plant J 67:395–405
11. Walter M, Chaban C, Schutze K, Batistic O, Weckermann K, Nake C, Blazevic D, Grefen C, Schumacher K, Oecking C, Harter K, Kudla J (2004) Plant J 40:428–438
12. Grefen C, Donald N, Hashimoto K, Kudla J, Schumacher K, Blatt MR (2010) Plant J 64: 355–365
13. Sparkes IA, Runions J, Kearns A, Hawes C (2006) Nat Protoc 1:2019–2025
14. Kerppola TK (2013) Cold Spring Harb Protoc 2013:727–731
15. Kerppola TK (2013) Cold Spring Harb Protoc 2013:714–718

Chapter 16

N-Glycosylation and Plant Cell Growth

Christiane Veit, Ulrike Vavra, and Richard Strasser

Abstract

N-linked glycosylation is one of the most prevalent cotranslational protein modifications in plants. It is initiated by a conserved process in the endoplasmic reticulum and subsequently involves a series of different *N*-glycan maturation steps that take place in the ER and Golgi apparatus. Despite our vast knowledge on the different processing steps we still understand very little about the role of characteristic glycoforms present on individual plant glycoproteins. Here, we describe convenient tools that allow the fast and reliable characterization of N-glycosylation on plant glycoproteins. The presented protocols can be adopted to other plant species and to the characterization of *N*-glycans from different glycoproteins.

Key words N-glycosylation, Glycoprotein, Oligomannosidic *N*-glycans, Complex *N*-glycans, Immunoblot, Endoglycosidase, Underglycosylation, Endoplasmic reticulum, Golgi, *Arabidopsis thaliana*

1 Introduction

Proteins destined for the secretory pathway are subjected to folding and maturation in the endoplasmic reticulum (ER). N-glycosylation is one of the most abundant protein modifications in eukaryotes and is initiated in the ER by transfer of a preassembled oligosaccharide to asparagine residues within the conserved glycosylation site (Asn-X-Ser/Thr, where X can be any amino acid except proline). The cotranslational transfer of the oligosaccharide can directly affect folding of proteins and subsequently plays a crucial role during glycan-mediated quality control processes like the calnexin/calreticulin cycle and ER-associated degradation of aberrant or surplus proteins. These fundamental functions of N-glycosylation are highly conserved in eukaryotes [1].

In *Arabidopsis thaliana* it has been shown that the absence of any catalytic subunit of the oligosaccharyltransferase (OST) complex is lethal [2]. In addition, the first two *N*-glycan processing steps

José M. Estevez (ed.), *Plant Cell Expansion: Methods and Protocols*, Methods in Molecular Biology, vol. 1242,
DOI 10.1007/978-1-4939-1902-4_16,

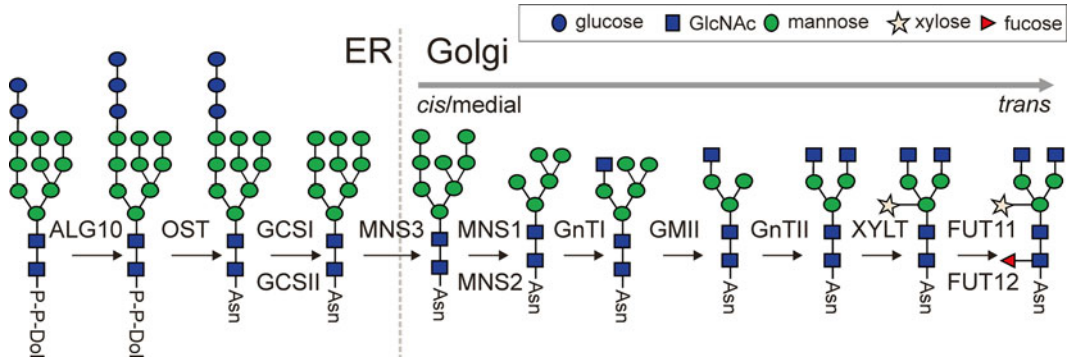

Fig. 1 Simplified schematic presentation of the N-glycosylation and *N*-glycan processing pathway in plants leading to the formation of the most abundant processed glycoform termed GnGnXF ($GlcNAc_2XylFucMan_3GlcNAc_2$). The last step in the biosynthesis of the dolichol-linked oligosaccharide precursor mediated by the α1,2-glucosyltransferase ALG10 is indicated. Transfer of the fully assembled oligosaccharide to an asparagine residue of the nascent polypeptide chain is catalyzed by the oligosaccharyltransferase (OST) complex. *N*-glycan processing enzymes: GCSI: α-glucosidase I; GCSII: α-glucosidase II; MNS3: ER-α-mannosidase I; MNS1/MNS2: Golgi-α-mannosidase I; GnTI: *N*-acetylglucosaminyltransferase I; GMII: Golgi-α-mannosidase II; GnTII: *N*-acetylglucosaminyltransferase II; XYLT: β1,2-xylosyltransferase; FUT11/FUT12: core α1,3-fucosyltransferase. *Note*: Different *N*-glycan processing routes can take place in the Golgi of plants

mediated by glucosidase I and II are also essential for plants [3–5]. In contrast, a block in the following maturation steps that are performed by class I α-mannosidases result in a severe root growth phenotype, but the plants complete their life cycle and produce seeds [6]. All further downstream *N*-glycan modifications that take place in the Golgi and result in the formation of complex *N*-glycans (Fig. 1) are dispensable for *A. thaliana* growth under controlled laboratory conditions [7–10]. However, a recent study shows that complex *N*-glycans are crucial for the development and reproduction of rice [11]. Together, these findings highlight that the formation of distinct *N*-glycan structures is highly important for plant development. In order to understand the contribution of individual *N*-glycans and the role of certain sugar residues to plant growth, a comprehensive analysis of *N*-glycan structures on plant glycoproteins is required. Recently, significant progress has been made in N-glycosylation site analysis in *A. thaliana* [12] and the first comprehensive *N*-glycan analysis of two endogenous *A. thaliana* glycoproteins with multiple *N*-glycans has been demonstrated [13]. Here, we describe basic protocols for the analysis of changes in N-glycosylation, which focus mainly on immunoblots that can be performed without any specialized equipment. The described procedures are complementary to structural analysis by MS-based methods that have been described in detail recently [13–15].

2 Materials

2.1 Plant Growth

2.1.1 Plant Material

Arabidopsis thaliana cgl1 [7] (N6192/CS6192), *gntI* (SALK_073560) [16] and *alg10-1* (SAIL_515_F10) [17] seeds can be obtained from the Nottingham Arabidopsis Stock Center or Arabidopsis Biological Resource Center. The *fut11 fut12* and *fut11 fut12 xylt* [8] seeds can be obtained upon request from the Strasser group. Double and triple mutants were obtained by crossing of the respective single mutants. With the exception of *cgl1* all mutants are T-DNA insertion lines.

2.1.2 Plant Growth

Plants were grown in 0.5× MS medium (Duchefa) supplemented with 0.8 % agar and 1 % sucrose or on soil at 22 °C under long day conditions (16 h light/8 h dark).

2.2 Equipment

1. Vertical electrophoresis system (Mini-Protean, Bio-Rad).
2. Tank transfer system (Mini-Trans Blot, Bio-Rad).
3. Power supply (Power Pac Universal Power Supply, Bio-Rad).
4. Mixer mill (Retsch) with metal beads.
5. Container with liquid nitrogen.
6. Refrigerated bench-top centrifuge.
7. Thermo block.
8. Shaker.

2.3 Reagents and Solutions Needed

1. Handcast "*see* **Note 1**" SDS-PAGE (10 %) gels (*see* **Note 2**).
2. Tris/glycine/SDS-PAGE running buffer.
3. Laemmli sample buffer.
4. Protein standard (prestained protein marker, Fermentas).
5. Tris/glycine/methanol transfer-buffer (*see* **Note 3**).
6. Whatman 3MM blotting paper.
7. Hybond ECL nitrocellulose membrane (GE Healthcare).
8. 1× Phosphate-Buffered Saline (PBS) (137 mM NaCl, 2.7 mM KCl, 10 mM Na_2HPO_4, 2 mM KH_2PO_4, pH 7.4).
9. PBST: 1× PBS + 0.1 % (v/v) Tween 20.
10. 1× TBS: Tris-buffered saline (25 mM Tris–Cl, pH 7.5, 150 mM NaCl, 2 mM KCl).
11. TBST: 1× TBS + 0.1 % (v/v) Tween 20.
12. Blocking solution: PBST + 3 % (w/v) BSA (use for anti-xylose, anti-fucose and anti-PDI antibody).

13. Blocking solution: TBST + 3 % (w/v) skimmed milk powder (for anti-HRP and anti-TGG1 antibody) or TBST + 2 % (w/v) skimmed milk (for anti-BRI1 antibody).
14. SuperSignal West PICO Chemiluminescent Substrate (Pierce) or Amersham ECL Prime Western Blotting Detection Reagent (GE Healthcare).
15. Hyperfilm ECL film (GE Healthcare) (alternatively use a gel imaging system).
16. 1× PBS + 1 % (v/v) Triton X-100.
17. Film developer and fixer solutions.
18. Anti-xylose antibody (Agrisera: AS07 267): 1:10,000 diluted in PBST.
19. Anti-fucose antibody (Agrisera: AS07 268): 1:6,500 diluted in PBST.
20. Anti-horseradish peroxidase (HRP) antibody (Sigma, P7899): 1:10,000 diluted in TBST.
21. Anti-protein disulfide isomerase (PDI) antibody (custom-made polyclonal antibody against the peptide CGPREAEGIVTYLKKQSGP, *A. thaliana* gene ID: At1g21750): 1:5,000 diluted in PBST.
22. Anti-beta-thioglucoside glucohydrolase (TGG1) antibody (custom-made polyclonal antibody against the peptide AQNNQTIVPSDVHT, *A. thaliana* gene ID: At5g26000): 1:500 diluted in TBST.
23. Anti-BRASSINOSTEROID INSENSITIVE 1 (BRI1) antibody (custom-made polyclonal antibody against the peptide CGKRPTDSPDFGDNN, *A. thaliana* gene ID: At4g39400): 1:750 diluted in TBST + 2 % (w/v) skimmed milk.
24. Anti-rabbit IgG-peroxidase (Sigma, A0545): 1:50,000 diluted in PBST or TBST + 2 % (w/v) skimmed milk.
25. Concanavalin A-peroxidase (ConA-HRP, Sigma-Aldrich: L6397): ConA solution: 0.5 μg/mL Con A-HRP in PBST containing 1 mM $MnCl_2$, 1 mM $CaCl_2$, 1 mM $MgCl_2$.
26. Endoglycosidase H (Endo H, 500,000 units/mL, NEB) + G5 reaction buffer (NEB).
27. Peptide-*N*-Glycosidase F (PNGase F, 500,000 units/mL, NEB) + G7 reaction buffer (NEB).
28. Glycoprotein denaturing buffer (NEB).
29. 10 % solution of NP-40 (NEB).
30. Ponceau S staining solution (Sigma).
31. Buffer for isolation of microsomal fractions, prepared according to [18].

3 Methods

3.1 Protein Extraction and SDS-PAGE

1. Harvest 20–200 mg seedlings or leaf material and transfer to 2 mL Eppendorf tubes containing two metal beads per tube (*see* **Note 4**).
2. Submerge 2 mL tubes with plant material in container with liquid nitrogen.
3. Mount 2 mL tubes in mixer mill and run 2 min at 50–60 amplitude.
4. Add 4 μL PBST (*see* **Note 5**) per mg of leaf material, vortex shortly, transfer liquid into a 1.5 mL tube and incubate on ice for 15 min, invert tube every 3 min.
5. Centrifuge two times 15 min, 9.600 × *g* at 4 °C, transfer supernatant each time to a new tube.
6. Keep protein extracts on ice for subsequent SDS-PAGE (*see* **Notes 6** and **7**).
7. Mix samples with 3× Laemmli sample buffer and heat to 95 °C for 5 min.
8. Run gel for 1.5 h at 100 V.

3.2 Immunoblot and Detection of Overall Changes in Complex N-glycan Formation

This procedure will detect all extracted proteins carrying complex *N*-glycans with core α1,3-fucose and/or β1,2-linked xylose.

1. Soak nitrocellulose membrane, sponges, and blotting paper in transfer buffer.
2. Perform the gel-membrane assembly according to the user manual from Bio-Rad and insert gel-membrane sandwich into the transfer cell. Add ice pack for cooling and fill up with transfer buffer.
3. Blot 1 h at 100 V.
4. Disassemble gel-membrane sandwich, carefully rinse the membrane with ultrapure water, and incubate in blocking solution for 1 h at room temperature (*see* **Note 8**).
5. Rinse briefly with PBST or TBST (depending on the first antibody).
6. Incubate membrane on a shaker for 12–16 h at 4 °C in the antibody solution (use anti-xylose, anti-fucose, or anti-HRP antibodies) (Fig. 2).
7. After incubation, wash four times 5 min with PBST or TBST (depending on the second antibody).
8. Add second antibody solution to membrane, incubate for 1.5 h at room temperature on shaker.
9. Wash four times 5 min in PBST or TBST.

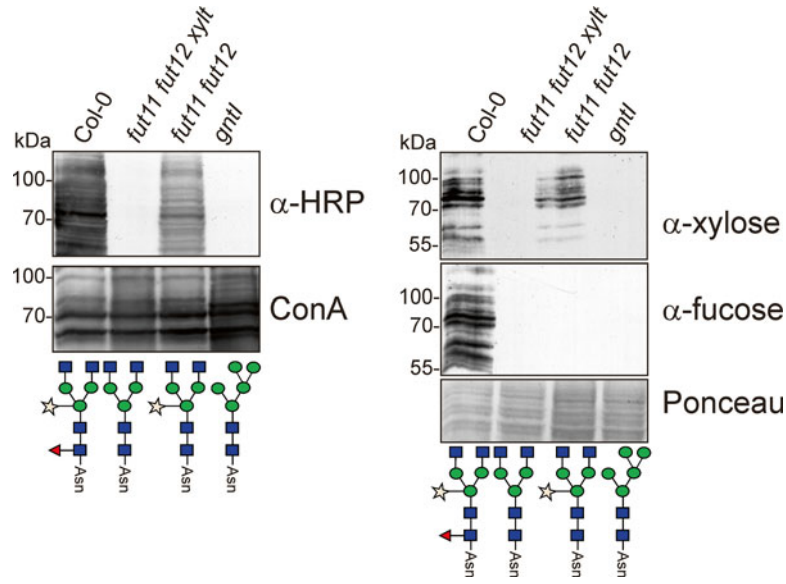

Fig. 2 Detection of complex *N*-glycans in total protein extracts from *A. thaliana* seedlings (anti-HRP antibody, ConA lectin) or leaves (anti-xylose, anti-fucose antibody). Col-0: wild-type plant; *fut11 fut12 xylt*: triple knockout plant lacking β1,2-xylosyltransferase and core α1,3-fucosyltransferases [8]; *fut11 fut12*: double knockout plant lacking core α1,3-fucosyltransferase activity [8]; *gntI*: GnTI knockout line (T-DNA insertion line) [17]. Ponceau S staining was used as a loading control. The most predominant *N*-glycan structure in these mutants is indicated

10. Perform detection using the chemiluminescent substrate.
11. Develop the film.
12. After developing the film the membrane can be stained with Ponceau S to monitor equal loading of protein extracts. Briefly rinse membrane in ultrapure water and subsequently incubate in Ponceau S staining solution for 5 min at room temperature. Destain with water until protein bands are clearly visible.

3.3 Lectin Lot and Detection of Changes in Oligomannosidic N-glycans

The lectin blot procedure is very similar to the detection of immobilized proteins using specific antibodies (Fig. 2). In brief, SDS-PAGE is done as described in Subheading 3.1 and blotting is carried as described in Subheading 3.2, **steps 1–5**. After blocking of the membrane in PBST + 3 % BSA the membrane is incubated on a shaker for 1 h at room temperature in ConA solution (*see* **Notes 9** and **10**). The subsequent detection is carried out as described in Subheading 3.2.

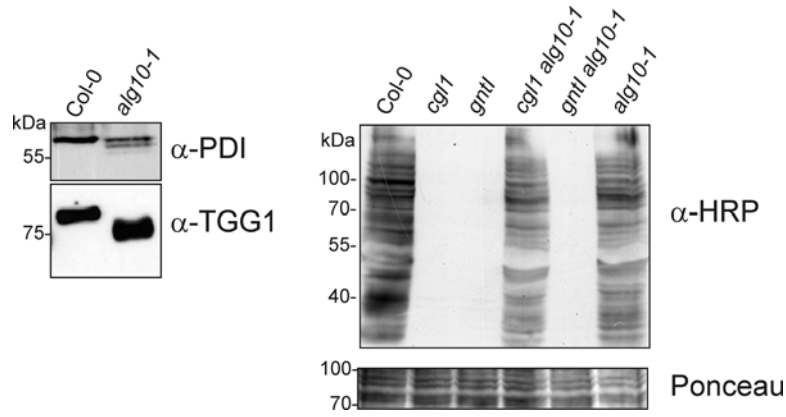

Fig. 3 Analyses of protein underglycosylation in *A. thaliana* seedlings (anti-PDI and anti-HRP antibody) or leaves (anti-TGG1 antibody). The *alg10-1* plants cannot perform the final step of the lipid-linked oligosaccharide biosynthesis (*see* Fig. 1) and therefore the incompletely assembled glycan is not transferred efficiently to N-glycosylation sites. Consequently, faster migrating protein forms (e.g., PDI and TGG1) are visible and CGL1-GnTI is not glycosylated at Asn144 resulting in the restoration of complex *N*-glycan formation in the *cgl1 alg10-1* double mutant (anti-HRP blot)

3.4 Monitoring of Protein Underglycosylation Defects in Arabidopsis thaliana Plants

3.4.1 Monitoring of Protein Underglycosylation in Seedlings

The ER resident *A. thaliana* PDI5 protein harbors two N-glycosylation sites, which carry oligomannosidic *N*-glycans. Underglycosylation of PDI5 results in the generation of two additional variants which carry either one residual *N*-glycan or no residual *N*-glycan. Both underglycosylated PDI variants can therefore be distinguished by faster migration upon SDS-PAGE separation (Fig. 3). PDI5 is very well detectable in protein extracts from *A. thaliana* seedlings (*see* **Note 11**) but less abundant in leaves [19]. Immunoblotting of PDI proteins has been used by different groups to characterize mutants that cause protein underglycosylation [17, 20–23].

3.4.2 Monitoring of Protein Underglycosylation in Rosette Leaves

The myrosinase TGG1 is a heavily glycosylated protein with nine N-linked oligomannosidic glycans [13]. TGG1 is involved in defense reactions against insects and other pathogens and is very abundant in *A. thaliana* leaves [24]. Consequently, analysis of TGG1 mobility upon SDS-PAGE separation and subsequent immunoblotting (Fig. 3) is a highly suitable tool to detect changes in *N*-glycan site occupancy that can occur in leaves of plants with defects in the OST complex or assembly of the lipid-linked oligosaccharide precursor. Changes in TGG1 N-glycosylation have been detected in different underglycosylation mutants [2, 17, 22, 23, 25] (*see* **Note 12**).

3.4.3 Monitoring of Protein Underglycosylation by Analysis of Complex N-glycan Restoration in the cgl1 Mutant

An elegant tool to investigate the occurrence and level of a protein underglycosylation defect in different plant organs is the restoration of complex *N*-glycan formation in the *cgl1* mutant. The *cgl1* mutant harbors a single point mutation in the gene coding for *N*-acetylglucosaminyltransferase I (GnTI) resulting in an amino acid change from Asp144 to Asn144 (CGL1-GnTI) [26]. This mutation has two effects: first, it reduces GnTI activity. Second, it generates an additional N-glycosylation site resulting in ER retention of GnTI and presumably degradation due to a glycan-mediated ER quality control process [27]. In a protein underglycosylation mutant (e.g., in *alg10-1*), lack of N-glycosylation on Asn144 of CGL1-GnTI results in the formation of a partially active GnTI protein. As a consequence of CGL1-GnTI underglycosylation, the enzyme is found in the Golgi and complex *N*-glycan formation that is initiated by GnTI is restored in these double mutants (e.g., *cgl1 stt3a*, *cgl1 alg10*, *cgl1 ost3/6*) [17, 23, 27] (*see* **Note 13**). This can be readily monitored using anti-HRP antibody (or alternatively anti-fucose or anti-xylose antibodies) (Fig. 3). Crossing to the GnTI T-DNA insertion line (*gntI*), which completely lacks GnTI activity serves as a control.

3.5 Deglycosylation to Monitor Trafficking of Proteins Through the Golgi

Prepare microsomal membrane fractions using the following procedure (*see* **Note 14**): 200 mg Arabidopsis seedlings were harvested and the plant material was homogenized following the procedure from Subheading 3.1. Extraction of proteins, preparation of cleared homogenate, and preparation of membrane pellets by centrifugation were performed as described in detail recently [18] (*see* **Note 15**). The occurrence of PNGase F-insensitive *N*-glycans shows that the glycoprotein is processed in the Golgi and carries complex *N*-glycans (*see* **Note 16**). The occurrence of Endo H-sensitive oligomannosidic *N*-glycans indicates that the protein is (1) either an ER-resident protein (like PDI), (2) bypasses the Golgi by direct trafficking from the ER to other downstream compartments (e.g., vacuoles) within the endomembrane system, or (3) the *N*-glycans of the glycoprotein are not accessible for the processing enzymes in the Golgi (e.g., buried in the protein structure upon folding in the ER).

3.5.1 Endo H Digestion to Monitor the Presence of Oligomannosidic N-glycans on a Distinct Glycoprotein

Endo H cleaves within the chitobiose core of oligomannosidic *N*-glycans (Fig. 4). Consequently, Endo H treatment results in removal of all oligomannosidic *N*-glycans from glycoproteins (*see* **Note 17**). Presence of complex *N*-glycans (initiated by the GnTI-mediated transfer of a single *N*-acetylglucosamine (GlcNAc)-residue [28]) blocks Endo H activity.

1. Solubilize membrane pellet in 75 µL 2× Laemmli sample buffer by incubation on ice for 15 min.
2. Incubate 22.5 µL solubilized membrane faction with 2.5 µL 10× Glycoprotein denaturing buffer for 10 min at 50 °C, transfer to ice and cool for 5 min.

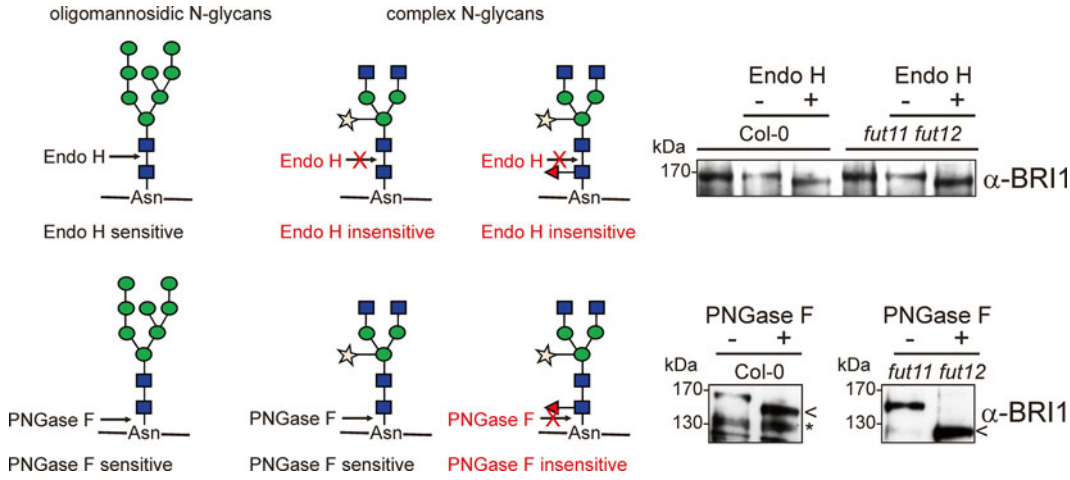

Fig. 4 Analyses of the N-glycosylation status of individual plant proteins by Endo H and PNGase F digestion. Endo H removes oligomannosidic *N*-glycans. Transfer of a single GlcNAc residue to the $Man_5GlcNAc_2$-Asn structure in the Golgi renders the glycan Endo H resistant. All other complex *N*-glycan structures are also Endo H insensitive. In contrast, PNGase F removes all *N*-glycans except those carrying the core α1,3-linked fucose. The analysis of BRI1, which has 14 potential N-glycosylation sites in its extracellular domain shows that it has oligomannosidic (shift upon Endo H treatment) and complex *N*-glycans with core α1,3-fucose (additional shift in *fut11 fut12* upon PNGase F digestion). The specific band is marked by an *arrow head* and an unspecific band is marked by an *asterisk*

3. Mix 22.5 µL of the denatured glycoproteins with 3 µL 10× G5 reaction buffer, 3 µL ultrapure water, and 1.5 µL Endo H. For the control reaction replace the 1.5 µL Endo H with ultrapure water.
4. Incubate for 90 min at 37 °C and stop the reaction by heating to 50 °C for 5 min.
5. Load samples on the SDS-PAGE gel and perform immunoblotting for example with anti-BRI1 antibody (Fig. 4).

3.5.2 PNGase F Digestion to Monitor the Presence of Complex N-glycans on a Distinct Glycoprotein

PNGase F removes the attached oligosaccharide by cleavage between the innermost GlcNAc and the asparagine residue (*see* **Note 18**) (Fig. 4). It is important to note that PNGase F is inactive against plant complex *N*-glycans carrying α1,3-fucose linked to the innermost GlcNAc [29]. This particular fucose is attached in the Golgi apparatus by core α1,3-fucosyltransferase [30]. In order to confirm the presence of Golgi-processed complex *N*-glycans (*see* **Note 19**) perform the same experiment in Col-0 wild-type plants and in the *fut11 fut12* double knockout mutant [8] (*see* **Note 20**).

1. Perform solubilization and denaturation as described for the Endo H digestion.
2. Mix 22.5 µL of the denatured glycoproteins with 3 µL 10× G7 reaction buffer, 3 µL NP-40, and 1.5 µL PNGase F. For the control reaction replace the 1.5 µL PNGase F with ultrapure water.

3. Incubate for 90 min at 37 °C and stop the reaction by heating to 50 °C for 5 min.
4. Load samples on the SDS-PAGE gel and perform immunoblotting for example with anti-BRI1 antibody (Fig. 4).

4 Notes

1. Wear goggles and gloves during casting of the gel.
2. As an alternative to handcast gels it is also convenient to use precast gels. For the separation of microsomal membrane fractions and detection of BRI1 we found that precast gels like Mini-Protean TGX, 4–15 % gradient gels (Bio-Rad) gave a better resolution.
3. Precooled to 4 °C.
4. To prevent the loss of plant material during grinding with the mixer mill the use of safe-lock microcentrifuge tubes is highly recommended.
5. Can be supplemented with protease inhibitor cocktail (e.g., Sigma 9599) to prevent rapid degradation of proteins.
6. The protein concentration can be estimated using a BCA Protein assay kit (Pierce).
7. Samples can be frozen, but be aware that freezing and storage can alter the protein composition in the extracts, which might be caused by degradation or precipitation of proteins.
8. Alternatively, blocking can be done for 12–16 h at 4 °C.
9. We use ConA conjugated to peroxidase (ConA-HRP). However, ConA can also be monitored due to its ability to bind the oligosaccharides of horseradish peroxidase.
10. ConA needs metal ions for binding.
11. There are almost no commercial antibodies available that detect endogenous *A. thaliana* glycoproteins. With our custom-made anti-PDI antibody PDI5 is readily detected in seedlings and young rosette leaves.
12. For some *A. thaliana* glycoproteins (e.g., KORRIGAN1) underglycosylation leads to much lower protein abundance [16, 23] presumably as a consequence of reduced stability and faster degradation in the ER.
13. Exceptions: false negatives—the OST complex is not well characterized in plants and the overall understanding of site-specific N-glycosylation is still in its infancy [1, 12].
14. In our hands preparation of microsomal fractions strongly reduced the background for detection of BRI1 on immunoblots.

15. Membrane pellets can be stored at −80 °C.
16. To draw this conclusion form PNGase F insensitivity, the N-glycosylation of the protein has to be determined first (e.g., by isolation of the protein and mass spectrometry analysis of glycopeptides or tunicamycin treatment and monitoring of differences in mobility upon SDS-PAGE or PNGase F digestion in plants lacking core α1,3-fucose).
17. To enable access to all N-glycosylation sites the proteins should be denatured prior to Endo H or PNGase F treatment.
18. When comparing the mobility of Endo H and PNGase F treated glycoproteins on SDS-PAGE keep in mind that Endo H treatment does not lead to a complete deglycosylation (Fig. 4). Consequently, heavily glycosylated proteins could migrate slower than PNGase F treated proteins due to the presence of the innermost GlcNAc linked to asparagines residues.
19. In most plants, including *A. thaliana*, the majority of all complex *N*-glycans is modified with core α1,3-fucose [8, 31].
20. In *A. thaliana* there are two redundant core α1,3-fucosyltransferases (FUT11 and FUT12) [8].

Acknowledgements

This work was supported by a grant from the Austrian Science Fund (FWF): P23906.

References

1. Aebi M (2013) Biochim Biophys Acta 1833:2430
2. Koiwa H, Li F, McCully M, Mendoza I, Koizumi N, Manabe Y, Nakagawa Y, Zhu J, Rus A, Pardo J, Bressan R, Hasegawa P (2003) Plant Cell 15:2273–2284
3. Boisson M, Gomord V, Audran C, Berger N, Dubreucq B, Granier F, Lerouge P, Faye L, Caboche M, Lepiniec L (2001) EMBO J 20:1010–1019
4. Gillmor C, Poindexter P, Lorieau J, Palcic M, Somerville C (2002) J Cell Biol 156: 1003–1013
5. Soussilane P, Soussillane P, D'Alessio C, Paccalet T, Fitchette A, Parodi A, Williamson R, Plasson C, Faye L, Gomord V (2009) Glycoconj J 26:597–607
6. Liebminger E, Hüttner S, Vavra U, Fischl R, Schoberer J, Grass J, Blaukopf C, Seifert G, Altmann F, Mach L, Strasser R (2009) Plant Cell 21:3850–3867
7. von Schaewen A, Sturm A, O'Neill J, Chrispeels M (1993) Plant Physiol 102:1109–1118
8. Strasser R, Altmann F, Mach L, Glössl J, Steinkellner H (2004) FEBS Lett 561: 132–136
9. Strasser R, Schoberer J, Jin C, Glössl J, Mach L, Steinkellner H (2006) Plant J 45:789–803
10. Strasser R, Bondili J, Vavra U, Schoberer J, Svoboda B, Glössl J, Léonard R, Stadlmann J, Altmann F, Steinkellner H, Mach L (2007) Plant Cell 19:2278–2292
11. Fanata WI, Lee KH, Son BH, Yoo JY, Harmoko R, Ko KS, Ramasamy NK, Kim KH, Oh DB, Jung HS, Kim JY, Lee SY, Lee KO (2013) Plant J 73:966–979
12. Zielinska DF, Gnad F, Schropp K, Wiśniewski JR, Mann M (2012) Mol Cell 46:542–548
13. Liebminger E, Grass J, Jez J, Neumann L, Altmann F, Strasser R (2012) Phytochemistry 84:24–30

14. Kolarich D, Jensen PH, Altmann F, Packer NH (2012) Nat Protoc 7:1285–1298
15. Ruiz-May E, Thannhauser TW, Zhang S, Rose JK (2012) Front Plant Sci 3:150
16. Kang J, Frank J, Kang C, Kajiura H, Vikram M, Ueda A, Kim S, Bahk J, Triplett B, Fujiyama K, Lee S, von Schaewen A, Koiwa H (2008) Proc Natl Acad Sci U S A 105:5933–5938
17. Farid A, Pabst M, Schoberer J, Altmann F, Glössl J, Strasser R (2011) Plant J 68: 314–325
18. Abas L, Luschnig C (2010) Anal Biochem 401:217–227
19. Andème Ondzighi C, Christopher D, Cho E, Chang S, Staehelin L (2008) Plant Cell 20:2205–2220
20. Lerouxel O, Mouille G, Andème-Onzighi C, Bruyant M, Séveno M, Loutelier-Bourhis C, Driouich A, Höfte H, Lerouge P (2005) Plant J 42:455–468
21. Henquet M, Lehle L, Schreuder M, Rouwendal G, Molthoff J, Helsper J, van der Krol S, Bosch D (2008) Plant Cell 20:1652–1664
22. Zhang M, Henquet M, Chen Z, Zhang H, Zhang Y, Ren X, van der Krol S, Gonneau M, Bosch D, Gong Z (2009) Plant J 60: 983–999
23. Farid A, Malinovsky FG, Veit C, Schoberer J, Zipfel C, Strasser R (2013) Plant Physiol 162:24–38
24. Ueda H, Nishiyama C, Shimada T, Koumoto Y, Hayashi Y, Kondo M, Takahashi T, Ohtomo I, Nishimura M, Hara-Nishimura I (2006) Plant Cell Physiol 47:164–175
25. Zhang H, Ohyama K, Boudet J, Chen Z, Yang J, Zhang M, Muranaka T, Maurel C, Zhu J, Gong Z (2008) Plant Cell 20:1879–1898
26. Strasser R, Stadlmann J, Svoboda B, Altmann F, Glössl J, Mach L (2005) Biochem J 387: 385–391
27. Frank J, Kaulfürst-Soboll H, Rips S, Koiwa H, von Schaewen A (2008) Plant Physiol 148: 1354–1367
28. Strasser R, Mucha J, Schwihla H, Altmann F, Glössl J, Steinkellner H (1999) Glycobiology 9:779–785
29. Tretter V, Altmann F, März L (1991) Eur J Biochem 199:647–652
30. Leiter H, Mucha J, Staudacher E, Grimm R, Glössl J, Altmann F (1999) J Biol Chem 274:21830–21839
31. Wilson I, Zeleny R, Kolarich D, Staudacher E, Stroop C, Kamerling J, Altmann F (2001) Glycobiology 11:261–274

Chapter 17

Peptide Separation Methodologies for In-depth Proteomics

Sajad Majeed Zargar, Rie Kurata, Randeep Rakwal, and Yoichiro Fukao

Abstract

The integration of proteomics to other omics technologies and generation of proteome maps of a particular cell/tissue requires the identification and quantification of a maximum number of proteins. Traditional 2-D gel-based approach though provides a clear proteome map has its limitations, such as time consuming, requiring high skill, and most importantly, inability to identify low-abundance proteins. The most common drawback of 2-D gel electrophoresis is the masking of low amount proteins by the highly expressed (high abundance) proteins. Therefore, the elucidation of complete regulatory networks of a cell/tissue demands identification of low-abundance proteins. Low-abundance protein identification requires the use of usually gel-free mass spectrometry (MS)-based approaches. Using *Arabidopsis thaliana* as a model system, in this chapter, we describe all the steps followed for the extraction of microsomal proteins to MS analysis of separated peptides with a major focus on three different methods, namely, OFFGEL fractionation, 2D-LC, and long-column method for the identification of low-abundance proteins. Separation of such peptides will lead to in-depth proteomics-based investigations to answer biological questions.

Key words Peptide fractionation, Low-abundance proteins, C-18 resin, Peptide desalting, MS

1 Introduction

Twenty-first century has been marked as the era of functional genomics, and where "omics" is the keyword for high-throughput technologies in deciphering the vast genomic information. Within omics, proteomics can be considered as the most prominent approach, as it focuses on proteins/molecules that catalyze/control essentially all biological processes [1]. Since proteins serve as critical components of major signaling and diverse biological processes, the study of the molecular moieties (proteins) that regulate various biological processes will reveal molecular mechanisms responsible for plant growth, development, and interaction with environment [2]. In other words, proteomics is a key technology for the study of highly complex and dynamic biological systems. At genomic as well as transcriptomic levels, we simply predict the protein/s. Since proteins undergo numerous modifications posttranscription like alternate splicing, mRNA processing, protein proteolysis,

José M. Estevez (ed.), *Plant Cell Expansion: Methods and Protocols*, Methods in Molecular Biology, vol. 1242,
DOI 10.1007/978-1-4939-1902-4_17,

and posttranslational modifications (PTMs), it is not one but many proteins for a gene [2]. As such, proteomics authenticates the presence and functionality of a specific protein. Two-dimensional gel electrophoresis (2-DGE) coupled to mass spectrometry (MS) has become routine in plant proteomics for the identification of differentially expressed proteins. However, despite advances in proteomics tools and with availability of immobilized pH gradient (IPG) and large-format gels, proteomic analysis of membrane proteins is still a major challenge. Nevertheless, due to lack of quantitative reproducibility, poor representation of low-abundance proteins and some other limitations, researchers have considered a shift to gel-free proteomics approaches.

In order to discover and examine the regulatory network of a cell, it is necessary to have detailed information on the maximum number of proteins that are expressed in a cell. Since the last few decades, various methodologies have been utilized for the identification of as many proteins as possible because identification of low-abundance proteins is essential to generate proteome maps of a particular cell/tissue and to integrate the proteomics with other omics technologies and for deciphering the molecular switches regulating various metabolic processes/networks of a cell. Holistically, availability of a complex proteome map would have great impact on life science research. It is our belief that the detection and coverage of certain categories of proteins such as membrane proteins and low-abundance proteins can be enhanced by various strategies.

Focusing on low-abundance proteins, in this chapter we describe three peptide separation methodologies (OFFGEL fractionation, 2D-LC, and long-column method) for their identification. These are schematically depicted in Fig. 1. We believe that these methodologies apply to various plants, model and nonmodel, although it must be emphasized that the protocols presented below have been developed using the dicot weed model plant *Arabidopsis thaliana*.

1.1 Current Status and Update on MS-based Gel Free Approaches for the identification of Low-Abundance Proteins

Proteomics is an analytical and technical approach to study the structural and functional determinant of cells. Proteomics can be defined as the entire complement of proteins, which are fundamental components of the physiological and metabolic pathways vital for growth, development, and interaction of living organism within the environment. The protein complement or proteome varies with time, among tissues and stimuli or stresses that a cell or organism undergoes. Proteomic approaches can be used (1) for proteome profiling to understand how proteins influence biological processes, (2) for comparative expression analysis of two or more protein samples, where proteins may fold into specific three-dimensional structures that determines function, (3) for the localization and identification of PTMs which are the major regulatory mechanisms controlling numerous basic cellular processes, (4) for

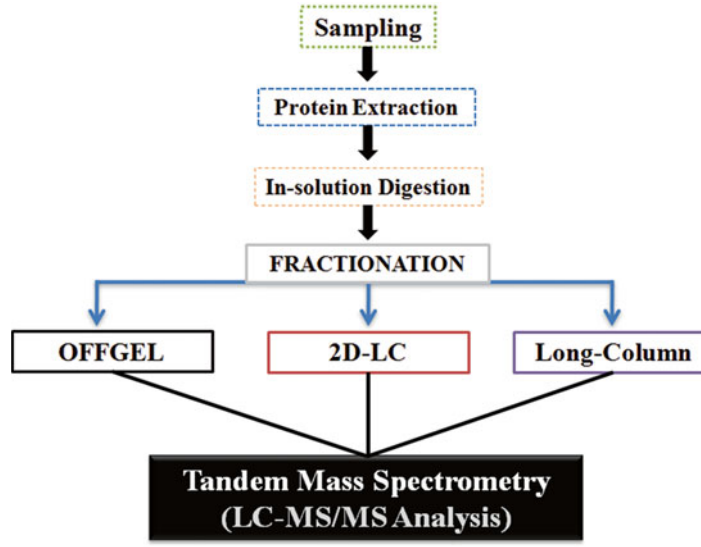

Fig. 1 Methods of peptide separation. Schematic view of methods used for identification of low-abundance proteins (LAP) from microsomal fraction of Arabidopsis shoots and roots. OFFGEL fractionation, 2D-LC, and Long-column method are the tools that help in peptide separation which assist in identification of low-abundance proteins. The identification of these proteins was done by LTQ-Orbitrap XL-HTC-PAL-Paradigm MS4 system

the study of protein–protein interactions, and (5) for identifying new biomarkers for detection and monitoring of specific stress manifestations [3]. Identification of low-abundance proteins is the key to generate as far as possible complete proteome maps of a particular cell/tissue that will help in decoding the molecular switches regulating various metabolic processes/networks of a cell. Over the years, fractionation of proteins into subproteomes based on biochemical, biophysical, and cellular properties had been used. Fractionation may involve: (a) sequential extraction of proteins with a series of reagents having differential protein solubility [4, 5]; (b) phase partitioning using various detergents or organic solvents [6, 7]; (c) LC fractionation [8]; and (d) isolation of highly enriched organelles or subcellular compartments including chloroplasts [7], mitochondria [9, 10], nuclei [11, 12], vacuoles [13, 14], peroxisomes [15], microsomal membranes [6], plasma membranes [16, 17], cell walls [4, 18], and the apoplast [19]. It is worth noting that proteome coverage has steadily increased over the past decade by great efforts, especially at the technical level, in the plant proteomics field (readers are referred to further study in Agrawal et al. [20] and Agrawal and Rakwal [21]). Nevertheless, the identification of low-abundance proteins has received and is still receiving great attentions because of lower identification numbers in traditional studies. Therein, MS-based 2D-gel free proteomics approaches

come into picture, and these techniques are recently being employed in plant proteomics for quantitative proteomics studies.

The OFFGEL fractionation is one of the methods for the separation of peptides via IPG strips that retains peptides or proteins in the liquid phase [22]. To identify maximum number of proteins, reducing the peptide complexity prior to MS proves effective. To give a background of OFFGEL fractionation, we need to look at early studies on bacterial and human models. OFFGEL fractionation of the *Escherichia coli* protein revealed around 90 % of the identified peptides in one or two shotgun analysis, demonstrating the high resolution of this technique [23]. Moreover, OFFGEL fractionation was demonstrated for peptide separation from human secretome and human plasma, and where it was observed that such peptides are compatible with iTRAQ labeling quantitative studies [24]. OFFGEL fractionation has been used to determine differences of the physiological, pathological, and biochemical distinct extraocular muscle allotype in comparison to hind-limb muscle [25]. In a single OFFGEL electrophoresis close to 70 % of the peptides separated were detected in a single fraction. To determine the separation repeatability of four samples, the ion volumes of multiple peptides were compared [25]. Of the 474 proteins identified, 61 proteins were differently expressed between the two muscle allotypes and were involved in metabolism, muscle contraction, stress response, or gene expression. As such it was considered that peptide OFFGEL fractionation is effective and efficient in addition of being a label-free quantitative proteomics technique [25]. What is the status in plants? Abdullah and coworkers [26], analyzed microsomal proteins of *Medicago truncatula* roots using OFFGEL electrophoresis fractionation of peptides and identified more than expected number of unique peptides.

On the other hand, 2D-LC method of peptide separation is based on strong cation exchange and reverse phase (RP) chromatography that offers good repeatability of separation but suffers from poor concentration, particularly of high-abundance peptides to a single fraction [27, 28]. Gilar and coworkers [29] investigated the efficiency of 2D separation for selected types of RP stationary phase, ion-pairing agents, and mobile phase pH. The greatest orthogonality was achieved for the system with C18 columns using pH 10 in the first dimension and pH 2.6 in the second LC dimension. The achievable peak capacity and overall performance indicates its efficiency in proteomic analysis. Furthermore, long monolithic silica capillary columns were found efficient in peptide separation [30]. The examples cited above clearly indicate the precision, efficiency, as well as reproducibility of these peptide separation methods for identification of low-abundance proteins for in-depth proteomics studies.

2 Materials

2.1 Plant Materials

A. thaliana ecotype Columbia (Col-0) plants were used as the experimental material. The seeds were sterilized, placed on the Murashige and Skoog (MS) medium, and incubated in a growth chamber till used for analysis.

2.2 Seed Sterilization Solution

Take a sterile 1.5 mL microfuge tube and mix 0.0002 % Triton X-100 and sodium hypochlorite solution (0.3 %) in sterile distilled H_2O (dH_2O).

2.3 MS Medium

Prepare MS medium containing 2.3 mM MES-KOH, pH 5.7, 1.0 % (w/v) sucrose, and 1.5 % agar [31]. Sterilize it at 121 °C for 20 min. Pour about 70 mL MS medium into plastic plates (10 × 14 × 1.5 cm).

2.4 Isolation of Microsomal Fraction from Arabidopsis Leaves or Roots

1. Preparation of extraction buffer

1 M Hepes-KOH	0.5 mL
0.5 M EDTA	0.1 mL
2 M Sucrose	2 mL
Proteinase inhibitor*	1 tablet
dH_2O water	7.4 mL
Total	10 mL

*Complete Mini, EDTA free (Roche).

2. Preparation of 100 mM ammonium bicarbonate (NH_4HCO_3). Take a calibrated glass reagent bottle and add 240 mg of NH_4HCO_3 in 30 mL of dH_2O.
3. Preparation of 6 M urea. Take a sterile 1.5 mL microfuge tube and add 0.4 g of urea in 1 mL of 100 mM NH_4HCO_3, and vortex the solution.

2.5 In-Solution Digestion

1. Preparation of 100 mM dithiothreitol (DTT). Take a sterile 1.5 mL microfuge tube and add 15 mg of DTT in 1 mL of 100 mM NH_4HCO_3, and vortex the solution (*see* **Note 1**).
2. Preparation of 200 mM iodoacetamide (IAA). Take a sterile 1.5 mL microfuge tube and add 36 mg of IAA in 100 mM NH_4HCO_3. Cover the tube with aluminum foil (*see* **Note 2**).
3. Preparation of trypsin solution. Take a sterile 1.5 mL microfuge tube (low-peptide binding) and add 100 µg of trypsin (Promega; Trypsin Gold, Mass Spectrometry Grade, catalog number V5280) in 100 µL of 50 mM acetic acid (*see* **Note 3**).

2.6 OFFGEL Fractionation

1. Preparation of peptide OFFGEL stock solution (1.25×).
   Take a 50 mL Falcon tube and add 6 mL of 50 % glycerol solution. Add 600 μL ampholyte (*see* **Note 4**). Mix the components and make up the volume to 50 mL with dH_2O (*see* **Note 5**).
2. Preparation of peptide IPG strip rehydration solution.
   For a 24-cm strip with 24 well frames, prepare a solution with 0.96 mL peptide OFFGEL stock solution (1.25×) and 0.24 mL dH_2O to obtain a final volume of 1.2 mL. For a 13-cm strip with 12 well frames, prepare a solution having 0.56 mL peptide OFFGEL stock solution (1.25×) and 0.14 mL dH_2O to have final volume of 0.7 mL.
3. Preparation of OFFGEL peptide sample.
   For a 24-cm strip with 24 well frames, take 2.88 mL of peptide OFFGEL stock solution (1.25×) and add 0.72 mL of sample (**Note 6**). For a 13-cm strip with 12 well frames, take 1.44 mL of peptide OFFGEL stock solution (1.25×) and add 0.36 mL of sample (**Note 6**).
4. IPG strip

   10 % trifluoroacetic acid (TFA).

   0.1 % (v/v) acetic acid/5 % (v/v) acetonitrile.

   0.1 % (v/v) acetic acid/90 % (v/v) acetonitrile.

   C-TIP (T300 10 μL; AMR).

   0.1 % (v/v) formic acid/5 % (v/v) acetonitrile.

   Plastic vial (PSVial 100; AMR).

2.7 2D-LC

100 % formic acid.

Sep-Pak Light C18 cartridge (Waters).

Sep-Pak solution A: 0.1 % formic acid.

Sep-Pak solution B: 75 % acetonitrile and 0.1 % formic acid.

Zapluos columnαP (200 μm internal diameter, 10 cm; AMR).

2D-LC solution A: 20 mM ammonium formate, pH 9.2.

2D-LC solution B: 20 mM ammonium formate and 45 % (v/v) acetonitrile in H_2O, pH 9.2.

0.1 % (v/v) formic acid/5 % (v/v) acetonitrile.

Plastic vial (PSVial 100; AMR).

2.8 Long-Column Method

0.1 % (v/v) acetic acid.

Sep-Pak Light C18 cartridge (Waters).

Sep-Pak solution A: 0.1 % formic acid.

Sep-Pak solution B: 75 % acetonitrile and 0.1 % formic acid.

0.1 % (v/v) formic acid/5 % (v/v) acetonitrile.

Plastic Vial (PSVial 100: AMR).

3 Methods

3.1 Plant Growth Conditions

1. Sterilize seeds of *A. thaliana* in 1 mL sterilizing solution for 15 min followed by washing the seeds three times with 1 mL sterile dH_2O.
2. Place the sterile seeds on MS medium having 0.1 % agar (*see* **Note 7**).
3. Incubate seeds for 3 days at 4 °C under the dark.
4. Grow the Arabidopsis seedlings vertically for 10 days at 22 °C under 16 h light/8 h dark conditions in a growth chamber.

3.2 Isolation of Microsomal Fraction from Arabidopsis thaliana Leaves and Roots

1. Weigh 200 mg (fresh weight) of leaf or root sample.
2. Place the leaf or root sample in a mortar placed on ice.
3. Add 1 mL of extraction buffer.
4. Crush the sample with a pestle on ice (*see* **Note 8**).
5. Transfer homogenate to a 2 mL microfuge tube and centrifuge at 1,000 × *g* for 20 min at 4 °C.
6. Take the supernatant and transfer into a new sterile microfuge tube.
7. Centrifuge at 8,000 × *g* for 20 min at 4 °C.
8. Transfer the supernatant into a 1.5 mL microfuge tube and centrifuge at 100,000 × *g* for 1 h at 4 °C (*see* **Note 9**).
9. Discard the supernatant, and add 200 μL of the extraction buffer. Solubilize the pellet using a tip followed by vortexing and ultrasonication for 1 min each. Add 1 mL of extraction buffer, and centrifuge again at 100,000 × *g* for 1 h at 4 °C (*see* **Note 10**). All steps are carried out on ice.
10. Repeat the **step 7** (*see* **Note 11**).
11. Add 100 μL of 6 M urea solution to each tube and dissolve the pellet with a tip by vortexing followed by ultrasonication for 1 min each.
12. Transfer the solubilized sample solution to a new microfuge tube (*see* **Note 12**).
13. Keep the samples on ice and quantify the protein using NanoDrop 2000 spectrophotometer (Thermo Fisher Scientific).
14. Store the samples at 4 °C (for immediate use) or –80 °C (for long-term storage), and use for the next step of in-solution digestion.

3.3 In-Solution Digestion

1. Add >5 μg protein in 90 μL of 6 M urea solution and mix by vortexing (*see* **Note 13**).
2. Add 5 μL of 100 mM DTT for reduction and mix by vortexing (*see* **Note 14**).

3. Incubate the solution at 37 °C in dry bath with light shaking for 1 h.
4. Add 20 μL of 200 mM IAA for alkylation. Mix the contents.
5. Incubate for 1 h at 37 °C in dark with slight shaking.
6. Add again 20 μL of DTT, mix the contents, and incubate for 1 h at 37 °C.
7. Add 775 μL of 20 mM NH_4HCO_3, and mix by inverting.
8. Add trypsin (in the ratio of trypsin:protein (1:20–30)).
9. Incubate at 37 °C overnight without shaking.
10. The digested protein is ready to use for further experiments. However, if required, the digested protein sample can be stored at −80 °C till future use.

3.4 OFFGEL Fractionation

1. Mix >20 μg of trypsin-digested peptides and OFFGEL buffer. The peptide purification can be avoided some times, however if there are many impurities in the peptide samples, peptides should be purified (*see* **Note 15**).
2. Load peptides onto the immobilized pH gradient strip using loading cup in liquid phase (*see* **Note 16**).
3. Use 3100 OFFGEL fractionator (Agilent Technologies) for separation of peptides into 12 or 24 fractions (*see* **Note 17**).
4. Add 4 μL of 10 % TFA into each fractionated peptide samples, to obtain a pH of 2.5–3.5.
5. Condition C-TIP (AMR) with 10 μL of 0.1 % (v/v) acetic acid/90 % (v/v) acetonitrile once and then 10 μL of 0.1 % (v/v) acetic acid/5 % (v/v) acetonitrile twice.
6. Load each peptide sample prepared at **step 4** into a C-TIP one by one.
7. Wash the peptides with 10 μL of 0.1 % (v/v) acetic acid/5 % (v/v) acetonitrile. This step is required for the desalting of peptides once (*see* **Note 18**).
8. Elute peptides from column into vials with 10 μL of 0.1 % (v/v) acetic acid/90 % (v/v) acetonitrile.
9. Dry the eluted samples in air (*see* **Note 19**).
10. Dissolve the dried samples in 20 μL of 0.1 % (v/v) acetic acid/2 % (v/v) acetonitrile in water. (Figure 2 gives an overview of the setup involved in identification of low-abundance proteins using OFFGEL fractionation method of peptide separation.)

3.5 2D-LC

1. Mix >10 μg of digested peptides and 5 μL of 100 % formic acid to get a pH of 2.5–3.5 (*see* **Note 20**).
2. Condition Sep-Pak (Waters) using 2 mL of Sep-Pak solution B followed by 2 mL of Sep-Pak solution A.

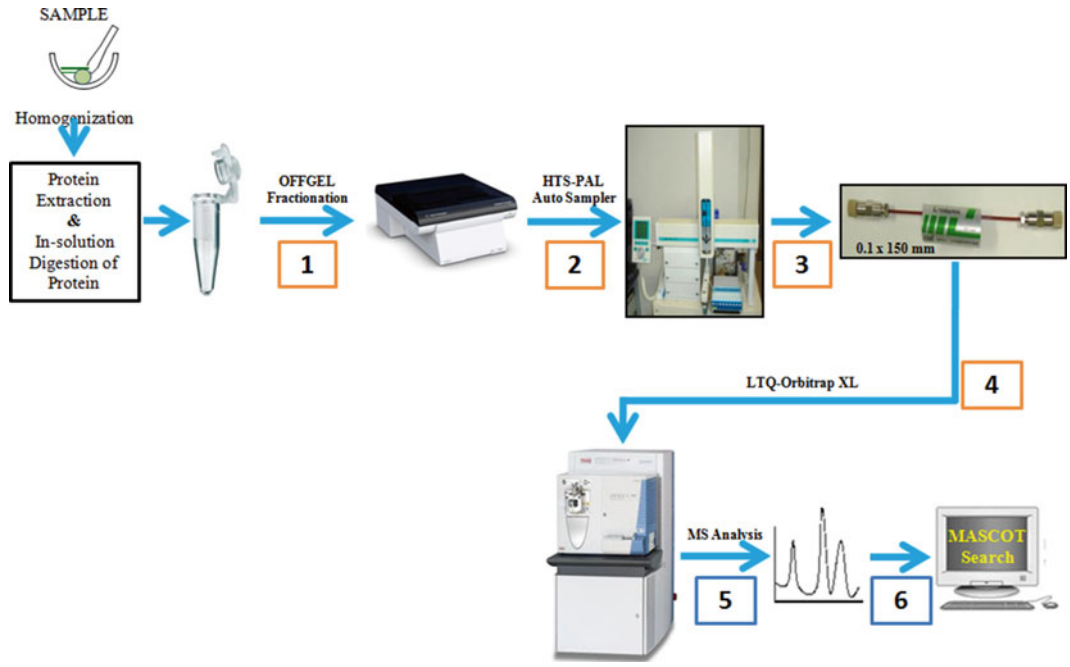

Fig. 2 Overview of peptide identification using OFFGEL fractionation method of peptide separation. The extracted proteins after in-solution digestion are subjected to OFFGEL fractionation. The fractionated peptides are purified by C-TIP using HTS-PAL autosampler. The purified peptides are separated by L-column OSD column and directly introduced to MS (LTQ-Orbitrap XL). The results are finally interpreted using MASCOT analysis

3. Load peptides prepared at **step 1** on Sep-Pak column (*see* **Note 21**).
4. Wash the column by 1.5 mL of Sep-Pak solution A.
5. Elute the peptides from column into 1.5 mL microfuge tube with 600 µL of Sep-Pak solution B.
6. Dry up the eluted solution using vacuum concentrator then dissolve in 10 µL of 2D-LC solution A (*see* **Note 22**).
7. Condition the column with 50 % 2D-LC solution A/50 % 2D-LC solution B for 5–10 min, and then with 98 % 2D-LC solution A/2 % 2D-LC solution B for 5–10 min.
8. Load less than 10 µg and less than 10 µL of purified peptides to a column (*see* **Note 23**). HTC-PAL autosampler was used.
9. Peptides are eluted by a linear gradient of 2 to 100 % 2D-LC solution B for 20 min, followed by 100 % 2D-LC solution B for 4 min, a linear gradient of 100 to 2 % 2D-LC solution B for 1 min, and 2 % 2D-LC solution B for 6 min. The separated peptides are collected into seven vials over an equal time period.
10. Air dry the samples for 1–2 overnight.
11. Repeat the procedure to obtain a yield of about 10 µg of dried fractionated peptides. This is an optional step.

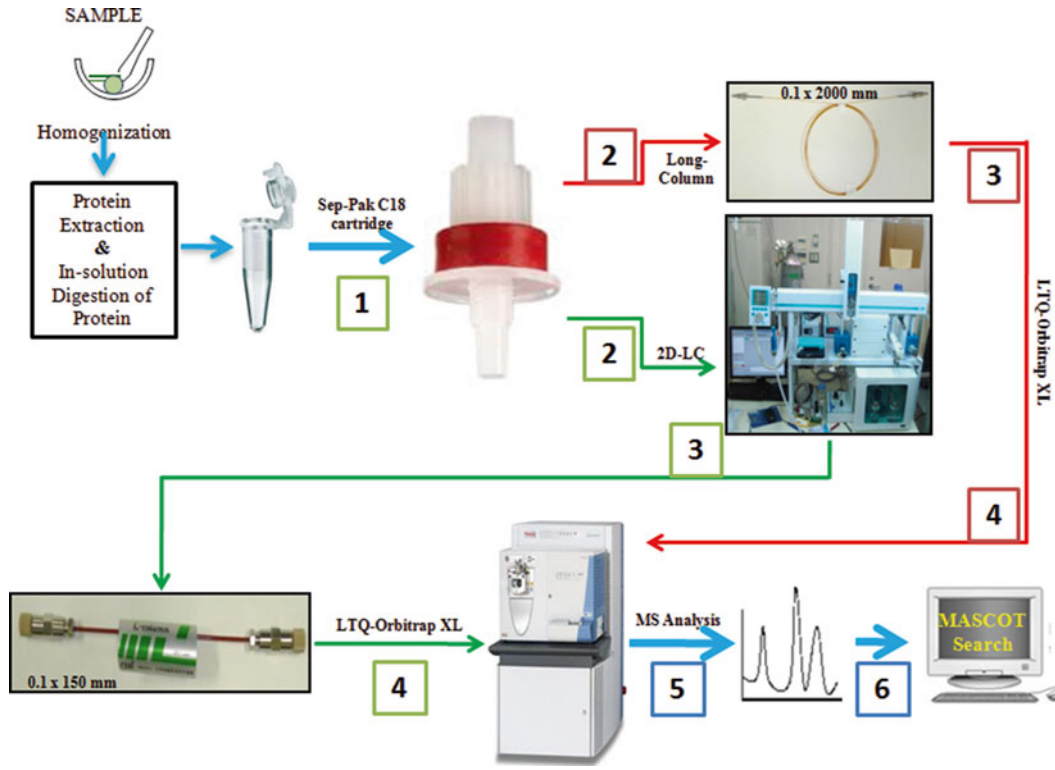

Fig. 3 Overview of peptide identification using 2D-LC and Long-column methods of peptide separation. The extracted proteins after in-solution digestion are purified using Sep-Pak C18 column, and then subjected to 2D-LC or directly to the long column. In case of 2D-LC method, the purified peptides are separated under alkaline conditions on a revere-phase column (Zapluos column αP) by the gradient as the first dimension, prior to LC–MS analysis. Then, each peptide fraction is separated under acidic conditions in a 150 mm reverse-phase column (L-column OSD) by the gradient as the second dimension and directly analyzed by MS (LTQ-Orbitrap XL). However, in case of long-column method, the purified peptides are separated under acidic conditions in a 2,000 mm monolithic silica capillary column (MonoCapC 18 High Resolution 2000 column) and then directly analyzed by MS (LTQ-Orbitrap XL)

12. Dissolve the dried peptides in 20 μL of 0.1 % (v/v) acetic acid/2 % (v/v) acetonitrile in water (*see* **Note 24).** (Figure 3 gives an overview of the setup involved in identification of low-abundance proteins using 2D-LC method of peptide separation.)

3.6 Long-Column Method

1. Desalt >10 μg of peptides on Sep-Pak (Waters), similarly as done for the 2D-LC method.
2. Concentrate these peptides to 5 μL (*see* **Note 25**).
3. Add 0.1 % (v/v) acetic acid/2 % (v/v) acetonitrile in dH_2O to have final volume of 20 μL. (Figure 3 gives an overview of the setup involved in identification of low-abundance proteins using long-column method of peptide separation.)

3.7 LC-MS Analysis

The purified fractionated peptides obtained from all three above mentioned methods were analyzed by an LTQ-Orbitrap XL combined with HTC-PAL-Paradigm MS4 system.

1. For OFFGEL fractionator and 2D-LC method, peptides were loaded onto the L-column ODS column (0.1 mm internal diameter, 150 mm; CERI), and for long-column method, peptides were loaded on the MonoCapC 18 High Resolution 2000 column (0.1 mm internal diameter, 2,000 mm; GL Sciences).
2. A linear gradient of 5 to 45 % for 26 min should be applied for the samples separated by OFFGEL fractionation and 2D-LC methods, and a gradient of 5 to 40 % for 320 min should be applied for the samples separated by LC method.
3. Introduce the eluted peptides from column directly into an LTQ-Orbitrap XL Mass Spectrometer (Thermo Fisher Scientific), with a flow rate of 500 μL/min and a spray voltage of 2.0 kV. Keep the range of MS scan m/z 450–1,500 and subject the top three peaks to MS/MS analysis (*see* **Note 26**).
4. Finally compare the spectra with available information resource (Arabidopsis information resources, TAIR 10; http://www.arabidopsis.org) using MASCOT software (version 2.4, Matrix Science).

3.8 Zinc (Zn)/Iron (Fe)-Regulation in Arabidopsis thaliana: A Case Study

Our laboratory at NAIST has been working extensively on the identification of peptides/proteins induced by the application of excess or deficient micronutrients such as Zn and Fe in Arabidopsis. The aim of our studies has been to use proteomics for understanding the regulatory system altering the transport of these minerals. Our early investigations have resulted in the identification of numerous zinc responsive proteins in the roots of Arabidopsis plants, which in turn has helped in the exploration of the mechanisms leading to growth defects in Arabidopsis roots due to excess zinc transport [32, 33]. The main target was to identify the low-abundance proteins. In a recently published study, we have been successful in increasing the efficiency of identification of low-abundance proteins many folds by using protoplasts collected from the epidermal cell layer of Arabidopsis roots after fluorescence-activated cell sorting [34]. Three different methods of peptide fractionation, i.e., OFFGEL fractionation, 2D-LC, and the long-column method were followed to decrease the peptide complexity prior to MS. Using these three approaches for peptide separation, we have improved the identification of peptides to a large extent. The number of proteins identified using these three different methods (OFFGEL electrophoresis, 2D-LC, and the long monolithic silica-C18 capillary column method) of peptide separation corresponds to 1,132, 836, and 795, respectively. In total, 1,493 proteins were identified with less than 1.0 % false discovery rate

and no redundancy. Two-thirds of the identified proteins have been reported for the first time from epidermal cell layer of Arabidopsis roots. The readers are referred to the work of Fukao and colleagues for further details [34].

3.9 Concluding Remarks

Different techniques are being employed for enhancing the resolution of peptides and this is due to (1) improved protein extraction methods, (2) development of efficient peptide purification methods, and (3) decreasing the protein complexity prior to MS analysis. Peptide separation is critical to obtain an overall picture of regulatory elements involved in diverse biological pathways. Identification of low-abundance proteins is believed to be important for developing proteome maps. In our experiments we have used three different methods of peptide separation to resolve the low-abundance peptides and to decrease peptide complexity before MS analysis. Proteomics-based studies using the three methods of peptide separation (OFFGEL fractionation, 2-LC, and long-column method) described in this chapter have advantages over gel-based proteomics investigations. The results clearly indicate that these advantages are due to the efficiency, precision, and reproducibility of these three peptide separation methods for identification of low-abundance proteins. Identification of these proteins will help in proper understanding of molecular mechanisms involved in different metabolic pathways. We believe that our research in this direction represents a significant technical advance, which with further fine-tuning should facilitate elucidation of the complete proteome map in Arabidopsis roots. Moreover, their applicability to various model and nonmodel systems and integration with other "omics" approaches will help promote these techniques in the plant proteomics community. One major challenge however remains and that is the need for advanced automated peptide purification systems with high precision and greater reproducibility.

4 Notes

1. DTT is stored at −20 °C, and in aliquots. Use/thaw a single tube each time to avoid instability due to repeated thawing and freezing.
2. Tubes are covered to prevent IAA from photodecomposition. Always prepare fresh IAA solution for each experiment.
3. The trypsin solution should be placed on ice and can be stored at −20 °C.
4. As an example; IPG Buffer, pH 3-10NL (GE Healthcare). Choose matching ampholyte, depending on the IPG strip.
5. Store OFFGEL solution at −20 °C and about 4 mL for 24 cm strip and 2 mL for 13 cm strip is used. Avoid multiple freeze/thaw

cycles, aliquot the OFFGEL stock solution into smaller microfuge tubes.

6. The final salt concentration in diluted sample should not exceed 10 mM.
7. About 100 seeds were placed on plates.
8. Crushing of samples should be carried out using sea sand (200–600 μm; 30–50 mesh).
9. Before ultracentrifugation, ensure the weight of tubes is equal to avoid problems in the ultracentrifuge due to imbalance.
10. The tip is put in the tube for disturbing pellet on vortexing so that the pellet will dissolve in the extraction buffer.
11. The repeated washing helps in removal of soluble proteins from the microsomal fraction to a large extent.
12. This is mainly to avoid transfer of pellet, if any.
13. The concentration of protein depends on purpose of experiment.
14. Keep DTT on ice.
15. By repeated purifications, peptide losses occur. Therefore, it is always advisable to desalt peptides before OFFGEL fractionation. Moreover, in case of Arabidopsis the protein samples were purified after OFFGEL fractionation just to make sure that different reagents like glycerol, etc., are removed from peptides, which are known to interfere in LC–MS analysis. Therefore if purification is repeated, it may lead to low peptide concentration.
16. pH gradient range from 3–10. However, it may vary, depending on the analyte.
17. 24 cm IPG gel, pH 3–10 (GE Healthcare) at 4,500 V for 50,000 Vh at 50 μA (as per instructions of the manufacturer).
18. HTC-PAL autosampler (CTC analytics) was used for desalting of protein and conditioning of column.
19. Samples are dried overnight, sometimes two nights.
20. In case of Sep-Pak, larger amounts of protein sample are preferred because low amount peptides can be lost easily.
21. Sep-Pack purification will help in desalting of peptides to avoid clogging the LC. Hence, it is always better to desalt peptide samples before 2D-LC. And once desalting is done at this stage, it is not required prior to LC–MS. We used this approach in our experiments, but are not sure about the consequences of not following this step. We believe that, if desalting is avoided, it may spoil/damage the column used for LC–MS.
22. The solubilization of sample in 2D-LC solution depends on the size of sample loop of column at **step 8**.
23. 10 μg is the maximum column capacity and 10 μL is the maximum sample loop capacity.

24. Vortexing at this stage is avoided to minimize the loss of peptides as they may splatter and get dried in the vial upon vortexing.
25. Vacuum concentrator/lyophilizer are used for the sample concentration. It takes 3–4 h for a sample to get concentrated.
26. The MS run time is 50 min, and number of scan events are 4, which are MS analysis for 1 scan event and 3 scan events MS/MS analysis.

Acknowledgments

This work was supported by a Grant-in-Aid for Scientific Research on Innovative Areas (No. 23119512 to Y.F.) from the Ministry of Education, Culture, Sports, Science and Technology of Japan; a Grant-in-Aid for Scientific Research from Nara Institute of Science and Technology supported by The Ministry of Education, Culture, Sports, Science and Technology, Japan. This research was supported by Japan Advanced Plant Science Network. S.M.Z. acknowledges the DBT, New Delhi, India for award of CREST, Overseas postdoc fellowship. R.R. acknowledges the great support of Professors Yoshihiro Shiraiwa (Provost, Faculty of Life and Environmental Sciences, University of Tsukuba) and Koji Nomura (Organization for Educational Initiatives, University of Tsukuba) in promoting interdisciplinary research and unselfish encouragement.

References

1. Ahrens CH, Brunner E, Qeli E et al (2010) Generating and navigating proteome maps using mass spectrometry. Mol Cell Biol 11: 789–801
2. Chen S, Harmon AC (2006) Advances in plant proteomics. Proteomics 6:5504–5516
3. Chandramouli K, Qian PY (2009) Proteomics: challenges, techniques and possibilities to overcome biological sample complexity. Hum Genomics Proteomics 8:23920
4. Robertson D, Mitchell GP, Gilroy JS et al (1997) Differential extraction and protein sequencing reveals major differences in patterns of primary cell wall proteins from plants. J Biol Chem 272:15841–15848
5. Molloy MP, Herbert BR, Walsh BJ et al (1998) Extraction of membrane proteins by differential solubilization for separation using two-dimensional gel electrophoresis. Electrophoresis 19:837–844
6. Borner GHH, Lilley KS, Stevens TJ et al (2003) Identification of glycosylphosphatidylinositol-anchored proteins in Arabidopsis: a proteomic and genomic analysis. Plant Physiol 132: 568–577
7. Peltier JB, Ytterberg AJ, Sun Q et al (2004) New functions of the thylakoid membrane proteome of Arabidopsis thaliana revealed by a simple, fast, and versatile fractionation strategy. J Biol Chem 279:49367–49383
8. Brown JWS, Flavell RB (1981) Fractionation of wheat gliadin and glutenin subunits by two-dimensional electrophoresis and the role of group 6 and group 2 chromosomes in gliadin synthesis. Theor Appl Genet 59:349–359
9. Werhahn W, Braun HP (2002) Biochemical dissection of the mitochondrial proteome from Arabidopsis thaliana by three-dimensional gel electrophoresis. Electrophoresis 23:640–646
10. Heazlewood JL, Tonti-Filippini JS, Gout AM et al (2004) Experimental analysis of the Arabidopsis mitochondrial proteome highlights signaling and regulatory components, provides assessment of targeting prediction programs, and indicates plant-specific mitochondrial proteins. Plant Cell 16:241–256

11. Bae MS, Cho EJ, Choi EY et al (2003) Analysis of the Arabidopsis nuclear proteome and its response to cold stress. Plant J 36:652–663
12. Pendle AF, Clark GP, Boon R et al (2005) Proteomic analysis of the Arabidopsis nucleolus suggests novel nucleolar functions. Mol Biol Cell 16:260–269
13. Carter C, Pan S, Zouhar J et al (2004) The vegetative vacuole proteome of Arabidopsis thaliana reveals predicted and unexpected proteins. Plant Cell 16:3285–3303
14. Szponarski W, Sommerer N, Boyer JC et al (2004) Large-scale characterization of integral proteins from Arabidopsis vacuolar membrane by two-dimensional liquid chromatography. Proteomics 4:397–406
15. Fukao Y, Hayashi M, Nishimura M (2002) Proteomic analysis of leaf peroxisomal proteins in greening cotyledons of *Arabidopsis thaliana*. Plant Cell Physiol 43:689–696
16. Santoni V, Kieffer S, Desclaux D et al (2000) Membrane proteomics: use of additive main effects with multiplicative interaction model to classify plasma membrane proteins according to their solubility and electrophoretic properties. Electrophoresis 21:3329–3344
17. Alexandersson E, Saalbach G, Larsson C et al (2004) *Arabidopsis* plasma membrane proteomics identifies components of transport, signal transduction and membrane trafficking. Plant Cell Physiol 45:1543–1556
18. Chivasa S, Ndimba BK, Simon WJ et al (2002) Proteomic analysis of the *Arabidopsis thaliana* cell wall. Electrophoresis 23:1754–1765
19. Haslam RP, Downie AL, Raveton M et al (2003) The assessment of enriched apoplastic extracts using proteomic approaches. Ann Appl Biol 143:81–91
20. Agrawal GK, Bourguignon J, Rolland N et al (2011) Plant organelle proteomics: collaborating for optimal cell function. Mass Spectrom Rev 30:772–853
21. Agrawal GK, Rakwal R (2008) Plant proteomics: technologies, strategies, and applications. Wiley, Hoboken
22. Bjellqvist B, Hughes GJ, Pasquali C et al (1993) The focusing positions of polypeptides in immobilized pH gradients can be predicted from their amino acid sequences. Electrophoresis 14:1023–1031
23. Horth P, Miller CA, Prekel T et al (2006) Efficient fractionation and improved protein identification by peptide OFFGEL electrophoresis. Mol Cell Proteomics 5:1968–1974
24. Chenau J, Michelland S, Sidibe J et al (2008) Peptides OFFGEL electrophoresis: a suitable pre-analytical step for complex eukaryotic samples fractionation compatible with quantitative iTRAQ labeling. Proc Natl Acad Sci U S A 6:1–8
25. Fraterman S, Zeiger U, Khurana TS et al (2007) Combination of peptide OFFGEL fractionation and label-free quantitation facilitated proteomics profiling of extraocular muscle. Proteomics 7:3404–3416
26. Abdallah C, Sergeant K, Guillier C et al (2012) Optimization of iTRAQ labelling coupled to OFFGEL fractionation as a proteomic workflow to the analysis of microsomal proteins of *Medicago truncatula* roots. Proc Natl Acad Sci U S A 10:37
27. Cargile BJ, Sevinsky JR, Essader AS et al (2005) Immobilized pH gradient isoelectric focusing as a first-dimension separation in shotgun proteomics. J Biomol Tech 16:181–189
28. Wolters DA, Washburn MP, Yates JR (2001) An automated multidimensional protein identification technology for shotgun proteomics. Anal Chem 73:5683–5690
29. Gilar M, Olivova P, Daly AD et al (1995) Two-dimensional separation of peptides using RP-RP-HPLC system with different pH in first and second separation dimensions. J Sep Sci 28:1694–1703
30. Miyamoto K, Hara T, Kobayashi H et al (2008) High-efficient liquid chromatographic separation uitilising long monolithic silica capillary columns. Anal Chem 80:8741–8750
31. Murashige T, Skoog F (1962) A revised medium for rapid growth and bioassays with tobacco cultures. Plant Physiol 15:473–497
32. Fukao Y, Ferjani A, Fujiwara M et al (2009) Identification of zinc-responsive proteins in the roots of *Arabidopsis thaliana* using a highly improved method of two-dimensional electrophoresis. Plant Cell Physiol 50:2234–2239
33. Fukao Y, Ferjani A, Tomioka R et al (2011) iTRAQ analysis reveals mechanisms of growth defects due to excess zinc in Arabidopsis. Plant Physiol 155:1893–1907
34. Fukao Y, Yoshida M, Kurata R et al (2013) Peptide separation methodologies for in-depth proteomics in Arabidopsis. Plant Cell Physiol 54(5):808–815

Chapter 18

Structural and Mechanical Characterization of Growing *Arabidopsis* Plant Cell Walls

Friederike Saxe, Ingo Burgert, and Michaela Eder

Abstract

This book chapter describes how structural and mechanical properties of living *Arabidopsis* hypocotyls can be measured by using small-angle X-ray scattering and micromechanical tensile tests. This approach is particularly useful to detect structural differences between selected mutants and to show how these differences are reflected in the tensile properties.

Key words Plant cell walls, Structural and mechanical properties, Hypocotyls, *Arabidopsis* - micromechanical tensile test, X-ray scattering

1 Introduction

Primary cell walls ensure the stability of the plant during growth while at the same time the cell wall is expanded and new material is added. These opposing demands lead to a complex structure [1–5] and several cell wall models have emerged [4, 6, 7] to address the relation between structure and function. While for secondary cell walls, the influence of structure on the mechanical properties is well established [8–12] this is still a matter of discussion for primary cell walls. Mostly larger systems like *Nitella* [13–15], onion epidermal cell walls [16–18], sunflower [19], celery collenchyma [20], or cucumber [21] have been studied. Apart from the characterization of these large primary cell wall systems, studies have also been performed on a smaller primary cell wall system—etiolated *Arabidopsis* hypocotyls [22–25]. The small size and the fragility of the system make such studies challenging, however, the knowledge about genetic and biochemical processes taking place during growth and the availability of a large number of cell wall mutants give striking advantages over other systems.

Structural characterization by small-angle X-ray scattering (SAXS) requires only minor sample preparation which allows for the analysis of living hypocotyls. The obtained cellulose orientation is

José M. Estevez (ed.), *Plant Cell Expansion: Methods and Protocols*, Methods in Molecular Biology, vol. 1242,
DOI 10.1007/978-1-4939-1902-4_18,

an integrated distribution over several cell layers and cells depending on the chosen beam size. Scanning of a larger area is generally possible. A drawback of the method is the indirect measurement. As a consequence, the results have to be calculated from the scattering pattern rather than being directly visible to the eye as in microscopy. Additionally, large facilities are necessary to produce the X-ray beam which reduces the availability of the method.

The mechanical characterization by microtensile testing can establish the link between cell wall composition and ultrastructure and the resulting ultimate tensile stress and Young's modulus. Like in SAXS, hypocotyls can be analyzed whilst still alive. The resulting mechanical properties are tissue properties.

The combination of both methods allows exploring the interplay between structure and properties of the primary cell wall system since besides bulk density the cellulose fibril orientation is the main factor to influence the mechanical properties. In this way, not only wild-type plants can be characterized but by the characterization of cell wall mutants the relation between genetic modifications, structural cell wall alterations, and the resulting properties can be established. The structural and mechanical characterization can provide insight into the respective roles of certain cell wall components.

Thus the combination of structural and mechanical characterization in living primary cell wall systems complements each other and broadens the understanding of systems that are well characterized by molecular biology methods.

2 Materials and Sample Preparation

2.1 Growth of Arabidopsis Hypocotyls

1. Prepare Petri dishes with, e.g., 8.8 g/l Murashige and Skoog basal medium in 0.8 % agar under sterile conditions, let them cool down afterwards, close them and store them under sterile conditions.
2. Sterilize *Arabidopsis* seeds (e.g., Col-0 and mutant).
3. For the sterilization prepare a mixture of TritonX and NaClO (20 %). Add 2–3 droplets of TritonX and shake.
4. Put a small amount of seeds into a 2 ml Eppendorf tube and add 1 ml ethanol. Shake well.
5. Remove the ethanol after 90 s and rinse twice with distilled water. Add 1 ml of the TritonX/NaClO solution and shake well. Shake again after 5 min. Remove the solution after 7 min as well as possible. Remove the remaining rest of the solution after 9.5 min and add 1 ml of water afterwards (the diluted solution with the seeds should be ready after 10 min in total). Rinse 5 times with H_2O. After 4 times no foam formation should be detectable.
6. Distribute the seeds with a pipette on the prepared Petri dishes. Close the petri dish and wrap them twice in aluminum

foil to keep the plate in the complete darkness (*see* **Note 1**).

7. Place the plates horizontally in a climate chamber (e.g., 22 °C) (*see* **Note 2**) for 4–7 days.
8. Rinse five times with H_2O. After four times no foam formation should be detectable.

2.2 Sample Preparation for Microtensile Tests Combined with Strain Measurement by Video Extensometry

Since one of the big challenges of testing a small hypocotyl in tension is sample clamping, particular care has to be taken in proper sample fixation in the tensile stage. The clamping can be realized by using foliar frames (e.g., Polyester, ~150 μm thick) as support structures for the tiny samples. The advantage is that the frames can easily be adapted to fit for a particular tensile testing device. The requirement of using glues to mount the hypocotyls onto the frame can be seen as a disadvantage since glues often require long times to cure. The problem can be solved by using a combination of cyanacrylate (e.g., Loctite 454) and dental cement (e.g., Ketac™ Cem).

1. Prepare a foliar frame that fits your tensile tester (e.g., Fig. 4a).
2. Carefully harvest a hypocotyl from the plate by using fine tweezers (*see* **Note 3**).
3. Put a small droplet of cyanacrylate glue by using a thin wire on a foliar frame (under a light microscope).
4. Place the hypocotyl on the foliar frame and make sure that its long axis is aligned in tensile direction to avoid high stress concentrations at the clamping site. Glue the other end of the hypocotyl free test span with cyanacrylate glue to the foliar frame (Fig. 4a).
5. Place a droplet of dental cement on top of the soft cyanacrylate glue (*see* **Note 4** for an explanation of glue combination).
6. Place the sample in a box with wet air (a folded piece of wet tissue can humidify the air) to avoid drying. Wait for 10 min until the dental cement is hardened. Then apply pressure on the dental cement with tweezers to harden the cyanacrylate glue.
7. Measure the free test span of the hypocotyl and the hypocotyl diameter with a microscope.

2.3 Structural Characterization by Small-Angle X-Ray Diffraction

In principle, small-angle X-ray scattering experiments can be performed on lab sources as well as at a synchrotron. However, the measurements on lab sources are performed in vacuum, which would immediately dry out the samples. Even if this problem could be solved by an appropriate measurement chamber with X-ray transmitting windows surrounding the samples, the cellulose content of hypocotyls is so low that the measurement time on the weaker lab sources would be very long (several hours to days). As

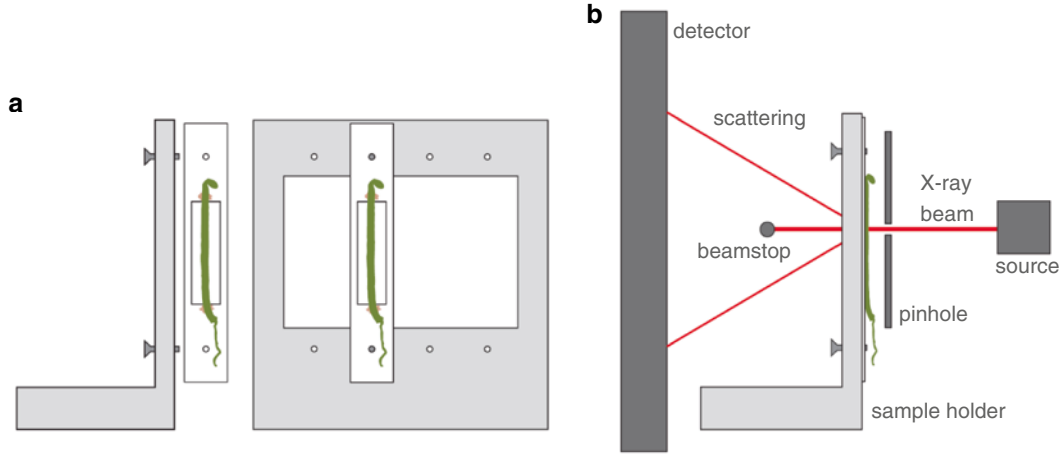

Fig. 1 (**a**) Sample holder for X-ray scattering experiments. The hypocotyls should be glued to foliar frames which can quickly and accurately be mounted on the sample holder by double sided tape. Small screws that stick out about 0.5 mm assure a reproducible positioning. *Left*: Side view, *right*: front view with mounted sample. (**b**) Setup at the synchrotron. The beam passes adjusting pinholes before hitting the sample. The scattered waves are collected with a two-dimensional detector while the primary beam is stopped by the beamstop

a living system is to be characterized, alterations due to growth and changes induced after exposition to light can appear during this time. At a synchrotron the beam brilliance is much higher which allows for shorter measurement times and measurements in air as with the stronger scattering signal air scattering can be neglected.

1. Prepare a sample holder (Fig. 1a and **Note 5**) and adjust the position of the sample holder at the measurement site as close to the pinhole as possible to avoid shadows in the scattering image from the sample holder (Fig. 1b). Mount a thread or wire with a width similar to the hypocotyls on the sample holder in the same way as the hypocotyls are mounted (see below) to find the coordinates of the sample position once the sample holder is fixed (*see* **Note 6**).
2. Prepare a foliar frame or a similar sample holder by applying small amounts of cyanacrylate glue above and below the measurement opening (Fig. 1).
3. Right before the measurement, take the dark grown seedlings off the plate to mount and fix it on the foliar frame or directly on the sample holder (*see* **Note 7**). Make sure that the glue only touches the plant in positions that cannot be exposed to the beam and that it cannot move along the plant to the region that will be analyzed (*see* **Note 8**).
4. Mount the foliar frames on the sample holder in the positions that have previously been determined. Immediately start to moisturize the sample via a humidifier (*see* tensile tests and **Note 9**).

3 Methods

The hypocotyls should always be kept hydrated to avoid drying artifacts.

3.1 Small-Angle X-Ray Diffraction

The cellulose orientation from primary cell walls in hypocotyls can be obtained because the SAXS signal originates from objects between 0.5 and 100 nm in size [26] that do not have to be crystalline (other than in wide-angle X-ray scattering). For the interpretation of the scattering pattern, we have to assume that it originates from a two-phase system, which means that there has to be a sufficient electron density contrast between the two phases for scattering to occur. In hydrated plant cell walls the highest electron density contrast is found between the cellulose and the surrounding water saturated matrix [26].

3.1.1 Measurement

1. The setup at the synchrotron should be arranged as described in Fig. 1.
2. Choose a beam size close to the diameter of the hypocotyl (*see* **Note 10**).
3. Finding the sample can be difficult due to low scattering intensities. The approximate position should be known from a measurement with a well-scattering thread or wire mounted on the same sample holder (*see* **Note 6**). Once the hypocotyl is mounted it can be found by scanning across the sample with very short measurement times (1–10 s each) in steps of ~100 μm (well below the diameter of the hypocotyl). When the hypocotyl is only partly illuminated by the beam, edge effects can appear. Thus, to ensure that the plant is placed in the middle of the beam a second scan across the sample in steps of 50 μm can determine the exact position of the sample once the hypocotyl is found.
4. Before starting the actual measurement the required measurement time has to be defined. It depends on the beam intensity as well as on the cellulose content in the sample and can be determined by several short consecutive measurements in the same sample position (10–60 s).
5. Once the minimum measurement time to obtain a good scattering signal is defined, beam damage has to be assessed. Again, short measurements are made in the same sample position until the scattering signal is altered due to burning or drying of the sample (*see* **Note 11**).
6. If you have placed several samples on the sample holder and determined the positions, which should be analyzed, the measurement can often be automated by a small macro. This gives some time to prepare the next samples.

7. Each series of measurements should be followed by the measurement of an empty beam (no sample) with the same measurement time, which allows subtracting air scattering. For every set of measurements (all samples on one sample holder) a standard (e.g., silver behenate), that is necessary to determine beam center and the exact distance of the detector, is required. It is sufficient to record a dark current file (no beam) once a day.

3.1.2 Data Evaluation

It is highly recommended to use a software like Fit2D [27] for (automation of) data evaluation. However, some basic theory will be provided to evaluate the data manually.

1. The results of the scattering experiments are two-dimensional scattering images (Fig. 2a). The beam center can be determined by graphically determining the center of the rings of the powder.
2. The distance of the sample to the detector D can be deduced by the (known) d-spacing of the standard:

$$D = \frac{rp}{\tan\left(2\arcsin\frac{\lambda}{2d}\right)}$$

   with r: radius of the scattering ring, p: pixel-size of the detector, λ: wavelength, and d: lattice spacing of the standard material.
3. To integrate the 2D pattern into a 1D curve, the pixel values from the detector are summed up. The radial profile $I(Q)$ with

$$Q = |Q| = \frac{4\pi \sin\theta}{\lambda}$$ (Fig. 2b)

   is calculated by binning all pixels with the same radial distance to the beam center. The azimuthal profile $I(\chi)$ is obtained by binning all pixels with the same azimuthal degree (Fig. 2c, d). This can, e.g., be done using the Radial Profile and Azimuthal Average Plugins for ImageJ (http://rsbweb.nih.gov/ij/plugins/radial-profile.html and http://rsb.info.nih.gov/ij/plugins/azimuthal-average.html) (*see* **Notes 12** and **13**).
4. The data is corrected for background scattering:
   (a) The empty beam is subtracted. This can either be done on the 2D scattering image or with the identically integrated data.
   (b) A baseline is drawn in the radial profile (Fig. 2e) and the constant value is subtracted from the azimuthal profile (Fig. 2f).

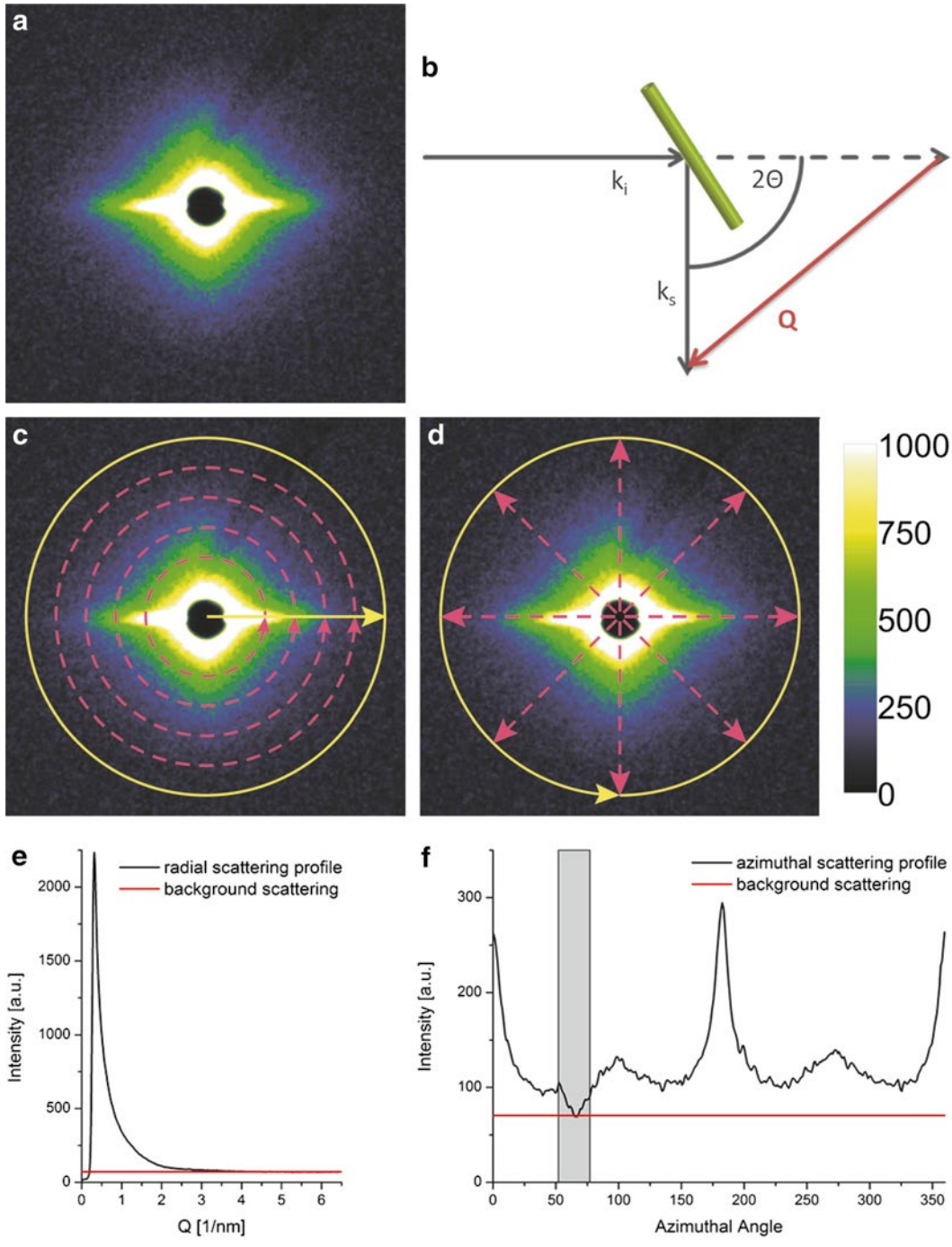

Fig. 2 (**a**) Typical two-dimensional scattering image from a 4-day-old *Arabidopsis* hypocotyl. (**b**) Elastic scattering. The incident beam (wavevector k_i) is scattered. The intensity of the scattered beam (wavevector k_s) is measured as a function of the scattering angle 2Θ. (**c**) Radial (*yellow arrow* indicates *Q*). (**d**) Azimuthal integration (*yellow arrow* indicates χ). (**e**) Baseline in radial scattering profile. (**f**) Baseline in azimuthal scattering profile. *Grey area* marks the region that is masked by the holder of the beamstop

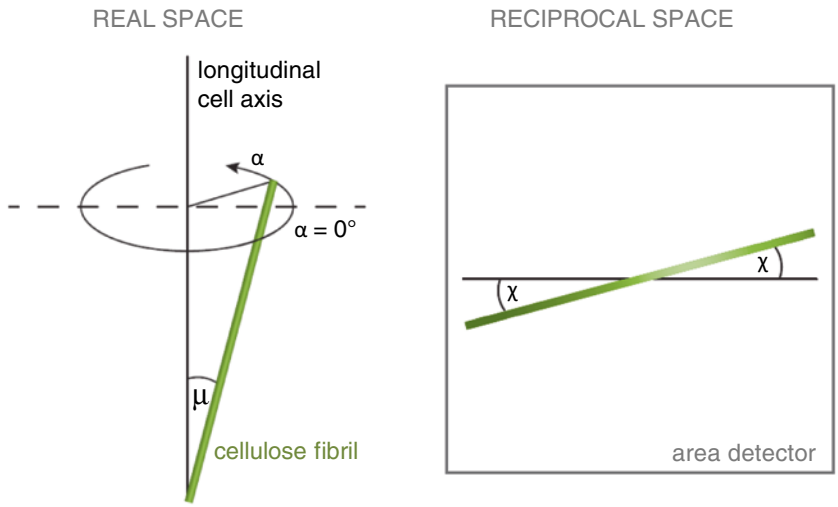

Fig. 3 In real space a cellulose microfibril is tilted toward the longitudinal axis of the cell by the microfibril angle μ and rotated by the cell wall orientation α. The microfibril causes a streak on the detector in reciprocal space that is tilted by the azimuthal angle χ. Redrawn from [36]

5. The positions of the streaks in the azimuthal profile are described by the following equation:
   $\tan\chi = \tan\mu\cos\alpha$ [9, 11] (Fig. 3).
6. For cylindrical cells it is possible to obtain an analytical solution by inverting the equation for the intensity distribution given by [28]:

$$I(\chi) = \frac{2}{\pi}\int_{\chi}^{\frac{\pi}{2}} \frac{p(\mu)\sin(\mu)}{\sqrt{\cos^2\chi - \cos^2\mu}}\,\mathrm{d}\mu$$

7. The inversion of the function can be done numerically [28], yet since $I(\chi)$ can only be determined from the detector image with limited precision, the SAXS data can be fitted by:

$$I(\chi) = \sum_{n\geq 0} a_n \cos^{2n}\chi \qquad \left(\text{for } 0 \leq \chi \leq \frac{\pi}{2}\right)$$

8. Then the probability for a microfibril to be aligned in an angle μ on a sphere $p(\mu)$ becomes:

$$p(\mu) = \sum_{n\geq 0} b_n \cos^{2n}\mu \qquad \text{with} \quad b_n = \frac{2a_n \;\; (n+1)/\Gamma\left(n+\frac{1}{2}\right)}{\sum_{k\geq 0} a_k \;\; (n+1)/\Gamma\left(n+\frac{3}{2}\right)}$$

9. The microfibril angle distribution in the cell wall of a cylindrical cell is $h(\mu) = p(\mu)\sin\mu$ [29] (*see* **Notes 12**, **13**, and **15**).

3.2 Microtensile Tests

Microtensile testing devices are often custom built, e.g. [19, 23, 30, 31]. All of them have in common that they consist of an accurate force sensor, a motor which allows the elongation of the sample and a system that records force and deformation. Since custom-built devices differ between each other we will describe two of our in-house built systems in detail and mention their strengths and weaknesses. These systems have been developed to address different research questions and can be used complementarily. After each description measurement protocols are given.

3.2.1 Microtensile Tester Combined with Strain Measurement by Video Extensometry

The tensile tester is equipped with a highly sensitive load cell (force sensor) with a maximum capacity of 500 mN (Fig. 4b). To avoid damage of the load cell the prepared foliar frames with the hypocotyls (Subheading 2.2) are fixed by a pin-and-hole system onto the tensile stage (Fig. 4b). To allow cutting off the remaining bridges of the foliar frame without damage of the hypocotyl a pressure bar with a spring (Fig. 4b) is mounted on the moveable table. Upon unscrewing the pressure bar is lifted up again with the attached metal springs and the only remaining link between the force sensor and the moveable table is the hypocotyl. During measurements the tensile stage is placed under a stereo microscope equipped with a camera. The black markers on the foliar frame serve for displacement measurement via videoextensometry. Motor displacement is controlled via a LabView-based program on a PC, simultaneously motor displacement, forces, and distance between the black markers are recorded. The mechanical properties of plant cell walls are known to be strain rate dependent, for that reason care needs to be taken by choosing the test speed.

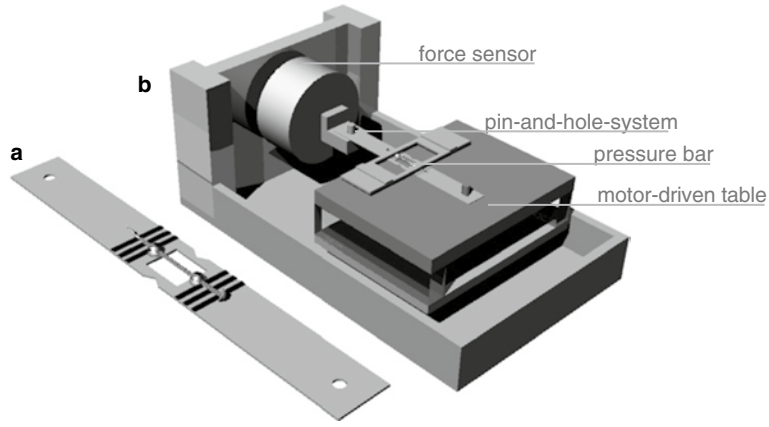

Fig. 4 Microtensile testing combined with videoextensometry for strain measurements. (**a**) Foliar frame with mounted hypocotyls, the black markers provide good contrast for videoextensometry. (**b**) Microtensile tester for operation in the horizontal position

3.2.2 Measurement with Microtensile Tester Combined With Strain Measurement by Video Extensometry

1. Place an air humidifier close to the tensile tester to keep the samples hydrated all the time (*see* **Note 16**).
2. Mount the foliar frame with the hypocotyl in the tensile tester by using the pin-and-hole system.
3. Fix the foliar frame to the table by tightening the screws of the pressure bar.
4. Carefully cut the remaining bridges of the frame with a cutter (*see* **Note 17**).
5. Unscrew to lift up the pressure bar again.
6. Place the microtensile tester under the microscope with the camera, focus on the black lines and illuminate well for good contrast, make sure that the sample is rinsed with wet air but avoid water droplets on the black markers (*see* **Note 18**).
7. Adjust the settings for the videoextensometry in the LabView-based program, choose the right test speed (*see* **Note 19**) and start the experiment.
8. After fracture, remove the sample and start with a new experiment, test at least 15–20 hypocotyls per batch. Keep the time between sample preparation and tensile test constant for each sample.

3.2.3 Microtensile Tester Combined with Strain Measurement Directly on the Sample

This vertically oriented experimental setup (Fig. 5d) allows tensile tests of hypocotyls completely immersed in any liquid that is useful for a particular research question, provided it does not damage equipment or sample clamping (*see* **Note 20**).

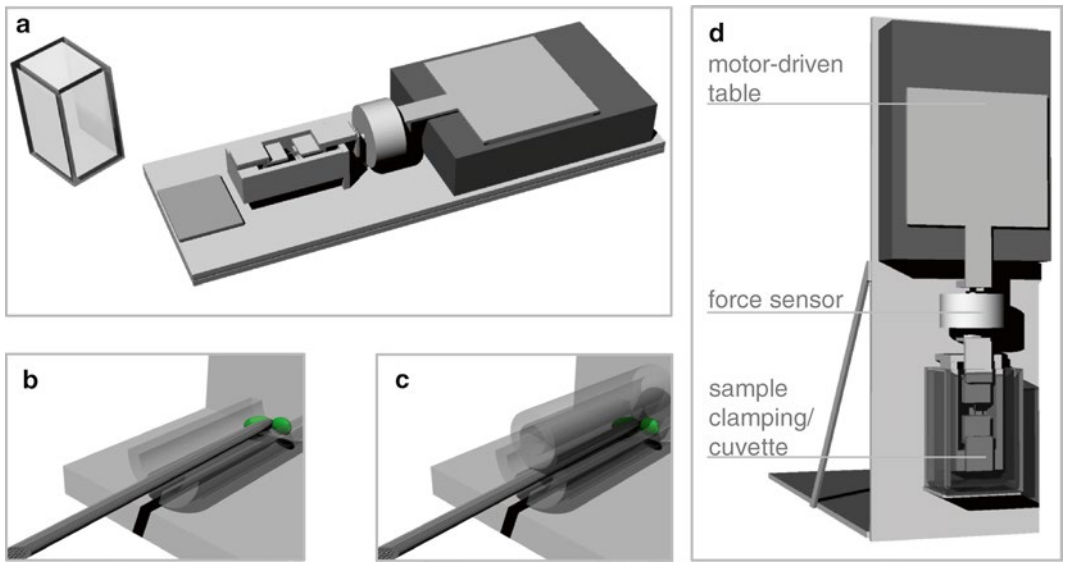

Fig. 5 Microtensile tester with strain measurement directly on the sample. (**a**) Microtensile tester in its horizontal position for sample mounting. (**b**) Hypocotyl placed on a silicone tube on the metal plate. (**c**) Hypocotyl placed between silicone tubes, just before the second metal plate from the top will finalize the clamping. (**d**) Microtensile tester in its vertical position, liquid filled cuvette for immersion of sample

Since dental cement partly dissolves in liquid, flexible silicone pipes with different diameters (commercially available infusion tubes, e.g., large tube with outer diameter of 3 mm and inner diameter of 1 mm combined with smaller tube with outer diameter of 2 mm and inner diameter of 1 mm) are used to transfer slight pressure onto a small amount of cyanacrylate glue for hardening without damaging the hypocotyl (Fig. 5b, c). The rigidity of this clamping system is limited but this is sufficient because strains are measured directly on the sample with a camera system on a microscope.

3.2.4 Measurement with Microtensile Tester Combined with Strain Measurement Directly on the Sample

1. Take a larger silicone pipe, cut it in half along its longitudinal axis and place it on the lower metal part of the clamping system (Fig. 5b). The microtensile tester is in a horizontal position (Fig. 5a).
2. Add a small amount of cyanacrylate glue onto the inner radius of the silicone tube.
3. Carefully harvest a hypocotyl from the plate and place the part with the roots in one tube and the other upper part in the other tube (Fig. 5b).
4. Place two pieces of a silicone pipe with smaller outer diameter on top of the hypocotyl ends (Fig. 5b).
5. Mount the upper metal clamps again, screw them on the lower parts to fix the silicone-tube—hypocotyl sandwich (the metal clamps can be seen in Fig. 5a).
6. Bring the tensile tester in a vertical position (Fig. 5d).
7. Fill the glass cuvette with liquid and immerse the sample in the cuvette by mounting the cuvette on the tensile tester.
8. Position a horizontally oriented light microscope in front of the sample.
9. Illuminate the sample both in reflection and transmission (through a hole/window in the plate of the tensile tester) (*see* **Note 21**).
10. Choose the right test speed (*see* **Note 19**) and start the test with the LabView-based program.
11. For strain analysis directly on the recorded images use image processing software (*see* **Note 22**).

3.2.5 Data Evaluation, Interpretation, and Limitations

The tensile tests allow immediate plotting of force–displacement curves (Fig. 6b). However, this does not tell much about the hypocotyl—and even less about the cell wall properties, since the mechanical properties depend on various additional factors. The most obvious is the geometry of the hypocotyls—lengths and diameters (Fig. 6a, c)—which can have considerable variation. In many cases, e.g., comparison between different mutants, the lower part of the hypocotyl is used for mechanical characterization. The free test span can be kept constant so that the hypocotyl length does not influence the mechanical data. In contrast the measured forces are directly

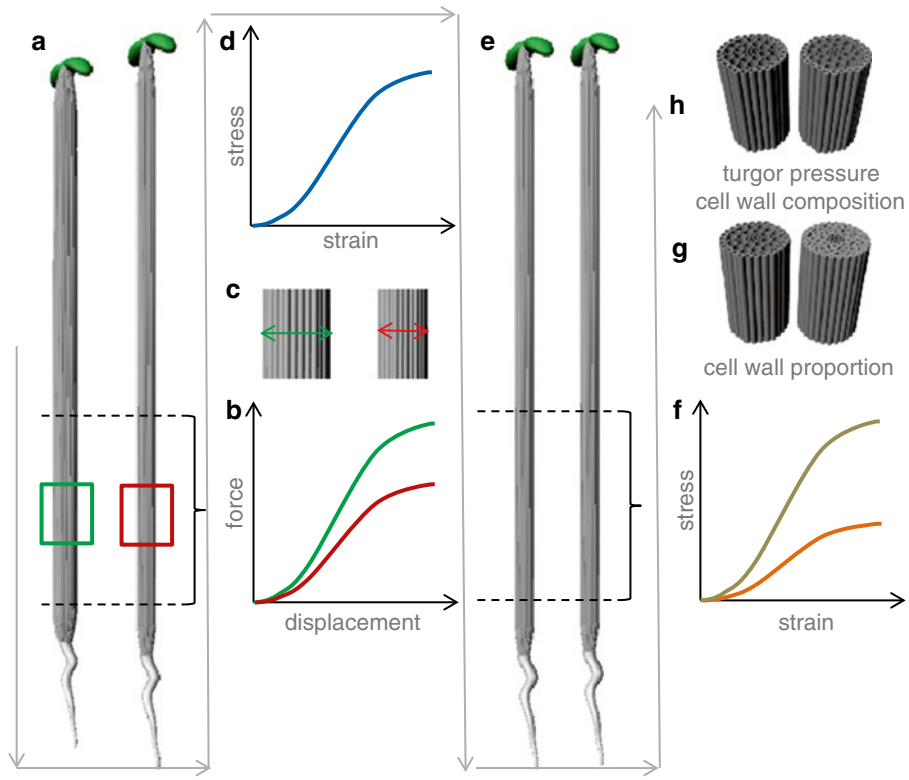

Fig. 6 Data evaluation procedure. (**a**) Hypocotyls with different diameters and lengths. (**b**) Possible force–displacement-diagrams of the hypocotyls in (**a**). (**c**) Hypocotyl diameters. (**d**) Stress–strain diagrams of hypocotyls (**a**), calculated on the hypocotyl cross sectional areas. (**e**) Hypocotyls with the same geometry. (**f**) Stress–strain diagrams of the hypocotyls (**e**). (**g**) Cell wall proportion might explain the different stress–strain-curves in (**f**). (**h**) If there are no differences in cell wall proportion between the hypocotyls (**e**), then turgor pressure or cell wall composition and structure can explain the curves in (**f**)

influenced by hypocotyl cross sections. A thick hypocotyl might require higher forces to break than a thin one with the same material properties (Fig. 6b). In a first data evaluation step stresses σ can be calculated, based on the measured forces F normalized by the hypocotyl cross sectional area A:

$$\sigma = F / A$$

This allows plotting stress–strain diagrams, and if the properties of the hypocotyls (Fig. 6a) would just depend on the cross sectional area then the two force–displacement curves shown in Fig. 6b would collapse into one stress–strain curve as shown in Fig. 6d. In another virtual experiment we tested two hypocotyls with equal lengths and diameters (Fig. 6e). However, the calculated stress–strain diagrams look quite different (Fig. 6f). The reason could be that one of the two hypocotyls has synthesized more cell wall material, e.g., thicker cell walls (Fig. 6g). However, even in

hypocotyls with equal cross sections and the same amount of synthesized cell wall material, the mechanical properties can still be different. So far differences in turgor pressure have not been considered but are known to influence mechanical properties as well [32]. Finally, if there are also no differences in turgor pressure, different stress–strain curves can be related to differences in cell wall composition and structure.

To experimentally access the above mentioned effects several options are possible. The relative cell wall proportion (~bulk density) can be accurately determined by Cryo-SEM [33], but this is extremely time consuming and might therefore not be possible for larger sample numbers. An alternative approach is to determine dry weight/volume, assuming that the measured mass mainly comes from cell wall material. Disadvantageous is, that this cannot be done on the same sample that has been tested. Instead collections of hypocotyls growing on the same plate can be used. For the determination of turgor pressure, pressure probes [34] can hardly be used on the small and delicate cells of the *Arabidopsis* hypocotyls. Alternatively, turgor pressure can be determined indirectly by knowing osmolarity and water potential which both can be measured on another batch of hypocotyls [22].

The presented tools are especially of interest when the effect of modifications on hypocotyls should be studied. The effect of turgor pressure on hypocotyl properties can be completely excluded by testing plasmolyzed cells [32]. The difficulties here are that the system becomes even more fragile and it is unknown what the treatment does to the hypocotyls. The time-dependent behavior can be studied in cyclic loading tests and long-term experiments to gain further insight into the specific deformation behavior of the cell walls, in particular in view of cell wall remodeling in the expansion process during growth (*see* **Note 23**).

4 Notes

1. Only if light could be excluded completely during growth.
2. The plates are placed in horizontal position during growth of the hypocotyls so that the plants can grow upright without a support, e.g., from the agarose as it would be the case if the plates were standing upright. During all the steps of the procedure care should be taken that the plants are kept in an upright position as they could otherwise bend which would influence the measured orientation and the system would not be clearly defined anymore.
3. Make sure not to touch the hypocotyl in the region that will be tested in the tensile test as this could damage the sample and thus influence the results.

4. The curing time of cyanacrylate glue is up to 24 h, if no external pressure is applied. It is clear that the hypocotyls would either not survive this long time or at least change their properties considerably. To overcome this problem a droplet of dental cement can be placed on top of the cyanacrylate glue, which accelerates the curing process. The hardening time of the cement is ~10 min. During hardening stresses cause curing of the cyanacrylate glue.
5. There might be geometrical constraints at the beamline that have to be considered when designing the sample holder. It should be made in a way such that (a) samples can be exchanged quickly and be prepared beforehand so that as much of the measurement time can be used, (b) the hypocotyls are brought as close to the pinhole as possible which means that no parts of the sample holder should jut out in the according direction, and (c) the depth of the material of the upper part that is close to the beam is rather low (0.5–1 cm maximum) to avoid shadowing of the scattering signal.
6. The exact determination of the measurement coordinates in the setup with a well scattering "dummy" like a thread or wire allows finding the hypocotyls much faster in the real measurement. Thus, drying or other alterations of the samples can be avoided. The usual procedure used at X-ray beamlines to locate the samples is to use a diode. However, the signal of the hypocotyls is so low that this method often does not work.
7. Foliar frames showed to be convenient as they are stable and allow an easy transport of the sample. However, other sample holders like flat metal grids are also possible. Care should be taken that the frame on which the hypocotyls are mounted is not too thick (<0.5 mm) because otherwise it could produce shadows in the scattering signal when measuring sample positions close to the frame.
8. Most glues will also scatter the beam when they are illuminated. The signal is likely to mask the scattering signal from the plant. Therefore good care should be taken that no traces of glue are present in the region that is supposed to be analyzed.
9. In the measurement huts at the beamlines there is often air-conditioning that can cause strong airflows. These can cause the steam from the humidifier to be blown away from the sample. When adjusting the humidifier, make sure that it really keeps the sample moist. Work quickly to avoid longer exposures to light before the measurement as the hypocotyl is a highly dynamic system, which can be altered very fast.
10. Choosing a beam size close to the diameter of the hypocotyl leads to a scattering signal that contains information on all cell types in the hypocotyl. As the cell walls in the epidermal cells

are thickest it can be assumed that most of the signal results from these cells. Separation of the different cell types is difficult as the integrity of the tissue is lost. Any additive that could stabilize dissected plants would also scatter the X-ray beam and likely mask the weak scattering signal from the plant.

11. Generally the time of the sample on the sample holder should be kept to a minimum to avoid drying and changes in the plant after light exposure.
12. Area masked by the beamstop should be excluded in the microfibril angle analysis (Fig. 2f).
13. One assumption of the model is that the cells of the hypocotyl are cylindrical. When characterizing plants or tissues with different shapes other models have to be used to deduce the microfibril angle distribution [29, 35].
14. Scattering images appear in reciprocal space rather than in real space (Fig. 3). The scattering pattern can be obtained by the Fourier transform of the sample in space. When the long cylindrical cellulose microfibrils are illuminated by the beam, a scattering pattern occurs in reciprocal space in which the microfibrils appear as flat disks. The angular intensity distribution in the azimuthal profile is influenced not only by the microfibril angle but also by the cell wall orientation α.
15. Depending on the cell geometry, different procedures have been developed to calculate the microfibril angle distributions [11, 26, 28].
16. Carefully keep the hypocotyls wet. This is of particular importance for some modified samples, which dry out faster than wild type hypocotyls. Wet boxes or rinsing with water saturated air during sample preparation and the mechanical test can help. Furthermore try to keep the time from sample preparation to the mechanical test as constant as possible, especially if you test living hypocotyls.
17. Successful cutting of the bridges of the foliar frames might require some training. Alternatively hot wires can be used for cutting.
18. The quality of the markers (system with videoextensometry) and illumination is crucial for strain measurements. Avoid water droplets on markers for videoextensometry (e.g., caused by condensation); they might lead to false strain measurements because of changing optical properties of water droplets.
19. The mechanical properties of plant cell walls are known to be strain rate dependent, for that reason care needs to be taken by choosing the test speed.
20. An isotonic liquid can be prepared, e.g., from polyethyleneglycol.

21. To get sufficiently good image quality illumination of the sample is crucial. The best results can be achieved by illuminating both in transmission and reflection.
22. For strain analysis the quality (contrast) of the images is crucial. Sometimes markers on the hypocotyls are necessary, this can be done with water proof pens but make sure that the ink does not alter the hypocotyl. If the contrast on the hypocotyl is good enough several areas can be marked and deformations tracked; creating strain maps along the hypocotyl should be possible, too. Choose a commercially available image analysis program that fits your purposes. Image analysis can also be done with LabView-based programs.
23. Since it is known that trace levels of iron might inhibit cell wall creep or relaxation try to avoid sample contact with metal parts when you plan long measurement times [32].

References

1. Somerville C, Bauer S, Brininstool G, Facette M, Hamann T, Milne J, Osborne E, Paredez A, Persson S, Raab T (2004) Toward a systems approach to understanding plant cell walls. Science 306(5705):2206–2211
2. Somerville C (2006) Cellulose synthesis in higher plants. Annu Rev Cell Dev Biol 22:53–78
3. Endler A, Persson S (2011) Cellulose synthases and synthesis in Arabidopsis. Mol Plant. doi:10.1093/mp/ssq079
4. Cosgrove DJ (2005) Growth of the plant cell wall. Nat Rev Mol Cell Biol 6(11):850–861
5. Cosgrove D, Jarvis M (2012) Comparative structure and biomechanics of plant primary and secondary cell walls. Front Plant Sci 3:204, doi:10.3389/fpls.2012.00204
6. Keegstra K, Talmadge KW, Bauer W, Albersheim P (1973) The structure of plant cell walls III. A model of the walls of suspension-cultured sycamore cells based on the interconnections of the macromolecular components. Plant Physiol 51(1):188–197
7. Preston RD (1974) The physical biology of plant cell walls. Chapman and Hall, London
8. Wardrop AB (1952) The low-angle scattering of X-rays by conifer tracheids. Text Res J 22(4): 288–291
9. Kantola M, Kähkönen H (1963) Small-angle X-ray investigation of the orientation of crystallites in Finnish coniferous and deciduous wood fibers. Suomalainen tiedeakatemia, Helsinki
10. Jakob HF, Fratzl P, Tschegg SE (1994) Size and arrangement of elementary cellulose fibrils in wood cells: a small-angle X-ray scattering study of Picea abies. J Struct Biol 113(1): 13–22
11. Reiterer A, Jakob HF, Stanzl-Tschegg SE, Fratzl P (1998) Spiral angle of elementary cellulose fibrils in cell walls of Picea abies determined by small-angle X-ray scattering. Wood Sci Technol 32(5):335–345
12. Lichtenegger H, Reiterer A, Stanzl-Tschegg S, Fratzl P (1999) Variation of cellulose microfibril angles in softwoods and hardwoods—a possible strategy of mechanical optimization. J Struct Biol 128(3):257–269
13. Gertel ET, Green PB (1977) Cell-growth pattern and wall microfibrillar arrangement—experiments with Nitella. Plant Physiol 60(2): 247–254
14. Green PB (1960) Multinet growth in the cell wall of Nitella. J Biophys Biochem Cytol 7(2):289–296
15. Richmond PA, Métraux JP, Taiz L (1980) Cell expansion patterns and directionality of wall mechanical properties in Nitella. Plant Physiol 65(2):211
16. Davies LM, Harris PJ (2003) Atomic force microscopy of microfibrils in primary cell walls. Planta 217(2):283–289
17. Hepworth DG, Bruce DM (2004) Relationships between primary plant cell wall architecture and mechanical properties for onion bulb scale epidermal cells. J Texture Stud 35(6): 586–602
18. Zhang T, Mahgsoudy-Louyeh S, Tittmann B, Cosgrove D (2014) Visualization of the

nanoscale pattern of recently-deposited cellulose microfibrils and matrix materials in never-dried primary walls of the onion epidermis. Cellulose 21(2):853–862

19. Kutschera U (1991) Determination of the longitudinal tissue stresses in the growing and non-growing regions of sunflower hypocotyls. J Plant Physiol 138(4):460–465
20. Kennedy CJ, Sturcova A, Jarvis MC, Wess TJ (2007) Hydration effects on spacing of primary-wall cellulose microfibrils: a small angle X-ray scattering study. Cellulose 14:401–408
21. Cosgrove DJ, Durachko DM (1994) Autolysis and extension of isolated walls from growing cucumber hypocotyls. J Exp Bot 45: 1711–1719
22. Abasolo W, Eder M, Yamauchi K, Obel N, Reinecke A, Neumetzler L, Dunlop JWC, Mouille G, Pauly M, Hofte H, Burgert I (2009) Pectin may hinder the unfolding of xyloglucan chains during cell deformation: implications of the mechanical performance of Arabidopsis hypocotyls with pectin alterations. Mol Plant 2(5):990–999
23. Ryden P, Sugimoto-Shirasu K, Smith AC, Findlay K, Reiter WD, McCann MC (2003) Tensile properties of Arabidopsis cell walls depend on both a xyloglucan cross-linked microfibrillar network and rhamnogalacturonan II-borate complexes. Plant Physiol 132(2): 1033–1040
24. Cavalier DM, Lerouxel O, Neumetzler L, Yamauchi K, Reinecke A, Freshour G, Zabotina OA, Hahn MG, Burgert I, Pauly M, Raikhel NV, Keegstra K (2008) Disrupting two Arabidopsis thaliana xylosyltransferase genes results in plants deficient in xyloglucan, a major primary cell wall component. Plant Cell 20(6):1519–1537
25. Pauly M, Albersheim P, Darvill A, York WS (1999) Molecular domains of the cellulose/xyloglucan network in the cell walls of higher plants. Plant J 20(6):629–639
26. Lichtenegger H, Reiterer A, Tschegg S, Fratzl P (1998) Determination of spiral angles of elementary fibrils in the wood cell wall: comparison of small-angle X-ray scattering and wide-angle X-ray diffraction. In: Butterfield BG (Ed) Proceedings of the International Workshop on the Significance of Microfibril Angle to Wood Quality, New Zealand, pp. 140–156
27. Hammersley A (1998) FIT2D V9.129 Reference Manual V3.1. ESRF internal report, ESRF98HA01T
28. Perret R, Ruland W (1969) Single and multiple x-ray small-angle scattering of carbon fibres. J Appl Crystallogr 2(5):209–218
29. Saxe F, Eder M, Benecke G, Aichmayer B, Fratzl P, Burgert I, Rüggeberg M (2014) Measurement of cellulose microfibril angle distributions in primary cell walls by small angle X-ray scattering. Plant Methods 10:25
30. Suslov D, Verbelen JP (2006) Cellulose orientation determines mechanical anisotropy in onion epidermis cell walls. J Exp Bot 57(10): 2183–2192
31. Burgert I, Frühmann K, Keckes J, Fratzl P, Stanzl-Tschegg SE (2003) Microtensile testing of wood fibers combined with video extensometry for efficient strain detection. Holzforschung 57(6):661–664
32. Cosgrove DJ (2011) Measuring in vitro extensibility of growing plant cell walls. Methods Mol Biol 715:291–303
33. Derbyshire P, Findlay K, McCann MC, Roberts K (2007) Cell elongation in Arabidopsis hypocotyls involves dynamic changes in cell wall thickness. J Exp Bot 58(8):2079–2089
34. Green PB (1968) Growth physics in Nitella: a method for continuous in vivo analysis of extensibility based on a micro-manometer technique for turgor pressure. Plant Physiol 43:1169–1184
35. Ruggeberg M, Saxe F, Metzger TH, Sundberg B, Fratzl P, Burgert I (2013) Enhanced cellulose orientation analysis in complex model plant tissues. J Struct Biol 183(3):419–428
36. Reiterer A, Lichtenegger H, Tschegg S, Fratzl P (1999) Experimental evidence for a mechanical function of the cellulose microfibril angle in wood cell walls. Philos Mag A 79(9):2173–2184

Index

José M. Estevez (ed.), *Plant Cell Expansion: Methods and Protocols*, Methods in Molecular Biology, vol. 1242,
DOI 10.1007/978-1-4939-1902-4, © Springer Science+Business Media New York 2015

G

H

I

L

M

N

O

P

R

S

T

V

W

X

Y